Consequences of Tyrosine Phosphorylation of Syntaxin4 and Munc18c on GLUT4 Trafficking

Mohammed Nasser Rashid Al Tobi

BSc MSc MSc

Thesis submitted in fulfilment of the requirements for the Degree of

Doctor of Philosophy

February 2018

Institute of Molecular, Cell and Systems Biology

College of Medical, Veterinary and Life Sciences

University of Glasgow

Abstract

Glucose homeostasis is regulated by the opposing actions of insulin and glucagon; insulin facilitates rapid glucose uptake from the blood stream to muscle and adipose cells. These tissues express the facilitative glucose transporter (GLUT4), which in response to insulin is translocated from intracellular compartments to the plasma membrane (PM) allowing glucose entry to cells. GLUT4 undergoes a complex intracellular trafficking itinerary, including recycling to and from the PM, but in the absence of insulin is mainly stored in GLUT4 storage vesicles (GSVs). When insulin binds its receptor, a complicated signalling cascade is initiated which results in the tethering, docking and fusion of GSVs to the PM. Fusion of the GSVs with the plasma membrane is mediated by SNARE proteins. The formation of a SNARE complex composed of Syntaxin4 (Sx4) and SNAP23 localised to the PM and VAMP2 on GSVs is a key event; the formation of this complex is in turn regulated by the Sec1/Munc18 protein, Munc18c. It has been shown that insulin stimulation leads to phosphorylation of Sx4 at two sites (Y115 and Y251) and Munc18c at Y521. The stoichiometry and order of phosphorylation are not yet known, and the biological consequences of this action to be uncovered. Therefore, the current study sought to ascertain the functional consequences of SNARE protein phosphorylation on GLUT4 trafficking. The approaches used include *in vitro* assessment of recombinant SNARE proteins and studies *in vivo* using 3T3-L1 adipocytes.

The results of this study confirmed that tyrosine 115 and 251 of syntaxin4 are phosphorylated in response to insulin in 3T3-L1 adipocytes; however, phosphorylation of Munc18c was ambiguous. Subsequently, phosphomimetic recombinant SNARE proteins were expressed and ternary SNARE complex formation was successfully recapitulated *in vitro* and the complex found to be SDS and heat resistant. Phosphomimetic syntaxin4 mutants showed increased formation of SNARE complexes, notably double phosphomimetic mutant. Moreover, binary interactions with other SNAREs (SNAP23 and VAMP2) revealed tighter binding and higher affinity of the double phosphomimetic syntaxin4 compared to wild-type syntaxin4. Additional spectroscopic evidences suggest these differences are due to conformational changes and syntaxin4 mutants are

more likely to be in the open form especially the double phosphomimetic mutant.

In order to translate *in vitro* findings into cell models, *in vivo* intervention tools were generated including phospho-specific antibodies against phosphorylated residues in syntaxin4 and lentivirus particles for 3T3-L1 adipocytes infection. Antibodies validated on recombinant proteins phosphorylated using recombinant insulin receptor tyrosine kinase indicated they are functional and specific. Efforts dedicated towards optimizing working conditions for phospho-specific antibodies using adipocyte lysates were extensively examined, yet signals detected were generally found to be non-specific.

A non-intrusive protein-protein interaction protocol, proximity ligation assay, was used to detect insulin-stimulated phosphorylation in adipocytes. A positive signal was detected confirming antibodies functionality in this assay; further work will be required to optimize this.

Lentiviruses were used to over-express phosphomimetic mutants of syntaxin4 in 3T3-L1 adipocytes and Hela cells. The functionality of the transfected syntaxin4 mutants was assessed by measuring basal and insulin-stimulated glucose uptake. Infected native 3T3-L1 adipocytes showed a trend towards an increase in glucose uptake under basal conditions with no effect observed on the maximal insulin-stimulated rate of glucose transport. We speculate this may reflect the presence of the endogenous Sx4 molecules masking any effects of mutant over-expression thus Sx4 knockout cell lines was considered as an alternative experimental system. Sx4 overexpression rescued insulin-stimulated glucose uptake in Sx4 knockout 3T3-L1 cells and was significantly enhanced in cells expressing the double phosphomimetic mutant.

Finally, our work showed that the native Munc18c native mouse gene sequence expressed poorly in bacteria; hence we used a gene-enhanced sequence that was found to express well and purify effectively. CD spectroscopy showed similar structures of expressed Munc18c using either sequences. Phosphomimetic Munc18c (Y521E) binds with higher affinity both wild type and double phosphomimetic syntaxin4 compared to wild type Munc18c.

The data presented in this study suggest strongly that phosphorylation influences GLUT4 trafficking by altering the frequency and affinity of SNARE protein

interactions. Such findings enrich knowledge about the mechanism of GLUT4 trafficking thus ultimately could help in understanding type 2 diabetes.

Table of Contents

Abstract i

Table of Contents iv

List of Tables x

List of Figures xi

Acknowledgement xiv

Author's Declaration xv

Definitions/Abbreviations xvi

1 Introduction 20

1.1 Membrane trafficking 21

1.1.1 Membrane trafficking in eukaryotic cells 21

1.1.2 Endocytosis and exocytosis cycles 21

1.1.3 Membrane fusion 24

1.1.4 Tethering, docking, and fusion 25

1.2 SNARE proteins: the SNARE hypothesis, and SNARE complex 26

1.2.1 Discovery of SNARE proteins 26

1.2.2 SNARE protein structure 27

1.2.3 The SNARE hypothesis 29

1.2.4 Classification of SNARE proteins 31

1.2.5 SNARE complex formation and structure 33

1.3 Sec1-Munc18 (SM) regulatory proteins 36

1.3.1 SM proteins 36

1.3.2 Tethers 40

1.3.3 Rab proteins 41

1.4 Glucose metabolism 42

1.4.1 Glucose homeostasis and diabetes 42

1.4.2 Glucose transporters 43
1.4.3 Insulin signaling 45
1.4.4 GLUT4 trafficking 47
1.4.5 SNARE-mediated GLUT4 trafficking 49
1.4.6 GLUT4 regulation by Munc18c 51
1.5 SNAREs and post-translational modification 52
1.5.1 Phosphorylation 52
1.6 Aim of this study 55
1.6.1 Aims of chapter THREE 55
1.6.2 Aims of chapter FOUR 55
1.6.3 Aims of chapter FIVE 56
1.6.4 Aims of chapter SIX 56
2 Materials and Methods 58
2.1 Materials 59
2.1.1 General reagents and kits 59
2.1.2 Solutions and media 59
2.1.3 Antibodies 62
2.1.4 Plasmids 66
2.1.5 Cell lines 71
2.1.6 Computer software 71
2.2 Molecular biology methods/techniques 72
2.2.1 Plasmid DNA purification – small scale 72
2.2.2 Plasmid DNA purification – large scale 72
2.2.3 Agarose gel electrophoresis 73
2.2.4 Digestion of plasmids using restriction endonucleases 73
2.2.5 Plasmid transformation 74
2.3 Protein methods 74
2.3.1 Recombinant proteins expression and purification 74

2.3.2 SDS-PAGE 77
2.3.3 Coomassie stain 78
2.3.4 Protein concentration estimation 78
2.3.5 Western blotting; Immunoblots (semi-dry & wet transfer) 78
2.4 Pull down 80
2.5 Complex assembly assay 80
2.6 CIRK phosphorylation 81
2.7 Cell culture 82
2.7.1 3T3-L1 maintenance and differentiation 82
2.7.2 Insulin stimulation of 3T3L1 adipocytes 82
2.7.3 Lentivirus production using HEK293 and concentration 83
2.7.4 Lentivirus infection 84
2.7.5 Cell transfection 84
2.7.6 Freezing cells 85
2.8 Proximity Ligation Assay (PLA) 85
2.9 Fluorimeter analysis & anisotropy 86
2.9.1 IANBD labelling 86
2.9.2 Fluorescence scanning 87
2.10 Oil Red O stain 88
2.11 Total membrane fraction preparation 88
3 Characterization of phosphomimetic Syntaxin4 mutants 90
3.1 Introduction 91
3.2 Results 91
3.2.1 Confirmation of tyrosine phosphorylation residues in Sx4 and Munc18c 91
3.2.2 MS analysis shows Y115 and Y251 are phosphorylated in adipocytes in response to insulin 93
3.2.3 Generation of recombinant Sx4 proteins 95

3.2.4 SNARE complex formation *in vitro* 97
3.2.5 2P exhibits enhanced SNARE complex formation in vitro 99
3.2.6 SNARE complex formation is independent of the Tag on the VAMP2 101
3.2.7 An alternative assay of SNARE complex formation 102
3.2.8 Pairwise interactions of Sx4 and Sx4-2P with VAMP2 and SNAP23 .. 105
3.2.9 Circular Dichroism (CD) spectroscopy and Isothermal Titration Calorimetry (ITC) to quantify binary interactions 109
3.2.10 Phosphorylated Sx4 is in the open conformation. 112
3.3 Discussion 113
4 Tools for *in vivo* work 120
4.1 Introduction 121
4.2 Results 121
4.2.1 Generation of anti-phospho antibodies for Sx4 and Munc18c 121
4.2.2 Syntaxin4 is a CIRK phosphorylation target 124
4.2.3 Phospho-specific syntaxin4 antibodies proved difficult to detect signal in cell lysates 127
4.2.4 Munc18c phospho-specific antibody demonstrate good detection signal though less than approved 132
4.2.5 PLA signals suggest Sx4 phosphorylation sites stoichiometry with more effort 132
4.2.6 Generation of Sx4 and Munc18c lentivirus 136
4.2.7 Sx4 versus 2P in HeLa cells expressing GLUT4 140
4.3 Discussion 142
5 Syntaxin4 phosphorylation consequences, *in vivo* 148
5.1 Introduction 149
5.2 Results 149
5.2.1 Primary data on over-expression of Sx4 or 2P and resulting consequences on glucose uptake in native 3T3-L1 adipocytes 149

5.2.2 Characterisation of Sx4 knockout cells. 152
5.2.3 Restored Sx4 is functional, evidence shown by glucose uptake assay 157
5.2.4 Knockout effects on GLUT4 machinery 163
5.2.5 Compensatory mechanisms. 165
5.2.6 Adipokine secretion – preliminary analysis of Sx4 knockout lines. . 167
5.3 Discussion 171
6 Munc18c phosphorylation effects on SNARE complex 174
6.1 Introduction 175
6.2 Results 176
6.2.1 Expression of enhanced gene and compare to mouse original sequence 176
6.2.2 Cloning enhanced gene into pQE30 177
6.2.3 Munc18c codon-optimised expression 178
6.2.4 Enhanced Munc18c usage in SNARE complex 179
6.2.5 Munc18c pull down assay with cognate SNAREs 184
6.3 Discussion 186
7 Discussion 191
7.1 Discussion 192
7.2 Future work 197
8 Appendices 200
8.1 Appendix-I: Primary data obtained from PLA analysis for indicated samples. 201
8.2 Basal versus 5 minutes insulin stimulation 203
8.2.1 SX4/M-115P/R BASAL 204
8.2.2 SX4/M-115P/R INSULIN 205
8.2.3 SX4/M-251P/R BASAL 206
8.2.4 SX4/M-251P/R INSULIN 207

8.2.5 SX4/M-SX4/R BASAL....208
8.2.6 SX4/M-SX4/R INSULIN....209
8.2.7 V2/M-S23/R BASAL....210
8.2.8 V2/M-S23/R INSULIN....211
9 List of References....212

List of Tables

Table 1 List of primary antibodies used in different experiments in this study.. 62
Table 2 List of secondary antibodies used for immuno-detection..... 65
Table 3 Plasmid constructs used for expressing study-targeted proteins. 67
Table 4 Mammalian cell lines used in this study. 71
Table 5 Recombinant protein purification buffers used in this study. 76
Table 6 Secondary structure content estimates for Munc18c mutants. 183

List of Figures

Figure 1-1 Cellular components of secretory and endocytic pathways. 23
Figure 1-2 Vesicle fusion through hemi-fusion intermediate transition. 25
Figure 1-3 SNARE proteins structure. 28
Figure 1-4 The SNARE hypothesis illustration. 29
Figure 1-5 SNAREs localisation within mammalian cell. 30
Figure 1-6 SNARE complex structure. 35
Figure 1-7 SM-Syntaxin binding modes. 39
Figure 1-8 GLUT4 diagram 44
Figure 1-9 Insulin signaling pathways in GLUT4 translocation. 46
Figure 1-10 GLUT4 trafficking model. 48
Figure 1-11 Munc18c-Syntaxin4 regulatory binding modes. 51
Figure 3-1 Immunoprecipitation of Sx4 from adipocytes is quantitative and can be used for MS. 92
Figure 3-2 MS analysis shows Y115 and Y251 are phosphorylated in 3T3-L1 adipocytes in response to insulin. 94
Figure 3-3 Representative purifications of Sx4-GST fusion proteins. 95
Figure 3-4 Purification of cleaved forms of Sx4, wt (A) and 2P (B). 97
Figure 3-5 SNARE complex formation requires Sx4, SNAP23, and VAMP2. 98
Figure 3-6 SNARE complex formation is enhanced in the phosphomimetic mutants. 100
Figure 3-7 SNARE complex formation is independent of participant tag. 101
Figure 3-8 Fluorescent environment-sensitive label show signal intensity change upon SNARE complex formation through time and Sx4 mutants status. 105
Figure 3-9 Phosphomimetic Sx4 mutants bind more SNAP23 than WT. 106
Figure 3-10 Phosphomimetic Syntaxin4 mutants show increased binding to VAMP2 compared to WT. 108
Figure 3-11 Far UV CD spectrum of ternary complex show conformation changes. 110
Figure 3-12 ITC data reveals that Sx4-2P binds SNAP23 tighter than Sx4-wt. ... 111
Figure 3-13 Sx4-Y115E and Sx4-Y115,251E show comparable sensitivity to limited proteolysis to the Sx4 open mutant. 113

Figure 4-1 Syntaxin4 tyrosine phosphorylation sites conserved among other species. 123
Figure 4-2 Tyrosine 521 in Munc18c conserved between human isoforms and mouse. 124
Figure 4-3 Syntaxin4 phospho-specific antibodies detect targeted CIRK-phosphorylated Sx4 in precision. 125
Figure 4-4 Monomeric Sx4 is a CIRK target but not in t-SNARE complex, Sx4/SNAP23 126
Figure 4-5 Syntaxin4 phospho-specific antibodies struggle detecting signal in 3T3-L1 adipocytes. 128
Figure 4-6 Syntaxin4 phospho-specific detection in different cell types. 129
Figure 4-7 Phospho-specific Sx4 antibodies are not reliable for blotting 3T3-L1 lysates. 130
Figure 4-8 Immunoprecipitation of Sx4 using generated phospho-specific antibodies as primary antibody 131
Figure 4-9 Generated Munc18c antibodies detected signal at right size in addition to non-specific. 132
Figure 4-10 Proximity Ligation Assay (PLA) principle. 134
Figure 4-11 Typical output data from BlobFinder software analysis. 135
Figure 4-12 Confocal imaging plan show different number of blobs at different focus points. 136
Figure 4-13 Sub-cloning Sx4 and Munc18c into lentivirus plasmids followed by transient expression of viral vectors shows they are functional. 138
Figure 4-14 Lentivirus produced for Sx4 are functional for transducing cells to overexpress target protein. 140
Figure 4-15 Virus infection of HA-GLUT-GFP HeLa cells. 141
Figure 5-1 Lentivirus infection of 3T3-L1 adipocytes resulted in an overexpression of Sx4. 150
Figure 5-2 Sx4 over-expression appears to elevate basal glucose transport in native 3T3-L1. 152
Figure 5-3 Sx4 is depleted in knockout 3T3-L1 cells. 154
Figure 5-4 Sx4 knockout decelerates the proliferation of cell fibroblasts as well as differentiation into adipocytes 155
Figure 5-5 Adipocyte differentiation protein markers. 156

Figure 5-6 Sx4 over-expression rescues insulin-stimulated glucose uptake in Sx4 knockout 3T3-L1 cells. 158
Figure 5-7 Lentivirus-mediated over-expression of Sx4 rescues levels of glucose uptake in knockout 3T3-L1 cells. 160
Figure 5-8 Sx4 re-expressed in infected knockout cells. 162
Figure 5-9 Sx4 knockout effects on glucose transport machinery. 164
Figure 5-10 Other SNARE protein levels in Sx4 knockout adipocytes. 166
Figure 5-11 Adipocyte secretions. 167
Figure 5-12 Over-expression of Sx4 in knockout cells approaches levels in wild-type cells. 168
Figure 5-13 Sx4 re-expression did not restore transcriptional factor PPARγ. ... 169
Figure 5-14 Re-introduction of Sx4 effects on other Sx proteins. 170
Figure 6-1 Munc18c expression using native mouse sequence. 176
Figure 6-2 Sub-cloning codon-optimised Munc18c into pQE30. 177
Figure 6-3 Munc18c purifications using codon-optimised gene sequence. 178
Figure 6-4 Munc18c influence on SNARE complex. 179
Figure 6-5 SNARE complex formation assay with Munc18c. 181
Figure 6-6 Far UV CD spectrum of cytosolic domains of Munc18c expressed by native mouse gene or codon-optimised. 182
Figure 6-7 Normalised far UV CD spectra of the cytosolic domains of native mouse and codon-optimised Munc18c gene. 184
Figure 6-8 Phosphorylation effect on binding affinity of Sx4 and Munc18c. 186

Acknowledgement

I would like to express my deep gratitude to Professor Gwyn Gould and Professor Nia Bryant, my research supervisors, for their patient guidance, enthusiastic encouragement and useful critiques of this research work. Apart from academic guidance, Professor Gwyn Gould was there for support and assistance whenever needed which is mostly appreciated and am honoured working with him. My gratitude extends to all lab241 staff and students, past and present, who were my second family in Scotland and supporting team in work. I would also like to thank Dr Dimitrios Kioumourtzoglou for introducing me to the project and his continuous support from York. A big thank you goes to my colleagues Kamilla, Silke, and my brother Peter; working together as one team and supporting each other all the time, I enjoyed your company. I owe thanks to Dr Hannah Black sharing knowledge and experience in this study. Special thanks to Dr Cheryl Woodhead and Sharon Kelly for their help with all spectroscopic analyses. I would also like to extend my thanks to the technicians of the laboratory of the department for their help in offering me the resources in running the study. My friends in Edinburgh and Glasgow, appreciate your support and help throughout this journey.

My family is my life. Thank you to my wife who was in support over this adventure and life journey as well as my children who were a joy-source at hard days. Taking care of family, while studying PhD, was challenging yet enjoyable with many memories to remember. I wish to thank my parents for their support and encouragement throughout my study and their prayers. I appreciate their efforts bringing me into what I am.

Last but not least, I am grateful to my country Sultanate of Oman, funding my study scholarship especially Ministry of Higher Education. Also, I would like to thank my working place, Sultan Qaboos University SQU, for their support.

Thank you all

شكراً جزيلاً لكم جميعا

Author's Declaration

I declare that the work presented in this thesis is my own, unless otherwise cited or acknowledged. It is entirely of my own composition and has not, in whole or in part, been submitted for any other degree.

Mohammed Nasser Rashid Al Tobi
February 2018

Definitions/Abbreviations

(v/v)	Units volume per unit volume
(w/v)	Units weight per unit volume
°C	Degrees Celsius
~	Approximately
ADP	Adenosine diphosphate
Amp	Ampicillin
APS	Ammonium persulfate
AS160	Akt substrate of 160 kilodaltons
ATP	Adenosine 5'-triphosphate
bp	DNA base pair(s)
BSA	Bovine serum albumin
CAP	c-Cbl associated protein
dH2O	Distilled water
DMEM	Dulbecco's modified Eagle's medium
DMSO	Dimethyl sulphoxide
DNA	Deoxyribonucleic acid
DNaseI	Deoxyribonuclease I
dNTP	Deoxynucleoside (5')-triphosphate
E. coli	Escherichia coli
ECL	Enhanced chemiluminescence
EDTA	Ethylenediaminetetraacetic acid
ER	Endoplasmic reticulum
FBS	Foetal bovine serum
FRET	Förster resonance energy transfer
g	Gram
GDP	Guanosine-5'-diphosphate
GFP	Aequorea victoria green fluorescent protein
GLUT	Glucose transporter
GST	Glutathione S transferase
GSV	GLUT4 storage vesicle

GTP	Guanosine-5'-triphosphate
HA	Influenza haemagglutinin epitope tag
HCl	Hydrochloric acid
HEPES	2-[4-(2-Hydroxyethyl)-1-piperazine] ethanesulfonic acid
His	Six-histidine residue tag
HRP	Horse radish peroxidase
IB	Immunoblot
IF	Immunofluorescence
IgG	Immunoglobulin G
IP	Immunoprecipitation
IPTG	Isopropyl-ß-D-thiogalactopyranoside
IR	insulin receptor
IRAP	insulin receptor-associated protein
IRS	insulin receptor substrate
Kan	Kanamycin
k	Kilo (prefix)
kb	Kilobase
kDa	Kilo daltons
L	Litre
LSB	Laemmli's sample buffer
m	Milli (prefix)
M	Molar
M18c	Munc18c
mA	Milliamp
mg	Milligram
min	Minute
ml	Millilitre
n	Nano (prefix)
N-terminal	Amino terminal
NCS	New-born calf serum
Ni-NTA	Nickel-nitrilotriacetic acid
NSF	N-ethylmaleimide sensitive factor
OD600	Optical density at 600nm

p	Pico (prefix)
PAGE	Polyacrylamide gel electrophoresis
PBS	Phosphate buffered saline
PBS-T	Phosphate buffered saline plus Tween-20
PCR	Polymerase chain reaction
PFA	Paraformaldehyde
PI	Phosphatidylinositol
PI3K	Phosphatidylinositol 3-kinase
PIP2	Phosphatidylinositol 4,5-bisphosphate
PIP3	Phosphatidylinositol 3,4,5-triphosphate
PKB	Protein kinase B/Akt
PKC	Protein kinase C
PLA	Proximity ligation assay
PM	Plasma membrane
PMSF	Phenylmethylsulfonyl fluoride
psi	Pounds per square inch
RNA	Ribonucleic acid
rpm	Rotations per minute
S. *cerevisiae*	Saccharomyces cerevisiae
SDS	Sodium dodecyl sulfate
SDS-PAGE	Sodium dodecyl sulphate- polyacrylamide gel electrophoresis
siRNA	Short interfering ribonucleic acid
SM	Sec1/Munc18
SNAP	Soluble NSF attachment protein
SNARE	Soluble NSF attachment protein receptor
SOC	Super Optimal Broth
Sx	Syntaxin
t-SNARE	Target SNARE
TAE	Tris acetate EDTA
Taq	Thermus aquaticus
TB	Terrific broth
TEMED	N, N, N', N' - tetramethylenediamine
TGN	*Tran*-Golgi network

TIRF	Total internal reflection fluorescent
Tris	2-Amino-2-(hydroxymethyl)-1,3-propanediol
Tween-20	Polyoxyethylene sorbitan monolaurate
v-SNARE	Vesicle SNARE
VAMP	Vesicle associated membrane protein
µ	Micro (prefix)

CHAPTER ONE

1 Introduction

1.1 Membrane trafficking

1.1.1 Membrane trafficking in eukaryotic cells

Cells are the building blocks of eukaryotes. Although small in size they are loaded with many organelles and their internal membranes are organized in a highly ordered and sophisticated manner. Organelles and macromolecules are compartmentalized in membrane engulfed vesicles that control the complicated and specific biochemical interactions within cells (Vellai and Vida, 1999). Communication and interactions, both intracellular and extracellular, are mediated through membrane trafficking such that signals are transduced at the right time and place, thus keeping cells functioning (Dacks and Field, 2007). For cells to function and survive, membrane trafficking is a very important process ensuring organelles within cells interact properly and that the cell is also communicating with the surrounding environment thus functioning in the whole body.

1.1.2 Endocytosis and exocytosis cycles

Membrane trafficking can be divided into two main types represented by endocytosis and exocytosis pathway. In the former pathway, plasma membrane (PM) proteins or molecules from outside the cell are engulfed by the plasma membrane into the cytoplasm, internalising cargo in the form of a vesicle that is be cleaved off the PM and delivered to its specific destination (Parkar et al., 2009). The destination of vesicles internalized from the PM differ. Some are recycled through early endosomes, delivering cargo then returning to the plasma membrane thereby maintaining and controlling the PM composition (Grant and Donaldson, 2009). Others are transported deeper into the cell to late endosomes or the trans-Golgi network. Some are also trafficked to and degraded by lysosomes as a final destination (Van Vliet et al., 2003). Such complexity reveals the need for careful homeostatic mechanism to control these different pathways.

An important study in the field of secretory pathway endocytosis/exocytosis used the pancreatic exocrine cell as a model (Palade, 1975). The study showed

that the newly synthesized proteins, for secretion, move across a successive sequence of organelles on their way to the final destination, in this case secretory granules destined for the PM, such that vesicles fuse with plasma membrane and proteins are released to the extracellular space (Figure **1-1**). The organelles involved include the endoplasmic reticulum, and the Golgi network. Secretory pathways are in general categorized into two types: constitutive and regulated exocytosis. Constitutive secretion is a continuous transport of newly synthesized proteins to the plasma membrane, usually through the *trans* Golgi network. On the other hand, regulated secretion involves the exocytosis of vesicle-containing proteins in response to a signal. In this case, the membrane proteins of the secretory vesicles are delivered to the plasma membrane and the contents delivered extracellularly. This type of regulated exocytosis is found in specialized types of cells responsible for secreting functional molecules such as hormones, neurotransmitters, or digestive enzymes. Molecules are synthesized within the cell and held in secretory vesicles often near the PM, waiting for an extracellular signal such that a vesicle fuses with PM and releases its content in a highly regulated process (Van Vliet et al., 2003). This process is of high importance in many cell types from nerve to endocrine cells.

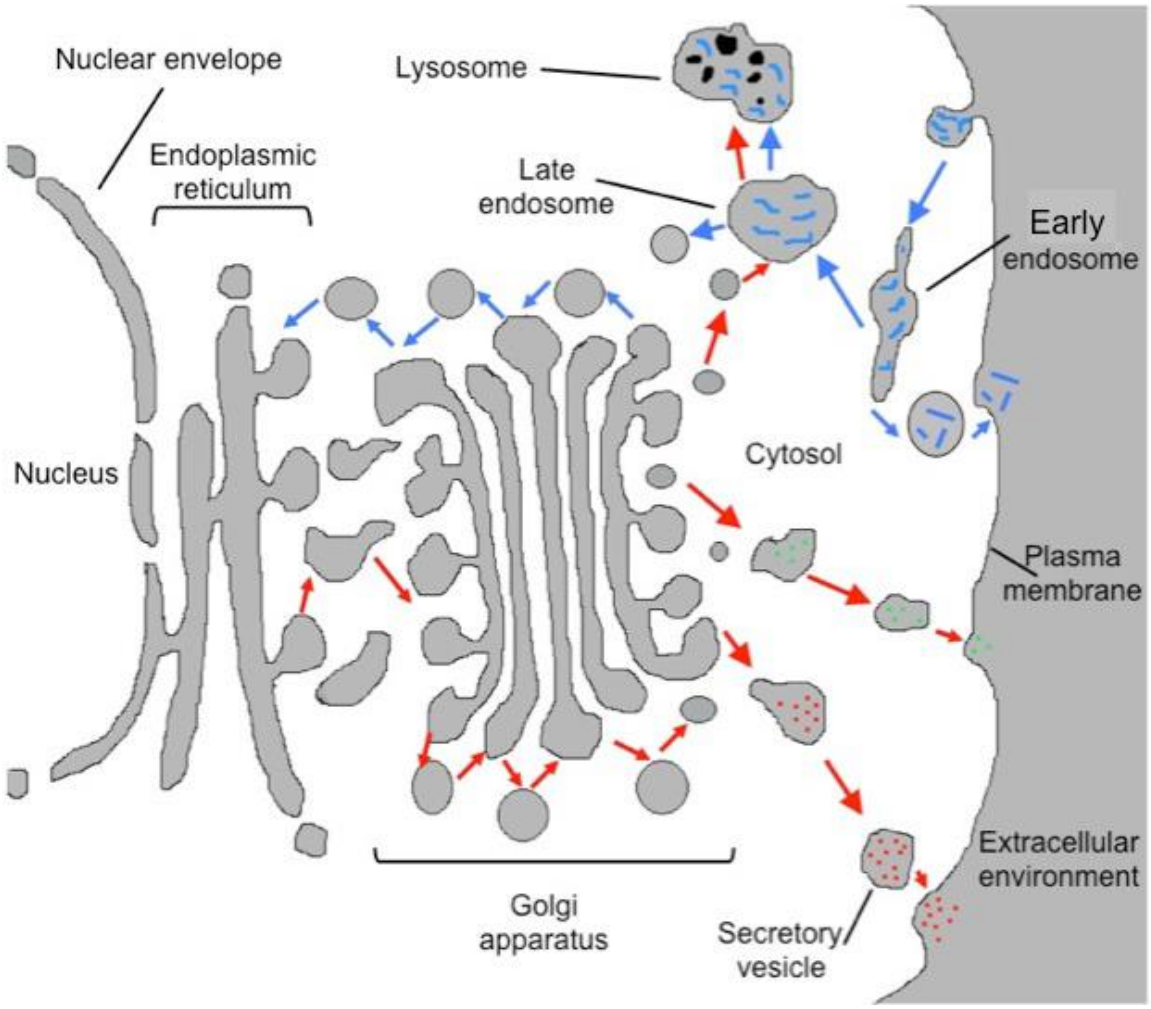

Figure 1-1 Cellular components of secretory and endocytic pathways.

This is an illustration of the main components of eukaryotic membrane trafficking pathways. The secretory (exocytic) pathway is shown in red which is directed from the nucleus to the plasma membrane (PM), and the endocytic pathway is shown in blue, delivering material from the plasma membrane towards the nucleus. Newly synthesized proteins in the endoplasmic reticulum (ER) are transported through Golgi apparatus to PM for secretion or alternatively to late endosomes then lysosome for either a further modification or termination. The endocytic pathway controls molecules entering the cell by engulfing them in PM-derived vesicles that pinch off and are transported through cell. Vesicles transported to early endosome can be either recycled back to PM or to late endosome from where they can be sent for destruction by lysosomes or travel to the Golgi apparatus. This figure was edited from Molecular Biology of the Cell, fourth edition, 2002.

1.1.3 Membrane fusion

Lipid bilayer membrane fusion is involved in all vesicle trafficking events at all stages of the secretory pathway. It is of a fundamental importance in membrane biology, resulting in structure and content mixing between the vesicle and its target membrane. The fusion process must be carefully controlled to insure specificity of vesicle trafficking, and the steps involved - tethering, docking, and fusion - are all carefully and tightly controlled.

Membrane fusion involves a donor compartment (usually represented by the vesicle carrying a synthesized protein or active substance) and an acceptor side (which could be the plasma membrane (heterotypic) or another vesicle membrane (homotypic)). Fusion is not a favorable process due to the hydrophobic nature of donor and acceptor membranes which provides a strong repulsive force. A widely accepted model was proposed explaining the energy requirements of membrane fusion called “hemi-fusion” by Chernomordik and Kozlov in 2005. The model suggested that the mechanism of membrane fusion occurs through an intermediate, such that contacting outer layers of membranes merge while the inner ones, in reference to the center of vesicle, do not. This is called “hemi-fusion” (Figure **1-2**). After this transition state, a trunk-like fusion is formed that later progresses into a pore followed by complete fusion and content mixing (Chernomordik and Kozlov, 2003). More will be revealed about fusion triggering factors and a complete picture of fusion process in subsequent sections of this thesis. Fusion, like almost all biological process, is highly organized and its execution is ordered. For all vesicle trafficking steps, the process involves tethering, docking, and finally fusion.

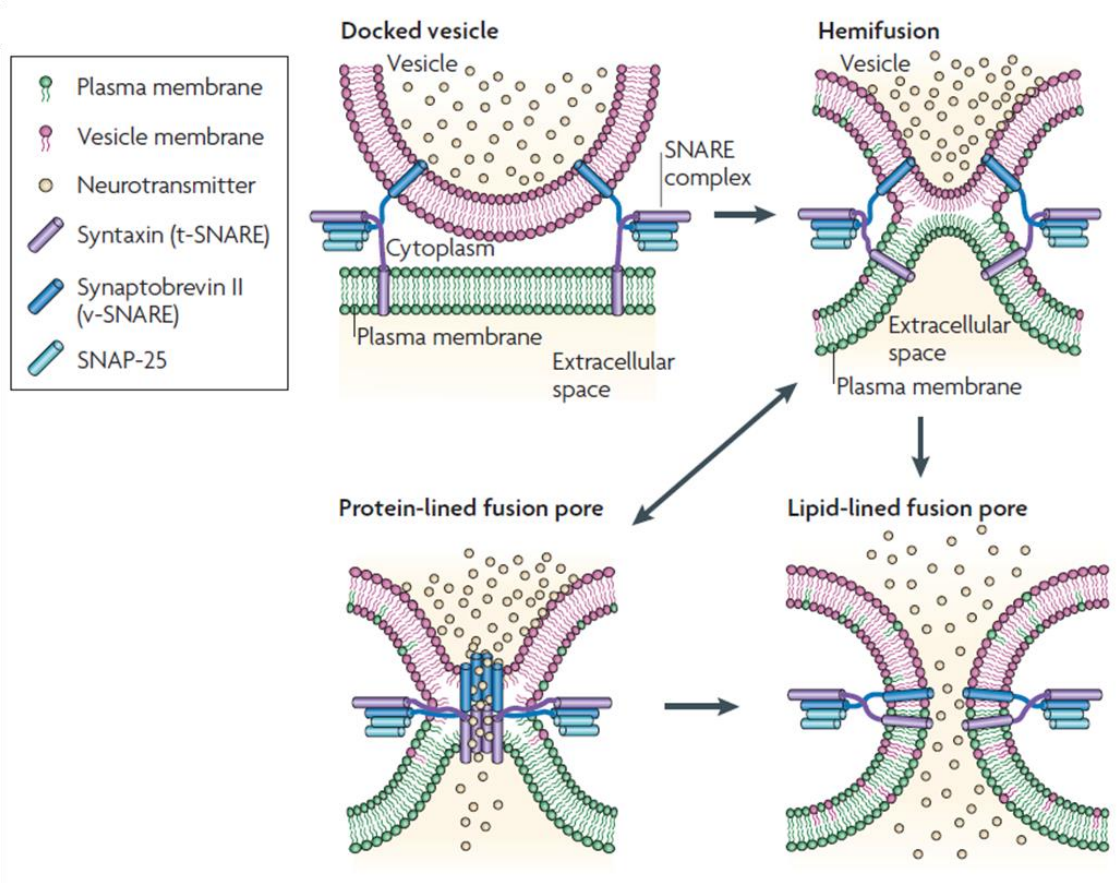

Figure 1-2 Vesicle fusion through hemi-fusion intermediate transition.

Following tethering, a donor vesicle approaches acceptor, target membrane and docks to plasma membrane by SNARE protein interactions, (top left panel). The distal or outer membrane leaflets from both vesicle and PM merge with each other while the inner leaflets are still intact and this intermediate state is called 'hemi-fusion' (top right panel). This state is primed for release. A protein-lined pore is then formed by two of the SNARE proteins, syntaxin and synaptobrevin (lower left panel). This step is assumed to be reversible. Otherwise, it can proceed into the complete fusion which is formed by a lipid-lined fusion pore, lower right panel. This figure is edited from (Lisman et al., 2007).

1.1.4 Tethering, docking, and fusion

Though poorly understood, the first point of contact between the vesicle and the target membrane is through tethering proteins that direct the vesicle into its target destination. These include large multi-subunit complexes capable of reaching out over distances two or three times larger than the vesicle itself. Engagement of the tethering process then leads to the docking step - the stage at which the vesicle and target membrane are lined up in a fusion-ready state

waiting for a trigger to initiate the final fusion. Intracellular membrane fusion involves a highly conserved family of proteins called SNAREs (Soluble N-ethylmaleimide sensitive factor Attachment protein Receptors). They are the minimal components needed for fusion to overcome the repulsive forces exerted by opposing membranes (Weber et al., 1998). Tethering proteins together with SNAREs are key factors in mediating vesicle/target specificity.

1.2 SNARE proteins: the SNARE hypothesis, and SNARE complex

All membrane trafficking steps utilize the SNARE machinery to drive fusion. This involves the formation of a so-called SNARE complex comprised of proteins on both the target and vesicle, the assembly of which into a complex provides the energy for fusion. Fusion can often be regulated, by hormones such as insulin, or other signals, such as elevation in cytosolic Ca^{2+} concentrations. SNARE proteins serve apparently two purposes: specificity and fusion. Therefore, their presence is crucial to the overall process and their role is essential as it is known to be involved in all known membrane fusion events (Malsam et al., 2008).

1.2.1 Discovery of SNARE proteins

The first identification of SNAREs was as indirect receptors for two known proteins participating in membrane trafficking steps known as NSF (N-ethylmaleimide Sensitive Factor) and its binding partner SNAP (Soluble NSF Attachment Protein) (Söllner et al., 1993a). NSF, purified from brain extract, was identified by its ability to recover the membrane trafficking in an *in vitro* system treated N-ethylmaleimide (NEM) (Malhotra et al., 1988). Later, SNAP was identified and purified (Clary et al., 1990). Using crude bovine brain membrane extract and the purified proteins NSF and SNAP, associated synaptic vesicle fusion proteins were identified. These included Syntaxin1, VAMP (synaptobrevin), and SNAP25 (synaptosome-associated protein of 25kDa) and collectively called Soluble NSF Attachment REceptors (SNAREs) (Söllner et al., 1993b). These discoveries suggested the existence of a fusion machinery composed of multiple protein sets. Indeed, SNAREs subsequently proved to

provide the minimal mechanism to overcome the repulsive force between membranes, and thus fusion (Hu et al., 2003; Weber et al., 1998). Many other isoforms of SNAREs were identified since the first discovery and the human genome listed 35 such genes (Bock et al., 2001). The genomic revolution identified 25 SNAREs in *Saccharomyces cerevisiae*, and 56 in *Arabidopsis Thaliana* (Malsam et al., 2008), and has led to a wealth of structural and regulatory information *in silico*.

1.2.2 SNARE protein structure

SNARE proteins are a well-conserved family with homologues found in all eukaryotes (Bock et al., 2001). They are small proteins which vary in structure yet have a common conserved domain consisting of 60-70 amino acids with eight heptad repeats; this domain is called the SNARE motif and this is the defining feature of the SNARE protein family. This common motif is crucial in membrane fusion as it forms a stable bundle of helices with similar domains present in associated SNAREs to facilitate first docking and eventually fusion (Antonin et al., 2002). Most SNAREs are anchored in the membrane, with the exception of SNAP25-family members which lack a transmembrane domain but is instead membrane anchored by palmitoylation, and is distinct in having two SNARE domains in the same polypeptide (Figure 1-3 **A**). Syntaxin is localized in the target membrane and is generally thought to be found in two conformations, open or closed, such that the regulatory Habc domain present in the N-terminus can fold back into the SNARE motif and prevent formation of the SNARE complex (Figure 1-3 **B**). Vesicular SNAREs such as VAMP2 are present on the approaching, donor vesicle.

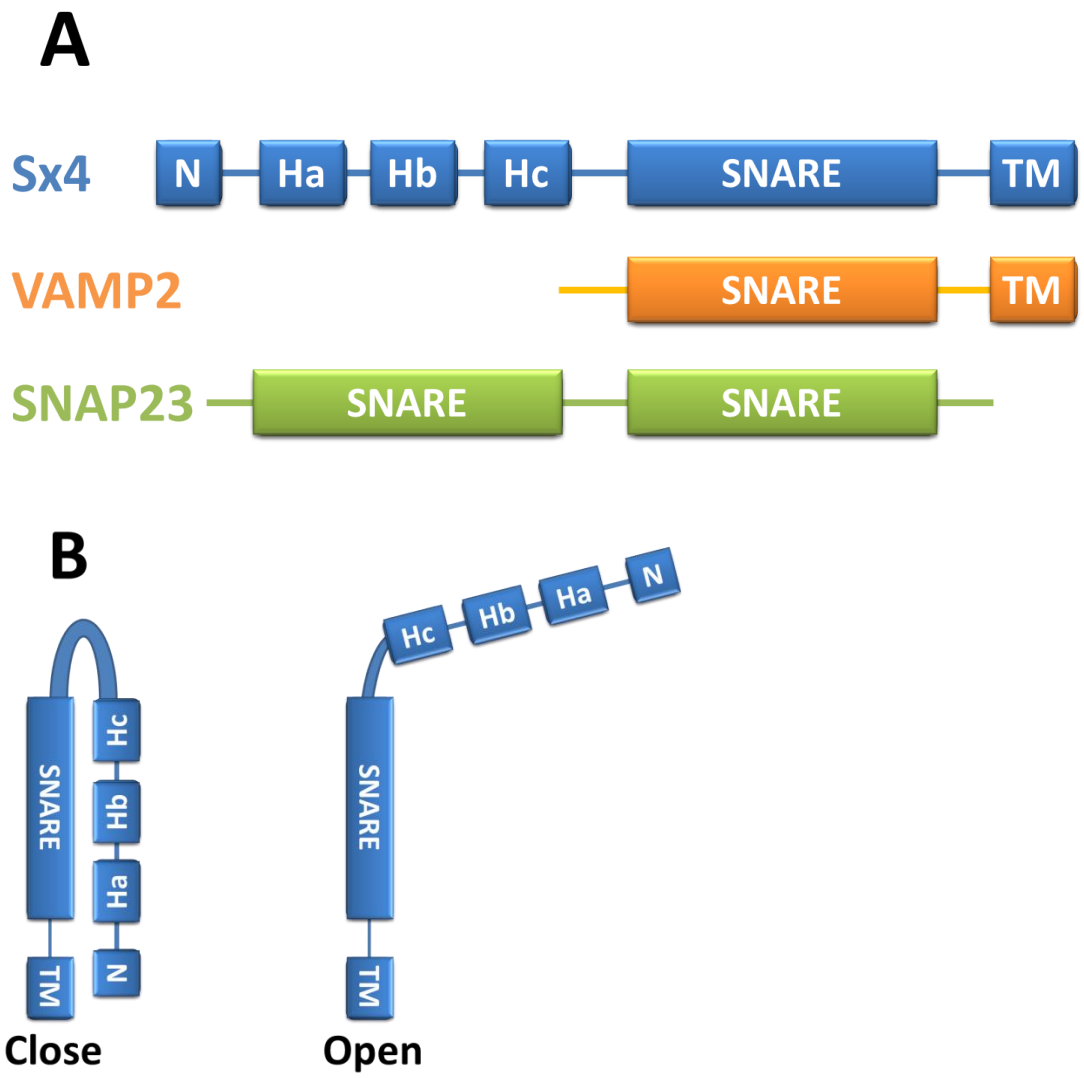

Figure 1-3 SNARE proteins structure.

SNAREs considered in this study are shown here. The conserved SNARE motif between the three SNAREs is aligned for clarity. Sx4 contains a transmembrane domain (TM) that anchors into plasma membrane, and an N-terminus that interacts with regulatory proteins such as Munc18c. There is a Habc (or H3) domain that controls participation of Sx4 in complex formation such that it can fold back and bind the SNARE domain in a closed conformation blocking its activity. Vesicular protein, VAMP2, has a TM domain anchored into the vesicle membrane plus the SNARE domain participating in complex formation. SNAP23, a member of the SNAP25-family, lacks a TM domain and uniquely has two SNARE domains.

1.2.3 The SNARE hypothesis

Accompanying the identification and analysis of SNAREs, a proposal was put forward to explain membrane fusion - called the SNARE hypothesis (Söllner et al., 1993b). This assumed that each vesicle transport and fusion event involves a distinctive vesicle SNARE (v-SNARE) which couples up with a unique cognate target SNARE (t-SNARE) at the specific target membrane. This specific interaction results in docking the vesicle in the correct membrane followed by assembly of the SNARE complex and membrane fusion. This was then followed by subsequent dissociation of the SNARE complex by the ATPase activity of NSF (Figure 1-4). It is assumed that localisation of SNAREs enhance specificity of fusion as well as influencing the protein functions (Chen and Scheller, 2001). The subcellular localisation of SNARE proteins is shown in (Figure 1-5), following figure which includes participating molecules in the secretory and endocytic pathways (Figure 1-5).

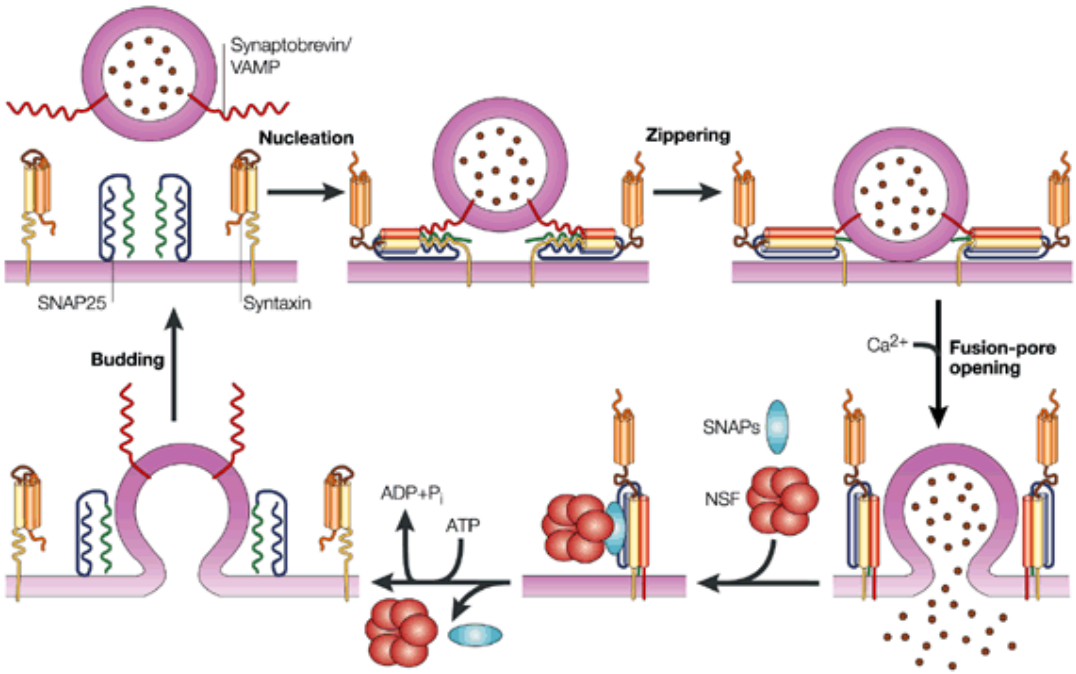

Figure 1-4 The SNARE hypothesis illustration.

Illustration to explain the SNARE hypothesis. First, the donor (vesicle) membrane approaches the acceptor (target) membrane and v-SNARE binds with its cognate t-SNARE forming the ternary complex. The stable complex provides the force to overcome the repulsive energy barrier between

membranes and thus fusions established, triggered with calcium influx here. As cargo content is delivered, NSF and SNAP bind and with ATPase energy the complex is disassembled.

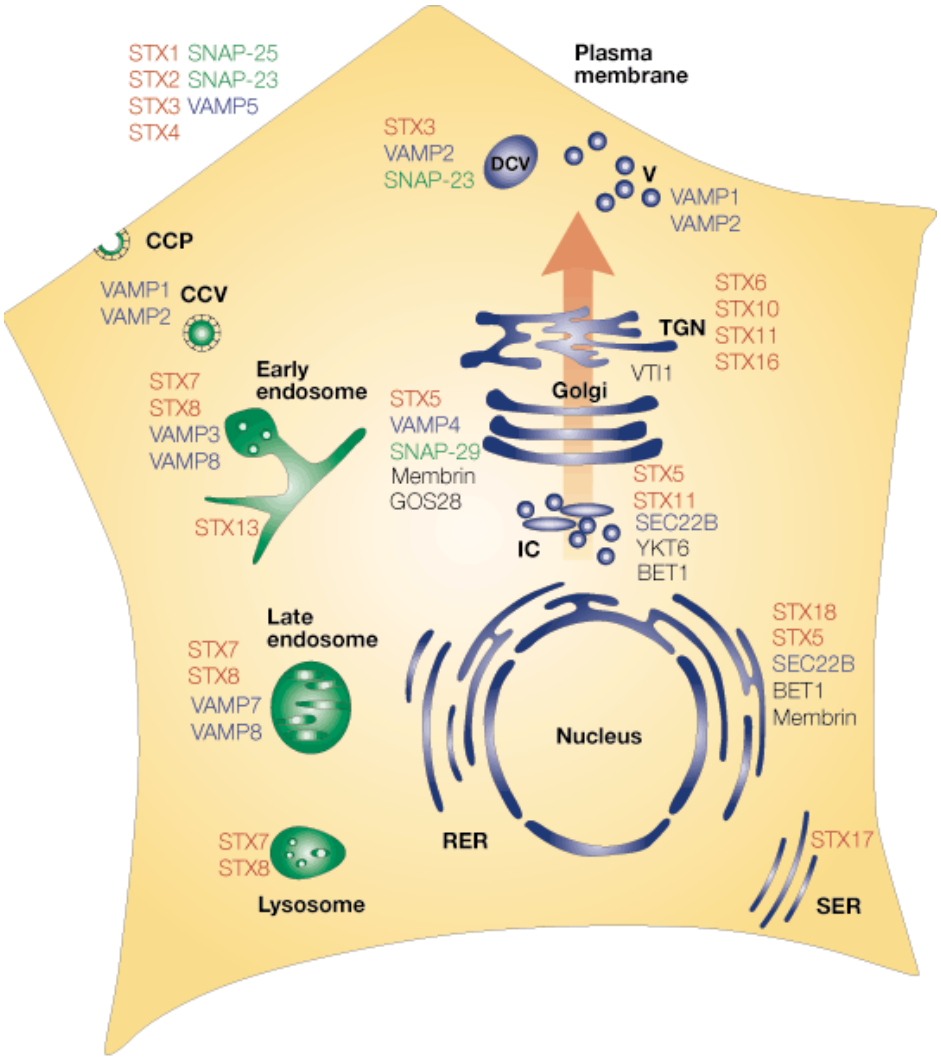

Figure 1-5 SNAREs localisation within mammalian cell.

This figure shows known mammalian SNAREs and their location within cell. Localisation improves the specificity of the SNARE-mediated fusion. The secretory pathway is displayed in red. Different SNARE's families indicated with different colour: Red, syntaxin family; blue, VAMP family; green, SNAP family; black, others. Abbreviations: CCP, clathrin-coated pit; CCV, clathrin-coated vesicles; DCV, dense core vesicles; IC, intermediate compartment; RER, rough endoplasmic reticulum; SER, smooth endoplasmic reticulum; SNAP-25, 25 kDa synaptosome-associated protein; TGN, trans-Golgi network; V, vesicles; VAMP, vesicle-associated membrane protein. Figure taken from (Chen and Scheller, 2001).

1.2.4 Classification of SNARE proteins

There are two terminologies used to describe different types of SNAREs. In accordance to SNARE's position, they are classified as vesicle (v-SNARE) and target (t-SNARE) (Rothman, 1994). Another nomenclature is used based on the amino acid sequence in the so-called zero layer of the SNARE complex (Figure 1-6) content such that they are called Q- or R-SNAREs (t- or v-SNARE, respectively). There are three Q-SNAREs and one R-SNARE in a complex. The Q-SNAREs contain a glutamine residue in its SNARE domain which is important in the core complex formation (Sutton et al., 1998). Depending on the position of the Q-SNARE in the complex, they have been further sub-classified into Qa, Qb, and Qc sub-families (Bock et al., 2001). Syntaxins are Qa family members, while Qb and Qc are for SNAP23 which contributes two chains. On the other hand, the R-SNARE contains an arginine residue at the core of the complex. Each functional ternary complex is composed of four SNARE domains each from one class of R, Qa, Qb and Qc SNAREs (Sutton et al., 1998). Further details about each of these SNARE protein families are described below.

1.2.4.1 Syntaxin family

Syntaxin proteins are classified as Qa SNAREs and are anchored to the membrane through a short C-terminal transmembrane domain (Masaki et al., 1998). The SNARE domain is immediately after the transmembrane domain containing the conserved glutamine essential for interaction with other SNARE proteins (Figure 1-3 **A**). The N-terminus contains three antiparallel alpha helices called the Habc domain which is capable of interacting with the SNARE domain through a long flexible linker (Fernandez et al., 1998). Syntaxins exist in two structural conformations, open and closed. The N-terminal domain can fold back and bind the SNARE domain forming the closed form that is consequently believed to be unable to participate in complex formation (Dulubova et al., 1999), Figure 1-3 **B**. This feature could be considered as a regulatory mechanism for Syntaxin and has been reported in many isoforms including Sx1a, Sx2, Sx3 and Sx4 (Bennett et al., 1992; Bock et al., 1996; Wong et al., 1998). Syntaxin proteins are localized within different compartments (Figure 1-5) suggesting their essential role in

membrane fusion events at similar (homotypic) or different (heterotypic) membranes.

1.2.4.2 Synaptosome Associated Protein (SNAP) family

Synaptosomal protein family members are Q-SNAREs that differ from other SNAREs as they lack the transmembrane domain (Figure 1-3 **A**) and thus are not integral membrane proteins. These proteins contain two SNARE domains, connected by a flexible linker, and hence contributes two helices, Qb and Qc, in the ternary SNARE complex (Lang and Jahn, 2008). It was discovered first in neuronal cells (Oyler et al., 1989) but other isoforms which included SNAP23 (Ran et al., 1996), SNAP29 (Yang et al., 1999) and SNAP47 (Holt et al., 2006) are widely expressed. It is believed to form a binary complex with Syntaxin (Steegmaier et al., 1998). The linker region in SNAP23 and SNAP25 contains a group of palmitoylated cysteine molecules which anchor the protein to target membranes (Gonzalo and Linder, 1998).

1.2.4.3 VAMP family

Vesicle-associated membrane proteins, VAMPs, also called synaptobrevins, are found in the approaching vesicular membrane so they are classified as R-SNAREs (also v-SNAREs). Like Syntaxin and SNAP families, VAMPs were first discovered in neuronal cells as a component of synaptic vesicles (Foster et al., 1998). The structure of VAMP proteins is similar to Syntaxin in that it contains a transmembrane domain, a SNARE domain, and a regulatory N-terminal region which is Proline-rich (Foster et al., 1998) (Figure 1-3 **A**). A considerable number of VAMP isoforms were identified in different intracellular compartments yet some are expressed in more than one location. An example of this is VAMP7 which is found in late endosomes and lysosomes (Yang et al., 1999) as well as at the PM (Williams and Pessin, 2008). VAMP isoforms include VAMP1 (synaptobrevin 1), VAMP2 (synaptobrevin 2), VAMP3 (cellubrevin), VAMP4, VAMP5 (myobrevin), VAMP7 and VAMP8 (endobrevin) (Hong, 2005a).

1.2.5 SNARE complex formation and structure

The aforementioned SNAREs form the core of the highly stable SNARE complex. The complex consists of Syntaxin (Qa), SNAP (Qb and Qc), and VAMP (R) proteins which are individually unfolded with low stability (Margittai et al., 2001) contrary to the fully assembled complex. The stability of the complex is high, such that it is resistant to proteases, high temperatures, and detergents such as sodium dodecyl sulphate (SDS) (Hayashi et al., 1994), a property used in this work to measure the formation of a functional complex. According to the SNARE's locations in the complex, two forms are identified: *trans* when they exist on different membranes (pre-fusion) and *cis* when they are on the same membrane (post-fusion). The process of complex formation is often described as a 'zippering' event, such that the N terminal residues of the SNARE complex start interacting and binding and move towards the C terminus ('zippering') forming the *trans* SNARE complex. This action results in bringing the two membranes into a close proximity which overcome the membranes repulsive force thus facilitating fusion (Pobbati et al., 2006). Moreover, a recent structural study discovered an interesting finding in neuronal complexes using rat syntaxin 1A, SNAP-25 and synaptobrevin 2, with the carboxy-terminal linkers and transmembrane regions at 3.4 Å resolution. The study showed that assembly continued over the known core complex which resulted in a continuous helical bundle extension (Stein et al., 2009). This is additionally stabilized by side-chain interactions in the linker region. The model suggests that complex formation is taking place in successive, distinct phases where in each phase SNARE domains interact with each other forming a layer followed by another and heading towards membranes thus 'dragging' opposing membranes to fuse.
A recent study has suggested a slightly different fusion mechanism, accomplished through a two-step SNARE complex assembly (Li et al., 2014). Here, a two-step folding pathway in sequence was required to achieve membrane fusion directed from the N-terminus toward the C-terminus. First, N-terminus of VAMP docks to the t-SNARE resulting in conformational rearrangement into a half-zippered active complex. This partially assembled SNARE complex results in locking the C-terminal domain at the t-SNARE into a post-fusion four-helix bundle, therefore creating binding site for VAMP at C-

terminus. Second, completing zippering of the rest of SNAREs domains including C-terminal, linker, and transmembrane domain is sufficient for fusion (Li et al., 2014). Further work will be required to define which of these models is most accurately reflecting the physiological mechanism, and indeed whether a single model applies to all SNARE-dependent fusion events.

As the identification of SNARE proteins began in neuronal cells (synaptic exocytosis), the most well-characterized complex is the neuronal SNARE complex and was documented by a structure of the core-region of the SNARE complex resolved at resolution of 2.4 Å (Sutton et al., 1998) which is used as a model for all subsequent complex structure studies using homology modelling. Structural crystallographic data from the endosomal SNARE complex exhibited similarity to neuronal complex such that helices alignment and the structure of interacting layers are analogous (Antonin et al., 2002).
The core of the complex consists of 16 stacked layers of interacting side chains from the four SNARE domains contributed by each protein (Figure 1-6). Interactions are mostly hydrophobic apart from the central layer, which is labeled as the 0-layer, and is an ionic interaction. The central layer consists of an arginine residue (R-SNARE) interacting with three glutamine molecules (Q-SNARE) which are conserved over evolution (Sutton et al., 1998) – see above on SNARE nomenclature. A study on yeast SNARE complex showed that relative Q and R SNARE positions within interacting layer is not seriously important in biological activity while Q-to-R substitutions would reduce complex stability and could lead to lethal defects (Katz and Brennwald, 2000). Interestingly, an all-glutamine central layer composition SNARE complex was fully functional for assembly in vitro and exocytic function *in vivo*.

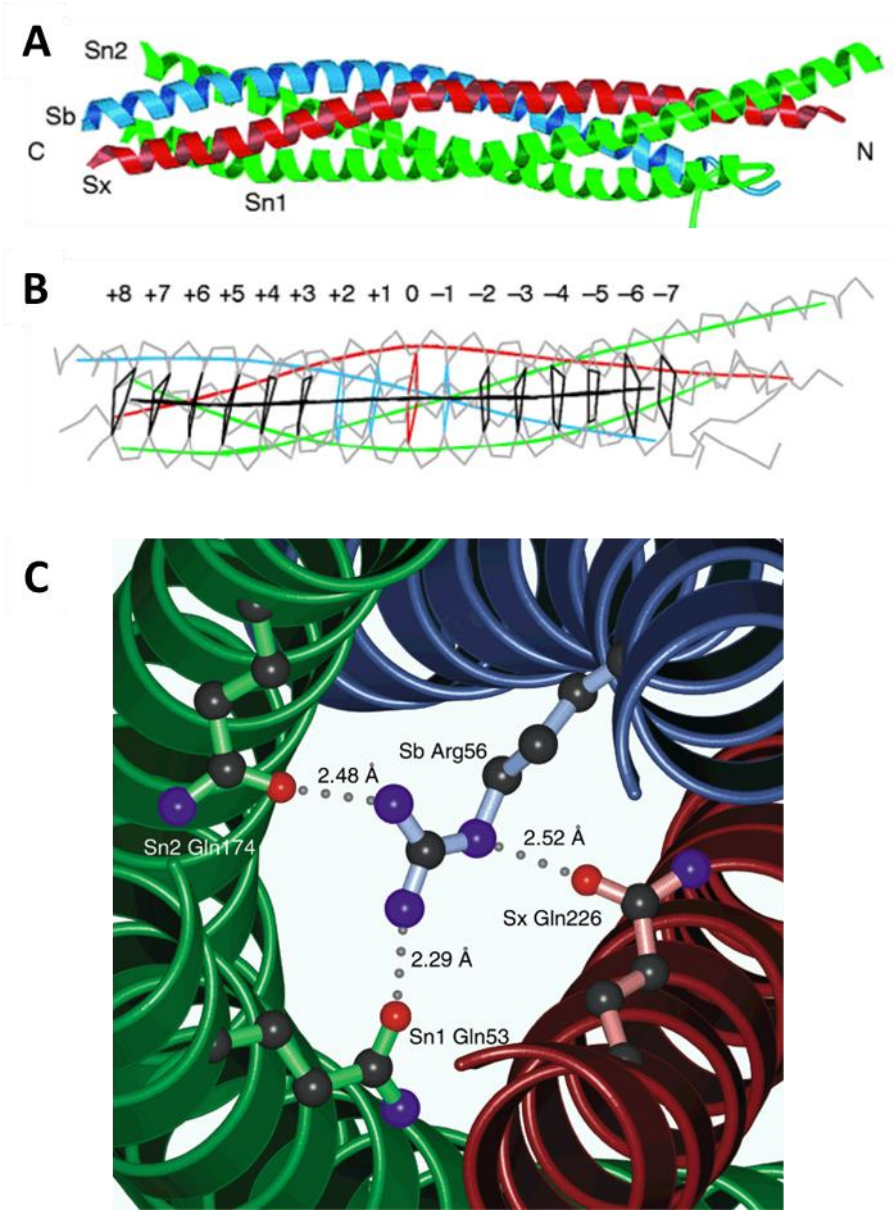

Figure 1-6 SNARE complex structure.

Upper panel: A/ Protein ribbon backbone diagram of an assembled SNARE complex showing parallel alignment of SNARE domains contributed by Syntaxin 1A (Sx, red), Synaptobrevin2 (Sb, blue), and two domains of SNAP25 (Sn1 and Sn2, green); B/ Layers of interaction, 16, at the core of complex where each square represents a single layer of interaction between the four SNARE domains from each SNARE and the central red square illustrates the unique ionic interaction between the four helices which is also called the central layer; C/ an expanded view of the ionic central layer displaying an arginine residue from Synaptobrevin (Sb, blue) interacting with three glutamine residues from Syntaxin 1 and SNAP25. Figure edited from (Sutton et al., 1998).

1.3 Sec1-Munc18 (SM) regulatory proteins

There are numerous examples in biology of tightly regulated exocytic events, from neuronal exocytosis, insulin release from beta cells and the regulated delivery of GLUT4 or aquaporin channels to the cell surface in response to a defined, usually extracellular, signal. Given the importance of SNAREs in such exocytic events, studies have sought regulators of SNARE complexes that control complex assembly events and degree of formation, i.e. partial or full assembly, as potential control points. The regulation of membrane fusion events and the degree of fusion specificity are accomplished through the organized coordination between different protein families (Lang and Jahn, 2008). These include protein families from Sec1/Munc18 (SM), tethers, Rab, and other complexes. The SM proteins are important in fusion and together with tethers they define specificity.

1.3.1 SM proteins

The regulatory Sec1/Munc18 (SM) protein family was first discovered through genetic screening for abnormalities related to neurological defects in the nematode *C. elegans* revealing mutations in UNC-18 (uncoordinated protein 18) which were linked with severe uncoordinated phenotypes and that reflected their role in the regulation of neurotransmitter release and membrane fusion (S. Brenner, 1974; Sydney Brenner, 2003; Gengyo-Ando, Kitayama, Mukaida, & Ikawa, 1996;). In *S.cerevisiae* defective secretion was reported due to defects in secretory protein 1 (Sec1) (Novick and Schekman, 1979; Novick et al., 1980). The mammalian homolog of these proteins is Munc18a which is required for neurotransmitter release through a syntaxin-dependent mechanism (Misura et al., 2000). Subsequent research established the importance of SM proteins in membrane fusion and highlighted their role in regulation. As a regulatory protein, SM proteins have been implicated in different trafficking pathways (Toonen and Verhage, 2003). There are 7 SM proteins in mammalian cells and 4 in yeast (Jahn et al., 2003). SM proteins are typically between 60-70 kDa, exhibit a high degree of sequence similarity and share a highly conserved structure of

three domains forming an arch-shaped protein with a central cleft (Bracher and Weissenhorn, 2002; Misura et al., 2000)(Südhof and Rothman, 2009). SM proteins are associated with syntaxins and are thought to regulate their conformation thus participation in complex formation and bind with high affinity, with a Kd in nano-molar level (Pevsner et al., 1994; Smyth et al., 2010). Despite their identification as syntaxin-binding proteins, SM proteins were also reported to bind other SNAREs such as Munc18c binding VAMP2 (Brandie et al., 2008). The mechanism of SM proteins regulating SNAREs, syntaxin in particular, proved to be challenging and contrasting in that in some occasions they enhance complex formation while in others they inhibit it (Toonen and Verhage, 2003).

1.3.1.1 SM-Syntaxin binding

SM proteins regulate the SNARE complex formation through binding their cognate syntaxin using potentially three different binding modes controlling the syntaxin conformation. The first mode was identified in neuronal cells where Munc18a bound its cognate syntaxin1a via an arched shaped cavity (Misura et al., 2000). Syntaxin was held in the closed conformation as the SNARE domain was binding the Habc region thus blocking syntaxin from participation in complex formation (Figure 1-7 A). This binding mode is thought to be inhibitory to SNARE complex formation, yet Munc18a interaction with syntaxin1a was found to be essential for neurotransmitters release (Verhage et al., 2000), hence enforcing the notion of a SM-SNARE positive regulatory role in membrane fusion via SNARE complex formation. Moreover, other studies showed that SM proteins are not inhibitory to SNARE complex formation (Carr et al., 1999; Scott et al., 2004).

Yeast models identified a different binding mode where syntaxin is in the open conformation and the SM proteins interaction via distinct binding site (Figure 1-7 B). The SM protein Sly1 interacted with the N-terminal 44 amino acids, preceding the Habc domain in Sed5 (Yamaguchi et al., 2002). Crystal structure analysis showed that this interaction is mediated by a hydrophobic pocket located on the outer surface of Sly1 (Bracher and Weissenhorn, 2002). This mode of binding is referred to as mode 2. This mode was reported for the mammalian Munc18c isoform interacting with syntaxin4 (Latham et al., 2006). Also, the

neuronal SM, Munc18a, was reported to bind the N-terminus of syntaxin1a (Khvotchev et al., 2007) and deletion of this domain resulted in ending the stimulatory effect exerted by Munc18a on membrane fusion using an *in vitro* fusion assay system (Shen et al., 2007).

A third mode of interaction described experimentally, though not studied structurally, revealed that SM can bind assembled SNARE complexes (Figure 1-7 C). The yeast SM protein, Sec1, was localized at sites of vesicle secretion, binding SNAREs Sso1, Sec9p and Snc1p which form the SNARE complex (Carr et al., 1999). Mutations in SNARE complex assembly (impaired-assembly mutants of SNAREs) in yeast resulted in mis-localised Sec1 expression and mutations in complex disassembly showed robust localization of Sec1 which suggest SM binding to an assembled SNARE complex. Binding assays using recombinant proteins revealed high affinity binding of Sec1 to the binary t-SNARE as well as to ternary complex and, interestingly less to Sso1 (Scott et al., 2004). Munc18a, also presented exhibited evidence of binding to the fully assembled SNARE complex containing its cognate syntaxin1a (Dulubova et al., 2007).

The three different binding modes of SM proteins with their cognate syntaxins, suggests existence of an essential role for SM proteins in membrane fusion at different levels in trafficking and at variable stages of assembly and disassembly of SNARE complexes. The nature of the SM-SNARE interaction, i.e. inhibition or enhancement, is in many cases contradictory and yet to be fully revealed. Despite this, a chaperone-like function for SM proteins can explain many of the findings so far and SM proteins could be thought of as complex-intermediate protector, at the assembly step, from the premature NSF-mediated disassembly mechanism (Xu et al., 2010).

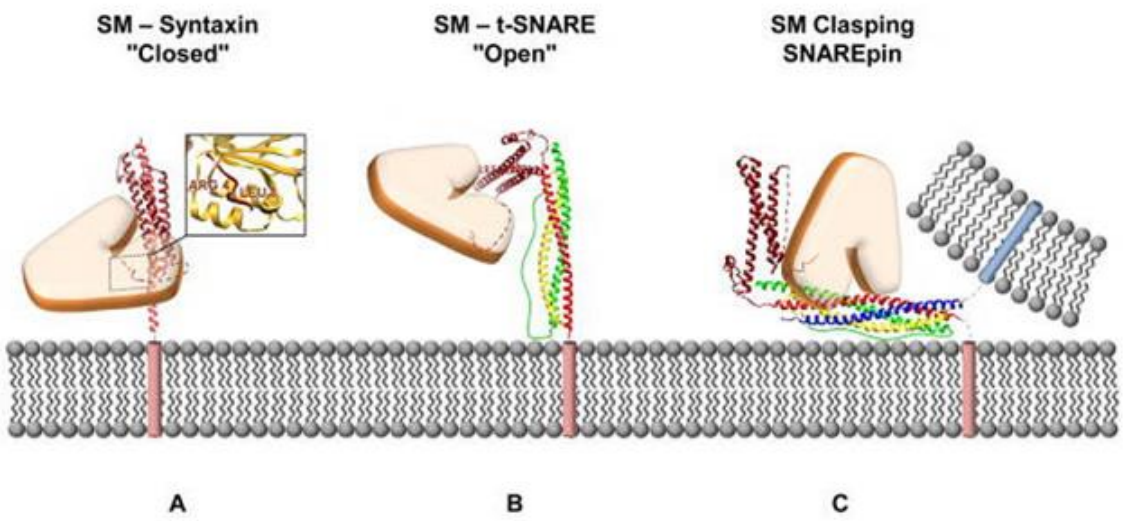

Figure 1-7 SM-Syntaxin binding modes.

The regulatory protein SM interacts with its cognate Syntaxin via three binding modes controlling activity of syntaxin. These modes were identified using biochemical, biophysical and/or structure crystallography experiments. A/ SM binds closed conformation of syntaxin in which the SNARE domain is bound to the Habc region and hence blocks its activity in complex formation; this is an inhibitory complex. B/ SM interacts with open syntaxin via the extreme N-terminus allowing the SNARE domain to interact with cognate SNAREs to form a fusion complex. C/ A less well-characterized binding mode where the SM binds a fully assembled SNARE complex and is thought to promote fusion. Key: syntaxin/red, SNAP/green and yellow, and VAMP/blue. Figure reproduced from Südhof & Rothman, 2009.

1.3.1.2 Munc18c

Munc18c is the regulatory SM protein specific for syntaxin4 and is required for insulin-stimulated GLUT4 translocation to the PM (Thurmond et al., 2000). It binds the syntaxin4 via the N-terminal domain by the hydrophobic pocket in its cleft – mode 2 binding (Latham et al., 2006) and is also thought to interacts with the closed conformation of syntaxin4 by mode 1 binding (Brandie et al., 2008). Munc18c was found to bind fully assembled SNARE complexes composed of syntaxin4/SNAP23/VAMP2 (Latham et al., 2006).
Munc18c has been found to be both facilitative and inhibitory to SNARE complex formation and thus membrane fusion (Latham et al. 2006; Brandie et al. 2008). Therefore, these different binding modes suggest strongly that Munc18c provides a mechanism by which insulin can regulate SNARE complex formation at

different stages and levels. Through this mechanism, Munc18c is inhibitory to fusion when it binds the closed form of syntaxin4 and facilitative when it binds the extreme N-terminal region of syntaxin4 in the open conformation such that the SNARE domain is exposed and ready for binding other SNAREs. Insulin stimulation results in increased GLUT4-vesicle fusion with the PM (Bryant and Gould, 2011), thus regulation of SNARE complex formation perhaps through phosphorylation events including Munc18c and syntaxin4 is of potential interest. It has been proposed that insulin stimulates Munc18c phosphorylation, preventing binding to closed syntaxin4 and driving the balance towards open forms (Aran et al., 2011; Jewell et al., 2011). This in turn facilitates SNARE complex formation and hence membrane fusion. This area will be returned to in future sections of this thesis.

1.3.2 Tethers

Membrane fusion is a very target-specific process mediated by SNAREs on vesicle and target membranes that control and direct fusion to take place in the right location. Upon a vesicle approaching its target membrane, the first tethers or binds lightly to the membrane and this is the first contact between membranes in a specific manner such that the SNARE on the vesicle would bind only to its cognate partner on the target membrane. Therefore, tethering proteins provide a layer of binding specificity into the membrane fusion process by being the first contact (Pfeffer, 1999). Tethers, also, play an essential role in regulating SNARE complex assembly and fusion; reviewed in (Dubuke and Munson, 2016; Hong and Lev, 2014; Sztul, 2005; Sztul and Lupashin, 2009). Tethering proteins can be classified, roughly, into two groups according to their composition; a first group of large multisubunit complexes and the second group of long coiled-coil proteins (Schuck, 2004). The long coiled-coil tethers are involved in SNARE complex regulation (Cheung and Pfeffer, 2016). There are many tethering proteins identified in different species, yeast or mammalian cells, belonging to the above mentioned classes with variable functions. Examples of the long coiled-coil proteins include Uso1p in yeast (Yamakawa et al., 1996) and its mammalian homologue p115 (Sapperstein et al., 1996).

Mutlisubunit tethering complexes (MTCs) are variable in number of subunits and structure yet a big number of them is found conserved across species (Schuck, 2004). These include the exocyst, octameric protein complex, first identified at S. cerevisiae (TerBush et al., 1996) involved in vesicle trafficking. A mammalian homologue to exocyst was identified showing the importance of this tethering protein in membrane fusion in eukaryotes (Kee et al., 1997). Indeed, mutational experiments showed significant role of exocyst in membrane trafficking such that mutations in its genes resulted in vesicle accumulation (Guo et al., 1999; TerBush et al., 1996) and an overexpression of Exo70 inhibited the insulin-stimulated glucose uptake in adipocytes (Inoue et al., 2003). MTCs are known to be compartment-specific complexes that promote the initial vesicle-target membranes interaction with a high specificity ensuring fusion of approaching vesicle at the right target membrane (Dubuke and Munson, 2016). They interact with Rab GTPases, SM proteins, coat proteins, and SNAREs thus controlling membrane trafficking at different stages.

MTCs subgroup of tethering complexes was defined according to its individual subunits structures similarity, though the overall complex architecture is different (Yu and Hughson, 2010). It was called the Complex Associated with Tethering Containing Helical Rods (CATCHR) family. Sub-families of CATCHR complexes have been identified at different compartments throughout trafficking pathways which include DSL1, GARP (Golgi Associated Retrograde Protein), COG (Conserved Oligomeric Golgi), EXOCYST.

1.3.3 Rab proteins

Ras-associated binding (Rab) proteins play a major role in vesicle budding (Carroll et al., 2001), uncoating (Semerdjieva et al., 2008), motility (Seabra and Coudrier, 2004) and fusion (Ohya et al., 2009) and are critical in coordinating membrane trafficking process. There are 60 Rab's in humans and mice, and another 11 isoforms in yeast and 29 in C. elegans. They are small in size, 20-29 kDa, ubiquitously expressed and are GTPases which are linked to all organelles and vesicles, functioning as molecular switches regulating different facets of membrane function (Hutagalung and Novick, 2011). Rab proteins are found in two states, inactive when bound to GDP and active when GTP is bound (Fukuda,

2008). Switching between the two states is under the control of guanine nucleotide exchange factors (GEFs) and GTPase activating proteins (GAPs). Active Rabs regulate trafficking by interacting with specific effector proteins (Zerial and McBride, 2001). As such, Rab proteins are important in membrane trafficking and essential in coordinating all process throughout fusion steps. Knockdown of Rab10 and to a lesser extent Rab14, resulted in inhibition of GLUT4 translocation in adipocytes (Sano et al., 2008). How these interact with SNAREs or SM proteins remains to be revealed.

1.4 Glucose metabolism

1.4.1 Glucose homeostasis and diabetes

Glucose is an essential source of energy for all eukaryotic cells. Physiological blood glucose level is tightly controlled around 4-7 mM to allow continuous glucose supplies to tissue such as brain and nerve (Kahn et al., 2006). This is achieved by different signalling molecules, such as insulin and glucagon, which act oppositely. These hormones are secreted from different cells within the islets of Langerhans in pancreas; glucagon is released from alpha cells while insulin from beta cells. Insulin signals for glucose uptake by adipocyte and muscle cells through glucose transporters such as GLUT4 which is a transmembrane protein allowing glucose to enter cells thus lowering blood glucose levels. In contrast, glucagon acts on liver, breaking down stored glucose in the form of glycogen by enhancing gluconeogenesis and release of glucose into blood stream, and hence an increase blood glucose level. The majority (90%) of blood glucose clearance is mediated by skeletal muscle (Kraegen et al., 1985) through the action of GLUT4 molecules on the PM. Insulin stimulates GLUT4 translocation from intracellular compartments into the plasma membrane and fusion. Depletion of GLUT4 in mice resulted in development of insulin resistance in skeletal muscle and also liver (Abel et al., 2001). Therefore, knowledge of the molecular mechanisms for glucose transport and how this is controlled across multiple tissues is essential.

Dysregulation of glucose homeostasis results in hyperglycemia such that the blood glucose level is high and cells within body are not using the excessive glucose due to a malfunction in signalling processes. At its extreme, this results in a condition called diabetes. There are two types of diabetes: type-1 in which insulin is not produced from pancreas in response to increase blood glucose levels. Type-2 diabetes (sometimes called non-insulin-dependent diabetes, or adult onset diabetes) is the main type of this disease, accounting for 90% of diabetes cases. The WHO indicate that the prevalence of this disease could reach 300 million cases by 2025 (Zimmet et al., 2001). Insulin is secreted in type-2 diabetes, but this is either non-functional ('insulin resistance') or eventually insulin secretion fails as the pancreas overcompensates for elevated blood glucose levels. This type of diabetes is sometimes referred to as life-style disorder caused because patients are consuming excessive amounts of food and sugar with little or no physical activity, thus overloading the body system with sugar, and exhausting the pancreas producing insulin.

Physiologically, excess blood glucose levels trigger insulin secretion which binds its receptor on cell surface and initiates an intracellular signalling cascade that results in GLUT4 translocation and fusion allowing glucose uptake (Bryant and Gould, 2011). Patients with Type 2 diabetes (T2D) exhibit impaired GLUT4 translocation (Rizza and Butler, 1990; Rothman et al., 1992) though the molecular mechanism is not fully understood, thus stimulating interest to uncover this defect.

1.4.2 Glucose transporters

Glucose transport in mammals is mediated by a family of facilitative glucose transporters (GLUTs) consisting of 14 proteins. These proteins are integral, transmembrane proteins that transport glucose and related hexoses across the plasma membrane. GLUTs cross the membrane 12 times, i.e. 12 transmembrane domains, and both amino- and carboxyl-termini are positioned toward the cytosol (Bryant et al., 2002) (Figure 1-8). They are classified into three subclasses according to structural similarities and the transported sugar, class-I

(1, 2, 3, 4, 14) transports glucose, class-II (5, 7, 9, 11) transports fructose, and class-III (6, 8, 10, 12, 13) (Bermúdez et al., 2007; Bryant et al., 2002; Thorens, 1996) which transport a range of other substrates, including the H+/myoinositol transporter (HMIT) which is primarily expressed in brain.

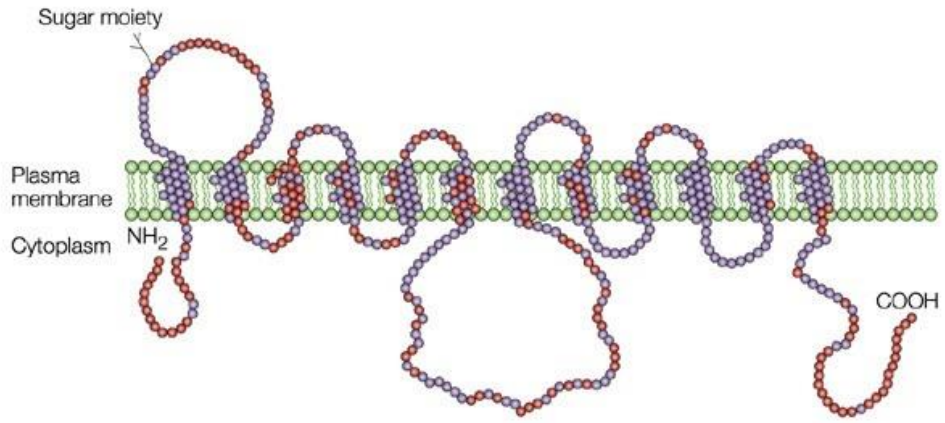

Figure 1-8 GLUT4 diagram

Shown is typical structural representation of the facilitative glucose transporters. 12 transmembrane domains span the plasma membrane with both termini, amino and carboxyl, facing the cytoplasm. Diagram is presenting homology structure between GLUT1 and GLUT4 such that residues in red are the ones unique to GLUT4 and those in blue are conserved between both. Reproduced from (Bryant et al., 2002).

Research into insulin action in adipocytes and muscle showed that insulin triggers translocation of glucose transporters from intracellular compartments within the cell to the plasma membrane (Cushman and Wardzala, 1980; Suzuki and Kono, 1980). Later, it turned that this translocation was restricted to one glucose transporter isoform - GLUT4 expressed predominantly in adipocytes and muscle that responded to insulin stimulation (James et al., 1988). This species was cloned (James et al., 1989). This subsequently was reported in other cells such the heart (Watanabe et al., 1984) and skeletal muscle (Hirshman et al., 1990).

GLUT4 is essential for glucose homeostasis, as its gene deletion (Kim et al., 2001; Stenbit et al., 1997) or over-expression (Tsao et al., 1996) can result in severe metabolic defects.

1.4.3 Insulin signaling

An excess blood glucose level triggers insulin secretion which binds its receptor in the cell membrane and initiates a complicated cascade of signaling events that result in GLUT4 translocation from the cell interior compartment into cell surface where it fuses allowing glucose uptake. Downstream signaling events are complicated involving many adaptor proteins and different pathways yet much research revealed details of insulin signaling. Despite the amount of research conducted, GLUT4 trafficking is not completely understood. To date, two pathways have been suggested for insulin signaling events in GLUT4 translocation in fat and muscle cells, summarized in Figure 1-9. These are the phosphoinositide 3-kinase (PI3K) pathway and the adaptor protein with pleckstrin homology and Src homology domains (APS) pathway. The insulin receptor (IR) is intrinsically kinase active and consists of two α-subunits and two ß-subunits (heterotetramer), linked with disulphide bonds (Gual et al., 2005). Upon insulin interaction with the α-subunit, a tyrosine autophosphorylation of the ß-subunit take place. Once activated, the insulin receptor generates multiple intracellular signalling cascades, some of which induce the rapid redistribution of the GLUT4 facilitative glucose transporter from intracellular compartments to the plasma membrane (Watson et al., 2007). To this stage, both signalling pathways, PI3K and APS, are common and the following steps are different.

In PI3K pathway (Figure 1-9), autophosphorylation of the IR result in recruitment of insulin receptor substrate (IRS) thus activating the PI3K signalling pathway (Jewell et al., 2010). Subsequently, active PI3K phosphorylates in turn phosphatidylinositol bisphosphate (PIP2), thus converting to phosphatidylinositol trisphosphate (PIP3) (Rowland et al., 2011). Then, PIP3 engage 3-phosphoinositide dependent kinase (PDK) and activate which then phosphorylate protein kinase B (PKB, also known as Akt). Akt in turn phosphorylates AS160, Rab-GTPase activating protein (Rab-GAP), that spread the signal downstream to other regulatory Rabs thought to coordinate GLUT4 trafficking. This pathway validated by blocking GLUT4 translocation using inhibitors such as wortmannin (Okada et al., 1994) and competitive inhibitor (Cheatham et al., 1994).

The second pathway, APS, starts from the activated IR recruiting the adaptor protein APS (Adaptor molecule containing Pleckstrin homology and Src homology 2 domains) which in turn engages a dimeric complex composed of c-CBL and c-CBL-associated protein (CAP). Phosphorylation of c-CBL results in interaction with the small adaptor protein CRK which then recruits C3G. C3G activates TC10, Rho-GTPase, through exchanging of GDP for GTP. The final step is when the activated TC10 interacts with group of effector proteins that regulate GLUT4 exocytosis though this step is not fully understood (Chiang et al., 2001). The Cbl proteins are regulator of amplitude and duration of signalling responses such that Cbl family of E3 ubiquitin ligases and adaptor proteins are key negative regulators of signals from many types of cell-surface receptors (Thien and Langdon, 2005). This pathway gained significance due to studies showing the vital role of lipid raft localization of TC10 (Watson et al., 2001). On the other hand, there was no evidence of reduced insulin-stimulated glucose uptake observed when siRNA-abolishment of key components in adipocytes (Mitra et al., 2004) was tested, and not even when c-CBL knocked-out mice (Molero et al., 2004) were used. Therefore, more studies are needed to define the final steps in insulin-stimulated glucose transportation as the early steps are thoroughly discussed and examined.

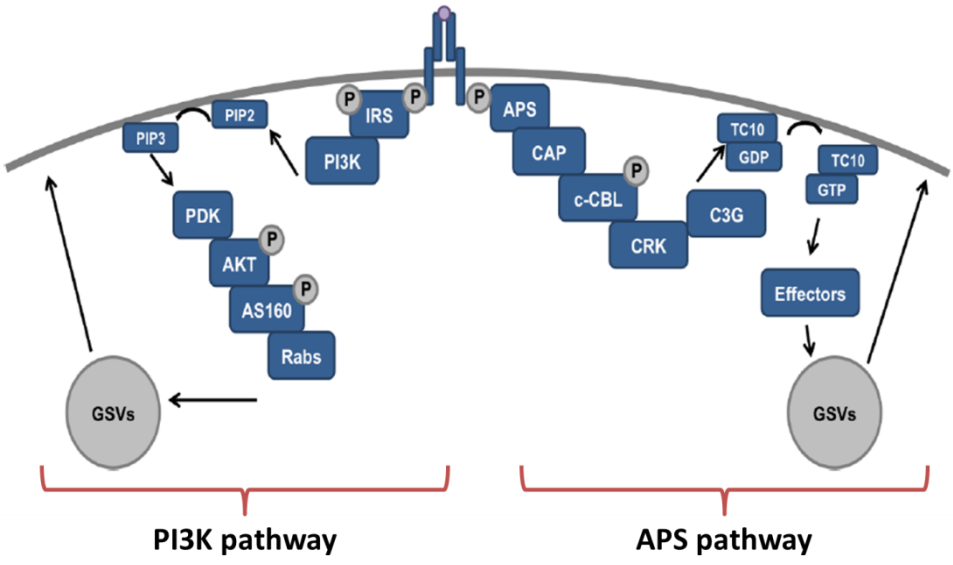

Figure 1-9 Insulin signaling pathways in GLUT4 translocation.

Proposed insulin-stimulated GLUT4 translocation signalling pathways, PI3K and APS which are described in detail in section 1.4.3. Insulin binds its receptor (IR) resulting in autophosphorylation and thereafter a signaling cascade is triggered which leads to the translocation of GLUT4 storage vesicles (GSVs) to plasma membrane and fusion allowing glucose uptake. Figure adapted from Hannah Black, PhD 2017.

1.4.4 GLUT4 trafficking

Upon insulin stimulation, GLUT4 storage vesicles (GSVs) translocate to PM from intracellular compartments (Leto and Saltiel, 2012) to dock and fuse resulting in elevated levels of GLUT4 (Bryant et al., 2002) thus allowing glucose uptake into adipose and muscle cells. GLUT4 molecules are recycled within the cell so post-insulin-stimulated glucose uptake, GLUT4 is internalised into vesicles, by endocytosis, to be transported intracellularly for another round. At the basal state, more than 95% of total GLUT4 is located in intracellular compartments such as endosomes and the trans-Golgi network (TGN) (Smith et al., 1991). It is found in small membrane-bound vesicles, 50nm, i.e. GSVs, clustered around the TGN. Numerous numbers of studies characterising GSVs showed that there are two pools for them and one of them is responsible for the rapid translocation in case of insulin stimulation while the other is endosome-associated (Hashiramoto and James, 2000; Livingstone et al., 1996). Insulin stimulation increases the GLUT4 population in plasma membrane by 10-20 fold over the basal level (Bryant et al., 2002). This suggested that there is an interlink between the two GLUT4 pools whereby one is recycling GLUT4 intracellularly while the other is ready to fuse in response to a trigger like insulin. Currently, the working model of GLUT4 trafficking states that in basal conditions it is circulated between two interacting cycles, such that the first cycle traffics GLUT4 fast between plasma membrane and recycling endosomes. The second cycle acts slowly and traffics GLUT4 through recycling endosomes, TGN, and the GSVs (Bryant et al., 2002), see Figure 1-10. It is assumed that the second cycle is the insulin-responsive population of GSVs (Kandror and Pilch, 2011). Study of GSVs revealed the two pools and categorising them according to the above-mentioned cycles showed that there are certain proteins found specifically for each route. One population

contained cellugyrin which is a transmembrane protein with unknown function while the other lacks cellugyrin (Kioumourtzoglou et al., 2015; Kupriyanova and Kandror, 2000). The second population, cellugyrin-negative, contained 5-6 more GLUT4 than the cellugyrin-positive and was the insulin-responsive. These vesicles were shown later to contain insulin responsive aminopeptidase (IRAP) and sortilin and were sourced from the cellugyrin-negative pool (Jedrychowski et al., 2010). All in all, two GSVs pools exist intracellularly that cycles differently such that one contains cellugyrin and recycle GLUT4 post insulin-induction maintaining levels at basal conditions. The second includes sortilin and reacts to insulin stimulation.

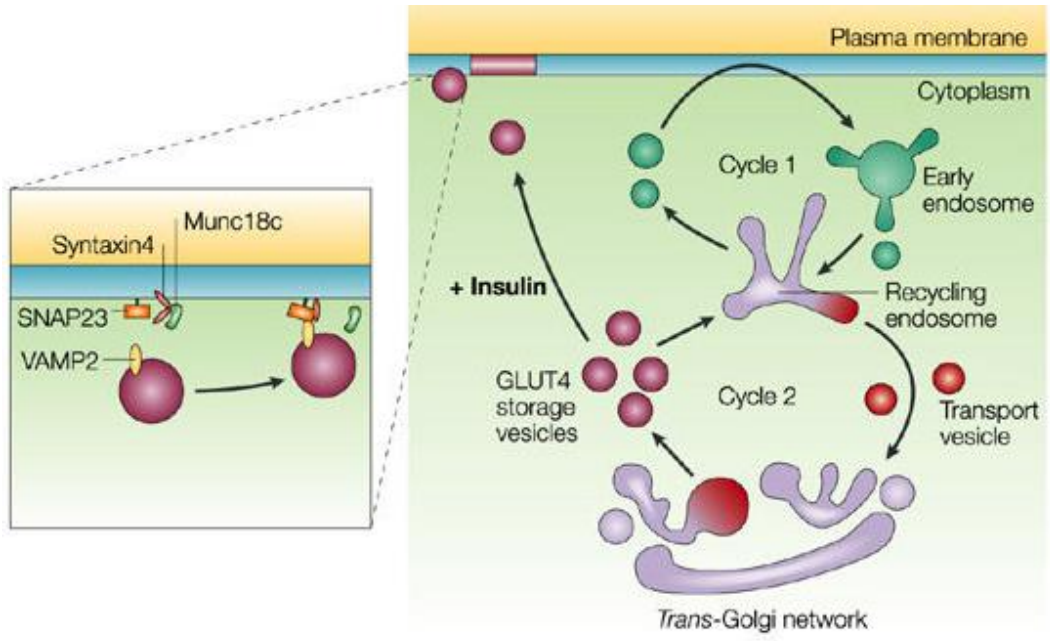

Figure 1-10 GLUT4 trafficking model.

GLUT4 is found in two pools of GSVs which have different cycles within the cell. Continuously it is trafficked between two cycles. Cycle-1 traffics GLUT4 internalised from plasma membrane (PM) to the early endosome then either back to PM or proceeds to cycle-2. The second cycle is slower and traffics GLUT4 to TGN followed by sorting into GSVs which either respond to insulin and translocate to plasma membrane for fusion, or head to the recycling endosome. Figure edited from (Bryant et al., 2002) .

1.4.5 SNARE-mediated GLUT4 trafficking

Eukaryotic cell trafficking between membrane compartments is mediated through formation of SNAREs (Soluble N-ethylmaleimide sensitive factor Attachment protein REceptors) complexes between carrier vesicles and the targeted destination (Cai et al., 2007). Fusion of GSVs with PM is mediated by formation of a SNARE complex, overcoming the energy barrier of fusion of the two hydrophobic membranes, i.e. PM and GSVs. Complexes formed between two proteins from the PM i.e. target (t-SNARE) Syntaxin4 and SNAP23, and one from the vesicle (v-SNARE), most likely, VAMP2 (Sadler et al., 2015), see Figure 1-10, catalyse the bilayer fusion event (Weber et al., 1998). Although studies have debated which VAMP isoform, i.e. VAMP2, VAMP3, VAMP4, VAMP5, VAMP7, or VAMP8 is involved in SNARE complex driving GSV fusion with the PM, recent work in our lab, analysed levels of expression, subcellular distribution, and co-immunoprecipitation of these different VAMPs and proposed that VAMP2 is the main v-SNARE facilitating GLUT4 translocation to PM of 3T3 L1 adipocytes (Sadler et al., 2015). Therefore, we built hypothesis upon this finding in the current study. GLUT4 trafficking is controlled by each component of the SNARE complex in addition to others such as Munc18c and more.

Syntaxin4 is a membrane-attached protein located in the plasma membrane and an essential component in the SNARE complex and thus is vital in GLUT4 trafficking. Syntaxin4 heterozygous knockout mice presented with reduced GLUT4 translocation accompanied with glucose uptake reduction (Yang et al., 2001). In contrast, overexpression of syntaxin4 showed a twofold greater translocation with enhanced glucose uptake following insulin stimulation (Spurlin et al., 2004). Together on the plasma membrane, syntaxin4 forms a binary complex, t-SNARE (Araki et al., 1997), with SNAP23 which was found by co-immunoprecipitation experiment using a solubilized rat adipocyte plasma membrane sample (St-Denis et al., 1999). Other isoforms of syntaxin proteins are reported to function in the GLUT4 trafficking process. Syntaxin6 and syntaxin16 were reported to be involved in GLUT4 sorting into GSVs. They together form the t-SNARE complex (Perera, 2003). Syntaxin16 co-localises strongly with GLUT4 (Shewan, 2003) and expression of dominant negative syntaxin16 resulted in

reduced insulin-induced glucose uptake (Proctor et al., 2006). Interestingly, it has been shown that a sub-domain of TGN is rich with both syntaxin6 and syntaxin16 suggesting that GLUT4 is trafficked from the plasma membrane through this domain to intracellular compartments (Shewan, 2003).

SNAP23 was first identified using yeast two-hybrid screening such that syntaxin4 was used as a bait and it shares 59% protein identity with SNAP25 with a molecular weight of 23kDa (Ran et al., 1996). It has a high binding affinity to syntaxin4, and they co-immunoprecipitate together and both are located in plasma membrane. Their interaction and localisation are not affected by insulin stimulation (St-Denis et al., 1999). Surface plasmon resonance (SPR) experiments showed formation of a stable SNARE complex composed of syntaxin 4, SNAP23 and VAMP2 by means of their conserved SNARE domains (Rea et al., 1998). A selective mutant of SNAP23 able to bind syntaxin4 but not VAMP2 was overexpressed and showed reduction in translocation of GLUT4 with insulin stimulation (Kawanishi et al., 2000).

The third main component of SNARE complex is VAMP2 which is a small size protein contributed by the donor vesicle. It was identified in rat adipocyte immunoblotting beside VAMP3 (Cain et al., 1992) which co-localise with GLUT4 and further is enriched in GLUT4-containing vesicles (Volchuk et al., 1995). The VAMP family contains several forms and it was proposed that other isoforms than VAMP2 can form the SNARE complex with syntaxin4 and SNAP23. It has been shown that VAMP isoforms 2, 3, 4, 5, 7, and 8 were able to form SDS-resistant SNARE complex with t-SNAREs syntaxin4 and SNAP23, in vitro (Sadler et al., 2015). Both VAMP2 and VAMP3 are inhibited by tetanus toxin which cleaves them and yet insulin-stimulated GLUT4 translocation was not stopped as it was added into rat adipocytes (Hajduch et al., 1997). On the other hand, the same inhibitor but in a different cell type, L6 myoblasts, diminished GLUT4 translocation by 60-70% (Randhawa et al., 2000). Furthermore, rescue translocation was achieved using a toxin-resistant form of VAMP2. In another study, inhibition of insulin-stimulated GLUT4 translocation was only achieved with blockage of VAMPs 2, 3, and 8 simultaneously and rescue with re-introduction of only one of them was enough (Zhao et al., 2009).

1.4.6 GLUT4 regulation by Munc18c

Glucose homeostasis is a tightly regulated process implying that regulation of SNARE complexe formation may be intimately involved. A key regulator is Munc18c, protein member of Sec1/Munc18 (SM) family, which acts on syntaxin4 (Sx4) participation on SNARE complex formation (Jahn, 2000). Sx4 can be found in two conformations i.e. open and closed (Aran et al., 2009; Jewell et al., 2010; Munson and Bryant, 2009). Binding of Munc18c to Sx4 in a closed form inhibits complex formation because it locks SNARE domain to its N-terminus domain (H_{abc}) (Figure 1-11). Munc18c also binds open Sx4 from its N-terminus which by contrast enhances complex formation. A third mode of Munc18c binding to the intact SNARE complex may directly control rate of complex formation (Latham et al., 2006; Munson and Bryant, 2009). Munc18c binding Sx4 might then result in inhibiting complex assembly (Kioumourtzoglou et al., 2014; Sudhof and Rothman, 2009; Thurmond et al., 1998) while any disruption to that binding may enhance GLUT4 translocation driven by stimulating SNARE complex formation (Kanda et al., 2005). Consistent with this, deletion of Munc18c in mice enhances insulin-stimulated glucose transport, and work from our group has suggested that Munc18c can positively regulate SNARE complex assembly (Kioumourtzoglou et al., 2014).

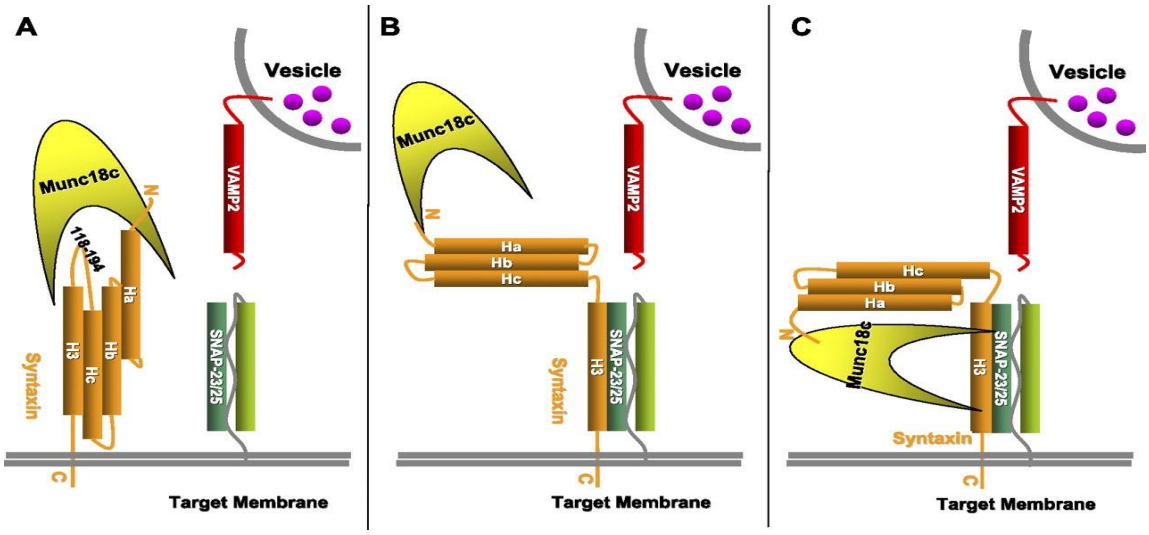

Figure 1-11 Munc18c-Syntaxin4 regulatory binding modes.

Munc18c binds Sx4 in closed/open modes and even the intact SNARE complex. Munc18c binds closed Sx4 conformation preventing SNARE complex formation(A), open Sx4 form interacts with Munc18c and bound to its N-terminus (B), intact SNARE complex shows Munc18c binding to the fully assembled complex (C). Figure cited from Jewell *et al.*, 2010.

1.5 SNAREs and post-translational modification

1.5.1 Phosphorylation

SNARE-mediated GLUT4 trafficking and fusion are regulated with the above mentioned proteins as well as with post-translational modifications such as phosphorylation (Snyder et al., 2006). All SNARE complex proteins were reported to be phosphorylated by different kinases and result in different effects on the overall complex formation or the process of fusion. Moreover, phosphorylation mediates numerous effects at multiple stages of the SNARE protein trafficking, including regulation of binding of SNARE-interacting factors, the 'zippering' of the trans SNARE complex and modulating the structure of the SNARE protein, reviewed in (Laidlaw et al., 2017).

A study by Schmelzle *et al*. 2006, investigated effects of insulin stimulation of 3T3 L1 adipocytes by an extensive, quantitative, mass spectrometry-based analysis of tyrosine phosphorylation in response to insulin. The study found 122 tyrosine phosphorylation sites on 89 proteins, two of which were syntaxin4 and Munc18c. Syntaxin4 was tyrosine phosphorylated on two sites, namely, Y115 and Y251 while Munc18c was phosphorylated at Y521. Treatment with insulin for 5 minutes increased phosphorylation by >10 fold for Munc18c and >3 fold for syntaxin4 (Schmelzle et al., 2006). Direct phosphorylation of Munc18c, *in vitro*, using recombinant cytosolic insulin receptor tyrosine kinase (CIRK) was found to phosphorylate the protein only at Y521 (Aran et al., 2011). Upon phosphorylation, Munc18c is unable to bind monomeric syntaxin4 and likewise phosphomimetic mutant Y521E is unable to bind syntaxin4. Therefore, such findings suggest strongly that Munc18c tyrosine phosphorylation upon insulin stimulation releases syntaxin4 from Munc18c binding thus allowing for syntaxin4 participation into SNARE assembly and ultimately fusion of GLUT4 into PM. Recent work using proximity ligation assays from our group have supported this conclusion (Kioumourtzoglou et al., 2014).

Neuronal SNAREs were thoroughly studied and characterized as they were the first to be identified in SNARE-trafficking and their importance for neurotransmitter release. Several kinases are used for phosphorylation which are diverse and represent various signaling paths and include those of protein kinase A (PKA), PKC, casein kinase (CK), death-associated protein kinase (DAPK), calcium/calmodulin-dependent protein kinase II (CaMKII), and cyclin-dependent kinases (Cdk). Following few examples presented as a representative sample of phosphorylation effects on membrane trafficking. Phosphorylation of syntaxin1a by CKII, *in vitro*, increased binding affinity to synaptotagmin 1, a Ca^{+2} sensor, which proposes the idea that this phosphorylation event might control neurotransmitter release (Risinger and Bennett, 1999). A more target-specific phosphorylation at serine-14, by CKII, localized syntaxin1 with SNAP25 into regions within axons that are thought to be fusion sites (Foletti et al., 2000). Furthermore, this phosphorylation site, serine-14, has been shown to be a regulatory residue in interaction with its regulator Munc18a (Rickman and Duncan, 2010).

In some occasions, the same SNARE is phosphorylated with different kinases and consequences are variable. Phosphorylation of SNAP25 using PKA showed no effects on either binary nor ternary binding with syntaxin1 or VAMP2 (Risinger and Bennett, 1999). In contrast, using PKC resulted in inhibition of interaction with syntaxin1a as well as VAMP2 (Shimazaki et al., 1996). Vesicular SNARE, VAMP2, phosphorylation by CKII and CaMKII showed indistinguishable effects thus functional consequences were not clear (Nielander et al., 1995).

The phosphorylation location within SNAREs affects resultant functional consequences. It is suggested that phosphorylations at sites close to C-terminal are inhibitory as they interfere with the zippering mechanism and thus halt membrane fusion (Hernandez et al., 2012). An example of this, phosphorylation of VAMP8 using PKC, resulted in suppression of secretory vesicle fusion in mast cells (Malmersjö et al., 2016). Vesicles were able to dock to target plasma membrane yet not fused.

The phosphorylation regulatory mechanism in other organisms like yeast showed functional consequences on membrane fusion. The t-SNARE Syntaxin1-like in yeast, Sso, is phosphorylated in the PKA-pathway resulting in inhibition of SNARE complex assembly (Marash and Gerst, 2001). De-phosphorylation of Sso using

ceramide activated phosphatase (CAPP), Sit4, increased the ability of Sso to bind Sec9, SNAP25-like. Therefore, these events show the impact of phosphorylation on binding affinity. Such findings trigger interest to explore more about phosphorylation's role in SNARE complex assembly, in particular, and membrane fusion, overall. Clearly SNAREs phosphorylation has functional consequences.

1.6 Aim of this study

Eukaryotic cells have a complicated and highly regulated membrane trafficking system. SNARE proteins are the main regulators beside other proteins as well as post-translational modifications such as phosphorylation. This study aimed at disclosure of biological consequences due to phosphorylation of SNAREs, syntaxin4 and Munc18c, key members in the insulin-stimulated SNARE-mediated GLUT4 trafficking process. Insulin stimulation results in tyrosine phosphorylation of synatxin4 (Sx4) at tyrosine-115 and tyrosine-251 as well as Munc18c at tyrosine-521. Therefore, in this study, I have looked into the biological consequences of these phosphorylations by means of *in vitro* and *in vivo* experiments and in single or combined conditions. Detailed aims for each results chapter are listed below.

1.6.1 Aims of chapter THREE

Schmelzle et al., 2006, showed syntaxin4 was tyrosine phosphorylated at 115 and 251 and insulin stimulation is known to increase GLUT4 trafficking to the plasma membrane as well as increasing the glucose uptake. The specific aims of this Chapter therefore are:

- To confirm previous studies on the phosphorylation of key tyrosine residues within Sx4 and Munc18c.
- To ascertain whether phosphorylation of Sx4 regulated function using the phosphomimetic mutant Sx4 species expressed in bacteria.
- To examine the suite of interactions between Sx4 and SNAP23 and VAMP2 and to assess how, if at all, phosphorylation of Sx4 modulated these.

1.6.2 Aims of chapter FOUR

Findings in the previous chapter were acquired from *in vitro* experiments and hence translation into an *in vivo* is necessary for validation: yet tools need to be developed for translation. The specific aims of this chapter are:

I. To develop phospho-selective antibodies to Sx4-Y115 and Sx4-Y251, and also Munc18c-Y521.
II. To ascertain whether there is a requirement for one or other of these tyrosine residues to be phosphorylated to allow phosphorylation of the other.
III. To develop lentivirus tools for expressing phosphomimetic mutants of these species in mammalian cells.

1.6.3 Aims of chapter FIVE

With the help of tools developed in the previous chapter, *in vivo* examinations about biological consequences of syntaxin4 phosphorylation using wild type (Sx4) and double phosphomimetic (2P) syntaxin4 were conducted. Therefore, aims pursued in this chapter were as follow:

I. Test produced Sx4-lentivirus infection efficiency and overexpression level followed by measuring changes in glucose uptake.
II. Characterisation of Sx4-knockout cells and examine effects on GLUT4 machinery.
III. Assessment of re-introduction of Sx4 into knockout model.

1.6.4 Aims of chapter SIX

The SM regulatory protein for syntaxin4 is Munc18c and it was shown to be phosphorylated by insulin together with syntaxin4 in the study of Schmelzle et al., 2006. The effect of Munc18c over syntaxin4 is contradictory, inhibition/enhancement, when participating in SNARE complex assembly. Therefore, I set following aims to study Munc18c:

I. Express Munc18c in a better yield using an enhanced gene compared to previously used low expression.
II. Characterise newly expressed Munc18c.
III. Use of enhanced gene expressed Munc18c in SNARE complex.

IV. Assess binding affinity of Munc18c towards other SNAREs.

CHAPTER TWO

2 Materials and Methods

2.1 Materials

2.1.1 General reagents and kits

General laboratory disposables, kits, and reagents used in this study were supplied by the following suppliers:

- Ambion, Austin, USA
- BD Biosciences, Oxford, UK
- BioRad Laboratories Ltd, Hertfordshire, UK
- Clontech Laboratories Inc, California, USA
- Fisher Scientific Ltd, Loughborough, Leicestershire, UK
- FormediumTM, Norfolk, UK
- GE Healthcare Bio-Sciences Ltd, Buckinghamshire, UK
- Invitrogen Ltd, Paisley, UK
- New England Biolads UK Ltd, Hertfordshire, UK
- Melford Laboratories Ltd, Ipswich, Suffolk, UK
- Merck Chemicals Ltd, Nottingham, UK
- Millipore Ltd, Livingston, UK
- New England Biolabs, Ipswich, USA
- Pierce, Perbio Science UK Ltd, Cheshire, UK
- Promega Ltd, Southampton, UK
- Roche Diagnostics Ltd, Burgess Hill, UK
- Severn Biotech Ltd, Worcestershire, UK
- Sigma Aldrich Company Ltd, Dorset, UK
- Spectrum Laboratories Inc, Netherlands
- Stratagene Technologies, California, USA
- Synaptic Systems, Göttingen, Germany
- VWR UK Ltd, Leicestershire, UK
- Whatman Plc, Kent, UK

2.1.2 Solutions and media

Solutions listed below were prepared using high quality distilled water, unless stated otherwise, and media autoclaved post preparation.

2X Laemmli Sample 100mM Tris, HCl pH 6.8, 4% (w/v) SDS, 20% (v/v)

Buffer (2X LSB)	glycerol, 0.2% (w/v) bromophenol blue, 10% (v/v) ß-mercaptoethanol
2YT	1.6% (w/v) tryptone, 1.0% (w/v) yeast extract, 0.5% (w/v) NaCl (20% Agar)
Ampicillin	100mg/ml, 1g dissolved in 10ml d.H2O (sterilized)
Buffer C	25 mM HEPES, 0.4 M KCl, 10 % (w/v) glycerol, pH 7.4
Coomassie blue stain	0.05% (w/v) Coomassie brilliant blue R-250 , 50% (v/v)methanol, 10% (v/v) acetic acid
Coomassie De-stain	15% (v/v) methanol, 15% (v/v) acetic acid
ECL solution 1	100mM Tris-HCl, pH 8.5, 2.25mM luminol in 2% (v/v) DMSO, 0.4 mM ρ-coumaric acid in 1% (v/v) DMSO
ECL solution 2	100mM Tris-HCl, pH 8.5, 0.018% (v/v) H2O2
GST-Elution Buffer	50 mM Tris base pH 8.0, 25 mM reduced glutathione, 10 % (w/v) glycerol
GST-Preparation Buffer	100 mM HEPES, 500 mM NaCl, 5 mM MgCl2, 5mM ß-mercaptoethanol, 10 % (w/v) glycerol, 1 tablet of complete protease inhibitor mix per 100 ml (Roche)
His-Preparation Buffer	100 mM HEPES, 1.6 M KCl, 4mM Imadazol, 5mM ß-mercaptoethanol, 40 % (w/v) glycerol, 1 tablet of complete protease inhibitor mix per 100 ml (Roche)
Immunoprecipitation (IP) buffer	50 mM HEPES pH 7.5, 5 mM EDTA, 10 mM sodium pyrophosphate, 10 mM NaF, 150 mM NaCl, 2 mM

	β-Glycerophosphate, 1 mM DTT
Kanamycin	50mg/ml, 0.5g dissolved in 10ml d.H2O (sterilized)
Krebs-Ringer phosphate buffer (KRP)	10 mM NaHCO3, 120 mM NaCl, 4 mM KH2PO4, 1 mM MgSO4, and 1 mM CaCl2
PBS	140mM NaCl 3mM KCl, 1.5mM KH2HPO4, 8mM Na2HPO4
PBST	140mM NaCl 3mM KCl, 1.5mM KH2HPO4, 8mM Na2HPO4, 0.1% (v/v) Tween-20
Ponceau S	0.2% (w/v) Ponceau S, 1% (v/v) acetic acid
RIPA Buffer	50mM Tris, HCl pH8, 150mM NaCl, 2mM MgCl2, 1% Triton, 0.5% sodium deoxycholate (w/v), 0.1% (w/v) SDS, 1mM DTT, 50 units/ml Benzonase
SDS-PAGE gel resolving buffer	75mM Tris-HCl, pH 8.8, 0.2% (w/v) SDS
SDS-PAGE gel stacking buffer	25mM Tris-HCl, pH 6.8, 0.2% (w/v) SDS
SDS-PAGE running buffer	25mM Tris, 190mM glycine, 0.1% (w/v) SDS
SDS-PAGE transfer buffer (semi-dry)	50 mM Tris base, 40 mM glycine, 0.1% (w/v) SDS, 10% (v/v) methanol
SDS-PAGE transfer buffer (wet transfer)	25 mM Tris-HCl, 192 mM glycine, 20% (v/v) Methanol (or Ethanol)
SOC media	2% tryptone, 0.5% yeast extract, 10 mM NaCl, 2.5 mM KCl, 10 mM MgCl2, 10 mM MgSO4, and 20

	mM glucose
TAE buffer	40mM Tris, 1mM EDTA
TB media	47.6g TB, 8ml 50% glycerol, up to 1l dH2O
TBST	20 mM Tris-HCl, pH 7.5, 137 mM NaCl, 0.1% (v/v) Tween-20
TBST (high salt)	20 mM Tris-HCl, pH 7.5, 250 mM NaCl, 0.1% (v/v) Tween-20
TST	50mM Tris Hcl pH7.6, 150mM NaCl, 0.05% (v/v) Tween-20

2.1.3 Antibodies

2.1.3.1 Primary antibodies

Primary antibodies used in this study for different experiments are listed in Table 1 for immunoblotting (IB), immunofluorescence (IF), or proximity ligation assay (PLA).

Table 1 List of primary antibodies used in different experiments in this study.

Antigen	Working dilution	Description	Source
HA	IF 1:500	Rat, monoclonal, clone 3F10	Roche applied sciences (11867423001)
His_6	IB 1:1000	Mouse, monoclonal	Sigma-Aldrich (H1029)

GAPDH	IB 1:10000	Mouse, monoclonal	Ambion, Cambridgeshire, UK. (#4300)
VAMP2	IB 1:1000	Mouse, monoclonal	Synaptic Systems (104211)
VAMP2	IB 1:1000	Rabbit, polyclonal antiserum	Synaptic Systems (104202)
Syntaxin 4	IB 1:1000	Rabbit, polyclonal antiserum	Synaptic Systems (110042)
Syntaxin 4	IB 1:1000	Mouse, monoclonal, clone 49	BD Bioscience (610440)
Syntaxin 4	IB 1:1000	Mouse, monoclonal	Abcam (ab77037)
Phosphotyrosine, PY	IB 1:1000	Mouse; monoclonal clone:4G10	Millipore Corporation, Billerica, MA, USA. (#05-321)
Munc18c	IB 1:100	Rabbit, polyclonal antiserum	Abcam (ab26331)
Munc18c	IB 1:1000	Rabbit, polyclonal antiserum	Synaptic Systems (116203)
Munc18c	IB 1:1000	Rabbit, Phospho-Munc18 (Ser515), Polyclonal	Thermo Fisher (PA1-4689)
Munc18c	IB 1:1000	Goat, polyclonal antiserum	Abcam (ab194954)
SNAP23	IB 1:1000	Rabbit, polyclonal, affinity purified	Synaptic Systems (111213)

PPARɣ	IB 1:200	Mouse, monoclonal clone:E-8	Santa Cruz Biotechnology, CA, USA. (#SC-7273)
FAS	IB 1:1000	FASN, Rabbit, polyclonal antiserum	Cell Signalling (#3189)
Adiponectin (ACRP30)	IB 1:500	Rabbit, anti-peptide C-terminus	Home-made
Adipsin	IB 1:500	Goat	Home-made
Syntaxin 2	IB 1:1000	Rabbit, polyclonal	Synaptic Systems (110022)
Syntaxin 3	IB 1:1000	Rabbit, polyclonal	Synaptic Systems (110032)
Syntaxin 16	IB 1:1000	Rabbit, polyclonal antiserum	Synaptic Systems (110062)
Phospho-specific Syntaxin4-Y115	IB 1:200	Rabbit, affinity purified	generated by Antagene Inc.
Phospho-specific Syntaxin4-Y251	IB 1:200	Rabbit, affinity purified	generated by Antagene Inc.
non-Phospho-specific Syntaxin4-Y115	IB 1:200	Rabbit, affinity purified	generated by Antagene Inc.
non-Phospho-specific Syntaxin4-Y251	IB 1:200	Rabbit, affinity purified	generated by Antagene Inc.
IRAP	IB 1:1000	Rabbit, polyclonal	Cell Signalling
GLUT4	IB 1:1000	Rabbit, polyclonal	Abcam (ab654)
GLUT1	IB 1:1000	Rabbit, polyclonal	Abcam (ab652)

2.1.3.2 Secondary antibodies

Immune reactivity detection, species-dependent, visualized using secondary antibodies listed in Table 2 according to suitability with assay used.

Table 2 List of secondary antibodies used for immuno-detection.

Antigen	Working dilution	Description	Source
IRDye® Donkey anti-Mouse IgG	IB 1:10,000	IRDye® optimized for use with the Odyssey® imaging systems, red fluorescent	LI-COR IRDye® 680LT Donkey anti-Mouse IgG (H + L), 0.5 mg [P/N 926-68022]
IRDye® Donkey anti-Rabbit IgG	IB 1:10,000	IRDye® optimized for use with the Odyssey® imaging systems, green fluorescent	LI-COR IRDye® 680LT Donkey anti-Mouse IgG (H + L), 0.5 mg [P/N 926-32213]
Anti-Mouse IgG (whole molecule)	IB 1:2000	Mouse, polyclonal, affinity-isolated, produced in goat; used for ECL detection	Sigma-Aldrich (G-7777)
Anti-Rabbit IgG (whole molecule)	IB 1:80,000	Rabbit, polyclonal, affinity-isolated, produced in goat; used for ECL detection	Sigma-Aldrich (G-7277)

Anti-mouse IgG	PLA 1:5	Mouse antibody produced in donkey conjugated to Duolink II oligonucleotide PLUS. Used for PLA assay	Olink Proteomics, Sweden, Olink AB (cat.# 92001-0100)
Anti-rabbit IgG	PLA 1:5	Rabbit antibody produced in donkey conjugated to Duolink II oligonucleotide PLUS. Used for PLA assay	Olink Proteomics, Sweden, Olink AB (cat.# 92005-0100)
Donkey anti-Mouse IgG (H+L) Highly Cross-Adsorbed Secondary Antibody, Alexa Fluor 488	IF 1:500	Secondary used for immuno-fluorescent detection of mouse primary.	Invitrogen (A-21202)

2.1.4 Plasmids

Details of plasmid constructs used in this study are listed in Table 3 including name of vector with insert, tag and its location, type of vector, and source obtained from or made by.

Table 3 Plasmid constructs used for expressing study-targeted proteins.

Plasmid	Description	Source
pETDuet-1-GST	*E. coli* expression vector encoding GST	Constructed by Dr Fiona Brandie
pETDuet-Sx4-GST	*E. coli* expression vector encoding C-terminally GST tagged Sx4 cytosolic domain, wild type.	Constructed by Dr Fiona Brandie
pETDuet-Sx4-GST (Y115E)	*E. coli* expression vector encoding C-terminally GST tagged Sx4 cytosolic domain. Contains a phosphomimetic mutation (Y115E)	Constructed by Dr Veronica Aran-Ponte
pETDuet-Sx4-GST (Y251E)	*E. coli* expression vector encoding C-terminally GST tagged Sx4 cytosolic domain. Contains a phosphomimetic mutation (Y251E)	Constructed by Dr Veronica Aran-Ponte
pETDuet-Sx4-GST (Y115,251E); 2P	*E. coli* expression vector encoding C-terminally GST tagged Sx4 cytosolic domain. Containing two phosphomimetic mutations (Y115/251E)	Constructed by Dr Veronica Aran-Ponte
pGEX-4T-1-GST-Sx4, cleavable	*E. coli* expression vector encoding N-terminally GST-tagged Sx4 cytosolic domain (Thrombin-cleavable)	Constructed by Dr Fiona Brandie
pGEX-4T-1-GST-Sx4(Y115/251E); 2P, cleavable	*E. coli* expression vector encoding cytosolic domain, N-terminally GST-tagged Sx4(Y115/251E) (Thrombin-cleavable)	Constructed by Dr Dimitrios Kioumourtzoglou

pGEX-4T-1-GST-VAMP2	*E. coli* expression vector encoding N-terminally GST-tagged VAMP2 cytosolic domain (Thrombin cleavable)	Constructed by Dr Dimitrios Kioumourtzoglou
pQE30-His-VAMP2	*E. coli* expression vector encoding N-terminally His_6-tagged VAMP2.	Constructed by Dr Fiona Brandie
pQE30:His-SNAP23	*E. coli* expression vector encoding N-terminally His_6-tagged SNAP23.	Constructed by Dr Fiona Brandie
pET41a-GST-SNAP23	*E. coli* expression vector encoding N-terminally GST-tagged SNAP23, cleavable i.e. Thrombin cleavage site.	Constructed by Dr Fiona Brandie
pcDNA3.1(+)-Sx4	pcDNA3.1(+) mammalian expression plasmid encoding un-tagged full length Sx4(wt)	Cloned by GenScript, USA
pcDNA3.1(+)-Sx4(Y115E)	pcDNA3.1(+) mammalian expression plasmid encoding un-tagged full length Sx4(Y115E)	Cloned by GenScript, USA
pcDNA3.1(+)-Sx4(Y251E)	pcDNA3.1(+) mammalian expression plasmid encoding un-tagged full length Sx4(Y251E)	Cloned by GenScript, USA
pcDNA3.1(+)-Sx4(Y115/251E), 2P	pcDNA3.1(+) mammalian expression plasmid encoding un-tagged full length Sx4(Y115/251E)	Cloned by GenScript, USA
pcDNA3.1(+)-Munc18c	pcDNA3.1(+) mammalian expression plasmid encoding un-tagged full length Munc18c(wt)	Cloned by GenScript, USA

pcDNA3.1(+)-Munc18c(Y521E)	pcDNA3.1(+) mammalian expression plasmid encoding un-tagged full length Munc18c(Y521E)	Cloned by GenScript, USA
pCDH-CMV-MCS-EF1-RFP	Lentiviral plasmid, empty	System Biosciences SBI, cat number CD512B-1
pLVX-IRES-mCherry	Lentiviral plasmid, empty	Clontech, cat number 631237
pCDH-CMV-MCS-EF1-RFP-Sx4	Lentiviral plasmid, Sx4(wt) sub-cloned into pCDH-CMV-MCS-EF1-RFP using restriction enzymes BamHI and NheI.	Sub-cloned in this study
pCDH-CMV-MCS-EF1-RFP-Sx4(Y115E)	Lentiviral plasmid, Sx4(Y115E) sub-cloned into pCDH-CMV-MCS-EF1-RFP using restriction enzymes BamHI and NheI.	Sub-cloned in this study
pCDH-CMV-MCS-EF1-RFP-Sx4(Y251E)	Lentiviral plasmid, Sx4(Y251E) sub-cloned into pCDH-CMV-MCS-EF1-RFP using restriction enzymes BamHI and NheI.	Sub-cloned in this study
pCDH-CMV-MCS-EF1-RFP-Sx4(Y115/251E), 2P	Lentiviral plasmid, Sx4(Y115/251E) sub-cloned into pCDH-CMV-MCS-EF1-RFP using restriction enzymes BamHI and NheI.	Sub-cloned in this study
pLVX-IRES-mCherry-Munc18c	Lentiviral plasmid, Munc18c sub-cloned into pLVX-IRES-mCherry using restriction enzymes XhoI and EcoRI	Sub-cloned in this study

pLVX-IRES-mCherry-Munc18c(Y521E)	Lentiviral plasmid, Munc18c sub-cloned into pLVX-IRES-mCherry using restriction enzymes XhoI and EcoRI	Sub-cloned in this study
pQE30	Bacterial expression vector, empty, encodes His_6 tag.	Qiagen Ltd.
pMA-RQ-Munc18c	Mammalian expression vector encoding codon-optimised gene for Munc18c, His-tagged at N-terminus.	Assembled by Life technologies
pMA-RQ-Munc18c(Y521E)	Mammalian expression vector encoding codon-optimised gene for Munc18c(Y521E), His-tagged at N-terminus.	Assembled by Life technologies
pQE30-His-Munc18c	Bacterial plasmid, Munc18c(wt) sub-cloned into pQE30 using restriction enzymes EcoRI and SalI positioned after His_6 at N-terminus.	Sub-cloned in this study
pQE30-His-Munc18c(Y521E)	Bacterial plasmid, Munc18c(Y521E) sub-cloned into pQE30 using restriction enzymes EcoRI and SalI positioned after His_6 at N-terminus.	Sub-cloned in this study
pETDuet -PrA	*E. coli* expression vector encoding two repeats of IgG binding domains if S. aureus protein.	Constructed by Dr Lindsay Carpp
pETDuet –VAMP2-PrA	*E. coli* expression vector encoding cytosolic VAMP2, PrA-tagged at C-terminus.	Constructed by Dr Fiona Brandie

pET28b-His-Munc18c	*E. coli* expression vector encoding native gene for Munc18c, His_6-tagged at N-terminus.	Constructed by Dr Fiona Brandie
pQE30-His-P-Munc18c	*E. coli* expression vector encoding native gene for Munc18c(Y521E), His_6-tagged at N-terminus.	Constructed by Dr Veronica Aran-Ponte

2.1.5 Cell lines

Two types of cells were used in this study, mammalian and different strains of *E. coli* including BL21(DE3), TOP10, DH5 alpha, and XL-1 blue.

Table 4 Mammalian cell lines used in this study.

Cell line	Description	Source
3T3-L1	Mammalian cell, mouse, fat fibroblasts can be differentiated to mature adipocytes.	American Type Culture Collection (ATCC)
HeLa	Mammalian cell.	American Type Culture Collection (ATCC)
HEK293NT	Human embryonic kidney cells 293, used for lentivirus particles production.	Invitrogen
HEK293FT	Human embryonic kidney cells 293, used for lentivirus particles production.an enhanced version.	gift from David M. Bryant

2.1.6 Computer software

Following software were used throughout this study for purposes of data analyses or designing an experiment.

- Blobfinder, Swedish University of Agricultural Science, Uppsala, Sweden

- Image J V1.41, National Institutes of Health, Bethesda MD, USA
- LSM Viewer Carl Zeiss AxioVision LE Rel 4.5, Hertfordshire, UK
- Vector NTI V10.3, Invitrogen, Carlsbad, CA, USA
- GraphPad Prism 5, GraphPad Software, Inc., CA, USA
- Odyssey Sa, LI-COR Biotechnology - UK Ltd

2.2 Molecular biology methods/techniques

2.2.1 Plasmid DNA purification – small scale

A single colony, from fresh transformed bacteria (section 2.2.5), was used to inoculate sterilized 10ml 2YT supplemented with appropriate antibiotic (100µg/ml Ampicillin or 50µg/ml Kanamycin) for selection purposes and grown overnight at 37^{o}C with continuous shaking. Plasmid DNA was extracted using a commercial kit following the manufacturers protocol (Wizard® Plus SV Minipreps DNA Purification Systems (Promega)). Concentration and quality (RNA/protein contamination) of DNA were assessed using NanoDrop spectroscopy. A sample was also run on an agarose gel to check integrity. Purified plasmids were checked for the presence of the correct insert by restriction digestion using enzymes flanking the cloned insert followed by gel electrophoresis.

2.2.2 Plasmid DNA purification – large scale

A single colony, from freshly transformed bacteria (section 2.2.5), was used to inoculate sterilized 5ml 2YT supplemented with the appropriate antibiotic (100µg/ml Ampicillin or 50µg/ml Kanamycin) for selection purposes and grown for about 6 hours. This culture was then used to innoculate 400ml 2YT culture at 37^{o}C with continuous shaking overnight. Cells were then harvested by centrifugation at ~5000 xg for 10 minutes at 4^{o}C. Plasmid DNA was subsequently extracted using a commercial kit, following the manufacturer's protocol. Plasmid DNA concentration, quality, and integrity were checked as above (2.2.1).

2.2.3 Agarose gel electrophoresis

Samples of DNA to be visualized for size assessment or integrity and quality were routinely run in agarose gels post purification, restriction digestion, or PCR. Gels used vary in concentration, 0.8-1.5% w/v, depending on fragment sizes. High quality agarose was mixed in TAE buffer (40mM Tris, 1mM EDTA) and boiled in microwave to melt. Melted agarose was left to cool to about 60^{o}C at which time Ethidium Bromide, 0.5µg/ml, was added to stain DNA molecules in the gel which was cast using the casting stand designed for each gel apparatus. Samples loaded after mixing with 6X sample buffer (New England Biolabs Ltd) alongside a DNA marker (100bp or 1kbp, New England Biolabs Ltd). Gels were run at 80 volts followed by band detection using ultraviolet transilluminator with a built-in gel documentation system.

2.2.4 Digestion of plasmids using restriction endonucleases

Restricted endonucleases digestion reactions were performed over a heating block using 1.5ml eppendorf tube at designated temperature for a single enzyme. In case of two enzymes used, we either digest sequentially, one at a time, or add both into digestion reaction using most compatible buffer and temperature. Enzymes, with buffer, used were either from BioLabs or Promega and followed their optimised protocol. Reactions were mostly done at 37^{o}C for 4 hours followed by analysis in agarose gel or freezing at -20^{o}C for later analysis, in rare occasions. Digested samples were subjected to 0.8-1% agarose gel electrophoresis to separate fragments according to their size. A size marker included in every gel allowing size of digested fragments determination in addition to undigested plasmid and the single digestion reaction too. Depending on later analysis, i.e. cloning, sequencing, the gel-resolved fragment could be purified off gel.

2.2.5 Plasmid transformation

Plasmids were transformed into different types of chemically competent cells for different purposes including recombinant protein expression or plasmid DNA (pDNA) extraction. Cells used included BL21(DE3) for protein expression and TOP10, XL1-Blue, or DH5-Alpha for plasmid DNA extraction and preparation of DMSO stocks. Cells were purchased from Invitrogen company and BL21(DE3) used from commercial as well as home-made sources. Cells were stored at -80^{o}C and on day of use transferred on ice and left to thaw for half an hour. Selected plasmid DNA for transformation, 1-5µl (1mg/ml), were added into an aliquot of 20-50µl competent cells in sterilised tube next to flame, for sterilization purpose, and swirl-mixed by cell's tip and the closed tube incubated on ice for 45 minutes. Cells were later subjected to heat shock, altering membrane fluidity creating pores, at 42^{o}C for 35 seconds followed by incubation on ice for 2 minutes. SOC or 2YT media, 200-250µl, were added to cells in sterilised condition followed by incubation at 37^{o}C for 45 minutes with continuous shaking. This step allows cells to develop antibiotic resistance encoded in the transformed plasmid backbone thus giving them ability to grow later in antibiotic-selective media or plate. Finally, cells were plated on 10cm 2YT-agar plates with appropriate antibiotic using two volumes, 50 or 100µl, to get proper colony distribution for later selection, singular colonies, and incubated overnight at 37^{o}C. A transformation control was always included which was competent cells without pDNA treated exactly like transformation reaction.

2.3 Protein methods

2.3.1 Recombinant proteins expression and purification

A common protocol was used for recombinant protein expression and purification with specific changes in some steps in accordance with the purification tag used. A starter culture was prepared using sterilized (autoclave) 10ml 2YT media inoculated with a single colony from freshly transformed E. coli

BL21 (DE3) with the construct of interest in the presence of selective antibiotic, Ampicillin or Kanamycin. The culture was incubated at 37°C overnight with continuous shaking, 210units/min. Next day, the starter bacteria culture was used to inoculate a larger volume, 1 litre, of commercially-prepared rich terrific broth (TB) media, sterilized, with appropriate antibiotic added and incubated at 37°C with continuous shaking, with monitoring cell growth to reach an optical density (OD600) 0.6-0.8 at which time the protein expression was induced by addition of 0.5mM IPTG. The culture was incubated overnight at 22°C with continuous shaking for protein expression. Next day, cells were harvested by spinning down cultured bacteria at 3000g for 30 minutes at 4°C and media supernatant was discarded while the cell pellet was either resuspended in preparation, lysis, buffer or stored at -80°C for later usage. Depending on the pellet size, cells were suspended in lysis buffer, containing protease inhibitor, to have a fine suspension and lysed by passing them through a microfluidic machine, Microfluidizer M-110P cell disrupter, at 10,000 psi while keeping lysates on ice throughout the whole process. Cell lysates were incubated with 10units/ml DNaseI, in the cold room for 30 minutes with continuous mixing. The cell membrane and nucleus were pelleted by centrifugation at 31,000g for 45 minutes at 4°C, in a Beckman JA-20 rotor. Clear lysate was incubated with appropriate affinity beads overnight at 4°C with continuous rotation mixing in order for tagged protein to bind and purify from crude cell lysate. Beads were collected by centrifugation at 1000g for 2 minutes. Hereafter, in accordance with the tag on protein, different procedures and buffers were followed to wash, elute, dialyse (Table 5) and later quantify the expressed recombinant protein. Bound proteins were washed 3-5 times using 10 bed bead volumes to remove any non-specific bindings and later eluted in three aliquots of about 1ml each by incubating them with elution buffer for 30 minutes, at least, in cold room with rotation mixing. Combined elution aliquots were dialysed against PBS buffer overnight to remove contaminations and concentrate protein using either dialysis tubes (Float-A-Lyzer, Spectrum Laboratories Inc.) or cassette (Dialysis cassette Pierce Slide-A-Lyzer, Thermo Scientific) and the suitable molecular weight cut off, i.e. smaller than protein size. Proteins were then stored at -80°C in small aliquots, 200ul. Dialysed proteins were quantified using known BSA standards. Throughout the purification process, samples were taken to assess

procedure and document stages and that included samples of lysate, flow, wash, beads before elution, elutions, beads after elution, and dialysis which were later subjected to SDS-PAGE and coomassie blue staining.

Table 5 Recombinant protein purification buffers used in this study.

	Beads	**Lysis buffer**	**Wash buffer**	**Elution buffer**
GST	glutathione-Sepharose 4B beads (GE Healthcare Bio-Sciences Ltd)	100 mM HEPES, 500mM NaCl, 5mM MgCl2, 5mM ß-Mercaptoethanol 10% (w/v) glycerol, 1 tablet of complete protease inhibitor mix per 50ml (Roche)	0.5M NaCl in PBS (85mM NaCl, 1.7mM KCl, 5mM Na2HPO4, 0.9mM KH2PO4, pH 7.4)	50mM Tris base pH 8.0, 25mM reduced glutathione, 10% (w/v) glycerol
His_6	Ni^{2+}-NTA	2.5mM imidazole and 5mM ß-Mercaptoethanol in Buffer C [25mM HEPES, 0.4M KCl, 10% (w/v) glycerol pH7.4, 1 tablet of EDTA-free protease inhibitor mix per 50ml (Roche)]	25mM imidazole in Buffer C	250mM imidazole in Buffer C
PrA	IgG-Sepharose TM 6 Fast Flow beads (GE Healthcare Bio-Sciences Ltd)	5mM ß-Mercaptoethanol in 1X PBS, 1 tablet of EDTA-free protease inhibitor mix per 50ml (Roche)	TST (50mM Tris-HCl pH 7.6, 150mM NaCl, 0.05% (v/v) Tween-20) 0.5M HAc (Acetic acid) pH 3.4 5mM NH_4Ac pH 5 (0.2g in 500ml d.H_2O) <u>Beads washes</u>	0.5M acetic acid, pH 3.4

			before addition to lysate: 4X TST → 2X HAc → 2X TST → 2X HAc → 2X TST Beads washes after incubation with lysate: 10X TST → 2X NH_4Ac	

2.3.2 SDS-PAGE

Sodium dodecyl sulfate (SDS) gels were prepared freshly in the lab, 10-15% polyacrylamide gels with different thicknesses, 0.7-1.5mm, in accordance the protein size and sample available with amount. Gels were prepared using Bio-Rad casting setup and running tanks, holds 2-4 gels per run. Gels consisted of two layers, stacking layer (4%) which helps in aligning samples front and concentrating samples, and the resolving layer which separates proteins in one sample according to their sizes. A ready-made 30% acrylamide-bisacrylamide (Anachem Ltd, Luton, Bedfordshire, UK) stock solution was used to prepare first resolving gel (resolving buffer: 75mM Tris-HCl, pH 8.8, 0.2% (w/v) SDS) and as it solidified then stacking gel (stacking buffer: 25mM Tris-HCl, pH 6.8, 0.2% (w/v) SDS) was added on top of resolving with desired comb size (10-15 wells) placed before stacking polymerisation, initiated by addition of ammonium persulfate (APS) and N, N, N', N' - tetramethylenediamine (TEMED). Protein samples were prepared for SDS-PAGE by addition of equal volume of loading buffer 2X LSB (100 mM Tris.HCl pH 6.8, 4% (w/v) SDS, 20% (v/v) glycerol, 0.2% (w/v) bromophenol blue, 10% (v/v) Β-mercaptoethanol) and boiling samples at 95^{o}C for 5 minutes, unless stated differently, followed by addition to assembled gels immersed in running buffer (25mM Tris base, 190 mM glycine, 0.1% (w/v) SDS) and

electrophoresis started. Each run always included pre-stained protein markers (Bio-Rad) guiding protein sizes and appropriate controls. At the end of the run, gels were either coomassie-stained or used for western blotting.

2.3.3 Coomassie stain

Subsequent to protein size resolving, gels were stained for proteins using coomassie stain to visualize fragment sizes. I used two types of coomassie staining methods, i.e. home-made and commercial (InstantBlue, Expedeon Ltd.) stain. The resolving gel was removed from running supporting-glasses and immersed in coomassie stain (0.05 % (w/v) Coomassie brilliant blue R-250, 50 % (v/v) methanol, 10 % (v/v) acetic acid) at room temperature for half an hour with gentle shaking. The stain was removed and gel rinsed with water to wash out excess stain then incubated in destaining solution (15 % (v/v) methanol, 15 % (v/v) acetic acid) for at least 45 minutes or until the background was clear. Commercial solution was faster (stained in 15 minutes) and more sensitive (5 ng per band to be detected (BSA) when staining overnight).

2.3.4 Protein concentration estimation

In order to setup experiments, protein concentrations of reactants were needed; thus an estimation of protein concentrations was accomplished using SDS-PAGE (section 2.3.2) followed by coomassie stain (section 2.3.3). Bovine serum albumin (BSA) standards were used to quantify recombinant protein concentrations with help of ImageJ software quantification by densitometry of only the band of the protein apart from contaminants. Total protein concentration was determined using the colorimetric Pierce™ BCA Protein Assay Kit (ThermoFisher, 23227) and BSA standards, and quantified through microplate reader spectrophotometer.

2.3.5 Western blotting; Immunoblots (semi-dry & wet transfer)

Post SDS-PAGE, proteins were transferred from the gel onto nitrocellulose membrane (Severn Biotech Ltd.) for immunoblotting with antibodies later. I used

two ways for transferring, i.e. semi-dry and wet transfers. Both shared the order of sandwich layers as following, in order: anode-to-cathode, 3 filter papers, nitrocellulose membrane, gel, 3 filter papers, and the current run from cathode to anode such that negatively-charged proteins, SDS-masked, move from gel into the membrane. Buffers used were different between semi-dry (24mM Tris base, 20mM glycine, 0.1% (w/v) SDS, 20% (v/v) methanol) and wet transfer (25 mM Tris-HCl, 192 mM glycine, 20% (v/v) Methanol or Ethanol), and the former sandwich moistened only while latter was immersed in transfer buffer. The semi-dry run was for only 45 minutes while wet transfer could be done for 1, 2 hours, or overnight. The following steps were similar. By the end of transfer, efficiency was checked using Ponceau S stain solution (0.2 % (w/v) Ponceau Stain, 1 % (v/v) glacial acetic acid) which is a universal non-permanent protein stain showing all transferred proteins from gel in membrane. The blot was immersed in stain for 5-10 minutes at room temperature then removed and destained using water. Band patterns were documented by capturing a picture for later analysis.

Following protein transfer, the membrane is blocked for free sites with blocking buffer (5% fat-free milk, 3% BSA, or neat SEA BLOCK blocking buffer). Buffers used were either PBST (85 mM NaCl, 1.7 mM KCl, 5 mM Na2HPO4, 0.9mM KH2PO4, 0.1 % (v/v) Tween-20, pH 7.4) or TBST (20mM Tris-HCl pH 7.5, 137mM NaCl, 0.1% (v/v) Tween-20) depending on primary antibody used later and if there is any cross-reaction of buffer with the blotting process. The blot is then incubated with primary antibody, prepared in 1% blocking buffer, for at least an hour, or overnight, followed by 3 washes for 30 minutes. Then secondary antibody of choice (Table 2), was incubated for 1 hour at room temperature with mixing followed by 3 washes and finally detection using either ECL or LI-COR. Detection using ECL required development of X-ray film after blot incubation with commercial substrate (Pierce™ ECL Plus Western Blotting Substrate, ThermoFisher) while LI-COR scanned the blot using a fluorescent detection instrument (Odyssey, LI-COR Inc.). Blots were documented and analysed by densitometry quantification using ImageJ software.

2.4 Pull down

Syntaxin4 binding affinity with other SNAREs was measured using pull down assay. Sx4 was immobilised in glutathione beads and incubated with excess cognate protein for different timings followed by extensive washes and analysis by SDS-PAGE. GST-tagged Sx4 was sourced from either freshly expressed and washed affinity purification beads, glutathione sepharose, which were used for the assay. Otherwise eluted Sx4-GST was immobilised to glutathione beads for 3 hours followed by extensive washes and then used. In either case, all pull down proteins, immobilised or free, were quantified before assay and similar Sx4 mutant proteins were used on beads beside adding excess of cognate SNAREs in the reaction. The pull down was reaction setup in 500ul PBS with 10-30µl beads bed volume (1-5µg) mixed with excess compared-protein, VAMP2, SNAP23, Munc18c, or Munc18c(Y521E). The assay reaction was incubated mixing at 4^{o}C for variable timings followed by bead collection at 1000g for 5 minutes. Beads were washed with 1ml PBS 3-5 times and then an equal volume of 2X LSB loading buffer was added to beads and boiled at 95^{o}C for 5 minutes. Samples were analysed by subjecting them to SDS-PAGE followed by western blotting for the chosen antibody and/or coomassie stain.
The Munc18c pull down assay had a more intensive washing steps. This included the following 1ml each washes, in-order, 3X 0.2% fish skin gelatine-PBS, 3X 5%(w/v) glycerol-PBS, 4X PBS. This was followed by a last spin at 1000g for 5 minutes to remove all liquids then loading buffer, 2X LSB, was added and sample treated as mentioned above.

2.5 Complex assembly assay

Two methods were used for complex assembly assay, i.e. on beads and in solution. The former used Sx4 immobilised on glutathione sepharose beads incubated with cognate SNAREs, SNAP23 and VAMP2, followed by several washes to remove unbound proteins, and analysed by SDS-PAGE loading the beads into gel. The latter method was set in liquid such that all complex components were mixed in reaction buffer for different timings followed by analysis by SDS-PAGE

and immunoblotting or coomassie stain. The reaction was run at different temperatures including 37ºC and 4ºC; it was concluded 4ºC is better as the speed of complex formation is maintained and protein integrity is stable. Bead loading was not consistent as the amount of beads loaded onto the gel was not controlled. Both methods gave similar results and we decided to work using the liquid form at 4ºC for simplicity and ease of repeat. In each reaction equal protein amount was noticed and also between different Sx4 mutants.

The complex assembly assay using beads was started by immobilising Sx4 onto glutathione sepharose beads, as mentioned in section 1.4. A beads bed volume of 10-20µl incubated with SNAP23 and VAMP2 in 1ml binding buffer (buffer C: 25mM HEPES, 0.4M KCl, 10% (w/v) glycerol pH7.4, 6mM ß-mercaptoethanol) and 100µg/ml BSA in rotor mixer at 4ºC for 5-60 minutes. Beads were collected by centrifugation at 1000g for 5 minutes at 4ºC and a sample of supernatant was taken for the protein input determination. Beads were washed in binding buffer 3-5 times followed by addition of a beads-equal volume of loading buffer, 2X LSB, and boiling samples at 95ºC for 5 minutes. Samples were subjected to SDS-PAGE analysis and western blotting and/or coomassie stain.

The liquid version of the assay was started by mixing equal molarity of all SNAREs in 1ml binding buffer and 100µg/ml BSA. The mixture was incubated at 4ºC in a rotor mixer and 100µl samples at chosen time points were taken into different tubes and immediately loading buffer was added and samples boiled at 95ºC for 5 minutes then kept on ice. All samples were then analysed as mentioned above.

2.6 CIRK phosphorylation

A tyrosine phosphorylation assay using recombinant activated cytoplasmic insulin receptor kinase (CIRK), prepared previously by Dr Veronica Aran-Ponte, was applied on Sx4 phosphomimetic mutants and the Sx4-SNAP23 combination in tSNARE. 2µg Sx4 was mixed with 5µl CIRK and made up to 50µl total reaction volume using sterilised buffer (50 mM HEPES pH 7.5, 4 mM MnCl2, 0.2 mM DTT, 100 µM ATP Na-salt). The reaction mixture was incubated at 30ºC in a heating

block for 150 minutes. Sample buffer, 50µl 2X LSB, was then added terminating the reaction and samples heated to 75°C for 10 minutes. Samples were subjected to SDS-PAGE followed by western blotting for Sx4 antibodies as well as total phosphotyrosine. TBST buffer was used routinely in developing blots for this assay including steps of washing, primary and secondary antibodies, and blocking.

2.7 Cell culture

2.7.1 3T3-L1 maintenance and differentiation

Cells were cultured at 37°C/10% CO_2. 3T3-L1 fibroblasts obtained from the ATCC were grown to confluence in DMEM containing 25 mM D-glucose, 10% new-born calf serum (NCS), and penicillin/streptomycin (5000 U/ml). 3T3-L1 pre-adipocytes were seeded and allowed to reach confluence. Two days after confluence, cells were differentiated in DMEM/25 mM glucose supplemented with 10% fetal bovine serum (FBS) and a cocktail of 1 µg/ml insulin, 250 nM dexamethasone, 5µM Troglitazone, and 500µM isobutylmethylxanthine. Forty-eight hours later, the media were changed to DMEM/ 25 mM glucose in the presence of 10% FBS and 1µg/ml insulin for two more days. Cells were then grown in DMEM/25 mM glucose supplemented with 10% FBS and used between days 8–12 after the addition of differentiation cocktail.

2.7.2 Insulin stimulation of 3T3L1 adipocytes

3T3L1 adipocytes were insulin stimulated to probe effects on glucose homeostasis machinery including GLUT4 translocation and glucose uptake plus any changes on protein expression levels. Cells were serum starved for two hours using DMEM media only without serum or antibiotics after removing all FCS-DMEM media. Cells were kept in their incubator, 37°C/10%CO_2, at all times after additions or removal of media. Insulin stimulation was started by addition of a

final concentration of 100nM (or sometimes 1μM) diluted in new serum-free media and incubated for 5-20 minutes. The resting or basal condition is treated in parallel but without addition of insulin. Immediately after the incubation time, cells were placed on ice to stop the effect of stimulation and cells washed with PBS or lysis buffer for forward analysis.

2.7.3 Lentivirus production using HEK293 and concentration

Lentivirus were produced using HEK293 cells with help of transfection reagent PEI (polyethylenimine, sigma 40-872-7) and envelop plasmids (pVSV-G) named pMDG and packaging plasmid called Int., cultured in T150 flasks followed by virus concentration using ultracentrifugation. Virion molecules were produced for full length un-tagged Sx4 phosphomimetic mutants (Y115E, Y251E, Y115/251E), and Munc18c mutant (Y521E) as well as the wild type. Lower passage number cells were favoured to use for the lentivirus production and cells were brought up freshly from N_2 such that they were split two times before usage in the process of production. One day prior to transfection, T150 flasks were seeded with $1.2X10^6$ cells/flask at 37°C and 5%CO_2. On the day of transfection, a transfection mixture was prepared, for one T150 flask, including 50μg vector construct (expression plasmid), 17.5μg pMDG, and 32.5μg Int mixed in 5ml OptiMEM and sterilised through a 0.22μm filter. In another tube, 1μl (5mg/ml) PEI was mixed with 5ml OptiMEM and sterilised through a 0.22μm filter. The two tubes were mixed together with a gentle shake followed by incubation in hood at room temperature for 20 minutes. Each T150 flask was washed with 5ml OptiMEM before addition of the transfection mixture. Flasks were incubated at 37°C and 5%CO_2 for 4-16 hours followed by removal of transfection mixture and addition of 20ml complete media. Post 48 hours from transfection, media were collected and stored at 4°C and a fresh complete media was added for collection at 72 hours. The two collections were combined together and filtered through 0.22μm filter prior to concentration using ultracentrifugation.

The centrifuge to be used was pre-cooled to 4°C and tubes rinsed with 70% ethanol. All balancing and aliquot distribution work was done in the hood with high sterilisation means such that it was disinfected using virkon and any

disposables got in contact with virus media soaked in virkon overnight before dispose. Centrifugation tubes were filled with media and balanced before spinning at 23,000 rpm for one hour at 4°C. Tubes were removed and media decanted carefully and gently then more media was added into same tube. After the last spin, media was discarded and tubes tilted upside down to dry excess media in hood over a clean tissue paper. 100µl OptiMEM was added into each tube and incubated in the hood for 20 minutes followed by virus resuspension by pipetting gently up and down several times. Aliquots of 10-30µl concentrated virus were distributed in eppendorf tubes and stored in -80°C freezer.

2.7.4 Lentivirus infection

Lentivirus infection used for 3T3-L1 was achieved by two ways and both gave a stable transduction. Virus was added when they were fully confluent then differentiation started. Alternatively, virus was added on day-5 of differentiation; the former was the choice. By the end of the intended day of infection, media was removed and replaced with minimum complete media with an appropriate volume of concentrated virus, 1µl/96-well or 10µl/12-well plate, and 8µg polybrene. Cells were incubated with infection media overnight, 16 hours, at 37°C and 5%CO_2 then media was replaced with complete media and used after two days, at least, from infection start. Infection efficiency was checked on live cells using fluorescent microscopy such that filters for red RFP or mCherry tags in constructed plasmids for Sx4 or Munc18c, respectively, could be detected showing infected cells, and their numbers quantified.

2.7.5 Cell transfection

We used different transfection reagents including pPACKH1 (System Biosciences LLC, SBI), Lipofectamine2000 (ThermoFisher), and PureFection (System Biosciences LLC, SBI). Infected cells included 3T3-L1 fibroblasts and adipocytes, Hela, and HEK293 using different plasmids such as pcDNA3.1, pCDH, and pLVX. According to transfection reagent, the manufacturer's protocol was followed.

2.7.6 Freezing cells

Cells were frozen at confluence of 70-90% by removal of media and washing with sterilised PBS then incubation with trypsin for 5 minutes at 37ºC in an incubator followed by tapping flask to dislodge cells. The cells were checked under the microscope, and then complete media added and transferred into falcon tubes and spun at 2000rpm for 5 minutes. Media were aspirated and cells resuspended in 1ml 10% DMSO-FCS serum and transferred into a cryotube then frozen overnight at -80ºC slowly by keeping them in a container containing isopropanol for slower freezing. Next day, the cells were moved into liquid nitrogen container for storage.

2.8 Proximity Ligation Assay (PLA)

Proximity ligation assay (PLA) is an *in situ* technique allowing identification of protein-protein interactions or modification, i.e. phosphorylation, without any distraction to cell structure or tag interferences. The protocol followed for the assay was as optimised and published by our research group, Kioumourtzoglou D. *et al*. 2018 (Kioumourtzoglou et al., 2018). We used this technique to probe insulin-stimulated phosphorylation of Sx4 at residue Y115 or Y251, using phospho-specific antibodies. 3T3-L1 fibroblasts were seeded into an 8-chamber slide, Lab-Tek® Chamber Slide™ System, with a glass bottom such that it can be used later for microscopic visualization. Post two days of full confluence, cells were differentiated and used by day 8-12. On day of use, adipocytes were insulin stimulated (section 2.7.2) followed by 3X PBS washes then fixed with 3% PFA (200µl per well) for 30 minutes. Fixed cells were washed two times with glycine solution (2% (w/v) BSA, 20mM glycine in PBS) quenching the PFA. Then, simultaneously, cells were blocked and permeabilised by incubation for 30 minutes with solution containing BSA and detergent (0.1% (w/v) saponin, 2% (w/v) BSA, 20mM glycine in PBS). Primary antibodies were prepared (1:200 dilution) in this solution too, and antibody-pairs were used for each well apart

from negative controls. 100µl primary antibody mix was added into each well and incubated overnight at 37°C in a humidified incubator, water-soaked tissue put next to plate. Next day, all liquids were aspirated and the well's boundaries were removed from glass slide. Cells were washed a couple of times using block/permeabilization solution and later proximity probes were diluted 1:5 in the same solution and cells incubated at 37ºC in a humidified chamber for 90 minutes. These probes are the secondary antibody, into which a single stranded DNA oligonucleotides is attached, for previously added primary; thus two different species were used, mouse and rabbit in our assay. Post incubation, cells were washed with 0.05% (v/v) Tween-20 in TBST followed by incubation with hybridization-ligation solution for 30 minutes at 37ºC with humidity. Another wash with 0.05% (v/v) Tween-20 in TBST after incubation was followed by incubation with amplification-detection solution for two hours at 37ºC with humidity. Thorough washings followed the last incubation using a series of dilutions of the kit's washing buffer (0.2M Tris base and 0.1M NaCl) and left to dry. The whole slide, 8 samples, was mounted using a kit-provided solution that contains DAPI stain for nucleus. Later, slides were examined using 63X oil immersion objective lens fitted to a Zeiss LSM Pascal Exciter confocal fluorescence microscope, and images were analyzed using LSM software (Zeiss). Obtained images were analysed using a special software for this assay called Blobfinder that can detect positive signals in the form of blobs and also determine the cytoplasm and nucleus area. Data collected from Blobfinder software was statistically tested for any significant differences between conditions using GraphPad Prism.

2.9 Fluorimeter analysis & anisotropy

2.9.1 IANBD labelling

Environmental changes in solution can be detected using fluorescent probes signalling changes in protein structural conformations. One of these probes is IANBD Amide [*N*,*N*'-Dimethyl-*N*-(Iodoacetyl)-*N*'-(7-Nitrobenz-2-Oxa-1,3-Diazol-4-yl)Ethylenediamine] which is a thiol-reactive amide that binds to cysteine

residues and can be excited to emit. Thus different proteins combinations or buffers affecting structure can be detected. We used IANBD (ThermoFisher, D2004) to label Sx4 and SNAP23 recombinant proteins. They were N-terminally GST-tagged with a thrombin cleavage site; proteins were labelled on beads then cleaved off beads and dialysed. Proteins were expressed in E. coli BL21(DE3) as described previously (section 2.3.1) and affinity purified using glutathione sepharose beads and left on beads after washes step. Beads were washed further using a suitable labelling buffer (20 mM Hepes pH 7.5). The reducing agent must be absent in these steps as it will interfere with subsequent labelling. IANBD was prepared in labelling buffer to a concentration of 25mg/ml and 3ml (2mM) were added into the beads and incubated for two hours at room temperature, or overnight at 4^{o}C, with tube covered in foil (light sensitive) and rolling mixed. Beads were collected by a spin at 1000g for 5 minutes and all liquid aspirated. The beads were then washed with PBS containing 10 mM ß-mercaptoethanol to quench the reaction followed by a wash without reducing agent, to ensure removal of free probe molecules.

Labelled protein was cleaved off beads using thrombin by incubation with thrombin in PBS for three hours at room temperature with rolling mixing. Beads were collected by centrifugation at 1000g for 5 minutes and liquid above contained the cleaved protein which was collected and kept on ice. Beads were washed with further 1ml PBS to obtain as much protein as possible and collected after beads spin in a separate tube than first collection. Both collections went through buffer exchange dialysis and 200µl aliquots stored in -80^{o}C covered in foil. Throughout the purification process, samples were collected and SDS-PAGE was run.

2.9.2 Fluorescence scanning

Prior to starting the assay, all SNAREs were quantified for protein concentration and scanned through the fluorimeter at 190-600nm. Equal protein molarity was used in all reactions and PBS was the reaction buffer at room temperature while reactants were kept on ice at all times before mixing to ensure integrity. Labelled protein, Sx4 or SNAP23, was added into PBS in the Fluorimeter cuvette

and scanned, followed by addition of participating proteins and mixing by inversion and removal of air bubbles, then scanned again. The initial scan was used as the baseline and its intensity subtracted from tested values. Results were analysed for significant differences using GraphPad Prism software.

2.10 Oil Red O stain

3T3-L1 cells were grown and differentiated as described above (section 1.10.1). In preparation, fresh stain is prepared from stock, passed through a filter to get rid of un-dissolved crystals, and kept in closed container since solvent evaporation causes stain precipitation. On the day of use, media was removed and cells washed 3X with PBS. Cells were fixed in 10% formalin for 2 hours to overnight at room temperature (4^{o}C for overnight). Fixing solution was removed and cells washed with water a couple of times followed by a rinse with 60% isopropanol. Freshly prepared stain was added to cells for 15 minutes at room temperature, to stain fat droplets (Lillie and Ashburn, 1943). Stain was discarded and cells rinsed with 60% isopropanol and briefly (1 minute) stained with haematoxylin (stains nucleus) followed by a water rinse and, after drying, mounting on microscope slide. The stained cells would show lipids in red and nuclei in blue. Images were taken using an inverted light microscope fitted with colour camera.

2.11 Total membrane fraction preparation

The total membrane fraction was prepared as described in a protocol developed in our group (Sadler et al., 2016).Cells were serum starved overnight using 5ml serum-free DMEM. Cells were washed in ice-cold PBS then scraped off dishes in 1ml of lysis buffer, lysed by passing through a 26G needle and nuclei pelleted by centrifugation at 3,000 xg for five minutes at 4^{o}C. A total membrane fraction was collected by ultracentrifugation of the supernatant from this spin at 100,000 xg for 60 minutes at 4^{o}C. The resulting membrane pellet was suspended in lysis

buffer, then sample buffer 2X LSB was added in equal volume. Samples were separated by 12% SDS-PAGE followed by immunoblotting for proteins of interest.

CHAPTER THREE

3 Characterization of phosphomimetic Syntaxin4 mutants

3.1 Introduction

Previous studies (Schmelzle et al., 2006) have reported that both Sx4 and Munc18c are phosphorylated on tyrosine residues in response to insulin, and our lab has shown that cytosolic insulin receptor tyrosine kinase (CIRK) can phosphorylate both of these proteins directly *in vitro* (Aran et al., 2011). We felt it important as a first step in understanding the functional role of these events to confirm that such phosphorylation processes are evident in our hands. With that in mind, we set about performing immunoprecipitation of these proteins for analysis by Mass Spectrometry. Subsequently, we examined the functional consequences of these phosphorylation events using a range of *in vitro* approaches. The specific aims of this Chapter therefore were:

i. To confirm previous studies on the phosphorylation of key tyrosine residues within Sx4 and Munc18c.
ii. To ascertain whether phosphorylation of Sx4 regulated function using phosphomimetic mutant Sx4 species expressed in bacteria.
iii. To examine the suite of interactions between Sx4 and SNAP23 and VAMP2 and to assess how, if at all, phosphorylation of Sx4 modulated these.

3.2 Results

3.2.1 Confirmation of tyrosine phosphorylation residues in Sx4 and Munc18c

Sx4 and Munc18c were immunoprecipitated from resting and insulin-stimulated differentiated 3T3-L1 adipocytes using commercially available antibodies. Data from a typical experiment are shown in (Figure 3-1). Colloidal Coomassie staining was employed in tandem with parallel immunoblots to identify Sx4 and Munc18c, as shown in the figure. The appropriate bands were excised and sent for mass spectrometry with two aims; to confirm residues identified by Schmelzle et al, and also if possible to measure levels of phosphorylation at each site. Sx4 and Munc18c were excised from the gels by aligning with immunoblots

to ensure cutting the bands at the right location in gels (Figure 3-1). MS analysis was performed by the FingerPrints Facility, University of Dundee.
Mass spectrometry was able to successfully identify both the previously reported insulin-stimulated phosphorylation sites within Sx4, i.e. Y251 and Y115 (Figure 3-2); however this was not the case for Munc18c (Y521). The reasons for this are not clear, but may reflect low protein recoveries in the IP which were observed using several different sources of commercial antibodies (not shown). Different total protein concentrations, various different primary antibodies and buffer/lysis modifications were employed in an attempt to promote sample quality (e.g. beads were washed with high salt buffers), but without effect on Munc18c phosphorylation detection. Hence, this arm of the project was abandoned.

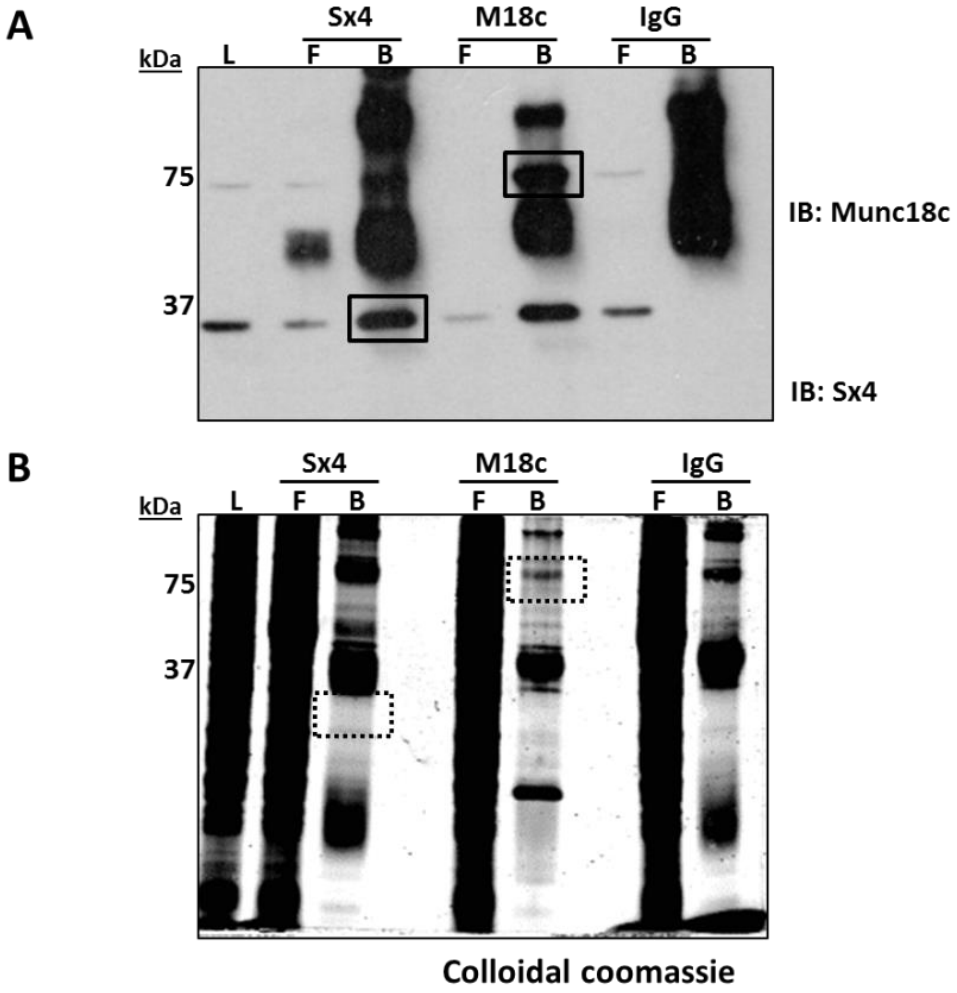

Figure 3-1 Immunoprecipitation of Sx4 from adipocytes is quantitative and can be used for MS.

Differentiated 3T3-L1 adipocytes were stimulated with 100 nM insulin for twenty minutes, lysed and used for IP as described. Samples of the lysate (L), flow through (F) and protein bound to beads

(B) were separated in 12% SDS-PAGE gels. Immunoblots (Panel A) and colloidal Coomassie stained gel (Panel B) are shown. Solid rectangles show positions of Sx4 and M18c in immunoblots while dashed boxes reveal the corresponding positions where the gel was cut and used for MS analysis. Note that in Panel A the nitrocellulose was incubated with anti-Sx4 and anti-Munc18c simultaneously and identified by the respective molecular weight. Note that Munc18c (M18c) and Sx4 co-immunoprecipitate in 3T3-L1 lysates. Data from a typical experiment is shown, repeated several times with similar results. In this experiment 10µl (84µg) was loaded for blots while 35µl (294µg) was used for the colloidal coomassie stained gel. The position of molecular weight markers is shown in kDa on the left.

3.2.2 MS analysis shows Y115 and Y251 are phosphorylated in adipocytes in response to insulin

Samples sent for analysis were first in-gel trypsin digested then injected into nanoLC system (Dionex/LC Packings) coupled to 4000 QTRAP (Applied Biosystems/Sciex), nLC-MS-MS. MS/MS fragment sizes from real sample were matched with expected values, using simulation software (i.e. prospector.ucsf.edu) to confirm the identity of the fragment. Levels of abundances of assigned peptides were compared (Figure 3-2) to look for changes between different conditions, in this case basal versus insulin. Control peptides from a different region were examined to exclude the possibility of total protein expression changes. The used technique called parent ion scanning, more commonly known as Parents of -79, to detect phosphopeptides prior to generation of tandem MS data that is then used to determine the site of phosphorylation.

Tyrosine sites 115 and 251 (Figure 3-2) were found to be phosphorylated in response to insulin, as shown previously in the study of Schmelzle et al. Although we have confirmed the identity of the sites noted by Schmelzle et al, we were unable to quantitate sites as detection of these sites is at the limit of the capability of the MS unit [FingerPrints Proteomics Facility (University of Dundee)] given the amounts of protein we can provide. One key aspect of this approach was to attempt to determine whether the same polypeptide was phosphorylated on both sites (i.e. Sx4-Y115 and Y251). We have approached this using other routes, which will be elaborated upon in later sections.

These sites may be functionally important, as Y115 is located in the N-terminal domain of Sx4, and this may be important in Munc18c binding (Latham et al., 2006) or binding to other components of the SNARE complex. This site may also be important in regulating the ratio of open/closed distribution of Sx4. Y251 is located in the SNARE domain hence may either regulate SNARE complex assembly or, like Y115, regulate the open/closed transition. Therefore, syntaxin4 phosphomimetic mutants in which tyrosine were replaced by the bulky glutamate residue were generated for further analysis. I generated single Y115E and Y251E mutants in full-length Sx4, in addition to the double phosphomimetic mutant, Y115, 251E, hereafter referred to as 2P. These mutants in the cytosolic domains of Sx4 (as C-terminal GST-fusions) have been previously made in the lab.

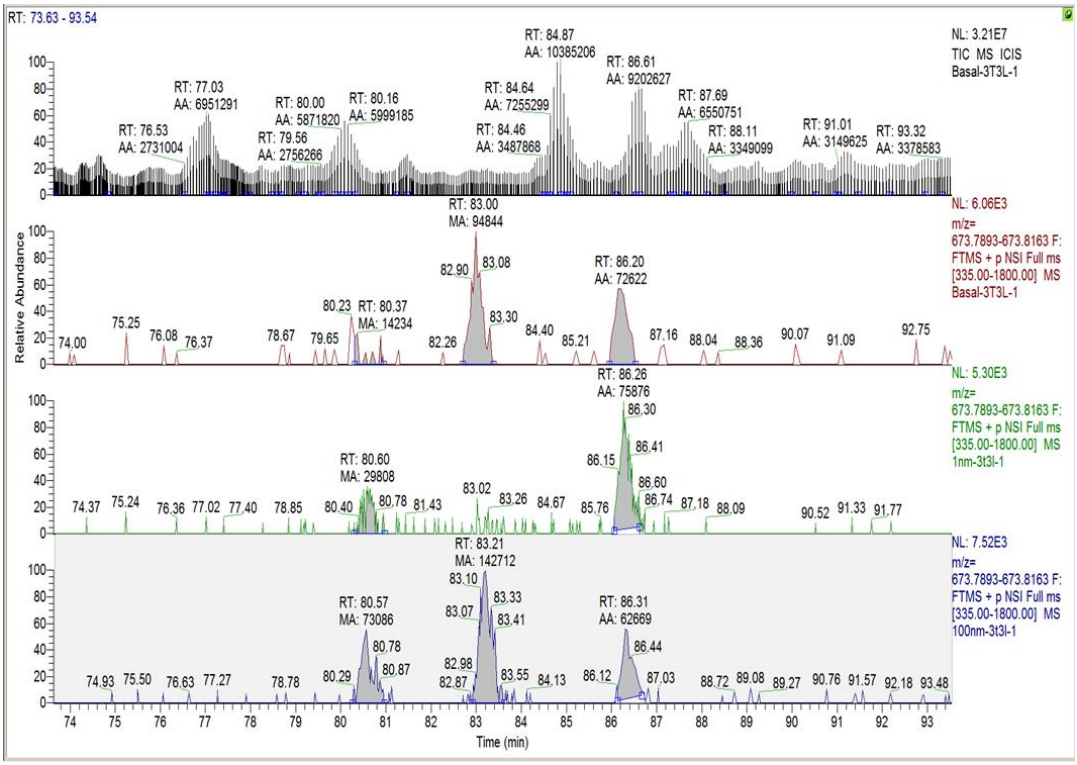

Figure 3-2 MS analysis shows Y115 and Y251 are phosphorylated in 3T3-L1 adipocytes in response to insulin.

MS/MS data for peptide NILSSADYVER, encompassing site Y-251 is shown. Here we present the relative abundance, total area under curve (AUC) for S4, S5, & Y8 (Y251) increased with insulin stimulation compared to basal control. Data from a typical experiment are shown; the MS analysis was repeated with three batches of immunoprecipitated material from three different cell platings. Shown in here, top panel represent HPLC chromatography spectrum showing separation of molecules according to their size or retention time, following three panels below are for the MS/MS

data showing different relative abundances of peptides at respective retention times found in the HPLC chromatogram. Mass spectroscopy (MS) spectrums shown, top-bottom, are for basal, 1nM, and 100nM insulin respectively.

3.2.3 Generation of recombinant Sx4 proteins

Expression of recombinant Sx4 mutants (Sx4 cytosolic domain 1-273 amino acids) was achieved using *E.coli* (BL21 DE3) using plasmids designed previously in our laboratory by Dr Veronica Aran-Ponte (University of Glasgow). Tyrosine 115 and 251 were replaced by a glutamic acid residue to mimic the negative charge of phosphorylated tyrosine and the bulky size. Expressed proteins were cytosolic and C-terminally GST-tagged (Figure 3-3). Other SNARE proteins were expressed including SNAP23, VAMP2, and Munc18c using different tags using similar approaches. Proteins of interest were purified in a good quality which was often further enhanced by dialysing samples to remove contamination. Proteins were stable within freeze-thaw cycles if kept at -20^{o}C prior to frequent usage and at -80^{o}C for longer-term storage (not shown).

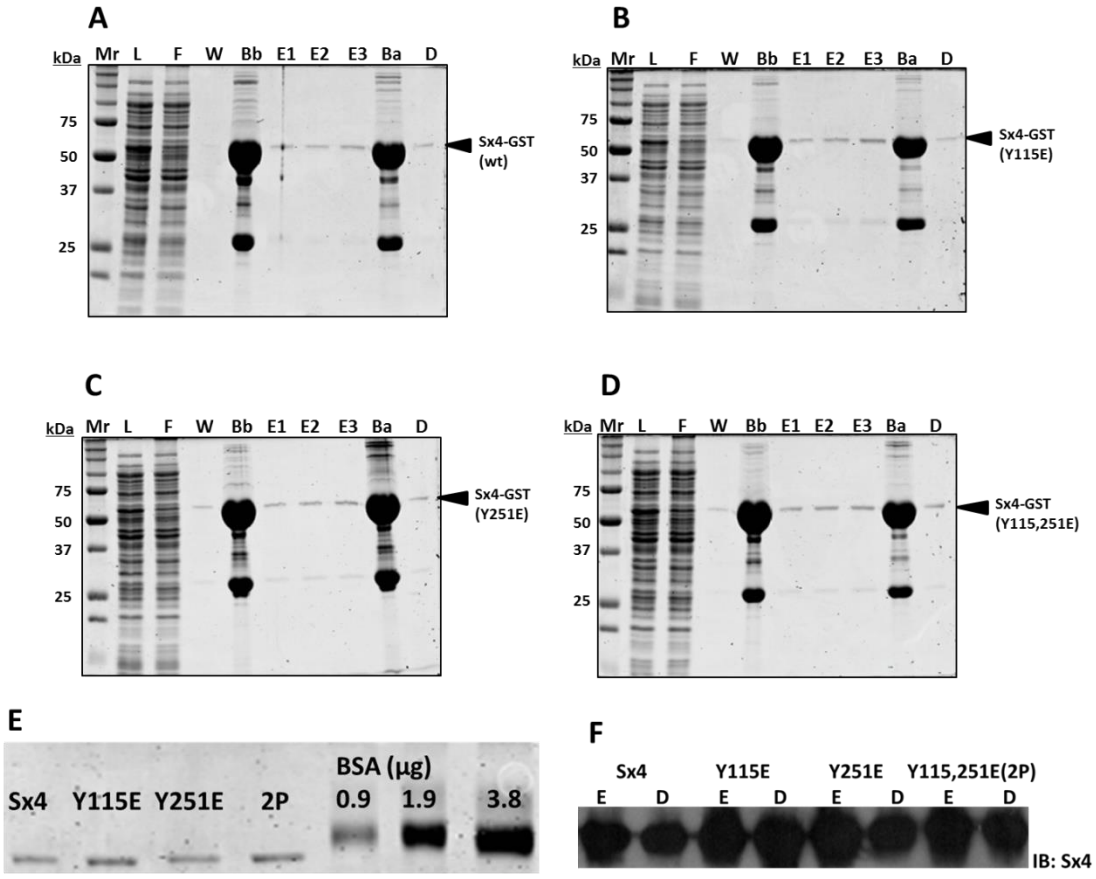

Figure 3-3 Representative purifications of Sx4-GST fusion proteins.

Sx4 species were over-expressed in *E. coli* BL21(DE3) and purified as outlined in section 2.3.1. Shown are representative Coomassie stained gels of fractions isolated from various stages of the purification of Sx4 phosphomimetic mutants: Panel **A** is wt Sx4; Panel **B** Sx4-Y115E; Panel **C** Sx4-Y251E, and Panel **D** is Sx4-2P. Shown are samples taken throughout purification process (L/Lysate, F/Flow, W/Wash, Bb/Beads before elution, E/Elution, Ba/Beads after elution, D/Dialysed sample), samples were boiled in 2X LSB at 95^{o}C for 5min prior to electrophoresis. Protein concentrations were quantified by comparison to BSA standards, and an example is shown in Panel **E**. Protein identity was subsequently confirmed by immunoblots, Panel **F**. Elution of these proteins from beads was not always effective, as shown by the high level of recombinant protein left on the beads (Ba); however sufficient protein was eluted for our needs so this issue was not optimised further.

Tag dimerisation and binding interference may result in misleading findings using recombinant proteins. Therefore, I generated variations of wild-type and Sx4-2P which harboured a thrombin cleavage site between the GST, present at the N-terminus, and the Sx4 cytosolic domain without transmembrane motif.
Figure 3-4 shows that a good yield of Sx4 or Sx4-2P was obtained using this method; this allowed examination of interactions free from potential interference of the purification tag.

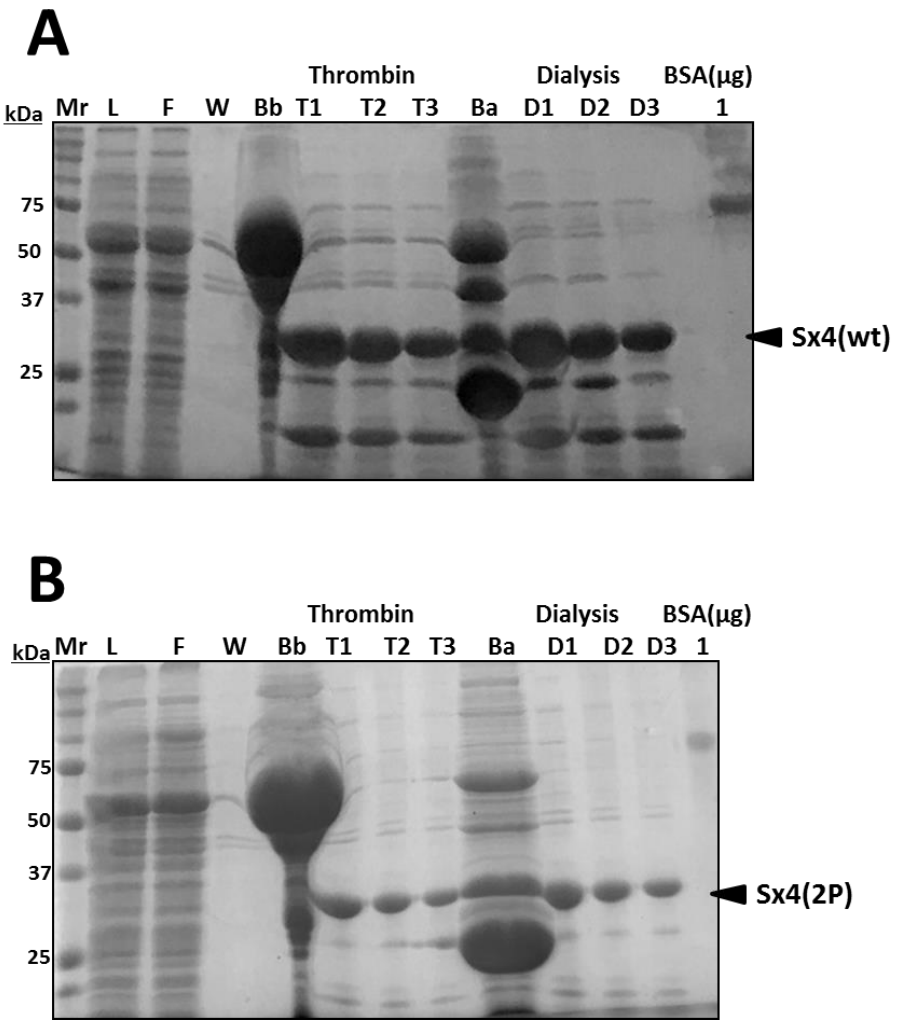

Figure 3-4 Purification of cleaved forms of Sx4, wt (A) and 2P (B).

Proteins were expressed using *E. coli* BL21(DE3) as an N-terminally GST-tagged with a Thrombin cleavage site. Coomassie-stained gels showing representative samples taken throughout the purification process (L/Lysate, F/Flow, W/Wash, Bb/Beads before cleavage, T/Thrombin cleavage, Ba/Beads after cleavage, D/Dialysed sample), samples boiled in 2X LSB at 95^{o}C for 5min. 12% SDS-PAGE gels were used to separate protein bands and gels were Coomassie stained.

3.2.4 SNARE complex formation *in vitro*

Ternary SNARE complexes form *in vivo* between tSNAREs from the plasma membrane, specifically Sx4 and SNAP23 and a vSNARE from the approaching GLUT4 storage vesicle (GSV) - VAMP2 (Kawanishi et al., 2000.; St-Denis, Cabaniols, Cushman, & Roche, 1999). This complex is highly stable, and is characterised as being both SDS- and heat-resistant (Flaumenhaft et al., 1998; Rea et al., 1998). This latter property has been used in this lab to assay the formation of SNARE complexes *in vitro* (Kioumourtzoglou et al., 2014). We

therefore used a modification of this assay to examine the effect of phosphomimetic mutations on SNARE complex formation mixed together in solution. To replicate these *in vitro*, purified recombinant SNARE proteins were mixed in equal molar ratios to first establish that an SDS and heat resistant protein complex was formed at high molecular weight in solution (Figure 3-5). Control experiments in which one of the three proteins was omitted did not show the formation of the complex (Figure 3-5).

A second complex formation assay was tested in which Syntaxin4 was immobilized in glutathione beads followed by addition of SNAP23 and VAMP2 incubated at 4ºC with mixing. Both assays gave qualitatively similar results, but the liquid based assay was used subsequently because of ease and reproducibility (this avoided the issue of aliquotting equal volumes of beads).

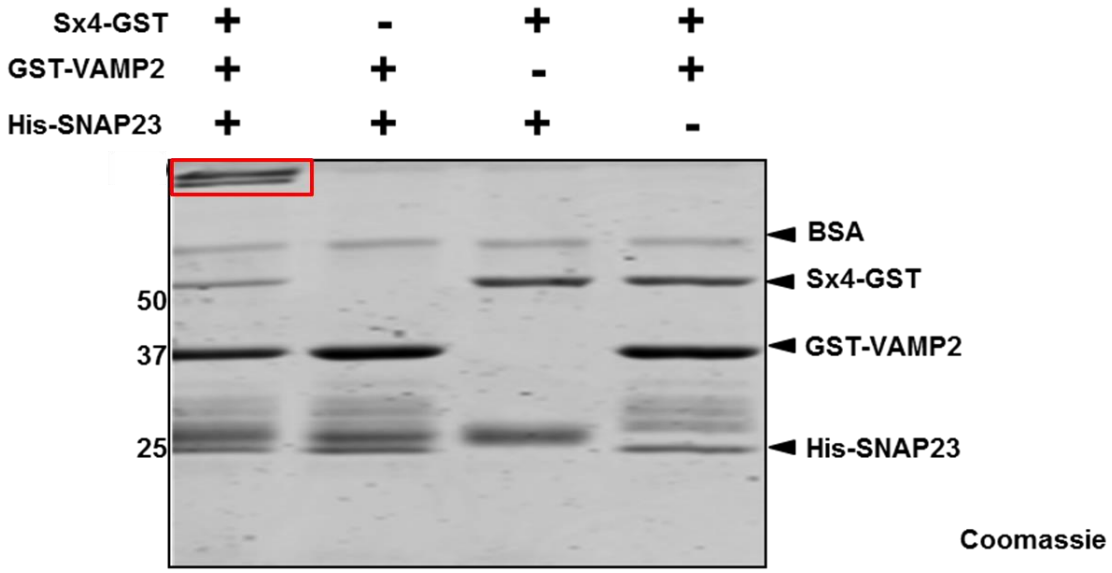

Figure 3-5 SNARE complex formation requires Sx4, SNAP23, and VAMP2.

Equal molar concentrations of the indicated proteins were mixed in PBS buffer at 4ºC and incubated for 15 minutes. A sample was then mixed with 2X LSB and boiled at 95ºC for 5min. Samples were analysed in 12% SDS-PAGE followed by Coomassie staining to reveal the presence or absence of the high molecular weight SNARE complex. Relative protein sizes are shown on left side of the gel in kDa.

We therefore used this complex as a tool to measure SNARE complex formation at different conditions such as time, the protein's phosphorylation status and different temperatures. It is important to note that the size of the SNARE complex cannot be estimated from this approach. Boiling in SDS-PAGE sample

buffer does not separate the constituent polypeptides as the ternary complex is stable under these conditions. Hence, it does not migrate as would be expected for a single, elongated polypeptide chain and its molecular weight does not equate to that of the individual components. Moreover, it is possible that higher order oligomers of SNARE complexes may form. Nevertheless, this assay is widely used to estimate the effectiveness of SNARE complex formation (Kioumourtzoglou et al., 2014).

3.2.5 2P exhibits enhanced SNARE complex formation in vitro

We tested whether there was a difference in SNARE complex formation using the phosphomimetic Sx4 mutants, i.e. Y115E, Y251E, and 2P compared to wild-type Sx4 in assays containing equimolar amounts of the different t- and v-SNAREs. The results of a typical experiment are shown in Figure 3-6; we consistently found that the amount of SNARE complex formed was higher in the phosphomimetic mutants compared to wild-type Sx4. The double phosphomimetic (2P) formed the highest amount followed by Y251E and Y115E (Figure 3-6). Y251E and 2P formed as much as 2-fold more complex than wt. Statistical analysis using one-way ANOVA showed significant differences between Sx4 and 2P (p-value 0.001-0.01) and phospho-mutant Y115E is significantly different to 2P (p-value 0.01-0.05).

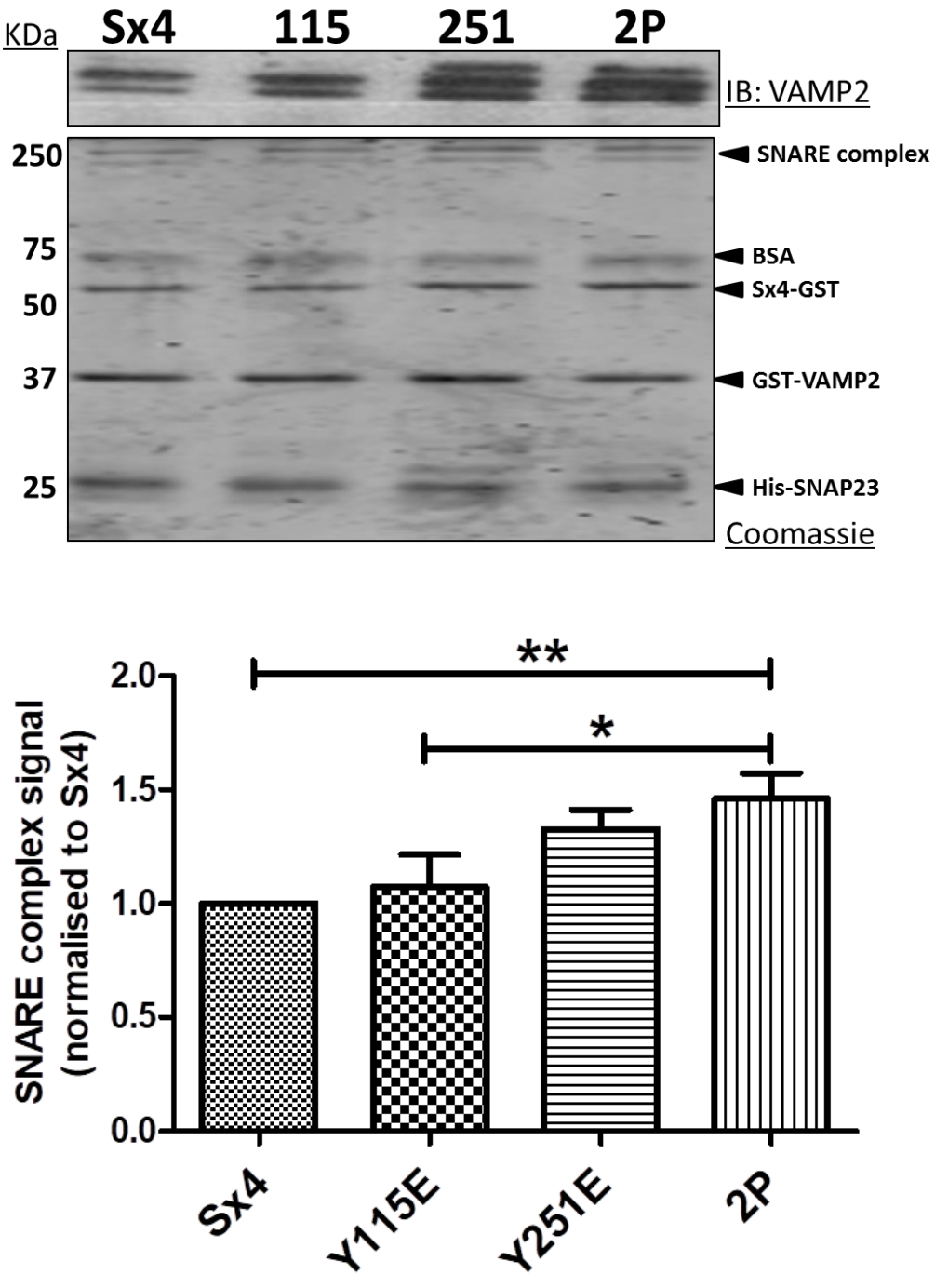

Figure 3-6 SNARE complex formation is enhanced in the phosphomimetic mutants.

Double phosphomimetic (2P) and 251 form more complex compared to wt while for 115 a slight increase is observed. Blots were analysed using ImageJ software to quantify band intensity and plotted as normalized to the wild type (Sx4). Syntaxin4 phosphomimetic mutants, wild type (Sx4), Y115E (115), Y251E (251), and Y115, 251E (2P), mixed with equal molar concentrations of SNAP23 and VAMP2 in PBS buffer supplemented with 10 µg BSA at 4^{o}C for 15 minutes. The sample was mixed with 2X LSB, boiled at 95^{o}C for 5 minutes, and proteins resolved in 12% SDS-PAGE. Proteins visualised by coomassie stained gel, lower panel, or developing immunoblot for VAMP2, upper panel. SNARE complex quantified from blot by densitometry using ImageJ software and plot in column graph shown. Experiment repeated with similar results and shown is

representative. Protein molecular weight sizes displayed on left of the figure, kDa. One-way ANOVA statistical test showed significant differences, p-value 0.0054. Significance label: *p-value 0.01 to 0.05; ** p-value 0.001-0.01).

3.2.6 SNARE complex formation is independent of the Tag on the VAMP2

In the experiments shown in Figure 3-6, GST-Sx4 and GST-VAMP2 were employed; we felt it important to evaluate whether the potential of GST dimerization might influence our data. To that end, we repeated the comparison of wild-type and 2P-Sx4 in the liquid SNARE complex formation assay using VAMP2 containing different tags (Protein-A tagged or hexa-his tagged). Consistently, 2P formed more complex than wt Sx4 using all the different tagged VAMP2 proteins (Figure 3-7) supporting the notion that the enhanced SNARE complex formation seen in Figure 3-6 is independent of the tag and reflects a real biological effect on SNARE complex formation. As expected, the sizes of the complexes formed differed, presumably reflecting the different sizes of the tags employed (Figure 3-7).

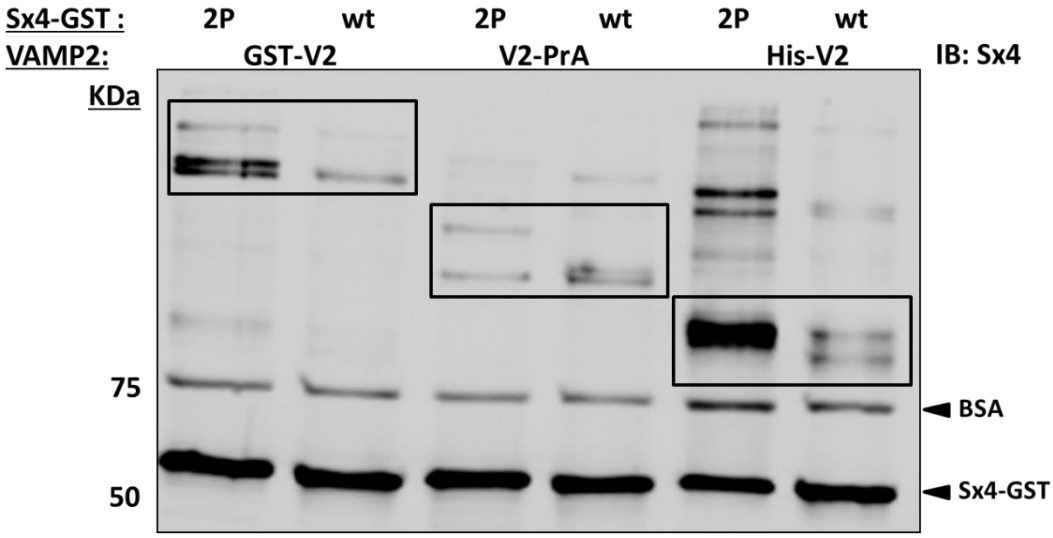

Figure 3-7 SNARE complex formation is independent of participant tag.

SNARE complex formation was assayed liquid form at 4^{o}C by mixing equal protein concentrations of Sx4-GST (wt or 2P) and His-SNAP23 with different VAMP2 forms, either GST-V2, V2-PrA, or

His-V2 in PBS buffer supplemented with 10 µg BSA at 4^{o}C for 15 minutes. Samples were mixed with 2X LSB, boiled at 95^{o}C for 5 minutes, and proteins resolved in 12% SDS-PAGE followed by immunoblotting for Sx4. The experiment was repeated with similar results and shown above is a representative blot. Protein molecular weight sizes displayed on left of the figure, kDa. Variable VAMP2 sizes, as a result of the different tags, result in different complex sizes. As predicted based on previous work, 2P gives stronger signal compared to wt through different tags on VAMP2.

3.2.7 An alternative assay of SNARE complex formation

Given the rather cumbersome assay of SNARE complex formation noted above, we have attempted to use other approaches to assay complex formation. IANBD amide (ThermoFisher; D2004) is an environmentally sensitive label and cysteine reactive fluorescent probe which may be used to monitor structural changes. We reasoned that this may report on environmental changes in this region as the Sx4 transitioned into a SNARE complex. Sx4 was fluorescently labelled at the only cysteine residue, located in the hinge region between the SNARE and Habc domains, using IANBD *in vitro*. Fluorescence intensity was monitored following different Sx4 interactions with both individual SNARE proteins and in the case of ternary SNARE complex formation. Minor fluorescent changes resulted from SNARE complex formation compared to signal from labelled Sx4 itself were observed, but these were small (data not shown). This region is likely to be in contact with solvent water and may not detect change in environment during interactions or complex formation. Therefore, we turned instead to SNAP23 for similar labelling, as there are five cysteine residues in this protein and it was hoped these would give a greater change in signal upon interactions.
Labelled SNAP23 gave clearer results than Sx4 probably due to the number of labelled cysteine residues, thus better signalling the conformational changes taking place. SNAP23 was expressed as an N-terminal GST fusion protein with a Thrombin cleavage site; the protein was labelled on beads followed by Thrombin cleavage and dialysis (Figure 3-8 **A**). Protein fluorescent label was examined spectrophotometrically compared to un-labelled SNARE proteins, and also checked by immunoblotting (Figure 3-8 **A**).

Labelled SNAP23 was mixed, in PBS, with Sx4 wt or Sx4-2P, followed by addition of the rest of the SNARE's and fluorescence readings were taken after additions

and at different time points from SNARE complex formation step. We observed fluorescence intensity increases upon binary interactions between Sx4 (wt) and SNAP23 (compare the blue and pink lines in Figure 3-8 **B**). Further increases were observed in a time-dependent manner presumably reflecting the formation of the SNARE complex (Figure 3-8 **B**). A similar trend was found using Sx4-2P (Figure 3-8 **C**). Previously, using the *in vitro* SNARE complex assembly assay (Figure 3-6), Syntaxin4 2P gave stronger signal for the complex compared to wt or other single phosphomimetic mutants. Similar results were observed here using labelled SNAP23 to report on SNARE complex formation. Hence, this technique supports our previous suggestion that Sx4-2P makes more complex than wild-type Sx4.

To quantify the difference between wt and 2P forms, the SNARE complex fluorescent signal at different time points after addition of all components was normalized to the original SNAP23 signal used in the reaction (Figure 3-8 **D**). Consistent with previous findings, Sx4-2P produced a higher intensity fluorescence signal than Sx4-wt. The change in fluorescence observed, which we interpret to reflect the formation of a ternary complex, was consistently found to take place faster and more extensively with Sx4-2P compared to wild-type Sx4 (Figure 3-8 **D**). The results from this assay are consistent with the hypothesis that double phosphomimetic (Sx4-2P) formed more complex, and faster, than wild type (Sx4-wt) (Figure 3-8 **D**).

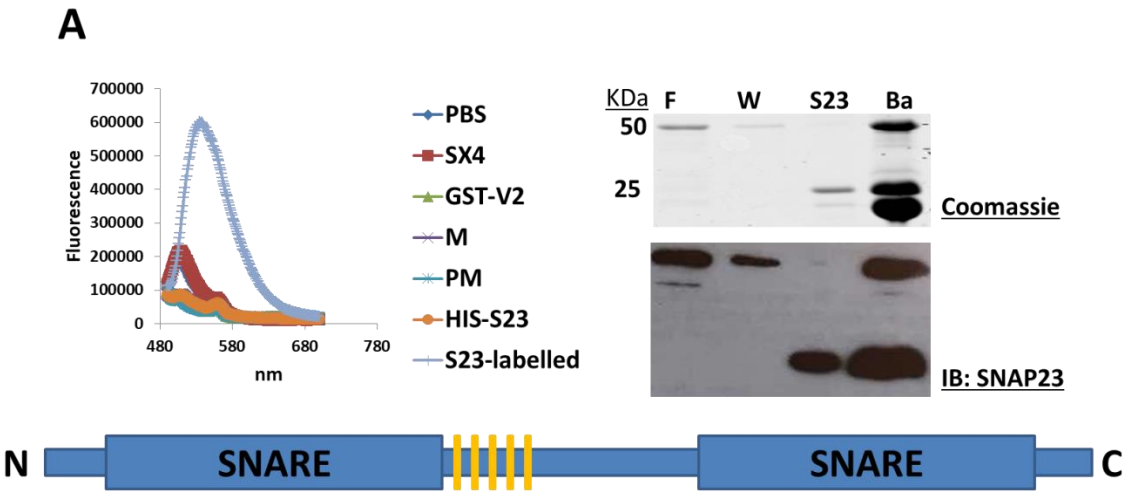

B

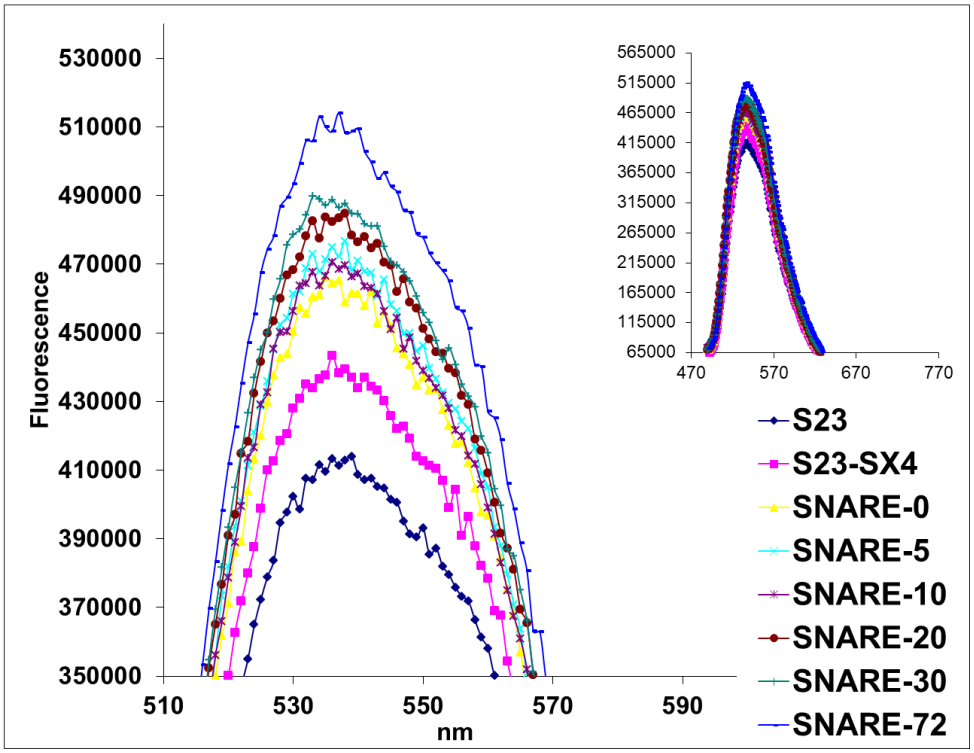
Fluorescence
530000
510000
490000
470000
450000
430000
410000
390000
370000
350000
510
530
550
570
590
nm
565000
515000
465000
415000
365000
315000
265000
215000
165000
115000
65000
470
570
670
770
S23
S23-SX4
SNARE-0
SNARE-5
SNARE-10
SNARE-20
SNARE-30
SNARE-72

C

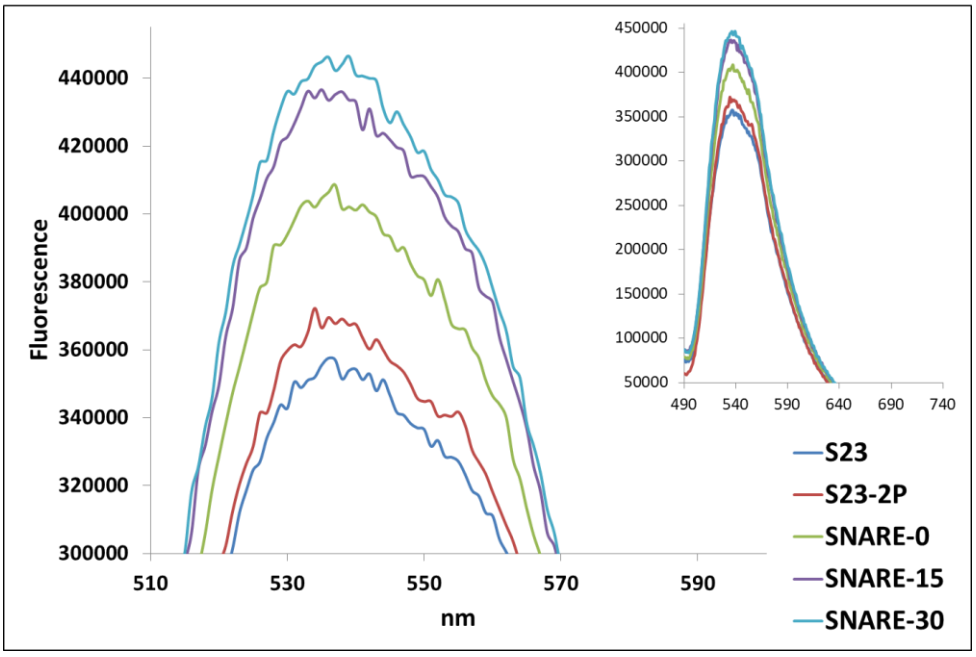
Fluorescence
440000
420000
400000
380000
360000
340000
320000
300000
510
530
550
570
590
nm
450000
400000
350000
300000
250000
200000
150000
100000
50000
490
540
590
640
690
740
S23
S23-2P
SNARE-0
SNARE-15
SNARE-30

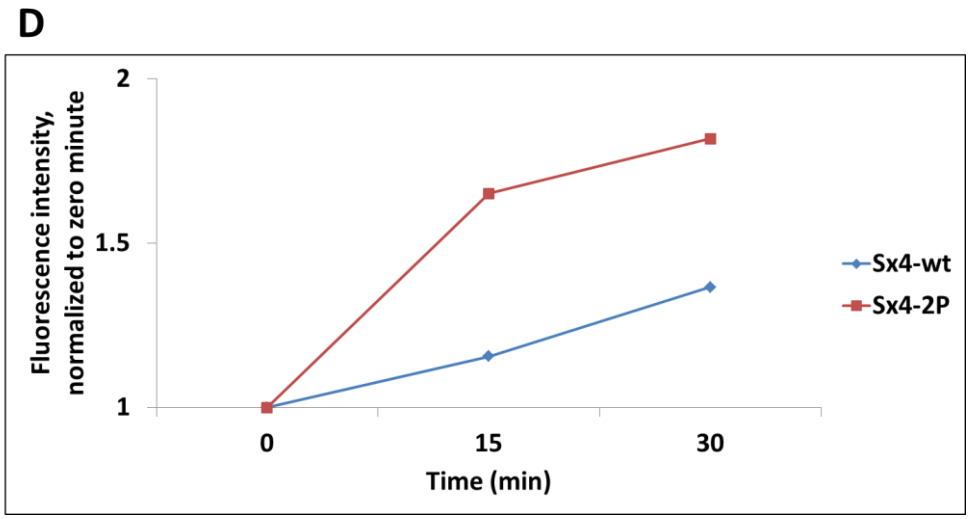

Figure 3-8 Fluorescent environment-sensitive label show signal intensity change upon SNARE complex formation through time and Sx4 mutants status.

Panel **A**: S23 was expressed and purified as N-terminus GST-Tagged with Thrombin cleavage site followed by labelling with IANBD fluorophore targeting cysteine residues, and then cleaved off beads. Samples run on SDS-PAGE and immunoblotted for S23 showing clean protein prep (F/Flow, W/Wash, S23/cleaved S23, Ba/beads after cleavage). Labelled S23 was scanned compared to all other (non-labelled) SNARE proteins to be used. Schematic representation of SNAP23 showing main domains and labelled cysteine residues, in orange. Panels **B** and **C** show representative examples of the changes in SNAP23 fluorescence with time as the indicated combinations of proteins were added. Thus in Panel **B**, the spectra of S23 is shown, then that after addition of Sx4, then at various times after addition of VAMP2. The same is shown in Panel **C** for Sx4-2P. Inset shows the full scan. Panel **D** shows that fluorescence intensity increases with time for both wild-type Sx4 and Sx4-2P, but the latter changes more extensively and faster. Readings at scan peaks, 530nm, plotted at different time points (normalized to S23 signal) showing higher signal from Sx4-2P compared to Sx4-wt. Data from several experiments revealed similar trends. These were not directly compared as the magnitude of the effect varied between batches of labelled protein. Rather, data from a typical experiment is presented.

3.2.8 Pairwise interactions of Sx4 and Sx4-2P with VAMP2 and SNAP23

The data presented above reveal that Sx4-2P appears to make more SNARE complex faster than wild-type Sx4. In order to dissect the reasons for these observations, we investigated the pair-wise interactions of Sx4 with either SNAP23 or VAMP2. To achieve this, several approaches were employed. Firstly, a

pull down assay was used to investigate binding. C-terminal GST-tagged Syntaxin4 phosphomimetic mutants were immobilized on glutathione-Sepharose beads followed by addition of SNAP23 or VAMP2 and incubation with mixing for 30 or 60 minutes at 4°C. In these experiments, an open mutant of Sx4 (L173A, E174A) was used as a positive control. These mutations which are in the linker region of Sx4, result in the protein maintaining an open conformation (Aran et al., 2009). After mixing with the target (SNAP23 or VAMP2), the beads were washed extensively, boiled, 95°C for 5 minutes in 2X LSB and the bound proteins analysed by SDS-PAGE and immunoblotting. The data is shown in Figure 3-9 (for SNAP23) and Figure 3-10 (for VAMP2). These experiments were performed jointly with Hannah Black.

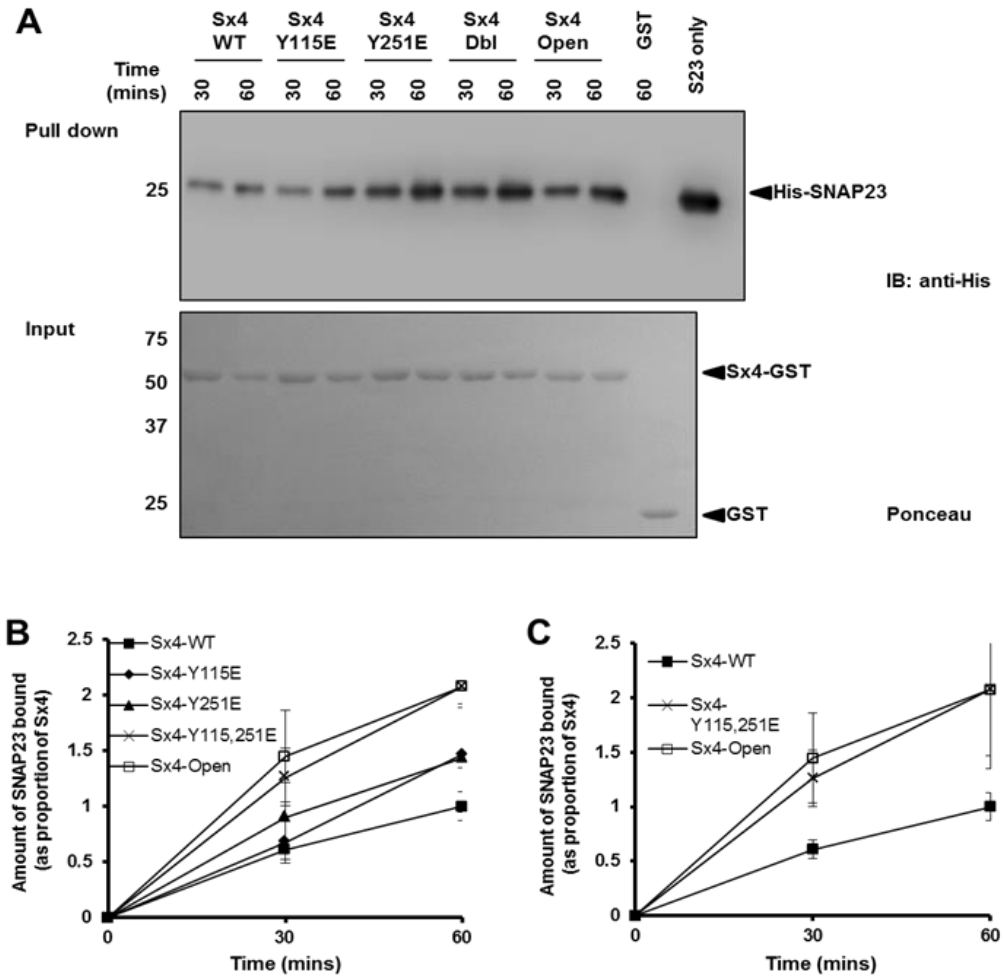

Figure 3-9 Phosphomimetic Sx4 mutants bind more SNAP23 than WT.

Immobilised Sx4-GST was incubated with an approximately equimolar amount of His-SNAP23 for 30 and 60 minutes at 4°C with rotation. Beads were collected and washed extensively before being subjected to SDS-PAGE and immunoblotting to analyse the amount of SNAP23 bound. Panel **A**:

Representative anti-His immunoblots (top) and ponceau stained membrane (bottom). The amount of SNAP23 pulled down by Sx4 beads was quantified using densitometry and expressed as a proportion of Sx4 (from the same sample shown in Ponceau). Panel **B** shows quantification of this data; Sx4-phosphomimetic mutants and the Open mutant showed an increase in SNAP23 binding compared to the WT protein. Normalized band intensity plotted at different time points. Panel **C**: A simplified graph demonstrating the difference between the Sx4-Y115,251E and Sx4-Open mutant compared to the WT protein. One-way analysis of variance comparing means at 30 and 60 minutes, showed p values of 0.2 and 0.5 respectively thus these differences are not statistically significant.

Overall, a trend towards higher signal for all phosphomimetic mutants was observed compared to wild-type Sx4 (Figure 3-9). This likely reflects the fact Sx4 and SNAP23 are thought to form a binary complex in the plasma membrane *in vivo*. This data suggests that this pairwise interaction might be increased by tyrosine phosphorylation of the Sx4 protein on either or both of these sites; we hypothesise this may be a consequence of the Sx4-2P adopting a more 'open' conformation thus facilitating interaction with SNAP23, a point we will return to below. The double mutant shows a trend towards increased binding compared to either individual mutant, probably reflecting an additive effect with both phospho-sites contributing to the tendency towards an open conformation.

Vesicle SNARE, VAMP2, binding to Sx4 was examined using a similar approach, also in collaboration with Hannah Black. Interaction between VAMP2 and Sx4 has previously been reported, but these appear to be of low affinity (Foster et al., 1998). Data from this analysis is presented in Figure 3-10. Longer incubations were needed for a good signal in pull down assays especially for wild type Sx4. Phosphomimetic Sx4 mutants consistently show a trend towards enhanced binding. The open mutant also showed enahnced binding to VAMP2 in this assay. Quantification of the data from multiple experiments of this type is presented in Figure 3-10 **B-C**.

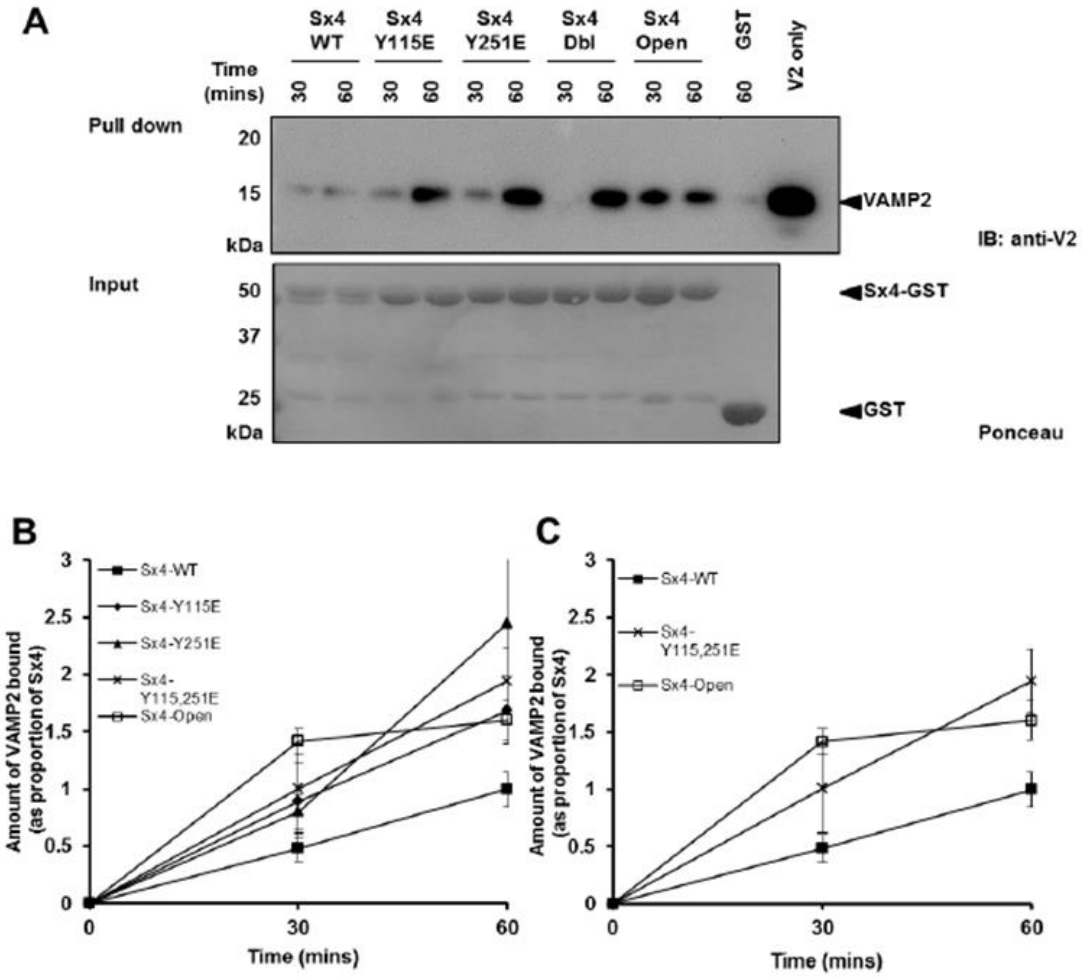

Figure 3-10 Phosphomimetic Syntaxin4 mutants show increased binding to VAMP2 compared to WT.

Immobilised Sx4-GST was incubated with VAMP2 for 30 and 60 minutes at 4°C with rotation mixing. Beads were collected and washed extensively before being subjected to SDS-PAGE and immunoblotting (anti-V2) to analyse the amount of VAMP2 bound. Panel A: Sx4 mutants bind more V2 compared to WT. A representative anti-VAMP2 immunoblot, top, and ponceau-stained blot, bottom, developed for all samples at different time points. The amount of bound protein was quantified using densitometry and expressed as a proportion of Sx4 (from the equivalent sample in ponceau-stained blot). Panel B: Normalized quantification of Sx4 binding, all samples, to VAMP2 plotted against incubation time. Sx4 mutant proteins show increased binding to VAMP2 when compared to WT. Panel C: A simplified graph demonstrating the difference between the Sx4-Y115,251E and Sx4-Open mutants compared to the WT protein. n=3, error bars show standard error of the mean. One way analysis of variance statistical analysis was applied; P values obtained of 0.19 when comparing means at 30 minutes, and 0.24 after 60 minutes hence statistically not significant differences.

Collectively, this hints that phosphorylation is an essential regulator for SNARE complex formation. This is revealed by a trend towards enanched interaction of

both the binary Sx4/SNAP23 and Sx4/VAMP2 interactions and enhanced complex formation. This likely reflects a key interface between the insulin receptor signalling cascade and the trafficking machinery, as the insulin signalling cascade is a tightly regulated process both in terms of time and location.

3.2.9 Circular Dichroism (CD) spectroscopy and Isothermal Titration Calorimetry (ITC) to quantify binary interactions

Recombinant SNARE proteins were examined for secondary structure contents i.e. alpha helix, beta sheets, beta turns and disordered structures using circular dichroism (CD) with the aim of identifying whether changes upon SNARE complex formation could be observed; these experiments were performed with Dr Sharon Kelly (Protein Characterisation Facility, University of Glasgow). Each individual SNARE protein, Sx4, SNAP23, or VAMP2, was scanned separately showing details of secondary structure present in that protein (data not shown). The three SNARE proteins were mixed to allow ternary SNARE complex formation and then scanned for structural details. Using the single protein scans, the expected sum of spectra was compared to the scan obtained from mixing proteins (Figure 3-11). A conformational change following the interaction of the proteins is clear from the difference in the spectrum obtained experimentally (in blue) compared with expected (in red) spectral sum of the individual components. Therefore, it has shown here that a conformational change following the interaction of the proteins is clear from the difference in the spectrum obtained.

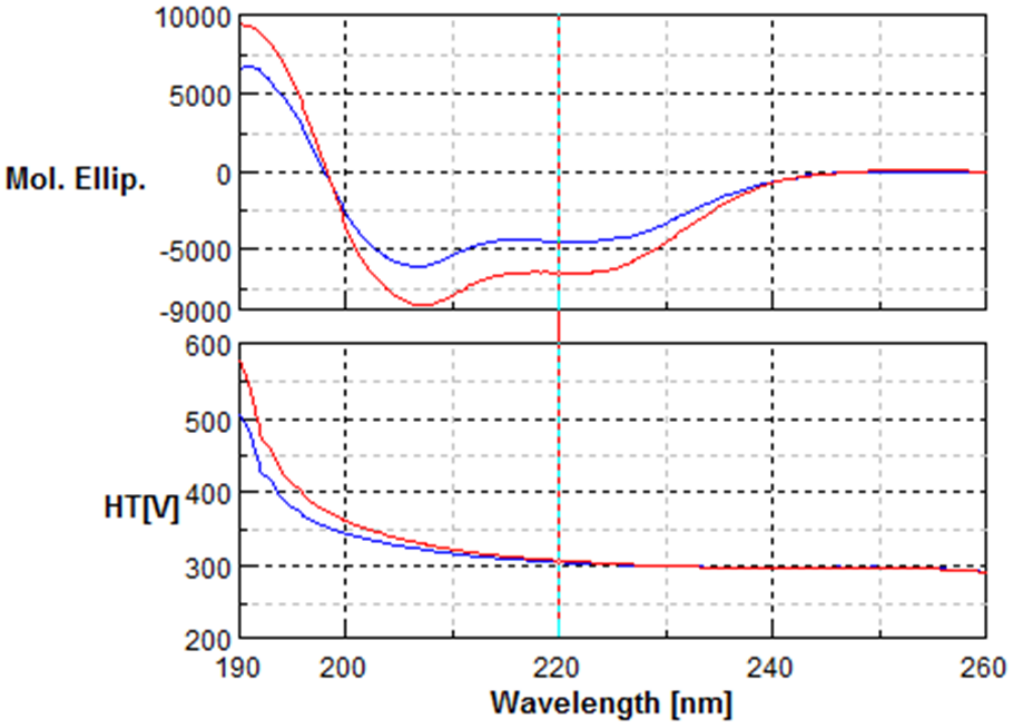

Figure 3-11 Far UV CD spectrum of ternary complex show conformation changes.

Following the mixing of VAMP2/Sx4/SNAP23 (blue) and the theoretical sum of the three singular spectra (normalised to reflect total protein concentration) (red). A conformational change following the interaction of the proteins is clear from the difference in the spectrum obtained compared with expected spectral sum of the individual components. Top graph shows molar ellipticity and second graph shows high tension voltage, HT[V]. HT stands for high tension, i.e. the voltage applied to the photomultiplier to keep the current constant and it roughly proportional to absorbance thus If the HT voltage goes above ~600 then the detector is saturated.

Quantification of the strength of binding between SNARE protein pairs might reveal how their pair-wise affinities are modulated by phosphorylation of Sx4. Although quantification of affinities can be obtained from pull-down type experiments, we approached this using more quantitative biophysical methodologies. Isothermal Titration Calorimetry (ITC) quantifies the affinity of two proteins and is widely used in analysis of SNARE proteins (Leavitt and Freire, 2001; Pierce et al., 1999). We therefore attempted to use ITC to quantify the Sx4/VAMP2 and Sx4/SNAP23 interactions. This approach required optimisation of the protein preparations used, as they were found in some cases to be contaminated with DNA.

Using highly purified protein preparations, a K_d of interaction between Sx4-2P and VAMP2 of 3.9 μM was measured; however, binding to wild-type Sx4 was either not detected or was found to be very weak with no end value reached in the titration experiments meaning that quantification cannot be attempted. It is not clear why no interaction is detected using this method; time constraints meant that this avenue was not further explored. However, the data does tentatively suggest that the interaction of Sx4 with VAMP2 is enhanced by the phosphomimetic mutations in Sx4-2P.

By contrast, evidence of interaction between Sx4-wt and SNAP23 was obtained. Sx4-2P showed tighter binding to SNAP23 (K_d 1.22μM) than Sx4 (K_d 5.6μM) (Figure 3-12). Syntaxin4 2P is ~5-times tighter binding than Sx4 wild-type. This finding is consistent with the pull down results where Sx4 2P binds more SNAP23 compared to wt.

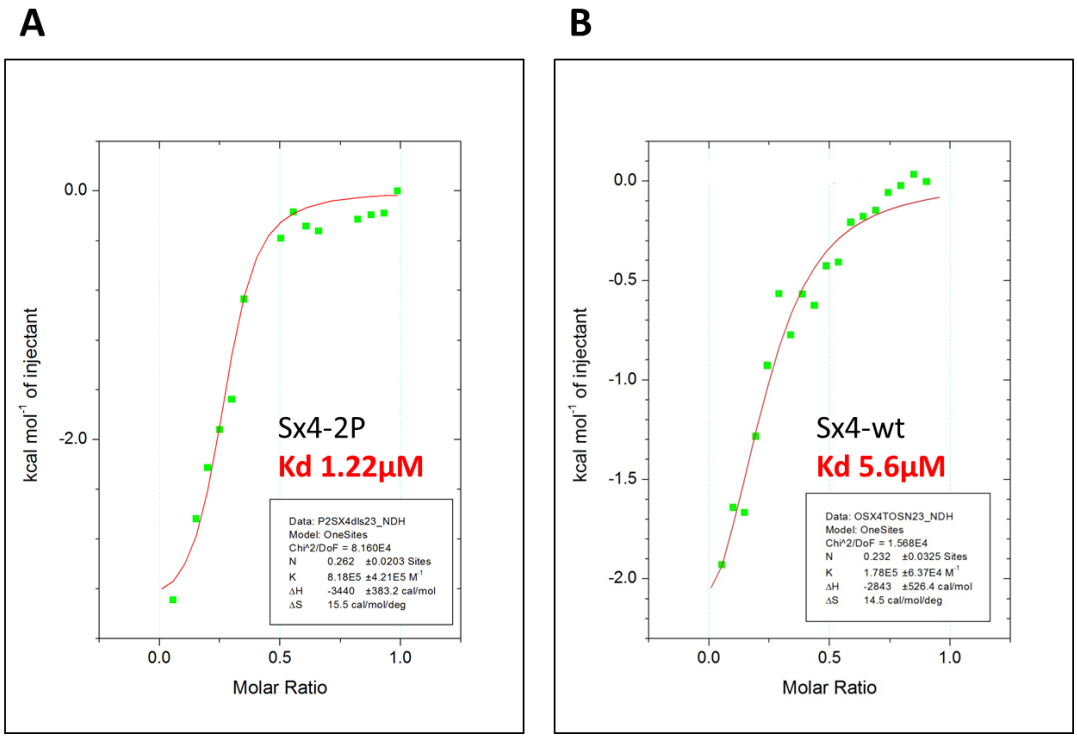

Figure 3-12 ITC data reveals that Sx4-2P binds SNAP23 tighter than Sx4-wt.

Panel A: Sx4-2P (308.25μM) in calorimeter was titrated with S23 (64μM) and the raw data fitted as shown with Kd 1.22μM. Panel B: Sx4-wt (298μM) was titrated with S23 (64μM) and the raw data fitted as shown with Kd 5.6μM. The Kd and stoichiometry of the interaction were calculated by fitting the data with a nonlinear least squares routine using Microcal Origin software. Measurements were performed using MicroCal VP-ITC instrument (Malvern). Parameters

measured: binding constants (Kd), reaction stoichiometry (N), enthalpy (ΔH) and entropy (ΔS). Shown is data from a representative experiment, repeated with similar results.

3.2.10 Phosphorylated Sx4 is in the open conformation.

Sx4 exists in two forms i.e. open and closed (Dulubova et al., 1999). Alternation between these conformers is thought to be regulated by Munc18c binding; in the closed form the SNARE domain is locked by Munc18c to the H_{abc} motif hence inhibiting Sx4 participation in ternary SNARE complex formation (Tamori et al., 1998). Munc18c also binds to the N-terminus which has been shown to enhance ternary complex formation (Brasher et al., 2017; Latham et al., 2006). Munc18c also binds to the assembled SNARE complex (Latham et al., 2006). Therefore, it was necessary to investigate which conformer the phosphomimetic Sx4 adopts, especially given our results showing higher affinity for SNAP23 and more ternary complex formed when 2P is used compared to wild-type Sx4. To address this, we used the approach of limited proteolysis. In this assay Sx4 proteins were incubated with Chymotrypsin for different times then samples analysed by SDS-PAGE; the open mutant has been previously shown to be more susceptible to chymotrypsin digestion than the wild-type Sx4 (Aran et al., 2009) (Figure 3-13 **A**). Sx4 mutants Y115E and 2P were digested to a degree comparable to the open Sx4, consistent with the hypothesis that phosphorylation alters the conformation of the Sx4 such that the open conformer is favoured. Syntaxin4 mutants Y115E, 2P, and open were digested to a significant degree compared to the wt (Figure 3-13 **B**). Interestingly, we consistently found that Y251E does not exhibit the same susceptibility to chymotrypsin digestion, suggesting that other hypotheses are required to explain enhanced binding/complex formation for this mutant.

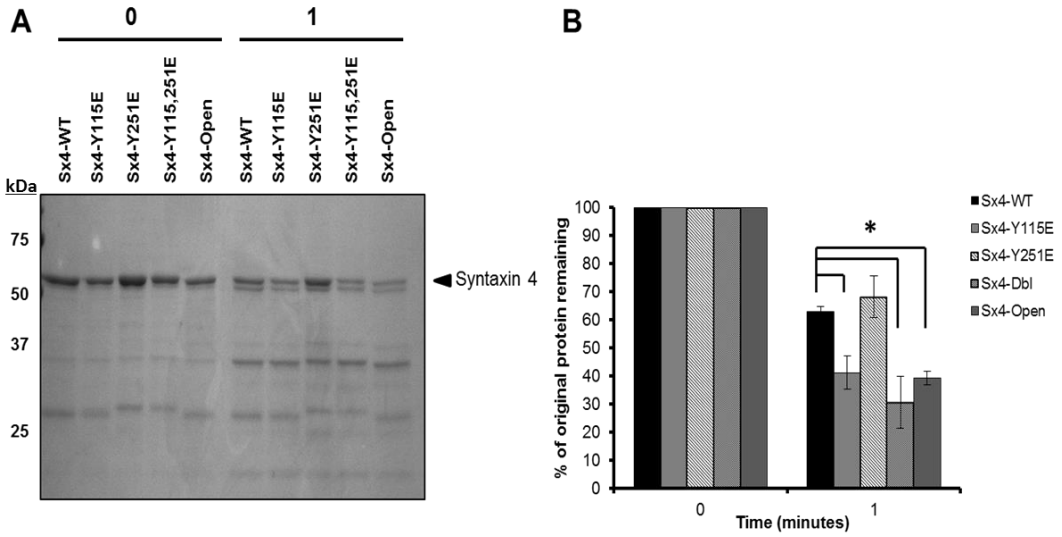

Figure 3-13 Sx4-Y115E and Sx4-Y115,251E show comparable sensitivity to limited proteolysis to the Sx4 open mutant.

Equal amounts of Syntaxin4 mutants WT, Y115E, Y251E, Y115,251E and Sx4-Open were incubated with chymotrypsin at room temperature for 0 and 1 minutes before the reaction was stopped by the addition of 2X LSB and samples boiled at 95°C for 5 minutes. Samples were analysed by SDS-PAGE and coomassie staining. Panel **A**: shows a representative coomassie stained gel showing samples digestion at time points. Panel **B**: Data were analysed using densitometry to calculate the amount of full length protein remaining compared to the protein at 0 minutes. Experiment repeated, n=3, error bars show standard error of the mean. Statistical significance was calculated using one-way ANOVA with a post-hoc Tukey test, * $p < 0.05$. This experiment was performed by Hannah Black, University of Glasgow using proteins prepared in Glasgow.

3.3 Discussion

Glucose homeostasis is mediated by the regulated trafficking of GLUT4 in adipocytes and muscle cells. They are stimulated with insulin. In response to insulin, GLUT4 is translocated from intracellular compartments to the cell surface, where the GLUT4-containing vesicles fuse into the plasma membrane through means of SNARE complex assembly. The SNARE complex for regulating GLUT4 fusion composed of syntaxin4, SNAP23, and VAMP2 (reviwed by Bryant & Gould, 2011). This process is tightly regulated in time and space, thus Sx4 complex participation is regulated by the Sec1-Munc18 family protein, Munc18c (Latham et al., 2006). Upon insulin stimulation, syntaxin4 (Sx4) is tyrosine phosphorylated in two sites, 115 and 251, and Munc18c at 521 in 3T3-L1 adipocytes (Schmelzle et al., 2006). Despite identification of these

phosphorylation events in Sx4, no further examination of biological consequences has been described. This chapter explores, *in vitro*, the effects of phosphorylation on Sx4 binary interactions, and Sx4 SNARE complex formation using recombinant, phosphomimetic Sx4.

Our first task was to confirm tyrosine phosphorylation sites in Sx4 and Munc18c. This was accomplished by immunoprecipitation (IP) of proteins and excision of the corresponding protein band, guided by blot-localised position (Figure 3-1) and sent to phosphorylation site mapping facility, University of Dundee-UK. Syntaxin4 and Munc18c were shown to co-immunoprecipitate from basal and insulin-stimulated 3T3-L1 adipocyte samples (Figure 3-1). Mass spectroscopy analyses confirmed Sx4 was tyrosine phosphorylated on residues Y115 and Y251; however Munc18c phosphorylation was hard to detect. Despite high sensitivity analysis and several attempts using different protein concentrations and enhanced IP modifications, we could not identify phosphorylation of Munc18c on Y521. The reasons for this are not clear. It is worth mentioning that the identified Sx4 sites were identified from raw data re-examined distinctly from the routine protocol – see Figure 3-2. Here, our approach included identification of tyrosine phosphorylation sites, within Sx4 and Munc18c; we hoped to ascertain whether one or other of the sites was phosphorylated with different kinetics; however, this approach was not robust enough to address this question. However, we will return to this point further in subsequent work.

The functional importance of Sx4 phosphorylation may be linked to roles in interactions with either regulatory proteins, for example with Munc18c through the N-terminus (Latham et al., 2006; Latham et al., 2007; Morey and Fasshauer, 2014), or via control of SNARE complex assembly, as Y115 and particularly Y251 which is located in the SNARE domain might be expected to exert an effect on SNARE complex formation. Therefore, it is vital to explore consequences of tyrosine phosphorylation at these sites on binary binding affinities with other SNAREs and equally important in formation of the ternary SNARE complex. Consequently, phosphomimetic mutants were expressed, using previously constructed plasmids in our group (Dr Veronica Aran-Ponte), where tyrosine replaced with glutamic acid to mimic negative charge on phosphorylated

tyrosine and occupy its bulky structure. The expressed proteins, corresponding to the cytosolic domain, are C-terminally tagged with GST in order not to affect its binding affinity to regulatory molecules (e.g. Munc18c binds the extreme N-terminus) or SNARE complex formation, which takes place by 'zippering' helices from N to C-terminal (Hu et al., 2007; Latham et al., 2007). Expression and purification of the phosphomimetic proteins resulted in good yields which were enhanced through dialysis (Figure 3-3). It is conceivable that sometimes tags on proteins may alter their interactions or binding affinities and in some cases could result in tags dimerisation. Therefore, tag-free versions of cytosolic wild type (Sx4) and double phosphomimetic (2P) were purified (Figure 3-4) to assure relevant interactions which represent physiological participating protein parts. Other SNAREs, SNAP23/VAMP2, and regulatory Sec1/Munc18, Munc18c, were also purified from bacteria.

Ternary SNARE complexes could be formed using recombinant proteins, *in vitro*, which yield a very stable high molecular weight protein complex that is resistant to SDS and heat (Kioumourtzoglou et al., 2014; Rea et al., 1998) and this feature was used to analyse Sx4 mutants on complex formation. Using purified recombinant proteins, SNARE complex was formed (Figure 3-5) only when complex components are all included in the reaction, i.e. Sx4/SNAP23/VAMP2. Complex size is more than collective masses of participating proteins; SNARE complexes may form oligomers and migrate much slower than the predicted sum of the component molecular masses (Rickman et al., 2005). Another factor is shape of complex such that boiling with SDS is unable to separate integrated polypeptides of the ternary complex and hence they would not migrate in gel similar to single, straight polypeptide chain as in normal cases. Consistently, phosphomimetic Sx4 mutants formed more complex compared to wild type and singular mutants increasingly showed more from mutant 251 to 115, in order (Figure 3-6). Statistical analysis revealed differences between Sx4 and 2P that are significant and Y115E is significantly different than 2P. These findings hint that Y251E contributed most to the enhanced complex formation of the Sx4-2P; Y115E consistently had a smaller effect in our hands. Figure 3-6 displays these interpretations more clearly. This suggests a significant and detectable effect of phosphorylation on SNARE complex formation. In this instance it serves as an

enhancer in agreement with physiological conditions such that insulin stimulation resulted in Sx4 phosphorylation (Schmelzle et al., 2006) and increased glucose uptake as a result of more GLUT4 vesicle fusion with the plasma membrane (Muretta et al., 2008; Pessin et al., 1999) mediated by increased complex formation. We wished to ascertain whether affinity-tag dimerization was a factor in promoting SNARE complex assembly, and so influence our results. Therefore, we designed an experiment where VAMP2 was purified using three different tags, i.e. GST/PrA/His; in SNARE complex assembly assays, all formed SNARE complexes, and all showed increased SNARE complex assembly when used with the Sx4-2P mutant. This confirmed that what we see is a genuine SNARE complex formed from participating proteins and not tag-mediated interactions. Moreover, 2P formed more complex than Sx4, consistent with previous findings, and hence supporting notion of a real biological effect.

SNARE complex formation, *in vitro*, using recombinant proteins showed consistent trends in complex signal intensity differences between phospho-mutants. On the other hand, signal intensity was variable between reaction repeats and immunoblots with different antibodies detecting different amounts though showed the same trends (data not shown). This resulted in a high standard deviation, thus an alternative technique was pursued. In solution, structural changes in proteins may be monitored using environmentally sensitive fluorescent probes such as IANBD which is cysteine reactive species. We started with labelling Sx4 looking into mutations effects on complex formation and binary interactions with other SNAREs. Labelled Sx4 showed small differences because it contains only one cysteine residue that is located in the linker region between the SNARE domain and H_{abc}; this single site of labelling did not prove particularly useful as any changes upon protein/protein interactions were small. Syntaxin4, *in vivo*, is in a binary t-SNARE complex with SNAP23 and SNAP23 was chosen next for labelling, as it contains five cysteine residues. This was hypothesised to provide a stronger signal and a greater likelihood of detecting environmental changes upon interaction with SNAREs. Using this fluorescent labelling approach, we focused on comparing Sx4 to 2P as they showed the main phosphorylation-related difference. The fluorescence signal increased very quickly upon addition of Sx4 to labelled SNAP23 (Figure 3-8 **B-C**) suggesting

conformational changes associated with t-SNARE formation. Furthermore, upon addition of v-SNARE, VAMP2, a time-dependent increase in fluorescence was observed. We interpret this to indicate more SNARE complexes forming with time. Similarly, Sx4-2P showed a similar trend, i.e. fluorescence signal increases with time. To control for different signal intensities used in different preparations of SNAP23, the data was normalised to the SNAP23 signal used. Signal at peak maximum at different time points was compared between Sx4 and Sx4-2P to allow comparisons with other experiments and with data obtained using liquid assembly assay. 2P displayed a higher signal than Sx4 (Figure 3-8 **D**). Therefore, we read these finding to indicate that 2P forms the ternary complex faster and more extensively than Sx4 (Figure 3-8 **D**). We speculate that this is possibly due to its conformation as we hypothesise Sx4-2P to be in the open from readily facilitating complex formation. All in all, we showed so far using two different approaches that double phosphomimetic Sx4 is forming more SNARE complex and faster than the wild type suggesting a strong effect of phosphorylation on ternary complex formation and in agreement with physiological observations such that insulin stimulation increases the glucose uptake mediated by GLUT4 translocation and complex assembly-dependant fusion.

Ternary complex formation speed or amount could be explained by changes in binary SNAREs binding affinities; thus pair-wise interactions were systematically investigated. This was approached through pull down assay in which Sx4 mutants immobilised to beads and bound amounts of either SNAP23 or VAMP2 analysed using immunoblots. An open mutant of Sx4 (L173A, E174A) was used as a positive control such that it maintains an open conformation (Aran et al., 2009).

Consistent with the SNARE complex formation assay in liquid (Figure 3-6), all phosphomimetic Sx4 mutants showed a trend for tighter binding to SNAP23 compared to wild type in pull-down assays, though this did not always reach statistical significance (Figure 3-9). Physiologically, Sx4 and SNAP23 form a binary complex, t-SNARE, thus their binding affinities expected to be high and current findings suggest that phosphorylation on Sx4 enhances binding in an additive manner, i.e. 2P higher than singular Y115E or Y251E, (see Figure 3-9 **B-**

C). The Sx4 open mutant presented the highest binding affinity hinting for a Sx4 conformational role in binding and the close relationship of phosphomimetic mutants to that of open Sx4. The open mutant facilitates accessible SNARE domains binding while wild type could be a mixture of opened and closed conformations.

Binary binding Sx4-VAMP2 is inhibitory to SNARE complex formation and this inhibition is proposed to be alleviated using Munc18c-Y521E (Kioumourtzoglou et al., 2014). It was also found to be the weakest pair binding among SNARE complex components, Sx4/SNAP23/VAMP2, (Foster et al., 1998). Accordingly, we found the binding to be weak, such that longer incubations were necessary to detect a measureable signal in the 30 minutes samples (Figure 3-10 **A**). Similar to SNAP23, mutants showed higher signal compared to wild type though the 30 minutes samples presented very close affinities and 60 minutes readings showed high variability (Figure 3-10 **B-C**). Also, the open mutant showed constant changes with double time incubation while 2P gave a higher binding signal. Despite these trends, statistical examinations revealed no significant differences between Sx4 and Sx4-2P in these binary interactions.

As noted above, SNARE complex formation using liquid form and ternary complex quantification using immunoblots was variable, thus a more sensitive and direct measurement was used. Circular dichroism (CD) spectroscopy examines secondary structure features of proteins thus can detect changes of conformations upon interactions or modifications. Individual SNAREs were scanned and the expected spectra sum was developed. Physical mixing to form ternary complex was scanned and compared to the expected (Figure 3-11). Spectra differences confirm structural changes upon physical mixing of SNAREs suggesting complex formation. This confirms that detected high molecular mass band in complex assay represent a real biological ternary complex consisted of Sx4/SNAP23/VAMP2, supported by data from labelled SNAP23 assays (Figure 3-8) and complex formation assay in liquid form (Figure 3-6).

Though binary binding affinity quantification using pull-down assays resulted in trends in the pairwise interaction strengths, in agreement with documented

studies, we sought to use more quantitative biophysical approaches, specifically Isothermal Titration Calorimetry (ITC). Measurements using ITC for syntaxin4-SNAP23 interactions (Figure 3-12) showed that 2P (K_d 1.22μM) is capable of five times stronger binding than wild type (K_d 5.6μM). This supports the notion of phosphorylation enhancing binding affinity.

The results reported here so far strongly suggest an important effect of phosphorylation on enhancing binary binding as well as on ternary SNARE complex formation. Syntaxin4 is known to exist in two forms, opened or closed, and we used an open mutant as a control to compare with phosphomimetic mutants in our pull-down experiments outlined above. Therefore, we speculated that phosphorylation may change Sx4 conformation to the open conformer; we were also interested to ascertain which of the two tyrosine residues, 115 or 251, may have the greater influence. To assay this, we employed limited proteolysis using Chymotrypsin and compared the rate of protease digestion of the mutants to the wild-type Sx4 (Figure 3-13). As previously reported, the open mutant is more sensitive to digestion compared to wild type (Aran et al., 2009). A similar result was observed with the Sx4-2P mutant, suggesting this is in a conformation akin to that of the open mutant. On the other hand, Y251E mutant was not consistent in degree of digestion between repeats thus it is not possible to draw a conclusion using this assay though it has presented more ternary complex than Y115E, constantly (see Figure 3-6).

In summary, *in vivo* Sx4 tyrosine phosphorylation at 115 and 251 upon insulin stimulation has been confirmed in 3T3-L1 adipocytes. Ternary SNARE complex formation was successfully recapitulated *in vitro* and the complex was found to be SDS and heat resistant. Syntaxin4 phosphomimetic mutants were expressed and they showed a higher amount of complex compared to the wild type. Double phosphomimetic Sx4 (2P) binds SNAP23 with a higher affinity in comparison to wt. Spectroscopic data suggests conformational changes upon ternary complex formation. Findings, so far, strongly suggest 2P is in the open form.

CHAPTER FOUR

4 Tools for *in vivo* work

4.1 Introduction

Findings in the previous chapter were based upon *in vitro* analysis of recombinant proteins. This needs to be translated into an *in vivo* model, such as a cell line, to be validated in a physiological environment. Therefore, Sx4 phosphomimetic mutants need to be expressed in an insulin-responsive cell model representative of GLUT4 translocation and glucose uptake enhancement, i.e. 3T3-L1 adipocytes. Tools are needed to both to detect specific tyrosine phosphorylation in Sx4 and to express mutant forms of Sx4 in cells to study functional consequences. Adipocytes of 3T3-L1 are known for their difficulty to transfect and hence lentivirus infection has been widely employed as the recommended approach. This chapter considers the development of tools to achieve this and their use to investigate physiological consequences of Sx4 tyrosine phosphorylation.

The specific aims of this chapter are:

I. To develop phospho-selective antibodies to Sx4-Y115 and Sx4-Y251, and also Munc18c-Y521.
II. To ascertain whether there is a requirement for one or other of these tyrosine residues to be phosphorylated to allow phosphorylation of the other.
III. To develop lentivirus tools for expressing phosphomimetic mutants of these species in mammalian cells.

4.2 Results

4.2.1 Generation of anti-phospho antibodies for Sx4 and Munc18c

Antibodies designed to specifically detect phosphorylated Sx4 at Y115 or Y251 and Munc18c at Y521 were generated on our behalf by Antagene Inc. who use phosphotyrosine derivatives (Fmoc-protected phosphorylated amino acids) to mount an immune response in rabbits to the phosphorylated peptide.

Prior to initiating this service, we compared the sequences of Sx4 around the putative phospho-sites. The Sx4 protein sequence is well conserved between

different species (Figure 4-1). Alignment of human and mouse Sx4 sequences showed that both tyrosine 115 and 251 sites are conserved and human isoform 3 is most identical to the mouse. These antibodies were therefore designed to detect phosphorylated Sx4 specifically at Y115 or Y251 and should in theory work across rat, mouse and human species.

Antibodies were produced by Antagene Inc. company following their standard 90 days protocol including peptide synthesis, one phosphorylation site modification, peptide-KLH conjugation, two rabbits immunization, and affinity purification. Two rabbits were immunized with designed peptide four times, i.e. day 1, 20, 40, and 60 followed by antisera collection on day 10 after the fourth immunization. Serum was then processed through phospho-peptide affinity purification resulting in the production of phospho-specific and non-phospho-specific antibodies. The phospho-peptide antibody purification included the extra phospho-specific peptide and non-phosphospecific peptide synthesis, two columns preparation and conjugation of AffiGel for phosphospecific antibody affinity purification and non-phosphospecific antibody depletion, and two-steps affinity purification of 100 ml serum from the two rabbits. The purified phosphospecific antibody (5-10mg) which does not cross-react with non-phosphospecific peptide (confirmed by ELISA) was provided. The phosphospecific and non-phosphospecific peptide ELISA titration of purified antibody from final bleeds was sent to us and confirmed the expected cross-reactivity (data not shown).

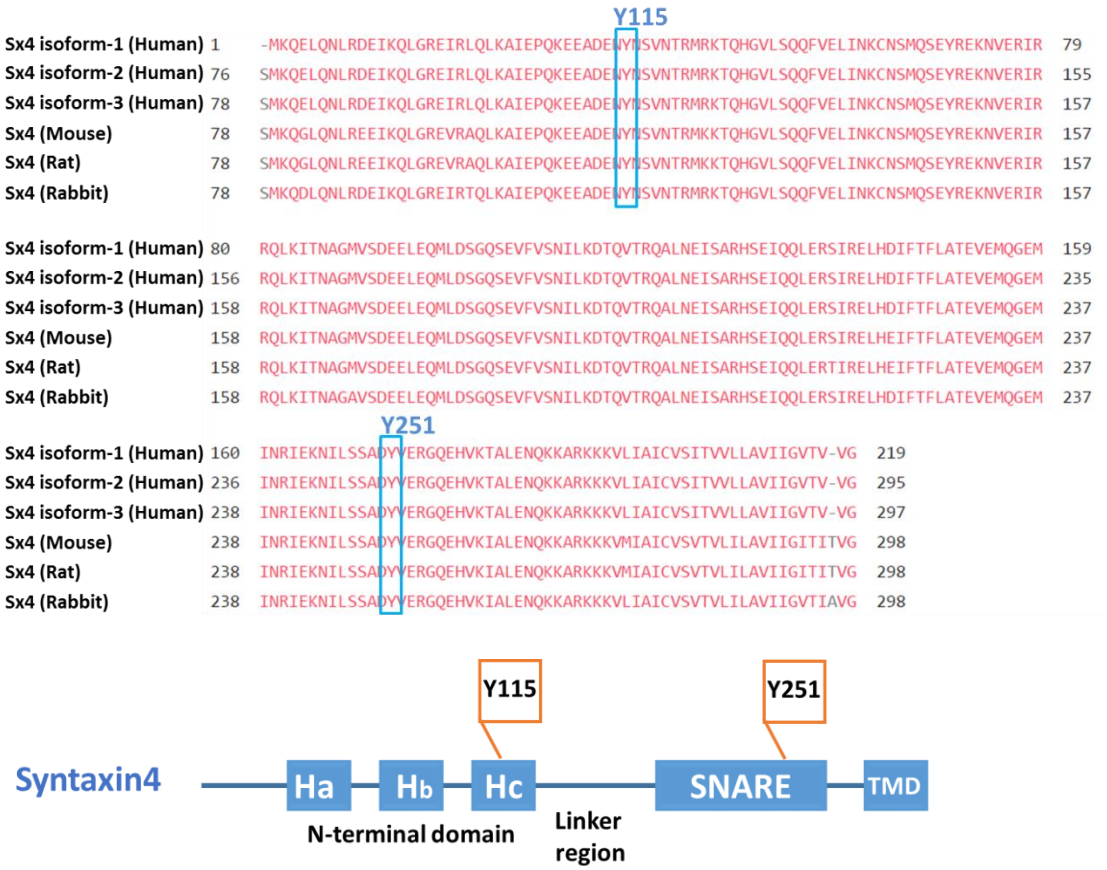

Figure 4-1 Syntaxin4 tyrosine phosphorylation sites conserved among other species.

Syntaxin4 sequence is conserved through different species as well as phosphotyrosine sites Y115 and Y251. Protein sequences of Sx4 were retrieved from NCBI for human isoforms 1 (NP_001259024.1), 2 (NP_001259025.1), 3 (NP_004595.2), mouse (NP_033320.1), rat (NP_112387.1), and rabbit (NP_002721779.1). Sequences were aligned using COBALT tool on the NCBI website. Phosphotyrosine sites Y115 and Y251 are identified by blue boxes at the respective location. Schematic representation of tyrosine phosphorylation sites within syntaxin4 presented in the lower panel.

The regulatory Sec1-Munc18 protein which binds to Sx4 is Munc18c; there are three isoforms of Munc18c in human. Full length protein sequences of the human isoforms together with that of mouse Munc18c were aligned to check for tyrosine 521 conservation (Figure 4-2). Tyrosine 521 site is well conserved between aligned sequences, and the flanking sequences are well conserved.

Figure 4-2 Tyrosine 521 in Munc18c conserved between human isoforms and mouse.

Munc18c protein sequence is conserved between different human sequences and mouse. Tyrosine 521 is conserved among all sequences shown, and the flanking regions are well conserved. Sequences obtained from NCBI website for human isoforms 1, 2, and 3 with reference numbers NP_009200.2, AAH47764.1, and AAH38099.1 respectively while mouse sequence is NP_035634.1. Sequences aligned using COBALT tool in NCBI website. Tyrosine 521 location is highlighted by the blue box.

4.2.2 Syntaxin4 is a CIRK phosphorylation target

Upon insulin stimulation, Sx4 is phosphorylated by the Cytoplasmic Insulin Receptor Kinase (CIRK). Recombinant CIRK was purified previously in our group and activated for phosphorylation (Dr Veronica Aran-Ponte, University of Glasgow). The CIRK construct consists of amino acids 941-1343 of the ß-subunit of the insulin receptor. It has been shown previously that CIRK is able to phosphorylate monomeric Sx4 and Munc18c but appears not to phosphorylate Sx4 when present in a ternary SNARE complex (Aran et al., 2011). CIRK-phosphorylated M18c, or phosphomimetic mutated Y521E, was unable to bind the SNARE proteins Sx4 or VAMP2 thus suggesting phosphorylation as layer of regulation for GLUT4 trafficking (Kioumourtzoglou et al., 2014). Therefore, we thought of testing CIRK on the phosphomimetic mutants as a way to determine whether phosphorylation of residue-x is a pre-requisite for phosphorylation of residue-y. Recombinant Sx4 phosphomimetic mutants were phosphorylated using CIRK, as described. Briefly, recombinant Sx4 proteins were mixed, individually, with recombinant CIRK in buffer (50 mM HEPES pH 7.5, 4 mM MnCl2, 0.2 mM DTT, 100 µM ATP) and incubated for 150 minutes at 30°C. Samples were mixed with 2X LSB loading buffer and heated to 65°C for 10 minutes. Proteins were separated on 12% SDS-PAGE followed by immunoblotting for total Sx4, phospho-site-specific, or total phospho-tyrosine antibodies. The result of a typical

experiment are shown in Figure 4-3. CIRK was shown to induce tyrosine phosphorylation of Sx4 wild-type and both phosphomimetic Sx4 single mutants as revealed using the phospho-specific antibodies for Sx4 (Figure 4-3). Antibodies phospho-specific for Sx4(Y115)-P did not recognise Sx4-Y115E (the phospho-site is mutated) but did recognise CIRK-phosphorylated Sx4 wild-type and Sx4-Y251E in which the Y115 site is intact. Similarly, anti-Sx4(Y251)-P recognised Sx4 wild-type and SX4-Y115, as in both cases the Y251 site is intact. Total phospho-tyrosine antibody showed a signal in all samples except in the double phosphomimetic Sx4 (2P) due to the fact that both tyrosine sites in 2P were mutated and hence cannot be phosphorylated. Therefore, this assay confirmed the specificity of the antibodies generated and CIRK-phosphorylated Sx4 detection. This data would also appear to suggest that the presence of a phosphomimetic group at either Y115 or Y251 is not inhibitory for the phosphorylation of the other site.

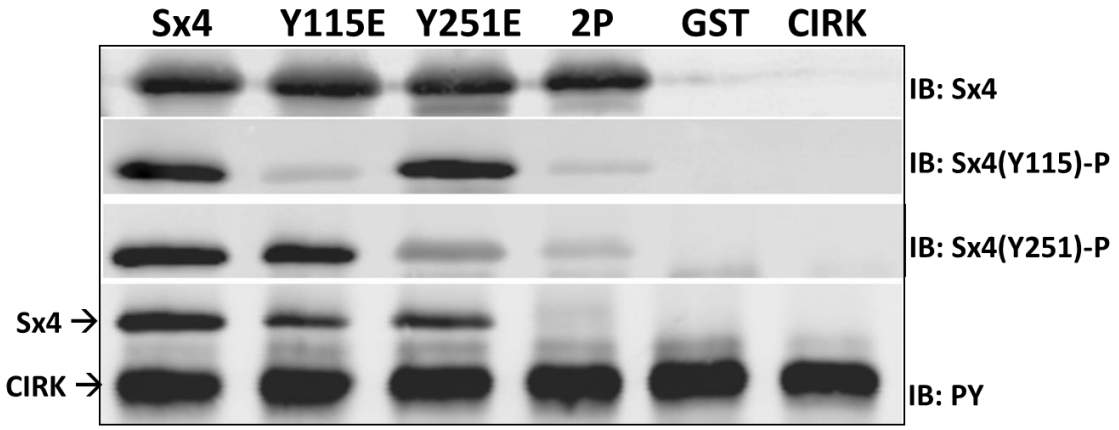

Figure 4-3 Syntaxin4 phospho-specific antibodies detect targeted CIRK-phosphorylated Sx4 in precision.

Phosphotyrosine-specific Sx4 antibodies detect Sx4 phosphorylated using CIRK. Equal amounts (2 µg) of either wild-type Sx4, or Sx4 phosphomimetic mutants were phosphorylated using recombinant CIRK for 150 min at 30^{o}C followed by mixing with 2X LSB and heating for 10 min at 65^{o}C. Samples were separated on 12% SDS-PAGE followed by immunoblot development for total antibody Sx4 (Sx4 on figure at right)), generated Sx4 tyrosine phospho-specific antibodies Sx4(Y115)-P & Sx4 (Y251)-P, and total phosphotyrosine antibody (PY on figure at right). Data shown are representative of several experiments of this type with qualitatively similar results.

Sx4 exists in cells in a complex with SNAP23 (the t-SNARE complex) but it is unknown whether Sx4 is phosphorylated as monomer, or in complex with SNAP23 or both. Recombinant t-SNARE complex was expressed using *E. coli* (BL21 DE3)

and used as a substrate for CIRK phosphorylation; the CIRK phosphorylation of monomeric Sx4 was compared in the same experiment. Monomeric Sx4 was phosphorylated by CIRK but not when present in the t-SNARE complex (Figure 4-4). Furthermore, increasing the amount of t-SNARE in the kinase reaction did not alter the finding. This suggests insulin stimulation does not influence Sx4 assembled in a t-SNARE complex in the plasma membrane, but rather may modulate the monomeric Sx4 pool. This result is a confirmation of a work previously done in our group (Dr Veronica Aran-Ponte, University of Glasgow) and hence was not repeated further.

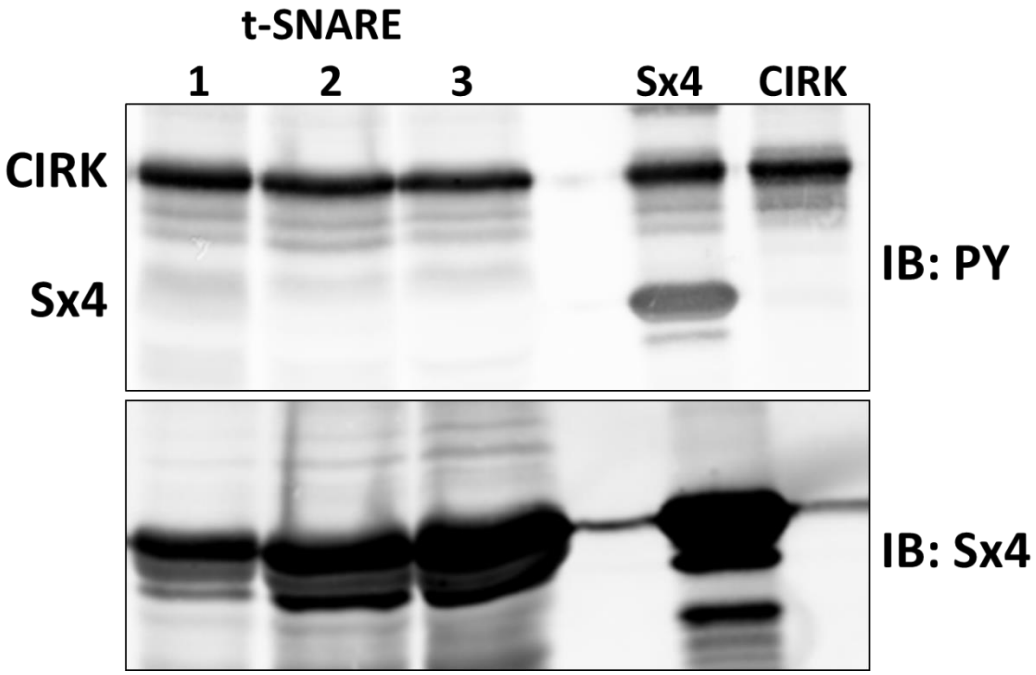

Figure 4-4 Monomeric Sx4 is a CIRK target but not in t-SNARE complex, Sx4/SNAP23.

CIRK is unable to phosphorylate Sx4 in a t-SNARE complex. t-SNARE complex was expressed in *E.coli* BL21 (DE3) by dual transformation of pQE30-His-Sx4 and pET41a-GST-SNAP23 and was then purified with glutathione beads followed by thrombin cleavage of SNAP23 resulting in pure t-SNARE. CIRK phosphorylation reaction was run at 30^{o}C for 150min by mixing 2ug recombinant CIRK with either 1.6 µg Sx4 or 14, 28, 52.5 µg t-SNARE (labeled as 1, 2, 3 respectively in the figure) in kinase buffer (50 mM HEPES pH 7.5, 4 mM MnCl2, 0.2 mM DTT and 100 µM Na-ATP). Samples were separated by SDS-PAGE and immunoblots were developed for either Sx4 or total phosphotyrosine, PY. Data shown is from representative experiments, repeated four times with similar findings.

4.2.3 Phospho-specific syntaxin4 antibodies proved difficult to detect signal in cell lysates

Our model of adipocyte cells is the 3T3-L1 fibroblasts which differentiate into adipocytes. They respond to insulin stimulation efficiently and thus we attempted to use the phospho-selective antibodies to identify Sx4 tyrosine phosphorylation using different insulin concentrations at different times of exposure. Phosphotyrosine changes at different time points could be detected using the phospho-specific antibodies, and might therefore reveal if there is a specific order of tyrosine 115 and 251 phosphorylation. Unfortunately, immunoblots using the phospho-specific antibodies did not detect a clear signal. Multiple bands were detected and it was hard to ascertain a band for Sx4 was being identified; the species identified often exhibited subtly different molecular weights to that for Sx4 detected using commercial antibody (Figure 4-5 **A**); this may be a reflection of post-translational modification, or may be non-specific. Lengthy optimization trials, included trying different blocking buffers, antibody dilutions, protein concentrations, and even immunoprecipitation (IP) of Sx4 followed by blotting using the phospho-specific Sx4 antibody with appropriate controls (Figure 4-5 **B** & **C**) did not clarify the data. This could be expected, to some degree, as detection of phosphorylated tyrosine residues using the proteomic mass spectroscopic approach was difficult and required deep analysis of the raw mass spectroscopic data below threshold values. Compared to CIRK phosphorylation of recombinant Sx4 mutants, which could be readily detected, these data collectively suggest a low concentration/stoichiometry of phosphorylated Sx4 present in 3T3-L1 lysates. However, this conclusion should be tempered with the difficulty in preparing high-affinity phospho-selective reagents.

A

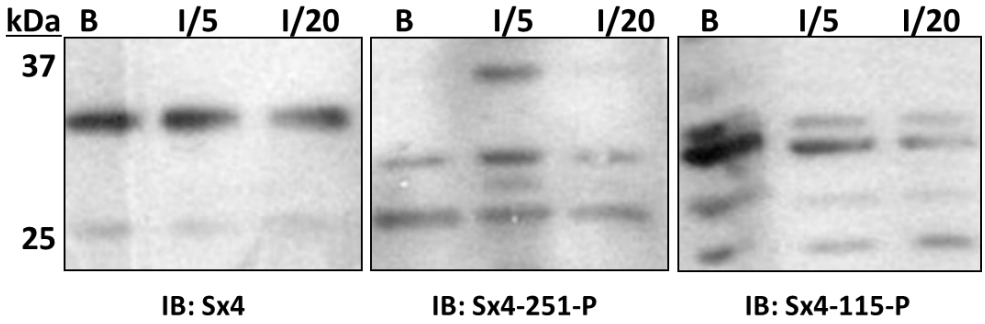

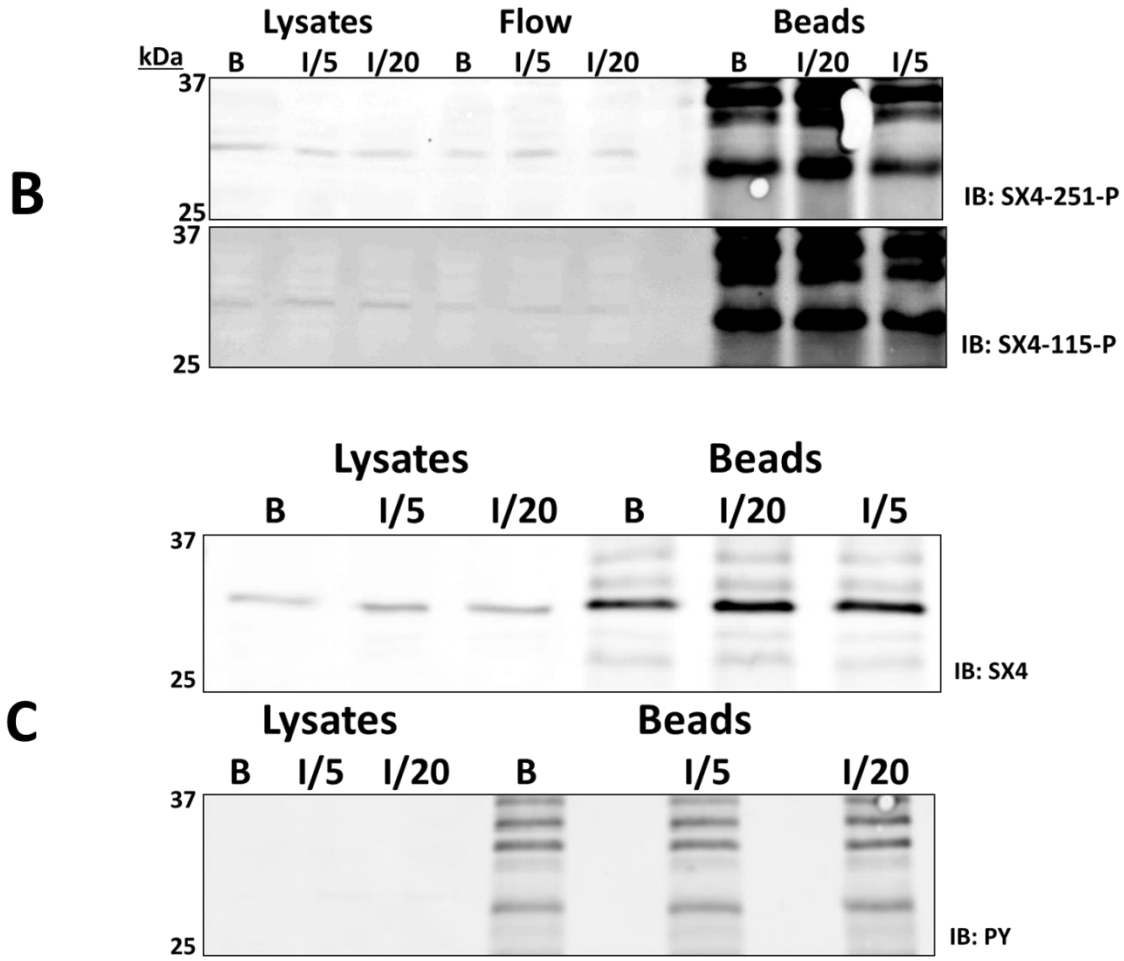

Figure 4-5 Syntaxin4 phospho-specific antibodies struggle detecting signal in 3T3-L1 adipocytes.

3T3-L1 adipocytes were lysed with phosphatase inhibitor added and samples run in 12% SDS-PAGE followed by immunoblots developed with marked antibody. Loaded samples included basal (B), and insulin stimulated (100nM) cells for 5 (I/5) or 20 (I/20) minutes. **A**/ blots were blocked using neat Sea Block blocking reagent, antibody diluted 1:100 in 50% Sea-Block in 0.05% Tween/TBS, and blot developed using ECL. **B & C**/ Sx4 immunoprecipitated first then blots developed, representative samples loaded i.e. lysate, flow (un-bound proteins), beads used to precipitate Sx4. Phospho-specific antibodies, Sx4-Y115-P or Sx4-Y251-P, detect weak signal for Sx4 in lysate and flow samples but much stronger on beads at un-expected sizes, **B**. Syntaxin4 size is around 35 kDa. Commercial Sx4 antibody detects same size band in both lysate and beads samples where signal is much stronger in the IP samples, as expected, **C**. Total tyrosine phosphorylation showed no signal in lysate samples and exact multi bands in the IP samples with similar intensities showing no difference for insulin stimulation, **C**. Protein sizes shown on left of blots, in kDa.

Different cell lines were compared to use with generated phospho-specific antibodies with the rationale that high levels of Sx4 phopsphorylation may be evident in other cell systems. Human liposarcoma cell line, SW872, and mouse

adipocytes, 3T3-L1, were cultured side-by-side and insulin stimulated similarly; cells were lysed using the same lysis buffer and sample preparation followed by SDS-PAGE separation and blot development (Figure 4-6). Commercial Sx4 antibody gave a strong signal in 3T3-L1 samples while SW872 lysates showed a weak signal. In contrast, the non-specific generated antibody showed a strong band intensity for both cell types (Figure 4-6,bottom panel) though the phospho-specific did not detect any specific, size-wise, signal for Sx4 (Figure 4-6,middle panel). This could reflect on cell expression issues on one hand and levels of variations too between the two types of cells.

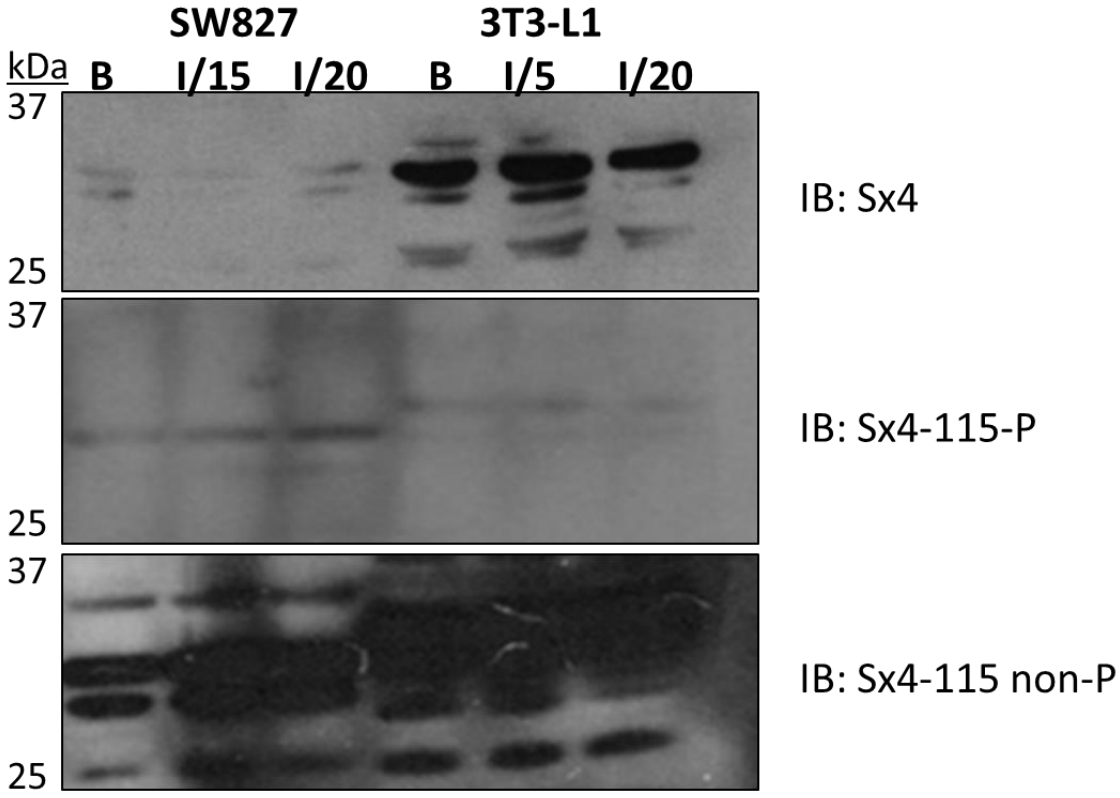

Figure 4-6 Syntaxin4 phospho-specific detection in different cell types.

Human liposarcoma cell line, SW827, and mouse adipocytes, 3T3-L1, were insulin-stimulated for indicated times, lysed and blotted using the antibodies shown. Basal (B) and insulin (I) stimulated samples were subjected to 12% SDS-PAGE followed by immunoblotting for commercial Sx4 and the phospho-specific (Sx4-115-P) and non-specific (Sx4-115 non-P) generated antibodies.

Previous finiding (Figure 4-6) hints that 3T3-L1 cells express more Sx4, and hence were used for further optimisation. Therefore, the two phospho-specific antibodies sets were compared using 3T3-L1 lysates. Commercial Sx4 antibody showed a strong and distinct signal at the expected size, around 35kDa

(Figure 4-7). Both phospho-specific antibodies showed multiple bands which mostly are not the right size, with exception of 5 minutes insulin stimulation and using Sx4-Y251-P antibody (Figure 4-7 **B**). Similarly, the non-phospho-specific also showed many bands at random protein sizes. Therefore, these data suggest that these antibodies will not be useful for *in vivo* work.

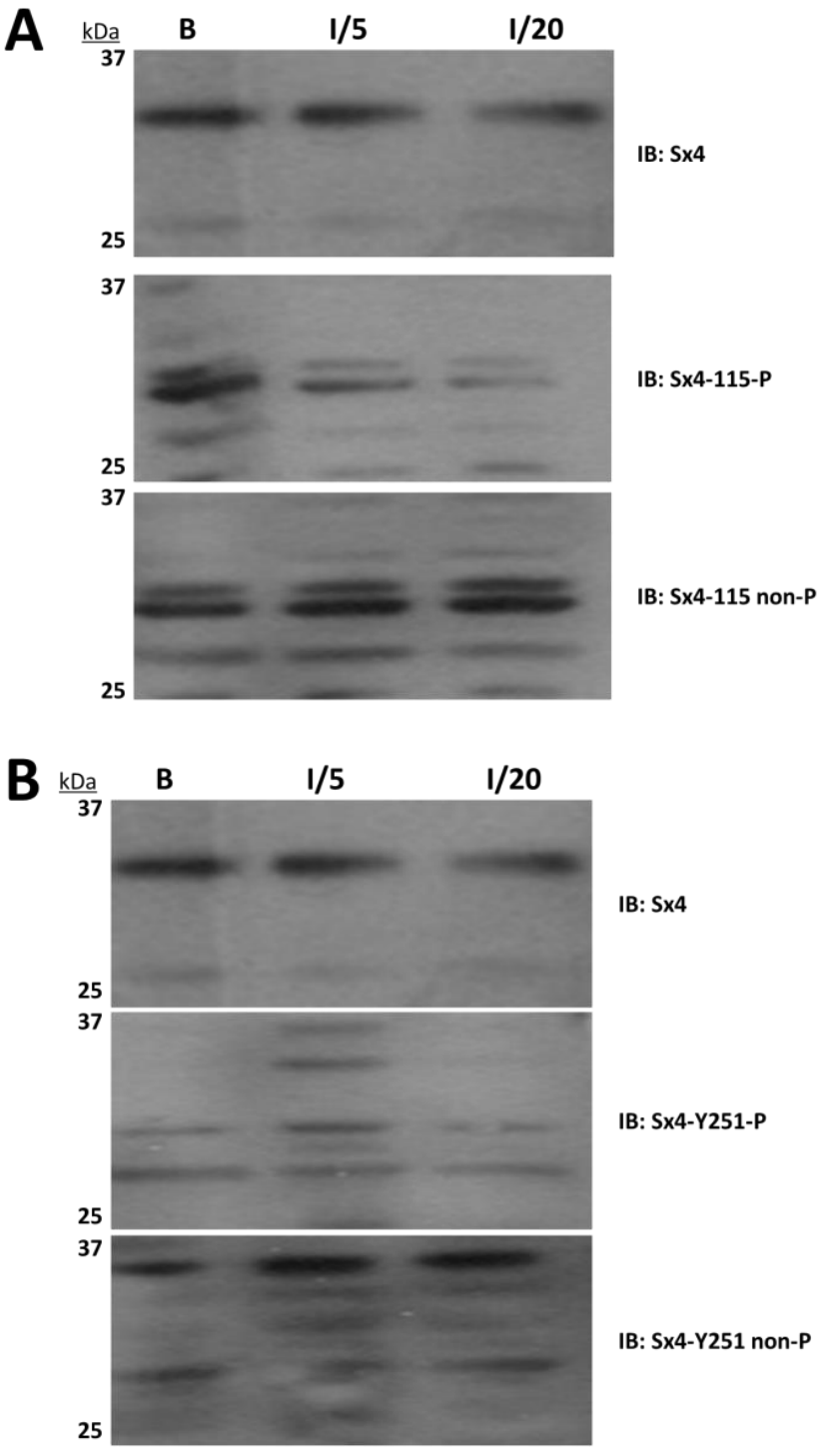

Figure 4-7 Phospho-specific Sx4 antibodies are not reliable for blotting 3T3-L1 lysates.

Cell lysates of basal (B) and insulin (I) stimulated, for 5 or 20 minutes, 3T3-L1 adipocytes were ran in 12% SDS-PAGE and immunoblots developed for the antibodies indicated at the right of the figure. Commercial antibodies were used in addition to the generated phospho specific or non-specific. Western blots were developed using wet transfer and visualized using fluorescent secondary antibody with LiCoR detection instrument. Antibodies versions of specific and non-specific compared for Y115 (**A**) and Y251 (**B**).

A further optimization step was attempted by first immunoprecipitating (IP) Sx4 using, as primary antibody, the generated phospho-specific antibodies, or commercial anti-Sx4, and also using total anti-phosphotyrosine agarose beads. Blots were developed using the same antibodies used for the IP (Figure 4-8). Syntaxin4 was detected, mainly, in lysate and commercial Sx4 IP samples at the right size. Total phospho tyrosine showed an increased signal with insulin stimulation but with a protein smaller than Sx4 though a band around Sx4 protein size was noticed and phospho-specific Y251 antibody also detected a signal of the size recognised by anti-phosphotyrosine antibodies. Most intense bands for Sx4 detected by Y115 and Y251 are bigger in size than commercial antibody which makes sense because, theoretically, phosphorylated Sx4 would be bigger, by added phosphate group, and hence its migration in gel might be slower.

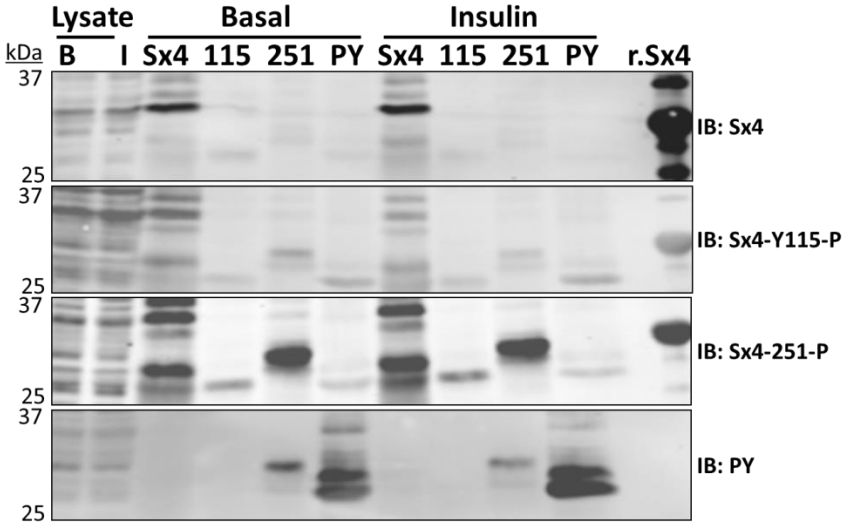

Figure 4-8 Immunoprecipitation of Sx4 using generated phospho-specific antibodies as primary antibody.

3T3-L1 adipocytes for basal and 20min insulin-stimulated were lysed and Sx4-immunoprecipitated using commercial, phospho-specific, and total phosphotyrosine antibodies. Beads were washed extensively and sample buffer, 2X LSB, was added followed by heating at 75^{o}C for 10 minutes. Proteins separated in 12% SDS-PAGE followed by wet transfer and immunoblotting for shown

antibodies. Recombinant Sx4 (r.Sx4) was loaded as an antibody control. Relative molecular weights are shown on left for guidance.

4.2.4 Munc18c phospho-specific antibody demonstrate good detection signal though less than approved

Similarly, the Munc18c phospho-selective antibody was hard to optimize though better signal was detected (Figure 4-9). Cell lysates of 3T3-L1 adipocytes were used to test the generated phospho-specific antibodies in parallel with commercial anti-Munc18c. A strong signal was detected using the commercial antibody while much less signal strength shown using the phospho-selective reagent. This reagent was not followed up further.

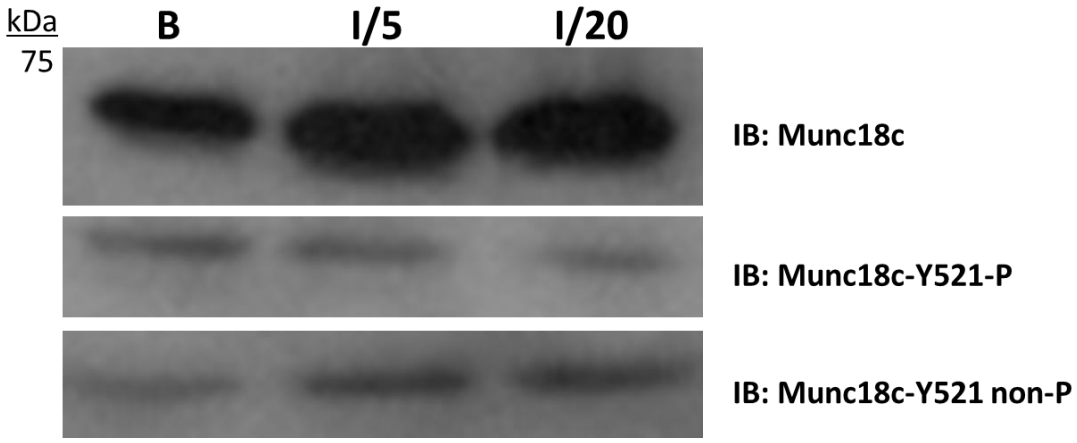

Figure 4-9 Generated Munc18c antibodies detected signal at right size in addition to non-specific.

Adipocytes lysates of 3T3-L1, basal (B) and insulin (I) stimulated, for 5 or 20 minutes, subjected to 12% SDS-PAGE followed by wet transfer and immunoblots for the commercial Munc18c antibody and the phospho specific or non-specific antibodies. Western blots developed using wet transfer and visualized using fluorescent secondary antibody with LiCoR detection instrument.

4.2.5 PLA signals suggest Sx4 phosphorylation sites stoichiometry with more effort

We reasoned that the phospho-specific reagents may function to bind native protein more efficiently than the material separated on SDS-PAGE gels. Hence,

we attempted to analyse their ability to recognise the native protein using a different approach. Proximity Ligation Assay (PLA) is an *in situ* proteomics technique for identifying protein-protein proximity using two primary antibodies raised in different species; if the two target proteins are close enough (<16nm) then a fluorescent signal would be detected. Briefly, the assay protocol involves a pair of antibodies which specifically recognize and bind to two potentially interacting targets (Figure 4-10**a**). These antibodies are conjugated to a matched pair (labeled +/-) of short single-stranded oligonucleotides. If the two respective targets interact, and hence remain in very close proximity, the oligonucleotide probes will hybridize and ligate with two additional "connector oligos" to form a continuous circular DNA structure (Figure 4-10**b**). DNA polymerase enzymes will amplify these circular molecules through simple, reliable rolling-circle amplification (Figure 4-10**c**). The result is a highly amplified circular DNA molecule that can be detected via standard fluorescent methods (Figure 4-10**d**), and that acts as a qualitative marker of interaction between the two proteins. The assay was performed following company's protocol, Sigma-Aldrich. Images were taken using confocal microscope and analysed using BlobFinder V3.2 software.

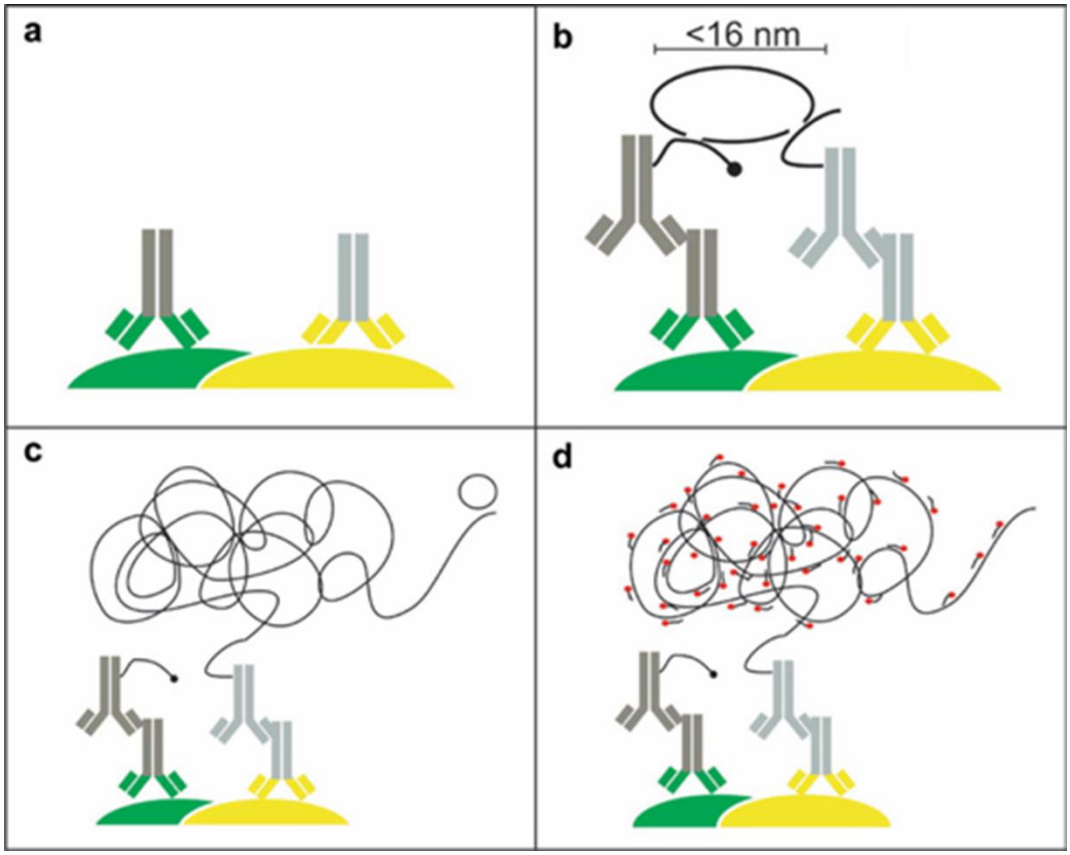

Figure 4-10 Proximity Ligation Assay (PLA) principle.

Panel a/ Primary antibodies against proteins of interest raised in different species. **Panel b**/ Secondary antibodies with oligonucleotides attached; Add two oligos complementary to those conjugated to the 2° antibodies. If the two proteins are in close enough proximity a ligation reaction circularises these two oligos. **Panel c**/ This can act as a template for rolling PCR (primed by one oligo, the other is blocked). Panel **d**/ Resultant single stranded DNA collapses into a bundle that can be detected through hybridisation of fluorescently labelled oligos.

The software, BlobFinder V3.2, has an algorithm able to detect positive fluorescent signals in the form of little red dots, called blobs. It can perform processing of image data and quantify, as well as localize cells and point like source signals in fluorescence microscopy images. It is possible to find signals hidden in over-stained areas or under DAPI stain thus yielding a reliable output. Cytoplasm size, nucleus, and number of blobs are the results obtained from this software (Figure 4-11 **A**) in addition to images of analysed data in the processed samples with facility of zoom in (Figure 4-11 **B**).

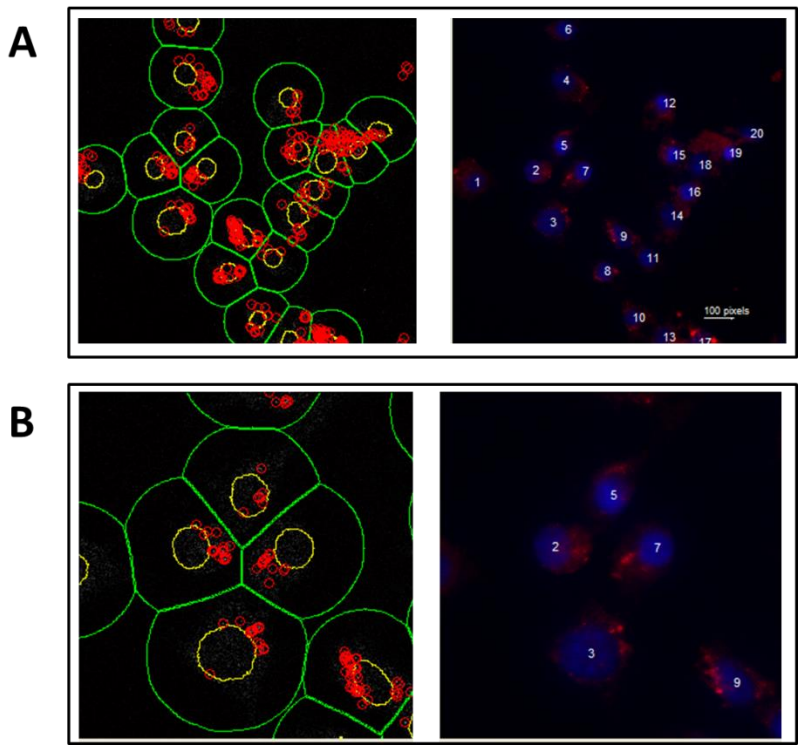

Figure 4-11 Typical output data from BlobFinder software analysis.

Antibody pair of Sx4/mouse, commercial, with phospho-specific Sx4-251 show fluorescent signals at insulin stimulated 3T3-L1 adipocytes. Panel **A** shows images obtained from confocal microscope analysed using BlobFinder V3.2 showing labelled cells in field, at right frame and in left cytoplasm size, green, and nucleus, yellow, while detected blobs shown in red circles. Panel **B** shows a zoom-in field showing more details of analysed image.

Phosphorylation modification of Sx4 gave a signal using the phospho-specific antibodies in combination with commercial antibody. We used PLA as a way to look for phosphorylation of Sx4, and used either Y115-P or Y251-P antibody in a PLA experiment with anti-Sx4, and compared the signal to Sx4-mouse/Sx4-rabbit combinations. Preliminary results are presented in Figure 4-12. Adipocytes are rounded in shape and PLA signals can be detected as a function of the focal plane (Figure 4-12). Signal detection is encouraging knowing that antibodies are working (Figure 4-11). Time limitations prevented exploring this more fully, but in the two separate experiments a positive PLA signal was observed suggesting that Sx4 is phosphorylated and the antibodies are recognising it. Control samples were included with only one of the pair of antibodies added but not the other. In such case, few, if any, signals were detected. A positive control was used from previous runs plus the use of Sx4/mouse with Sx4/rabbit.

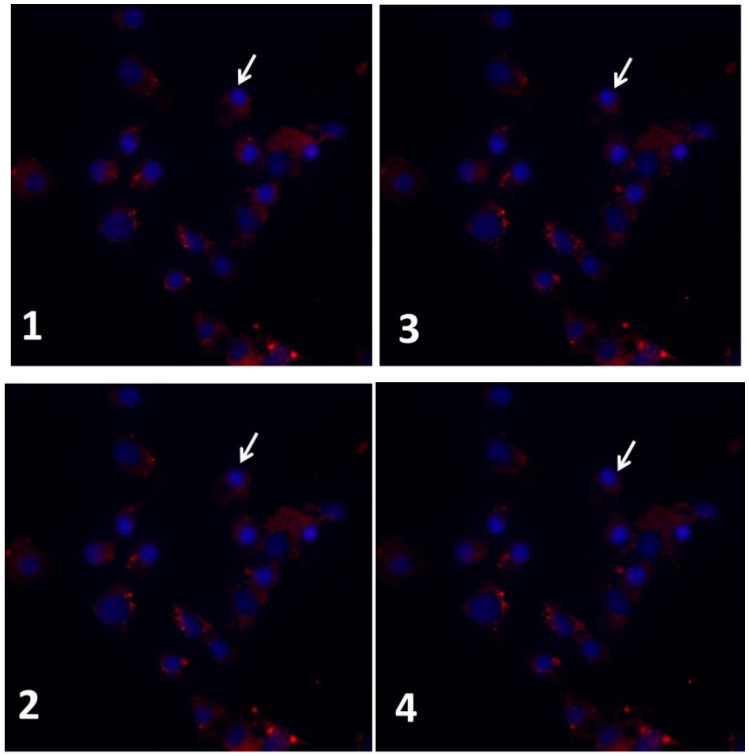

Figure 4-12 Confocal imaging plan show different number of blobs at different focus points.

Arrow-pointed cell, show different numbers of blobs as different images were taken at different zoom in-out. Images 1-4 are from same field with different zoom levels. Red dots represent positive signal and blue stain is for the nucleus. Arrows point at a single cell, selected as an example, showing different number of blobs at different zoom levels.

4.2.6 Generation of Sx4 and Munc18c lentivirus

Adipocytes are known for being difficult to transfect compared to other cell lines thus a lentivirus approach was the method of choice; this required sub-cloning Sx4 or Munc18c mutants into lentivirus plasmids. Full length, un-tagged, Sx4 and Munc18c, separately, wild type and mutants were cloned in mammalian expression plasmid pcDNA3.1(+) by GenScript. Syntaxin4 was then sub-cloned into the lentivirus plasmid pCDH-CMV-MCS-EF1-RFP (System Biosciences SBI, cat number CD512B-1) and Munc18c into pLVX-IRES-mCherry (Clontech, cat number 631237) (Figure 4-13 **A-B**). Restriction enzymes BamHI and NheI were used for Sx4 sub-cloning while XhoI and EcoRI were used for Munc18c (Figure 4-13 **A**). The size of Sx4 is about 1kbp and Munc18c about 2kbp while plasmid sizes are about 6.5kbp pCDH and 8.8kbp pLVX. Successful cloning trials were screened for positive ligation by digesting plasmid DNA extracted from selected colonies and check for the right insert size (Figure 4-13 **B**). Positive clones were used for later

analysis. Both plasmids, mammalian expression vectors and lentivirus expression vectors, were used for transfecting control cells i.e. HeLa, HEK293, and 3T3-L1 fibroblasts where both showed over-expression of Sx4 or Munc18c (Figure 4-13 **C**) (note that both vectors contain a promoter for eukaryotic expression). Therefore, this confirms that the constructs encode functional proteins in both vectors.

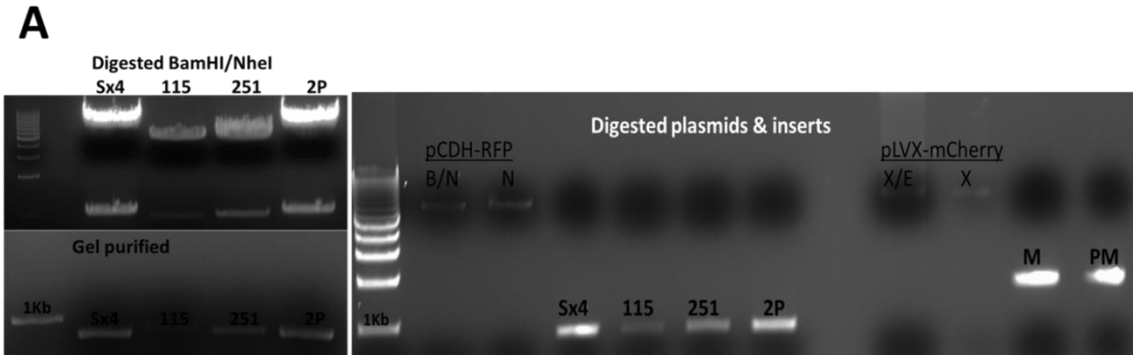

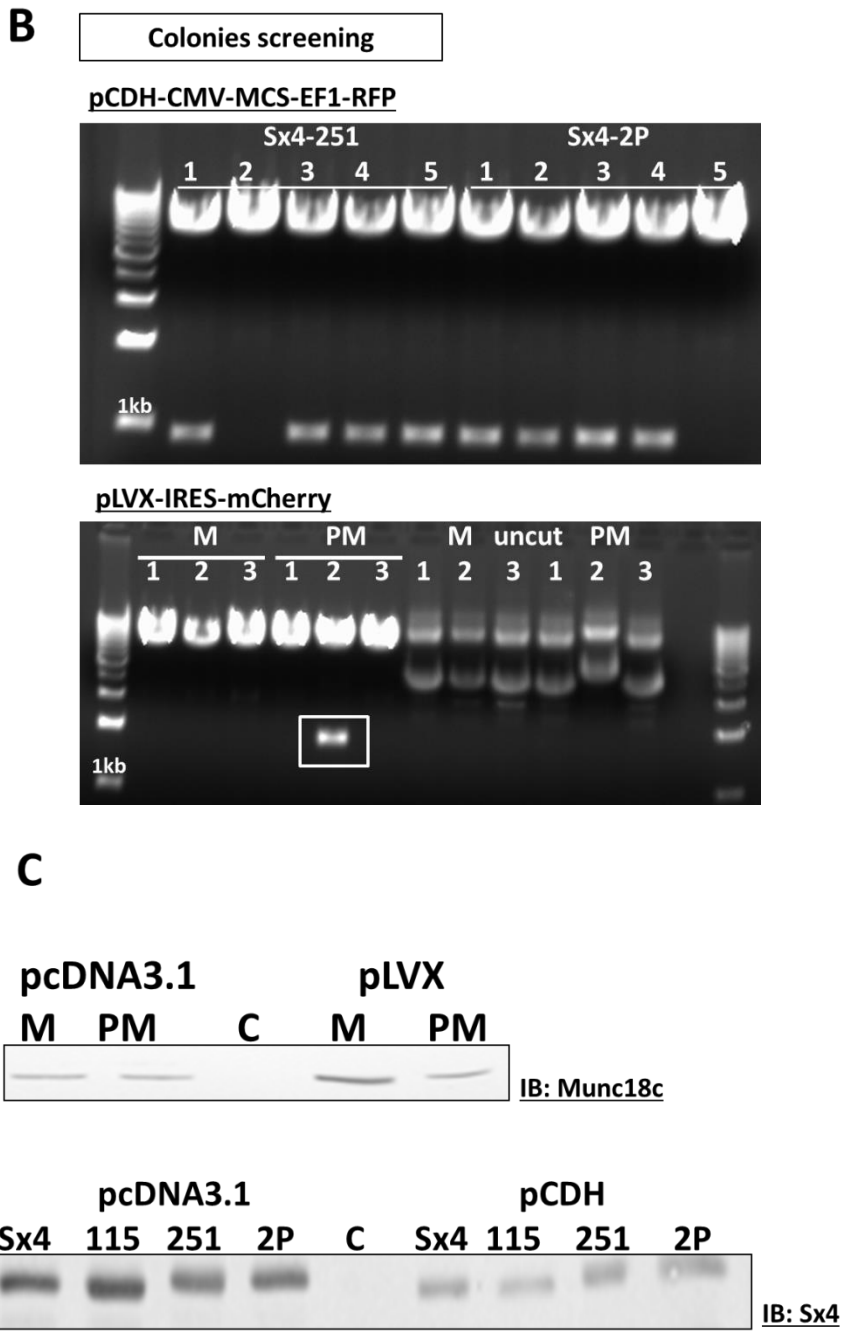

Figure 4-13 Sub-cloning Sx4 and Munc18c into lentivirus plasmids followed by transient expression of viral vectors shows they are functional.

Panel **A**/ Representative examples shown for the process of cloning Sx4 and Munc18c mutants as, first, they were digested from mammalian plasmid pcDNA3.1(+) followed by purification of the appropriate target band from agarose gel (left gels). Destination plasmids, pCDH for Sx4 or pLVX for Munc18c, were opened using the appropriate restriction enzymes followed by gel purification. Lentivirus plasmids and inserts for all mutants shown in gel at right, **A**. Panel **B**/ Successful ligations which produced colonies on the appropriate selective antibiotic were screened by digesting with BamHI/NheI for pCDH and XhoI/EcoRI for pLVX. Positive colonies drop out inserts of the expected size: Sx4 ~897bp and M18c ~2Kbp. Panel **C**/ HEK293 cells were transfected with mammalian plasmids, pcDNA3.1, and lentiviral plasmids, pCDH or pLVX, and both showed an

over-expression of Sx4 or Munc18c mutants; thus by transient expression, both vectors encode a protein of the expected molecular weight. Cells were transfected for 48 hours then lysed and subjected to SDS-PAGE followed by immunoblots developed for Munc18c (upper panel) or Sx4 (lower panel). Equal total protein concentrations were loaded per each lane. Abbreviations: B/BamHI, N/NheI, X/XhoI, E/EcoRI, Sx4/wild type syntaxin4, 115/Sx4-Y115E, 251/Sx4-Y251E, 2P/Sx4-Y115,251E, C/control, M/Munc18c, and PM/Munc18c-Y521E. Note that as these experiments were simply designed to confirm protein expression (yes/no), we did not perform loading control blots.

As plasmid transient transfections showed they are functional and can drive expression of protein of the expected molecular weight, the next step was to produce lentivirus to be used for the transduction of 3T3-L1 adipocytes. Lentivirus preps were made using HEK293TN or HEK293FT producer cells using different transfecting reagents including pPACKH1, Lipofectamine2000, PureFection, or PEI and packaging, envelop plasmids pInt and pMDG, respectively. Virus produced was concentrated using ultra-centrifugation (23,000 rpm/1h at 4^{o}C). Control cells, i.e. Hela, HEK293, and 3T3-L1 fibroblasts, were infected using the concentrated viruses with 8µg polybrene. Immunoblots showed overexpression of Sx4 (Figure 4-14 **A**) and Munc18c which was supported by confocal images showing red signal for RFP tag in Sx4 (Figure 4-14 **B**) and mCherry in Munc18c (not shown) which are part of the lentivirus plasmid construct thus confirming infection.

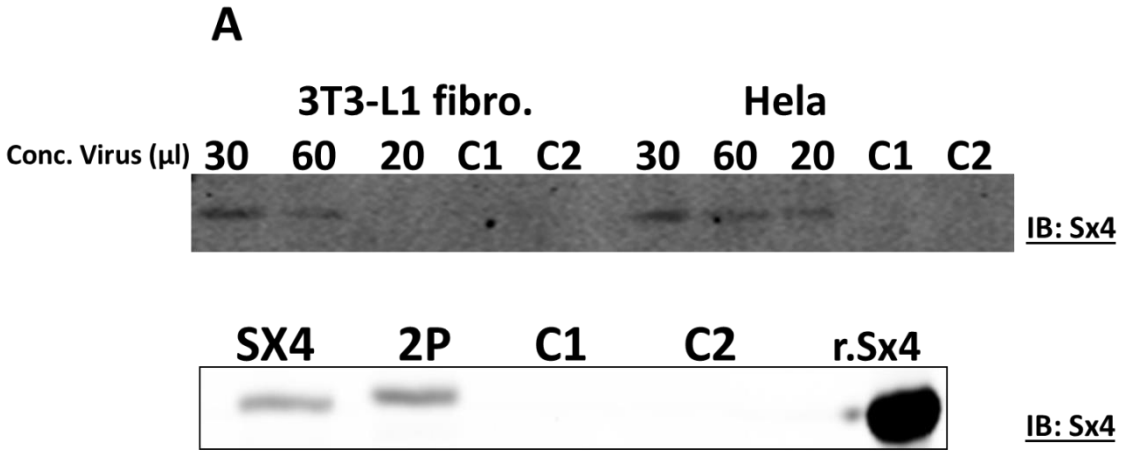

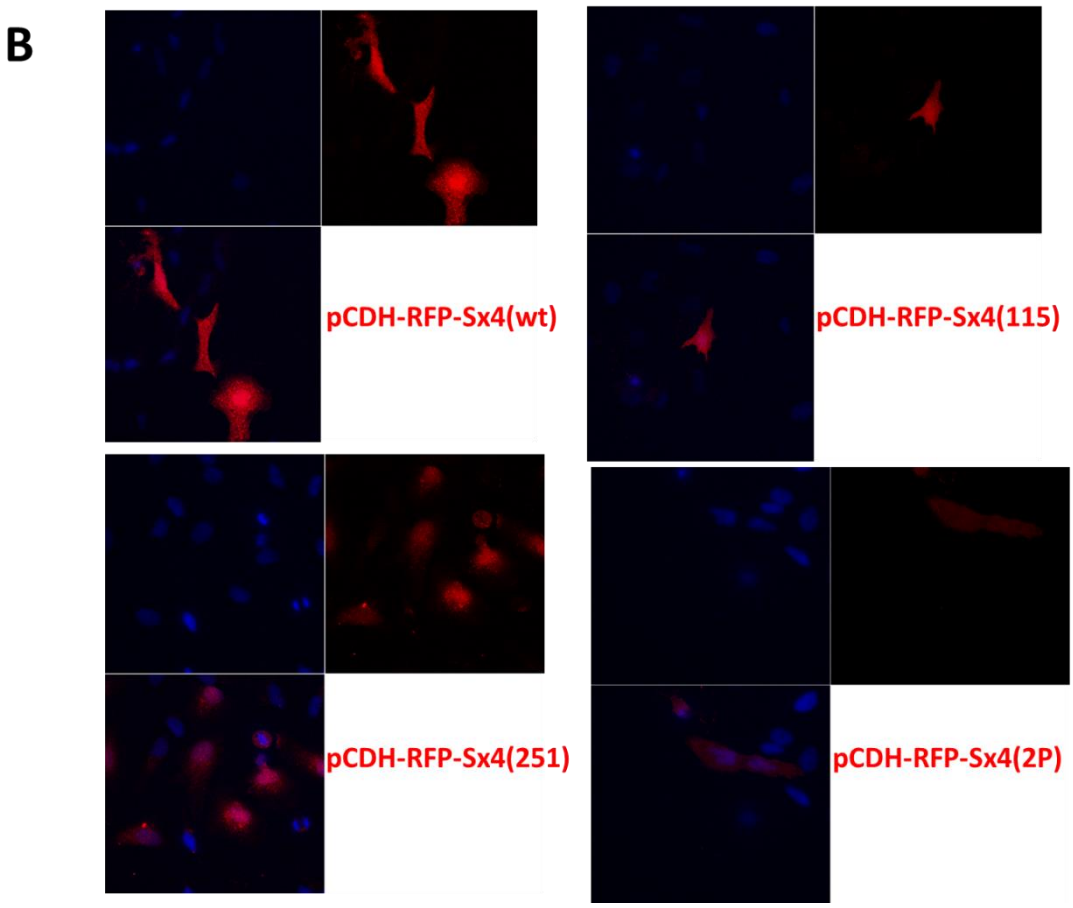

Figure 4-14 Lentivirus produced for Sx4 are functional for transducing cells to overexpress target protein.

Panel **A**/ Syntaxin4 over expression examined using different cell types including Hela, 3T3-L1 fibroblast, and HEK293 in which cells were infected with concentrated virus using 8µg/ml polybrene. Upper panel, HeLa and 3T3-L1 fibroblasts infection using concentrated Sx4-wt virus; lower panel, HEK293FT infection with concentrated virus 20µl Sx4-wt & 40µl Sx4-2P in 12 well plate for 48h using 8µg/ml polybrene. Panel **B**/ Positively infected HeLa cells indicated by RFP expression reveal efficient viral transduction. Images were taken using confocal microscope. DAPI staining is shown pseudo-coloured blue. Data shown representative of similar findings for other lentivirus preps.

4.2.7 Sx4 versus 2P in HeLa cells expressing GLUT4

HeLa cells are easier to infect compared to 3T3-L1 adipocytes and hence were chosen to examine the effects and consequences of overexpression of wild type (wt) and double phosphomimetic (2P) mutants of Sx4 on GLUT4 translocation. I used HA-GLUT4-GFP HeLa cells which express GLUT4 tagged with GFP showing total protein and HA can be stained to show the protein in the plasma membrane. This cell model was shown previously to respond to insulin

stimulation and GLUT4 translocation from intracellular compartments (Lampson et al., 2000; Martin et al., 2006). Infected HA-GLUT4-GFP-Hela cells with Sx4 or 2P did not show a definite difference between basal and insulin-stimulated GLUT4 translocation (Figure 4-15). HA-stain showed no difference between wt and 2P infected Hela cells and further the ratio of HA/GFP intensity was not significantly different (not shown). This may reflect the relatively small 'window' of the assay in these cells. Hence, we moved onto using 3T3-L1 adipocytes which give a more robust response (but are much harder to infect/transfect).

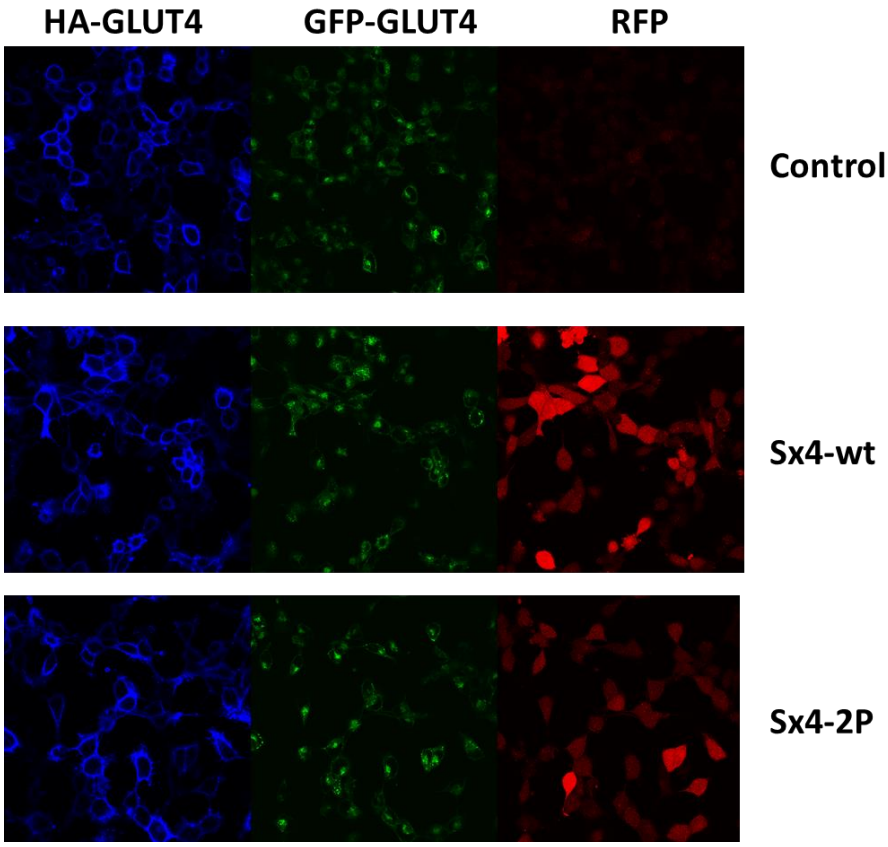

Figure 4-15 Virus infection of HA-GLUT-GFP HeLa cells.

HeLa cells were seeded in 24-well plates then infected with concentrated virus encoding wild type or double-phosphomimetic Sx4-2P. After 48h, cells were serum starved for 2 hours then washed, fixed and immunostained with anti-HA. RFP shown in red identified viral infected cells. HA-GLUT4 on plasma membrane is shown by anti-HA staining pseudo-coloured blue and total GLUT4 is shown in green from the GFP tag.

4.3 Discussion

We have shown in chapter 3 an interesting set of data suggesting important effects of posttranslational modification, i.e. phosphorylation, on SNAREs syntaxin4 and Munc18c that affected their interactions in binary bindings or SNARE complex formation. Yet these findings are *in vitro* and hence need to be translated in cellular systems. This requires tools for introducing phosphomimetic constructs into cells of interest thus mammalian type of plasmids are needed for sub-cloning constructs followed by transfection to check for viability of expressed protein. All of these and more were accomplished in this chapter.

In order to detect phosphorylated residues of either syntaxin4 or Mnuc18c, a set of antibodies capable of recognising tyrosine 115 or 251 in Sx4 and 521 in Munc18c were synthesised. Protein sequence alignments showed conserved polypeptide between different species and isoforms within human as well (Figure 4-1 and Figure 4-2). Antibodies synthesised were delivered as two sets including phospho-specific and another set which was non-phosphospecific. Both were affinity purified and tested for no cross-reactivity confirmed by ELISA.

As we received the phospho-specific antibodies the next task was to test them thus we set up experiments using recombinant proteins and cell lysates. Syntaxin4 is a direct target for phosphorylation, upon insulin stimulation, by tyrosine kinase. Recombinant cytoplasmic insulin receptor kinase (CIRK) (Kuhne et al., 1994) for examining consequences of insulin receptor phosphorylation on other proteins was used to mimic insulin stimulation and phosphorylation of Sx4. Syntaxin4 phosphomimetic mutants were employed to test phosphorylation using CIRK and detection using the phospho-specific antibodies. Interestingly, with purified proteins, the antibodies worked accurately as they detected predicted tyrosine residues to be phosphorylated in each mutant. For instance, antibody specific for Y115 phosphorylation detected phosphorylated Y115 within phosphomimetic Sx4-Y251E and wild type (Sx4) but not in Sx4-Y115E or 2P as these two have the site mutated while earlier two are still intact and hence susceptible to phosphorylation (Figure 4-3). Similarly data is seen using antibody specific for Y251 phosphorylation. Moreover, double phosphomimetic Sx4, 2P, showed no signal using neither of antibodies nor total tyrosine phosphorylation

(PY) antibody such that both sites are mutated. Total tyrosine phosphorylation (PY) antibody detected stronger signal for wild type Sx4 compared to single phosphomimetic, nearly double, in an indication of amount of tyrosine residues being phosphorylated. Commercial Sx4 antibody showed similar signal for all mutants confirming equal concentrations between all. These findings prove that CIRK is able to phosphorylate recombinant Sx4 at tyrosine residues 115 and 251 as it had been shown on 3T3-L1 adipocytes (Schmelzle et al., 2006). Also, generated antibodies were proven for detection specificity. Intriguingly, in regard to number of phosphorylated tyrosine residues upon stimulation, these data suggest that both sites, Y115 and Y251, might be phosphorylated together at the same time. Previous work in our group showed CIRK-phosphorylated Munc18c was unable to bind monomeric Sx4 or VAMP2 thus working as negative regulatory mechanism for GLUT4 translocation (Aran et al., 2011). Sx4 and SNAP23 are the t-SNAREs located in plasma membrane that participate in SNARE complex formation for GLUT4 fusion. Sx4 in adipocytes exists in two pools where it binds with SNAP23 forming t-SNARE, in the role of GLUT4 cycling through cell surface at basal conditions, and in another binds VAMP2 and Munc18c, serving as a reservoir ready to be mobilized upon insulin stimulation (Kioumourtzoglou et al., 2014). Therefore, we sought to ascertain if Sx4 in t-SNARE is phosphorylated by CIRK and hence facilitates Sx4 binding to the rest of SNAREs and ultimately complex formation and fusion. Dual expression of Sx4 and SNAP23 using *E.coli* BL21(DE3) was used for t-SNARE production and previous CIRK phosphorylation was used to phosphorylate Sx4 in the t-SNARE. Despite increasing t-SNARE concentrations, no phosphorylation signal was detected for Sx4 in contrast to the monomeric molecule (Figure 4-4). This is in agreement with similar experiments done in our group by mixing individual recombinant Sx4 and SNAP23 to form t-SNARE then CIRK phosphorylation. This data has implications regarding the locus of action of the insulin receptor on Sx4 function, implying this is not the assembled tSNARE complex.

Phospho-specific antibodies were generated using human full length sequences intended to detect phosphorylated residues in human or mouse samples as the phosphorylation sites are well-conserved within Sx4 and Munc18c (Figure 4-1 and Figure 4-2). Antibodies differ in immunoblotting conditions such that antibody

dilution, blocking buffer, lysis buffer, and washing buffer are factors that contribute to signal quality thus need to be optimised. Using 3T3-L1 adipocyte lysates, in contrast to commercial Sx4 antibody giving a single cross-reacting species at the expected molecular weight, Sx4 phospho-specific antibodies detected multiple bands in lysates at different sizes (Figure 4-5**A**). A set of optimisation criteria tested included blocking buffer, washing buffer, and antibody dilutions and yet non-specific bands still predominated. We turned therefore to immunoprecipitation of Sx4 using the phospho-specific antibodies. Discouragingly, blots showed a strong band but at a smaller size compared to band in lysates and un-bound (flow) samples (Figure 4-5**B**). Commercial antibody showed efficient immunoprecipitation such that a much stronger band for Sx4 was detected in beads samples while total phospho tyrosine showed non-specific bands (Figure 4-5**C**). A one step back approach was implemented by examining an adipocyte-derived human liposarcoma cell line (SW872) used in an identical treatment to 3T3-L1 insulin stimulation followed by a lysate immunoblot using phospho-specific antibodies (Figure 4-6). Syntaxin4 commercial antibody detected a very weak signal in SW872 and others were also not specific; thus no more work continued with this cell line.

Double hit methodology followed next by immunoprecipitating Sx4 using the phospho-specific antibodies and then using same antibodies for immunoblotting. This method suggested there is no phosphorylation in these cells or is too low to be detected by this method. It may be possible to send samples obtained from experiments using antibodies for immunoprecipitation and immunoblot (Figure 4-8) for mass spectroscopy analysis and phospho-peptide detection, to confirm if any of these bands contain predicted tyrosine. However, the reagents were not suitable for purpose for this investigation.

We also generated antibodies for Munc18c optimised for signal detection and these showed much weaker signal compared to commercial anti-Munc18c (Figure 4-9). Therefore, phospho-specific antibodies, for Sx4 or Munc18c, need more effort in optimisation as they worked with recombinant proteins but not with cell lysates which hint to concerns regarding expression level. In the future, overexpression of Sx4 or Munc18c followed by insulin stimulation then

immunoblot analysis may be useful to validate these reagents. Another approach could be by preparing a plasma membrane fraction post insulin stimulation thus enriching Sx4.

An *in situ* protein-protein interaction assay, free of complications of tags added, altered binding affinity, and tag oligomerisation or difficulties associated with cell lysing and immunoblot development, is the proximity ligation assay (PLA). PLA is the perfect technique to test protein interactions and modifications. It is superior in that detections are accomplished under endogenous protein expression levels (Weibrecht et al., 2010) and it has been used widely in research such as posttranslational modification, including phosphorylation (Blasic et al., 2012; Jarvius et al., 2007). PLA assays performed post insulin stimulation of fixed fully differentiated 3T3-L1 adipocytes using commercial Sx4 antibody raised in mouse and the phospho-specific antibodies, individually were employed. Positive control reactions contained mouse and rabbit anti-Sx4 antibodies and negative control assay had one antibody omitted in order to detect no signal. Both Sx4 phospho-specific antibodies, Y115-P and Y251-P, displayed PLA positive signals at basal and insulin-stimulated conditions (examples shown in Figure 4-11 and Figure 4-12). 3T3-L1 adipocytes are difficult to work with for examining cell surface interactions due to their shape, rounded, and fat droplets shielding parts of the cytosol. Therefore, PLA signal intensity and numbers vary with focal plane level changes (Figure 4-12). The obtained signal ratios between basal and insulin-stimulated adipocytes need more elaboration because of stated signal reading difficulties. Nevertheless, for initial documentation purposes, primary findings are included in appendices (Appendix-I). Moreover, PLA pairs VAMP2-SNAP23 showed a very significant insulin-stimulated increase compared to basal which had been documented in previous work done in our group (Kioumourtzoglou et al., 2014), data shown in Appendix-I. Hence, under conditions where we have shown the assay to be faithfully recording data from other studies, we can detect phosphorylation of these residues in 3T3-L1 adipocytes.

Data so far suggest phosphorylation of Sx4 and Munc18c exist and to a good degree of confidence in predicted sites. The next area of study is the effect of

phosphorylation of Sx4 (and Munc18c) on GLUT4 translocation and traffic and consequences on glucose uptake. Therefore, phosphomimetic mutant constructs need to be integrated in cells to be expressed thus their functionality could be examined. Studies using 3T3-L1 adipocytes are hindered by the fact that genetic modification of fully differentiated adipocytes is extremely difficult. Lentivirus intervention proved to be an efficient approach for genetic material insertion with low signs of toxicity or cytopathogenicity in the cultured adipocytes (Carlotti et al., 2004). Two plasmids were chosen for sub-cloning full length un-tagged Sx4 and Munc18c that contain fluorescent tags, for later infection assessment, pCDH-CMV-MCS-EF1-RFP and pLVX-IRES-mCherry, respectively. Cloning was successful and positively showed a transient expression as used in a transfection confirming viability of introduced constructs (Figure 4-13). To produce lentivirus molecules, HEK293 producer cells were employed using different transfection reagents followed by a concentration step using ultracentrifugation. Transduction efficiency was tested on relatively easy-to-infect cells such as HeLa, HEK293, and 3T3-L1 fibroblasts, before using our fatty cell model 3T3-L1 adipocytes. Infection using concentrated lentivirus was successful and confirmed by overexpression of Sx4 mutants visualised by immunoblots and confocal microscopy images showing infected cells in red corresponding to RFP tag constructed in the lentivirus plasmid (Figure 4-14). At this stage we decided to examine functionality of transduced constructs in a whole cell environment through GLUT4 translocation changes upon insulin stimulation. HeLa cells expressing HA-GLUT4-GFP were employed to examine consequences of overexpression of wild type Sx4 versus the double phosphomimetic (2P) and effects of that on translocation of GLUT4 as these cells are known to be efficiently viral transduced. The prediction was to detect more GLUT4 molecules on plasma membrane, gauged by HA stain, post insulin stimulation. The intracellular GLUT4 population would be distinguished such that they fluorescent green while plasma membrane-localised stain in blue. The HA epitope is in an extracellular loop which would be accessible to anti-HA antibody only when HA–GLUT4–GFP is inserted into the plasma membrane and this staining is achieved without cell permeabilization. Also, infected cells would fluorescent red for RFP in their construct, as described earlier (Figure 4-15). HA staining, showing GLUT4 in plasma membrane, was indistinguishable between basal and

insulin samples in these cells; this may be a function of viral transduction. We examined ratios of HA/GFP stain intensities: differences were not statistically significant (not shown). However, as we were assured of lentivirus transduction efficiency and overexpressed protein functionality, subsequent experiment work turned to 3T3-L1 adipocytes as cell model for GLUT4 trafficking.

CHAPTER FIVE

5 Syntaxin4 phosphorylation consequences, *in vivo*

5.1 Introduction

Fully differentiated 3T3-L1 adipocytes proved to be difficult for infection yet lentivirus approach is the most suitable route with high efficiency and low cytotoxicity (Carlotti et al., 2004). With the help of tools developed in previous chapter, *in vivo* examinations about biological consequences of syntaxin4 phosphorylation using wild type (Sx4) and double phosphomimetic (2P) syntaxin4 were conducted. Therefore, aims pursued in this chapter were as follow:

I. Test produced Sx4-lentivirus infection efficiency and overexpression level followed by measuring changes in glucose uptake.
II. Characterisation of Sx4-knockout cells and examine effects on GLUT4 machinery.
III. Assessment of re-introduction of Sx4 into knockout model.

5.2 Results

5.2.1 Primary data on over-expression of Sx4 or 2P and resulting consequences on glucose uptake in native 3T3-L1 adipocytes

In Chapter-4 we showed that cloned lentivirus plasmids were able to drive expression of Sx4 in HeLa cells after transfection and that virus produced from these packaging systems was able to infect HeLa and HEK293 cells. Our cell line of choice for study of insulin-stimulated glucose transport is 3T3-L1 adipocytes; these cells are known to be difficult to infect (Ross et al., 2003). Therefore, a set of different multiplicity of infection (MOI) controls, i.e. using variable volumes of concentrated virus, were tested first in an attempt to ascertain approximate ranges of viral dilutions for further experiments. Fully differentiated 3T3-L1 adipocytes were infected with concentrated lentivirus designed to express either wild type (Sx4) or double phosphomimetic (2P) Sx4 using polybrene to increase transduction efficiency (Aubin et al., 1994; Coelen et al., 1983). A further complicating aspect of this analysis is that we chose to design vectors and constructs which lacked an epitope tag. The addition of

epitope-tags to Sx's (and indeed other SNAREs) has been suggested to impact significantly on the interaction of the SNAREs with other members of the SNARE family and also with regulatory molecules such as Munc18c (Kioumourtzoglou et al., 2014). Furthermore, as part of infection optimization, 3T3-L1 cells were infected at different days before, during, or after differentiation in order to find out the best time and concentration (data not shown). In our hands, the choice of infection as fibroblasts followed by differentiation was favoured, as it involved infection of fibroblasts rather than adipocytes, provided the protein expressed remained present after differentiation in adipocytes. Immunoblot analysis of infected cells showed an increase in the Sx4-positive immunoreactivity at the expected molecular weight, which we interpret to represent over-expression; this was observed using both viruses (Figure 5-1) though to variable levels. Variable over-expression of Sx4 and 2P was observed (Figure 5-1), i.e. same volume of virus added result in different level of over-expression, although this may reflect differences in viral titre between batches. Both cDNAs were expressed in same plasmid backbone and have the same size of insert, apart from mutated nucleotides, hence this variability could be due to efficiency of lentivirus production, concentration, or transduction. Therefore, based upon the observed over-expression, we next used these cells to measure glucose uptake in the presence and absence of insulin, with the view of testing the hypothesis that a difference in transport rate might be evident between Sx4 and 2P over-expression.

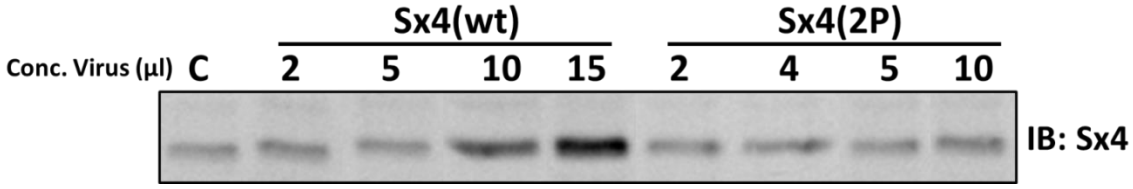

Figure 5-1 Lentivirus infection of 3T3-L1 adipocytes resulted in an overexpression of Sx4. 3T3-L1 adipocytes were infected with concentrated lentivirus containing wild type (Sx4) or double phosphomimetic (2P) Sx4 as indicated (500pfu/cell). 3T3-L1 cells were incubated for 48h then harvested in 50 µl lysis buffer and an equal volume of lysate added to each lane. Data from a typical experiment is shown; levels of over-expression vary with virus batch, but a dose-dependent increase in Sx4 immunoreactivity was observed for both viruses compared to control (which shows endogenous levels). C/ control, i.e. un-infected 3T3-L1 adipocyte.

To measure glucose transport rates, the accumulation of radioactive [3H] 2-deoxy-Glucose was the chosen approach, using non-infected 3T3-L1 cells as a control for insulin stimulation. Given the high volumes of virus required for this analysis, we re-designed the assay to be run in 96 well plates so minimizing the use of concentrated virus required. The optimisation process involved consideration of uptake times (for best signal/background ratio), the number of washes (aspiration washes were impossible to perform on small volumes with sufficient speed, hence we optimised the 'flip-and-dip' assay) and the best plasticware for optimal cell adhesion/differentiation (data not shown).
Figure 5-2 shows data from a typical experiment; these data hint at increased basal glucose transport rate upon over-expression of Sx4, consistent with data from transgenic mouse studies (Spurlin et al., 2004), this increased further when the 2P mutant was expressed (Figure 5-2). We hypothesised that the over-expression of Sx4 would lead to higher glucose uptake by having more Sx4 proteins to participate in SNARE complex formation thus GLUT4 fusion. We further hypothesised that this increases with over-expression of the double phosphomimetic version (2P) which is ready for complex formation, i.e. in the open conformation, and hence more fusion of GLUT4-containing vesicles resulting in elevated glucose transport. The data in Figure 5-2 support this. Interestingly there is no enhancement of insulin-stimulated glucose uptake; this may be logical given that insulin stimulated tyrosine phosphorylation of the endogenous Sx4 will still occur. These kinds of trends were not evident in all experiments of this type, perhaps reflecting some variability in levels of over-expression. Hence, we decided to focus our efforts on a recently developed CRISPR/Cas-9 knockout of Sx4 in 3T3-L1 cells, developed by Hannah Black in this group (H.L.Black, PhD thesis, University of Glasgow 2017). Prior to using these cells, some initial characterisation was required.

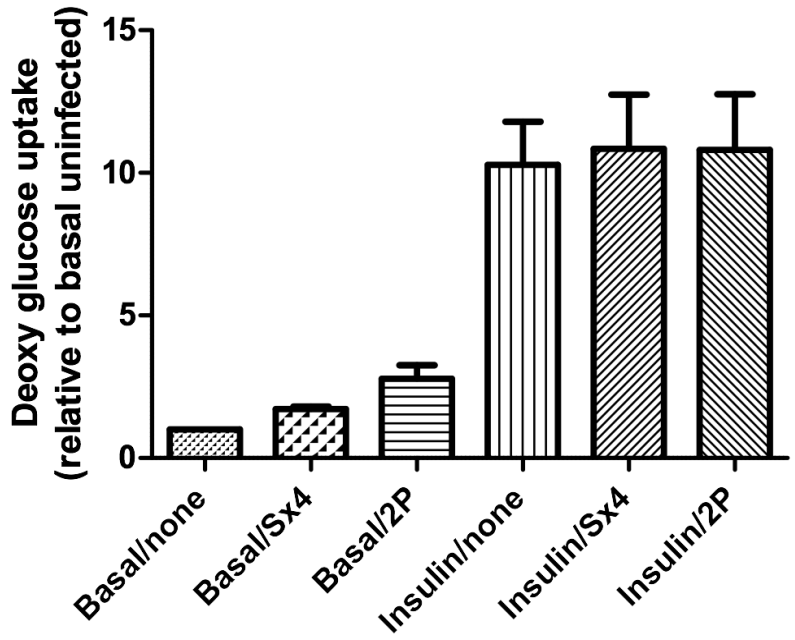

Figure 5-2 Sx4 over-expression appears to elevate basal glucose transport in native 3T3-L1. Differentiated 3T3-L1 cells were lentivirus infected for wild type (Sx4) or double phosphomimetic (2P) Sx4. 48h post-infection, cells were used for radioactive deoxyglucose uptake assay under basal or insulin stimulation (1μM for 20min) conditions. This is data from a single experiment, repeated with broadly similar results. Data plotted as mean ± SEM of triplicate wells for each condition; basal transport in control conditions is set as 1, and all data are expressed relative to that value. A trend towards elevated basal transport is seen, but this has not been quantified over a range of experiments for reasons elaborated in the text.

5.2.2 Characterisation of Sx4 knockout cells.

Syntaxin4 was knocked-out of native and HA-GLUT4-GFP over-expressing 3T3-L1 cells using CRISPR-Cas9 technology and their properties characterised; stages of this work were performed in tandem with Hannah Black, University of Glasgow. Cells were transfected with syntaxin4 CRISPR plasmid (pCMV-Cas9-RFP), obtained from GeneCellin, using manufacturer instruction. Post 24 hours, cells were washed in pre-warmed serum-free DMEM and dislodged from plating dish with Trypsin (0.05%) and 5 minutes' incubation at 37^{o}C. Cells were collected using centrifuge spin (800rpm/5minutes) followed by re-suspension in 1ml PBS. The plasmid used contain RFP tag. Transfected cells were sorted using a flow

cytometer (Beckman Coulter MoFlo Astrios flow cytometer and Summit 6.2 software) with good transfection efficiency, at 49% for 3T3-L1 cells and 48% for HA-GLUT4-GFP 3T3-L1 cells. Cells positive for RFP were diluted, in serious, and plated in 10cm dishes and 6-well plates with 10% NCS DMEM and 1% Glutamax until single colonies formed, media changed every 3 days. Selected colonies were removed, washed 3X with serum-free DMEM, using an autoclaved wide-end pipette fixed to bottom of plate with autoclaved silicon grease. Trypsin was added for one minute then cells were suspended by titration and plated for expansion. Positive cells were cultured and confirmed for Sx4 depletion by immunoblotting (Figure 5-3). The ability of these cells to differentiate, a vital characteristic for further utility, was examined using Oil-red O staining (Figure 5-4). Knockout cells were able to differentiate, though to a less extent compared to wild type cells as judged by Oil-red O staining; the HA-GLUT4-GFP 3T3-L1 cells were not able to differentiate at all and were also slower in growth. The latter were therefore not employed further in this study.

Characterization of the biological consequences of Sx4 knockout were important to explore and to explain any changes in the cell's slow growth, differentiation, adipogenesis, or glucose uptake. To this end, triplicate plates of native 3T3-L1 and knockout 3T3-L1 were grown and differentiated in 10cm dishes. Preparation of secreted proteins and cell lysate samples was performed as described (Sadler et al., 2016) in a protocol established in our lab.

Lysates obtained from native 3T3-L1 and knockout cells were blotted for marker proteins characteristic for adipocyte differentiation as well as proteins essential for the glucose uptake machinery such as GLUT4. Complete Sx4 depletion is clearly shown (Figure 5-3). This conformation ensures that forthcoming protein characterizations and biological consequences are accompanied by lack of Sx4 in these cells. (Note that multiple lines of 3T3-L1 cells devoid of Sx4 were used with similar results; here we focus on one line throughout the rest of this Chapter).

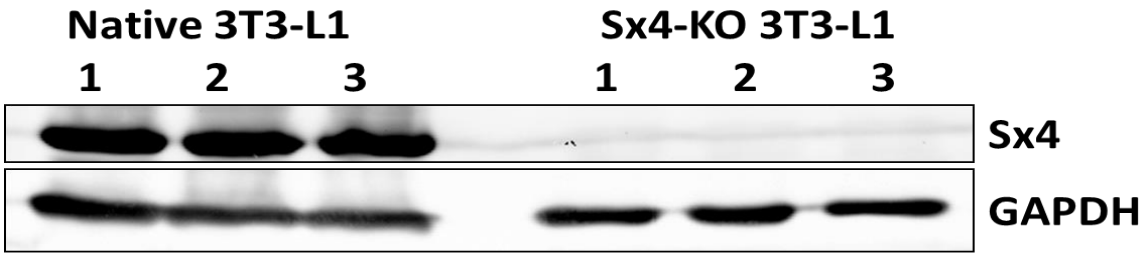

Figure 5-3 Sx4 is depleted in knockout 3T3-L1 cells.

Lysates from triplicate 10cm dishes (labelled 1,2 and 3 in figure) of differentiated native cells (three different plates) and knockout cells (three different plates of the same clone Sx4 knockout) were separate by 12% SDS-PAGE followed by immunoblotting for Sx4 and GAPDH (loading control). Equal protein loading for both cell lines was used; in this experiment 30ug of protein were loaded per lane.

Morphology of cells is an important measure of cellular organization and the physiological state of the cells in states of health or pathological conditions. Therefore, it is important to explore the effect of Sx4 knockout on fibroblast proliferation and differentiation by examining lipid accumulation which is characteristic of adipogenesis. Equal cell densities of native and knockout cells were seeded into 12-well plates, in duplicates, on glass coverslips and differentiated. Cells were grown to confluency then differentiation was initiated, labelled as day-0 (Figure 5-4). Briefly, on each assigned day, the media was aspirated; the cells were washed with PBS then fixed in formalin. Fixed cells were washed with isopropanol then incubated for 10 minutes with Oil Red O stain to stain lipid deposits and Haematoxylin to stain cell nuclei. Images were acquired using a light microscope fitted with a camera (Figure 5-4).
Knockout cells showed slightly different morphology to native cells from the first day of differentiation, day-0, as they were elongated compared to native cells which were more rounded (Figure 5-4). On day-3, more of the native cells stained red than knockout which become more obvious by day-6. The last set of samples was day-11 which showed clear difference between the two types of cells: native cells contain more lipid droplets which are bigger than those present in the knockout lines. These findings suggest an essential role of Sx4 in the process of cell proliferation and adipogenesis. Further work will be required to define this role. The absence of Sx4 slowed down these processes but

importantly did not halt them completely, as clear fat droplet accumulation has occurred even upon Sx4 knockout.

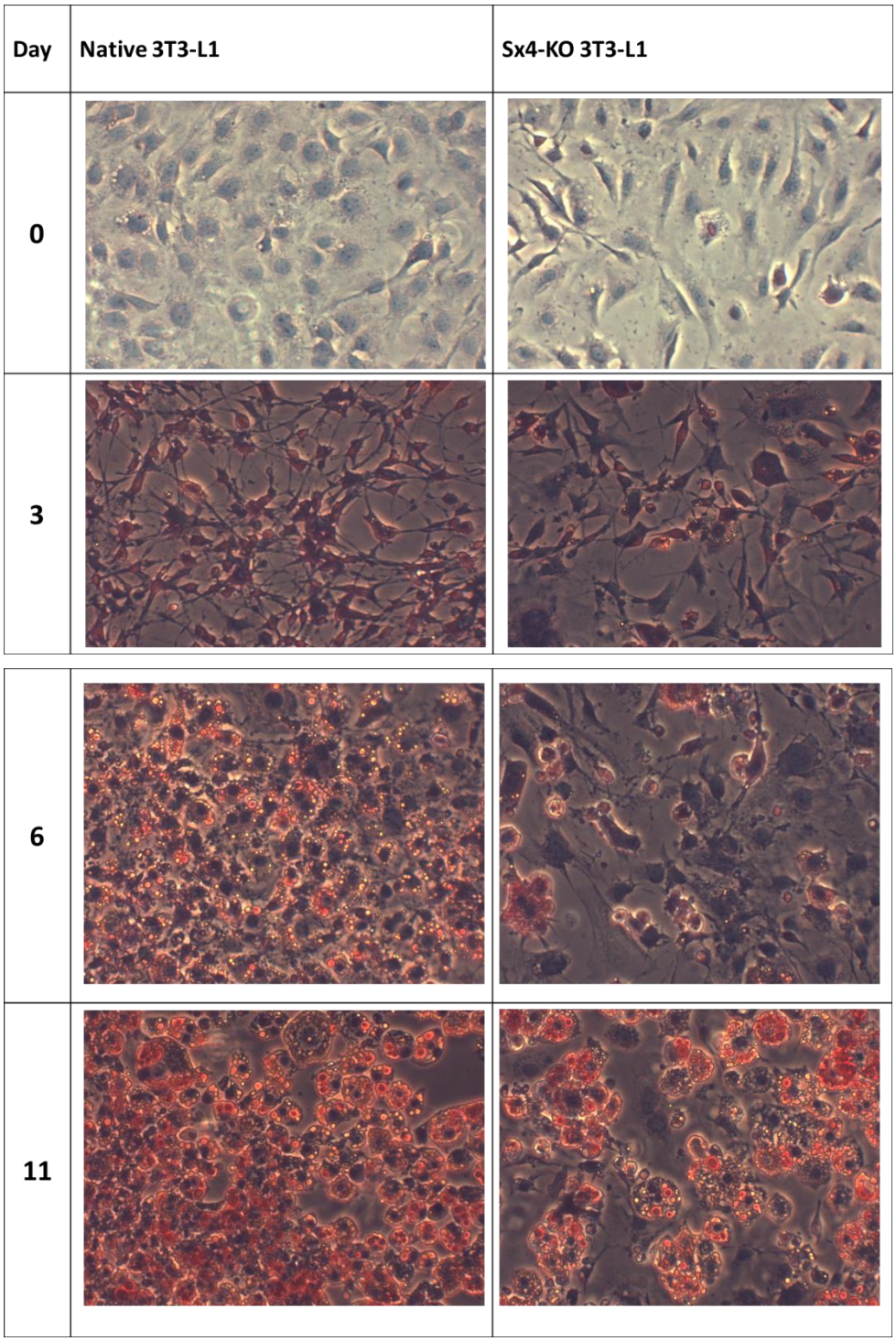

Figure 5-4 Sx4 knockout decelerates the proliferation of cell fibroblasts as well as differentiation into adipocytes.

Native 3T3-L1 and Sx4-KO 3T3-L1 cells seeded in coverslips in 12-well plates, differentiated, fixed, and fat droplets stained using Oil Red O stain, to examine the content of lipid in adipocytes, at indicated days. Images were taken using QCapture software and MicroPublisher Cameras (QImaging) installed on a light microscope. 'Day' indicates number of days from starting

differentiation (day-0). Microscopic views of cells at 20X magnification are shown. Lipid droplets stained in red and cell nuclei in blue.

The process of 3T3-L1 differentiation from fibroblasts into mature adipocytes can be monitored using different protein markers whose expression is known to increase during differentiation (Adams et al., 1997; Vishwanath et al., 2013). These include fatty acid synthase (FAS) responsible for lipid droplets formation, and peroxisome proliferator-activated receptor-γ (PPAR-γ) which is considered as a marker for differentiation. PPAR-γ is adipose specific and induced before transcriptional activation of most adipocyte genes (Adams et al., 1997). It is a key component in adipocyte differentiation and fat-specific gene expression (Brun et al., 1996; Lemberger et al., 1996). Almost an equal expression of FAS was presented by both native and knockout cells. On the other hand, PPAR-γ was dramatically reduced, if not absent, in knockout cells (Figure 5-5).

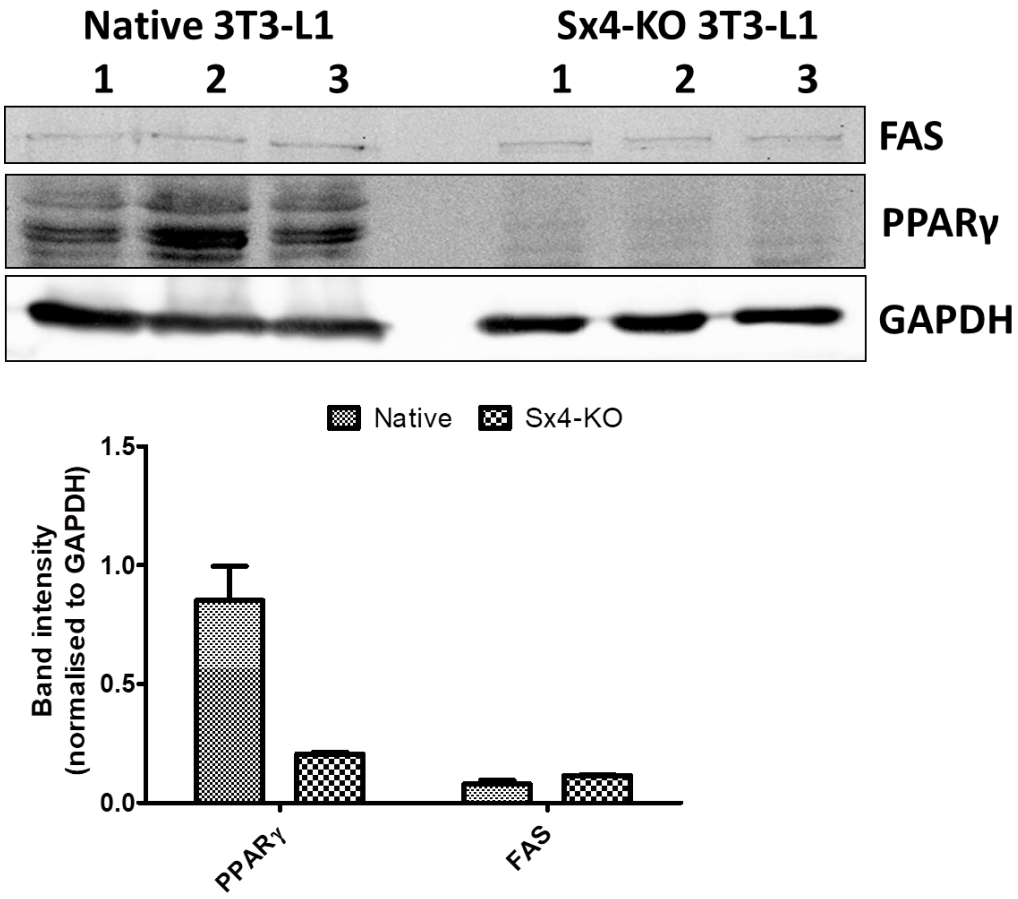

Figure 5-5 Adipocyte differentiation protein markers.

Triplicates of native or Sx4-KO 3T3-L1 fibroblasts seeded in 10cm dishes and differentiated followed by serum starvation overnight and harvested for total membrane fraction, individually.

Equal protein loads subjected to 12% SDS-PAGE and immunoblotting for differentiation markers FAS or PPAR-γ and loading control GAPDH.

Oil Red O stain (Figure 5-4) and differentiation protein markers (Figure 5-5), likely explain aspects of the slower differentiation and reduced fat droplet accumulation exhibited by knockout cells. The levels of lipid droplet in individual cells did not appear massively affected, but rather there were fewer adipocytes (Figure 5-4), and fatty acid synthase (FAS) continued to be expressed (Figure 5-5). Rather, our impression is that fat droplet formation in the knockout cells was delayed compared to the native probably as a consequence of the slower differentiation. In contrast, PPARγ expression exhibited a sharp decline; this may explain the observed slower adipocyte differentiation in the knockout cells. Collectively, we observed that knockout of Sx4 resulted in slower growth and delayed/reduced differentiation and reduced adipogenesis. We speculate that lack of Sx4 had an effect on cell growth because of its crucial role in regulating the glucose transport machinery, notably in the process of insulin stimulated glucose transport, and similarly at the differentiation stage. It is of interest, however that previous studies have shown that over-expression of PPARγ had no effect on Sx4 levels in NIH-3T3-L1 adipocytes all the way from start of differentiation to the point of being mature adipocytes (Gross et al., 2004).

5.2.3 Restored Sx4 is functional, evidence shown by glucose uptake assay

We next set out to ascertain whether the machinery involved in glucose uptake would be affected by Sx4 depletion, or whether other proteins would substitute for Sx4 function. Knockout cells were seeded, grown and differentiated, in 96-well plates for transport assays, and in parallel, a 24-well plate treated similarly was used for lysate samples to check for infection by blotting. On the day of use, media was replaced with serum-free medium for 2 hours followed by insulin stimulation for 20 minutes then glucose uptake for 5 minutes.
A typical representative dataset from knockout cells infected with wild type Sx4 or double phosphomimetic (2P) is shown in Figure 5-6, with data from four

experiments of this type shown collectively in Figure 5-7, together with comparison of wild-type 3T3-L1 adipocytes assayed under identical conditions (Figure 5-7 **B**).

Insulin stimulated glucose uptake in knockout cells at different levels between non-infected and cells infected with either wild type Sx4 or double phosphomimetic (2P) Sx4. Non-infected cells exhibited a 1.3-fold increase in glucose uptake upon insulin stimulation (Figure 5-6 **A**). Over-expression of Sx4 increased this to 2.3-fold. Interestingly, cells infected with double phosphomimetic Sx4 (2P) exhibited a further increase: 3.5-fold. The increases in fold effects in insulin-stimulation are statistically significant. Side by side, samples prepared for lysates using 24-well plate were used to blot for Sx4 and loading control, GAPDH (Figure 5-6 **B-C**). Sx4 signal was normalised to loading control in order to get an estimation of expression (Figure 5-6 **C**) and compare with the glucose uptake data described above.

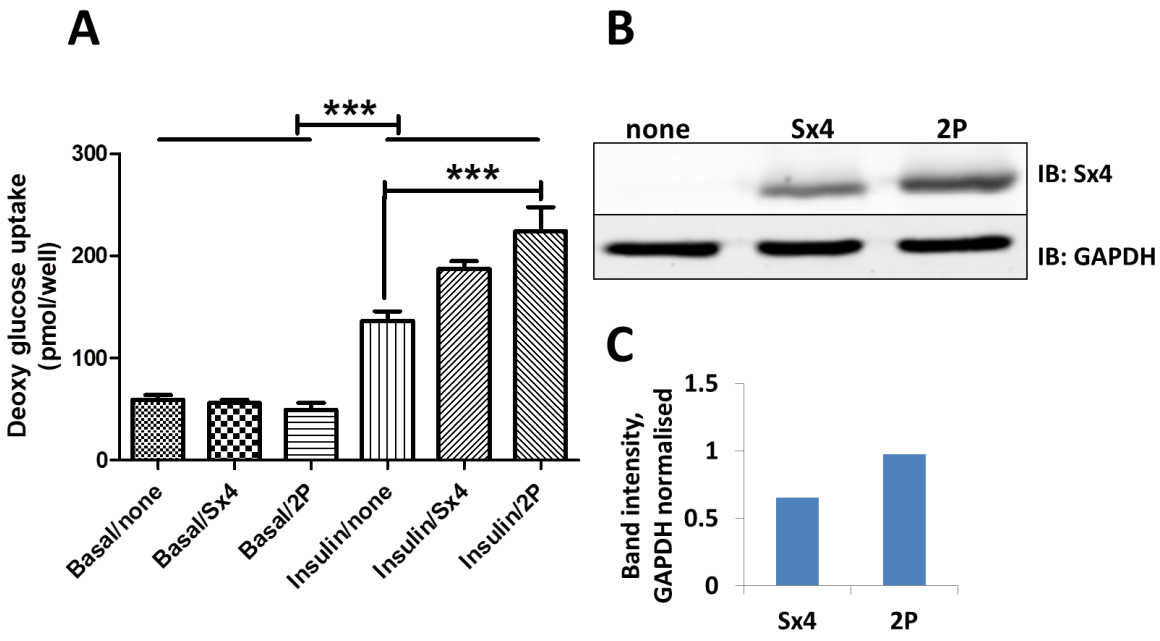

Figure 5-6 Sx4 over-expression rescues insulin-stimulated glucose uptake in Sx4 knockout 3T3-L1 cells.

Knockout cells seeded in 96-well plates and at full confluence were infected with lentivirus for either wild type (Sx4) or double phosphomimetic (2P) Sx4, followed by differentiation then glucose uptake assay on day 8-12 post-differentiation. A/ Typical glucose uptake readings from indicated samples obtained at basal or insulin-stimulated conditions. B/ Cell lysates from 24-well plate treated exactly like the uptake plate and used at same time were used to blot for indicated proteins. Equal protein

concentrations subjected to 12% SDS-PAGE followed by wet transfer and immunoblots for Sx4 or GAPDH. C/ Blot bands were quantified by densitometry and normalized to the GAPDH signal for each representative sample. Labels: none/ no lentivirus added, Sx4/ wild type lentivirus, 2P/ double phosphomimetic lentivirus. One-way ANOVA test showed highly statistical significant differences between group means, $p<0.0001$. Insulin stimulation of 2P-infected cells is significantly different than none-infected $p<0.0001$, n=4 per group.

Analysis of replicates of same experiment normalised to basal transport rate in unifected cells (Figure 5-7 **A**) shows consistent results. Knockout cells exhibit low rates of insulin-stimulated glucose transport, with a mean increase of ~1-fold compared to more than 5-fold in wild-type cells. Over-expression of wild type Sx4 increased slightly the uptake in both basal and insulin conditions; insulin stimulation increased deoxyglucose uptake by about one-fold (0.9-fold). Similarly, over-expression of the 2P-Sx4 increased basal uptake to same level as Sx4 and interestingly insulin-stimulated glucose transport demonstrated about three fold (2.66-fold). Overall, insulin stimulation resulted in statistically significant differences in glucose uptake in these cells; thus the GLUT4 machinery is active and can respond to insulin.

In comparison to native 3T3-L1 cells, the absolute values of glucose uptake are much less using the knockout cells which is relevant due to the fact the SNARE machinery for GLUT4 fusion is impaired. Typical data acquired using native 3T3-L1 is summarized in Figure 5-7 **B** from several replicates. Insulin stimulation results in about 4- to 5-fold increase in glucose uptake over basal in native cells. It is important to remember that native 3T3-L1 cells are more extensively differentiated adipocytes with a much better capacity and representative glucose uptake ability compared to the knockout lines.

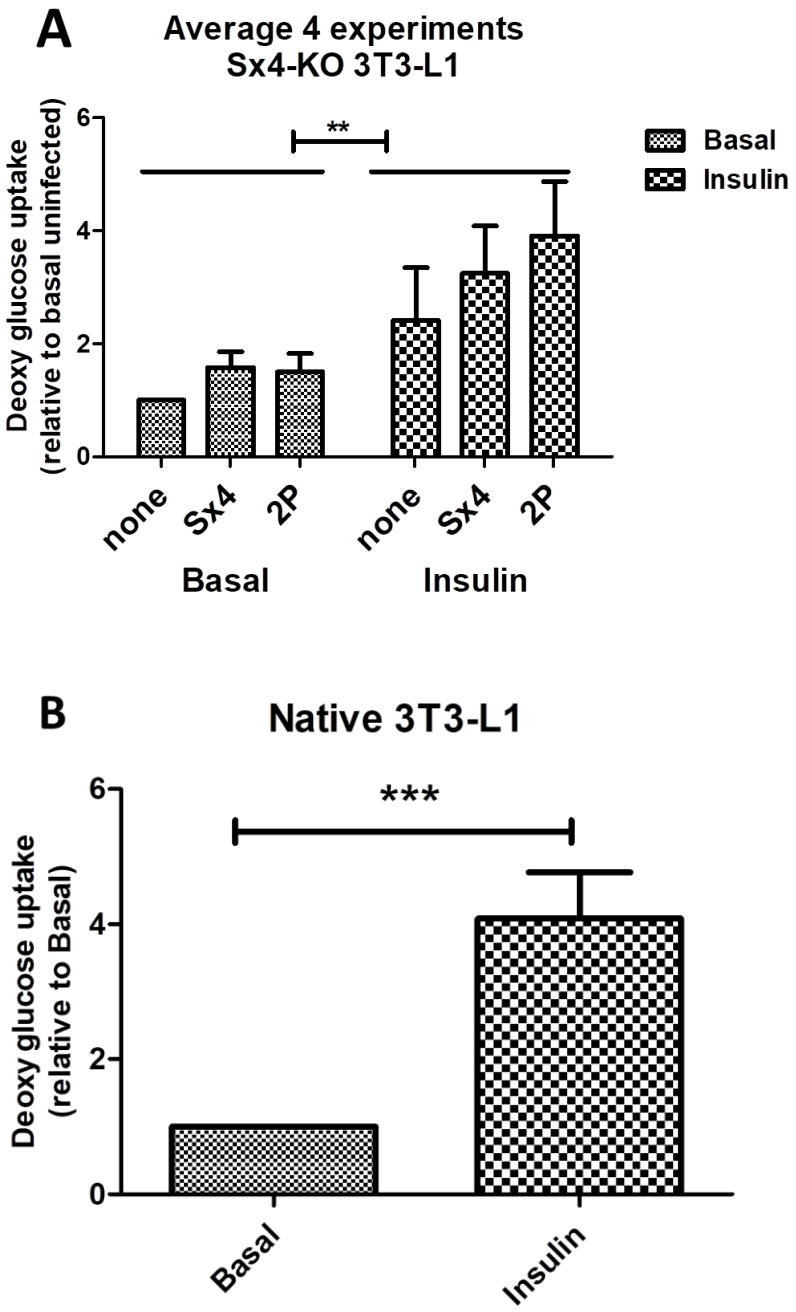

Figure 5-7 Lentivirus-mediated over-expression of Sx4 rescues levels of glucose uptake in knockout 3T3-L1 cells.

A/ Summary of four experiments where each had replicates of either 3 or 4 for each condition i.e. basal/insulin, virus infection none (no virus), Sx4, or 2P. Sx4-KO 3T3-L1 fibroblasts seeded in 96-well plates then either infected with lentivirus for wild type Sx4 (Sx4) or double phosphomimetic (2P) or no virus was added (none) and later differentiated. Following standard differentiation period, adipocytes were used for glucose uptake assay measurement and the response presented as uptake relative to basal uninfected samples ('none'). Data analysed using GraphPad Prism version 5.02, 2-way ANOVA test used with Bonferroni post-test. Error bars for SEM, $p<0.005$. B/ Typical insulin-stimulated increase in glucose uptake using native 3T3-L1, average of n=18. Data analysed

using GraphPad Prism version 5.02, Paired t-test was used to analyse data. Error bars for SEM, $p<0.001$.

These data suggest that insulin-stimulated glucose transport can be partially restored in Sx4 knockout cells upon over-expression of either type of 2P or Sx4, and further hint at differences between these two species. However, it is important to link these data with levels of over-expressed Sx4. Cell lysates were subjected to SDS-PAGE followed by blotting of Sx4 and loading control GAPDH (Figure 5-8 **A**) to compare levels of Sx4 over-expression. The plasmid construct used for the generation of lentivirus, pCDH, contained RFP. Thus images were taken for infected cells and compared to non-infected cells in order to confirm that the frequency of transduction was broadly similar between Sx4 and Sx4-2P by microscopic analysis (Figure 5-8 **B**). As shown, levels of expression were broadly comparable between Sx4 and Sx4-2P, and the numbers of infected cells were also similar. However, we found that levels of red fluorescence were difficult to analyse as the signal bleached quickly and interference from autofluorescence could sometimes complicate the results. Nonetheless, the analysis did not appear to revel significant differences in viral transduction between Sx4 and Sx4-2P, at least at a superficial level. Such observations suggest that differences in glucose transport rates outlined above may reflect functional distinctions between Sx4 and Sx4-2P (see Discussion).

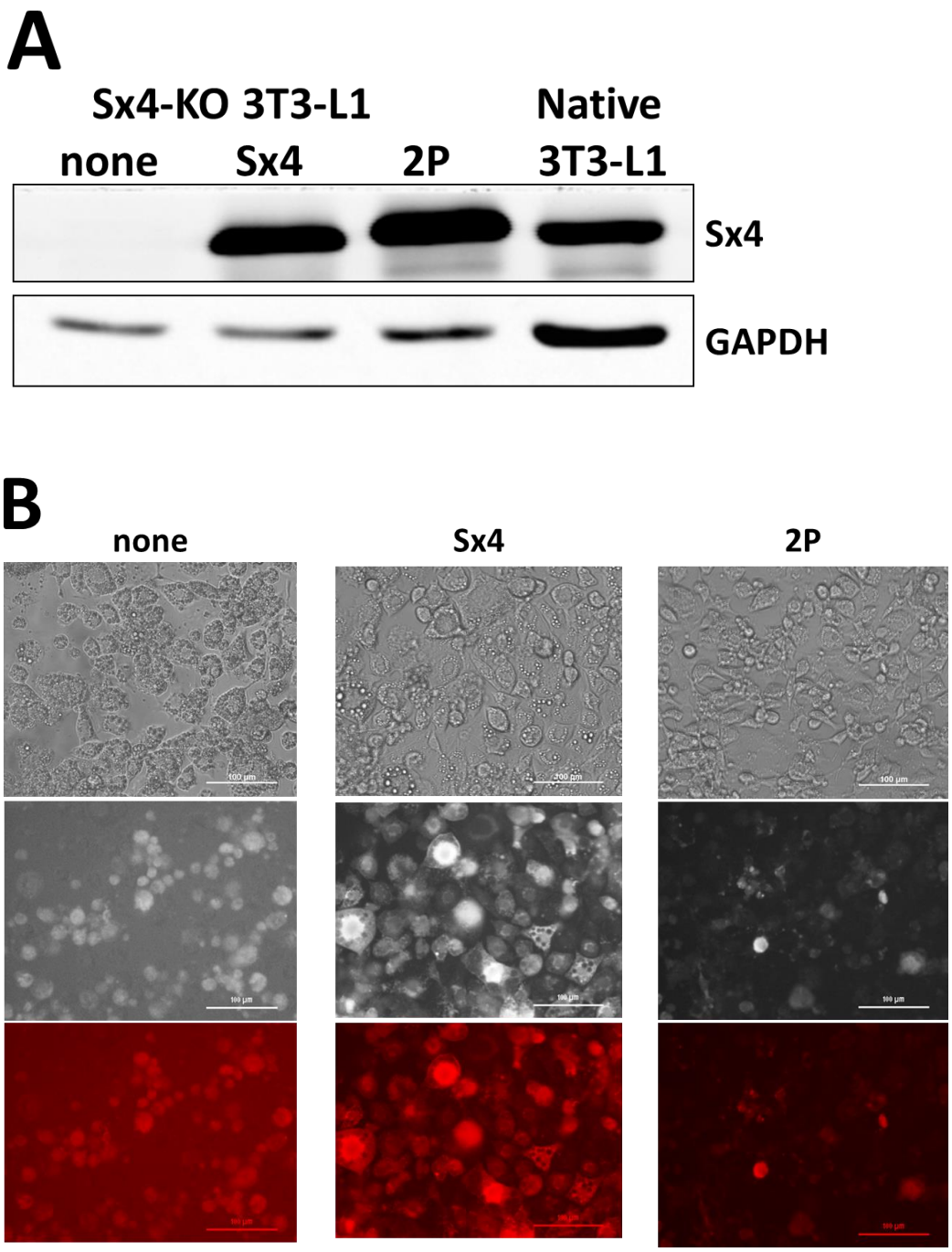

Figure 5-8 Sx4 re-expressed in infected knockout cells.

A/ Sx4-KO 3T3-L1 fibroblasts were grown in 24-well plates until fully confluent, then infected overnight with lentivirus for either wild type (Sx4) or double phosphomimetic (2P) Sx4 using 8ug/ml polybrene in complete media. Cells were differentiated and cell lysates prepared 8-12 day post induction. Equal protein loads (20µg) were subjected to 12% SDS-PAGE and immunoblot for Sx4 and GAPDH. B/ Bright field images, upper panel, of indicated cells taken using inverted light microscope and the microscope then switched to fluorescence to capture the middle panel in grey scale. Using ImageJ software, images were composited to red display in the lower panel. Cells were cultured in 96 well plastic plates.

5.2.4 Knockout effects on GLUT4 machinery

Insulin stimulates translocation of vesicles containing GLUT4 from intracellular compartments into the plasma membrane and fusion in 3T3-L1 adipocytes through a mechanism dependent on SNARE complex formation containing VAMP2, SNAP23, and Sx4. Sx4 is regulated by Munc18c operating either as an inhibitor or enhancer (Brandie et al., 2008; Christie et al., 2012; Hu et al., 2007; Latham et al., 2006; Thurmond et al., 2000). Insulin-responsive aminopeptidase (IRAP) is found in GLUT4-containing vesicles in 3T3-L1 adipocytes. GLUT1 facilitates the transport of glucose across the plasma membranes of mammalian cells (Olson and Pessin, 1996) and is expressed in 3T3-L1 adipocytes. Sx16, is known to function in early endosome-TGN transport and is involved in GLUT4 sorting and is up-regulated during adipocyte differentiation (Proctor et al., 2006; Roccisana et al., 2013). Therefore, we examined expression of these proteins to gauge the impact of Sx4 knockdown on the GLUT4 regulatory machinery (Figure 5-9). GLUT4 and GLUT1 are both expressed in 3T3-L1 at high levels (Robinson et al., 1992). GLUT4 decreased in expression dramatically in knockout cells compared to native cells. GLUT1 levels were also reduced but to a lesser degree than GLUT4. A sharp reduction in Sx16 was also documented (Figure 5-9).

By contrast, the IRAP levels in Sx4 knockout cells are only slightly reduced compared to native adipocytes. IRAP is present in fibroblasts and levels only modestly increase upon differentiation, but its trafficking changes as cells differentiate. Clearly, we cannot ascertain whether trafficking of IRAP is impaired in the knockout cells based upon the limited analysis performed here. The Sx4 regulatory protein, Munc18c, was sharply reduced in expression. Co-regulation of Sec1/Munc18 proteins and their cognate SNAREs has been reported in other systems, hence this result may not be entirely unexpected (Shanks et al., 2012). The changes reported here may reflect delayed adipocyte differentiation during the period of analysis, as discussed previously. Despite addition of protease inhibitors and working at low temperatures, samples on ice, the element of protein degradation is still valid especially with low-expressed proteins thus could be considered. Cell starvation results in downregulation of most endosomal membrane proteins and upregulation of autophagy.

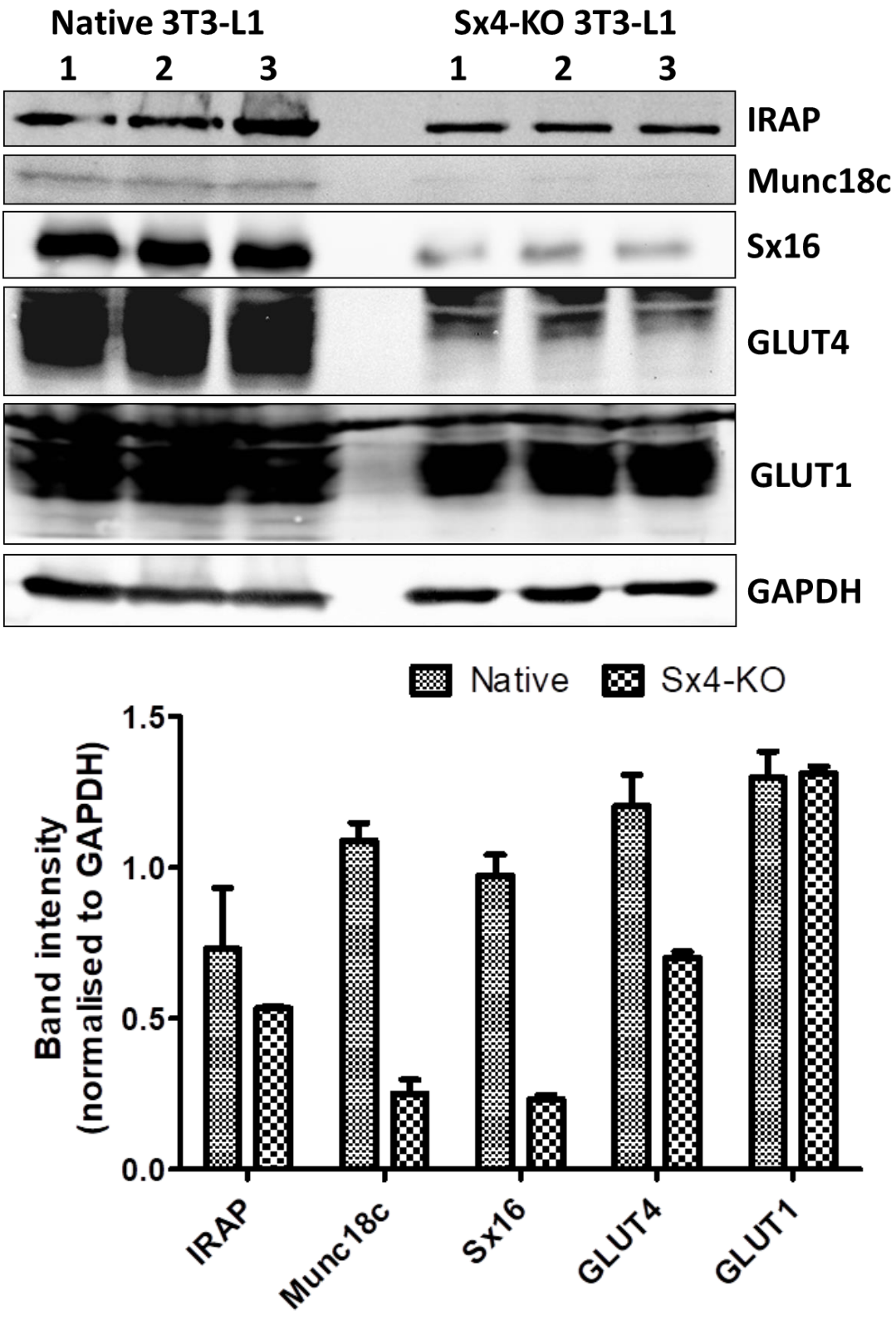

Figure 5-9 Sx4 knockout effects on glucose transport machinery.

Equal amounts of protein prepared from 10 cm dishes of native and knockout cell lysates, were separated by SDS-PAGE and analysed using immunoblotting with the indicted antibodies. Equal protein loading was confirmed using GAPDH as a control. Blots were developed using LI-COR detection system with the appropriate fluorescent IRDye®-conjugated secondary antibody.

Densitometry band intensity quantification comparing native to knockout cell lysates was normalized to loading control GAPDH. Graphs presents mean of 3 experiments of this type, with SEM shown.

5.2.5 Compensatory mechanisms.

There is a family of Sxs within the cell which localize to different compartments and share the SNARE domain, thus participating in a fusion process at different locations (Hong, 2005b). Therefore, our thoughts were directed to look for a compensating Sx that may exhibit increased expression to accommodate reduced Sx4. We focused on SNAREs localized to the plasma membrane as suitable candidates for GLUT4 fusion. Sxs 2 and 3 are located in plasma membrane, reviewed in (Teng et al., 2001), thus we tested for the presence of these molecules in knockout cell lysates compared to native 3T3-L1 adipocytes. Surprisingly, both were expressed in the native 3T3-L1 adipocytes but were reduced by almost half in the knockout (Figure 5-10). Sx 2, 3, and 4 are all reported to be located in the plasma membrane and known to function in exocytosis; but only Sx4 has been associated with GLUT4 translocation (Teng et al., 2001).

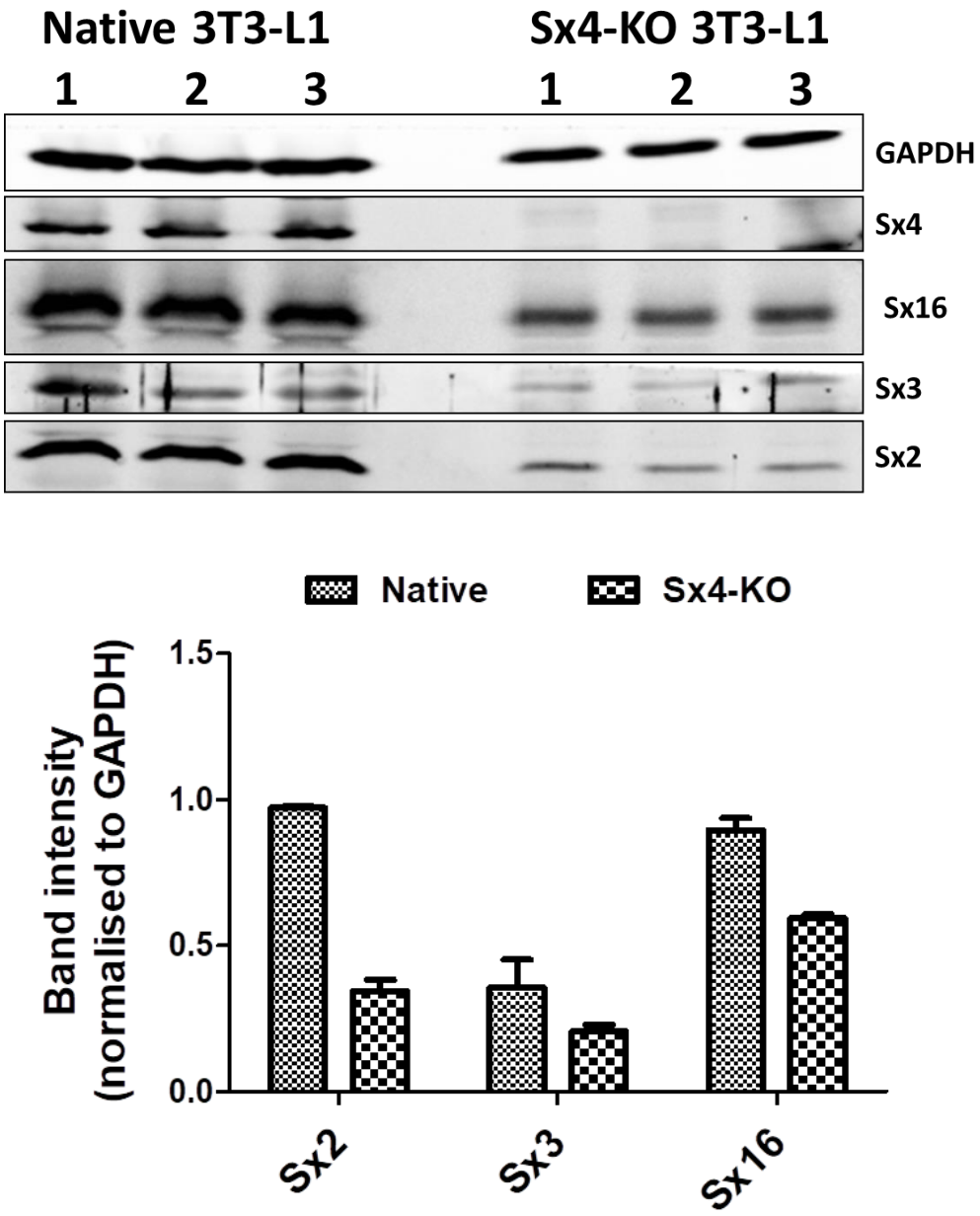

Figure 5-10 Other SNARE protein levels in Sx4 knockout adipocytes.

Native and knockout cell lysates, prepared from 10cm dishes, were separated by SDS-PAGE and examined by immunoblotting using the antibodies indicated. Equal protein loading was assessed using GAPDH as a control. Blots were developed using LI-COR detection system with the appropriate fluorescent IRDye®-conjugated secondary antibody. Densitometry band intensity quantification comparing native to knockout cell lysates was normalized to loading control GAPDH. Graph presents mean of 3 experiments with SEM.

5.2.6 Adipokine secretion – preliminary analysis of Sx4 knockout lines.

Adipocytes secret a number of peptide hormones which include leptin, adiponectin, and adipsin (Guerre-Millo, 2002). Secretions of cells were tested for the expression of adipocyte markers such as adiponectin and adipsin. Adipsin is known to be a factor expressed in differentiated cell lines of adipocytes (Doi et al., 2005; Lowell and Flier, 1990; Wilkison et al., 1990). Adiponectin gene expression and circulating concentrations are reduced in cases of obesity (Guerre-Millo, 2002). Secretion samples were obtained after an overnight serum starvation, and media collected next day followed by TCA precipitation. Knockout samples showed stronger signals for both adipsin and adiponectin (ACRP30) compared to the native (Figure 5-11) suggesting that both molecules were secreted at higher levels in the Sx4-knockout cell lines.

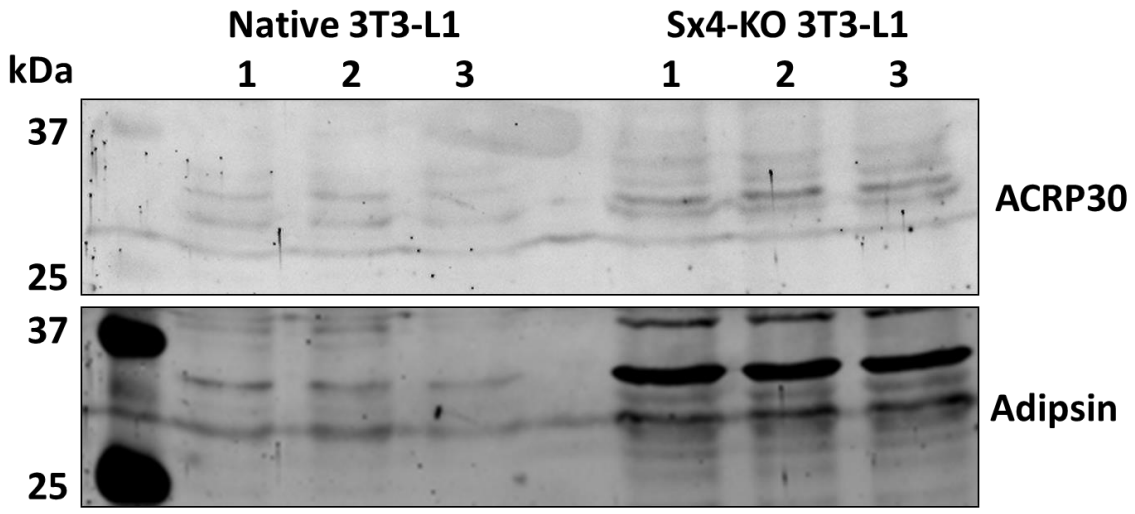

Figure 5-11 Adipocyte secretions.

Adipocyte-linked protein secretion varied with Sx4 knockout. Cells were serum-starved overnight and media collected next day to precipitate proteins using TCA. Replicates from 10cm dishes, three each, precipitated then re-suspended and mixed with equal volume of 2X LSB followed by boiling at 95oC for 5 minutes. Equal total protein concentrations were loaded into gel (25µg). Samples were immunblotted for adiponectin (ACRP30) and adipsin; data from a typical experiment is shown. The positions of molecular weight markers are shown on the left (kDa).

Given the data above, we felt it is important to estimate whether levels of Sx4 re-expression approaches those found in wild-type cells. Figure 5-12 revealed that Sx4 was well-expressed in the infected cells for both wild-type and 2P versions, compared to none in the non-infected Sx4 knockout cells (Figure 5-12). Comparison of wild-type 3T3-L1 adipocytes on the same blot revealed that the infected knockout cells over-expressed Sx4 to levels slightly higher than found in wild-type cells. Interestingly, with the re-expression of Sx4, Munc18c is also re-expressed to similar levels as the native (Figure 5-12).

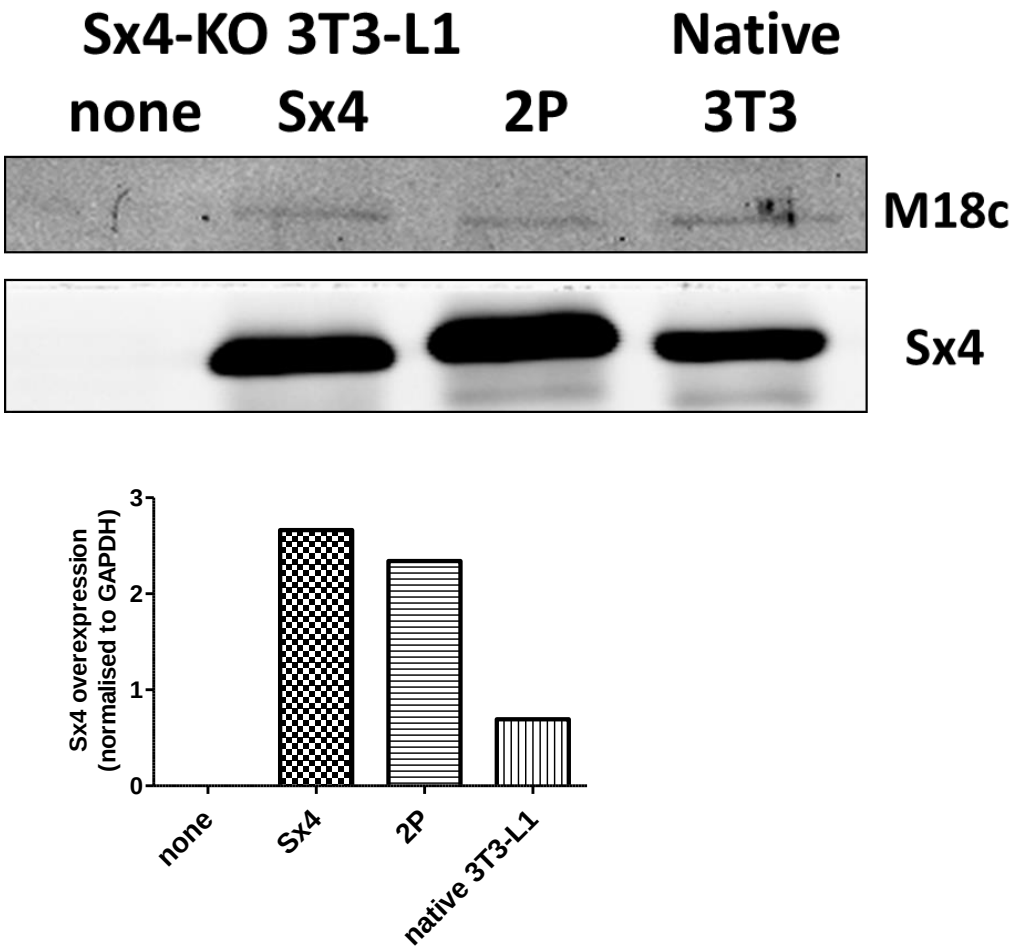

Figure 5-12 Over-expression of Sx4 in knockout cells approaches levels in wild-type cells.

Sx4-KO 3T3-L1 fibroblasts were grown on 24-well plates until fully confluent, then infected overnight with lentivirus for either wild type (Sx4) or double phosphomimetic (2P) Sx4. Cells were differentiated and cell lysates prepared 8-12 day post induction start. Equal protein loads (20µg) were subjected to 12% SDS-PAGE and immunoblot analysis for Sx4 and Munc18c. The quantification of this particular experiment is shown in graphical form where Sx4 levels are normalised to GAPDH expression.

As noted above, PPARγ levels were low in the Sx4 knockout cell lines. We therefore tested whether re-expression of Sx4 would restore or compensate for lack of endogenous Sx4 by restoring levels of this important transcription factor (Figure 5-13). It shows this was found to not be the case, with levels of PPARγ being low to undetectable regardless of Sx4 re-expression.

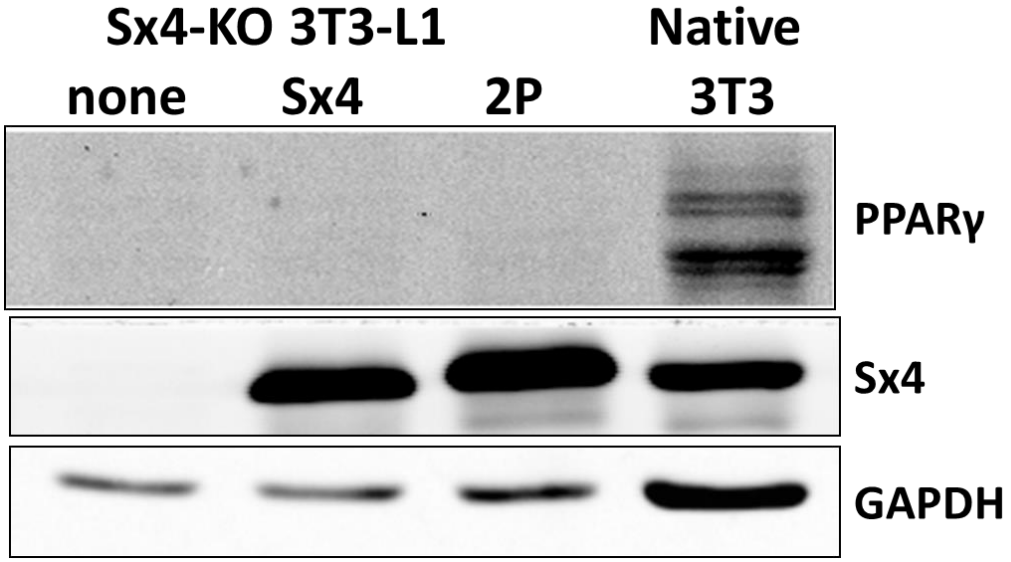

Figure 5-13 Sx4 re-expression did not restore transcriptional factor PPARγ.

The same used in Figure 5-12 were also probed for PPARγ expression. Data from a single experiment is shown.

Our data above showed that a predicted compensatory mechanism, increased Sx2, Sx3 or Sx16 expression, was not evident in these cells (Figure 5-10) as expression of each syntaxin was reduced upon Sx4 knockout. Therefore, we examined whether re-expression of Sx4 might bring their levels back to normal. Infected knockout lysates were immunoblotted for all three Sx proteins and their signals normalized first to the loading control GAPDH then compared to the un-infected (none) sample (Figure 5-14). In contrast to our expectation, Sx2 and Sx16 are lower in expression in the infected cells. Sx3 levels appeared slightly increased upon 2P expression; further data is required to ascertain whether this effect is reproducible or functionally significant.

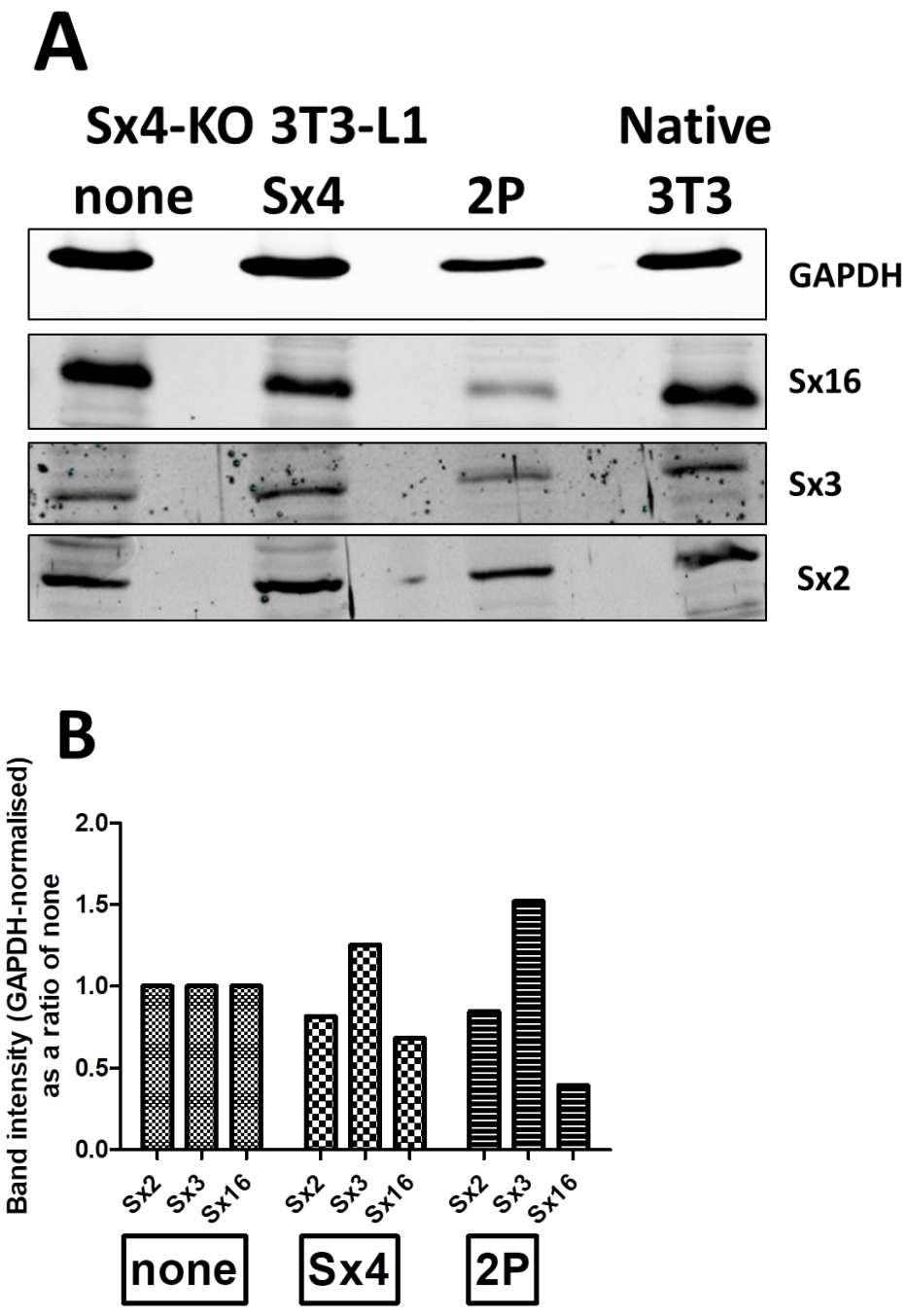

Figure 5-14 Re-introduction of Sx4 effects on other Sx proteins.

Equal protein loads (20µg) of Sx4-KO 3T3-L1 adipocytes either uninfected or infected with Sx4 or Sx4-2P were subjected to 12% SDS-PAGE and immunoblot analysis for the indicated proteins. Typical blots are shown in the upper panel; the data is then shown graphically below, where the band intensity/GAPDH signal for each SNARE is compared. The value observed in non-infected cells is set to 1, and changes upon Sx4 or Sx4-S2P expression are shown as a change in this value. Data from a typical experiment is shown.

5.3 Discussion

In the previous chapter, we showed the validity and viability of constructed lentiviral vectors which worked in transfections and later in producing lentivirus particles capable of infecting cells in culture. Sx4 over-expression in infected native adipocytes demonstrated their viability and functionality using a glucose uptake assay (Figure 5-1). The data in Figure 5-2 show a trend towards an increase in uptake in basal transport was observed but insulin stimulated glucose transport did not show a difference. We speculated this may reflect the presence of the endogenous Sx4 molecules masking any effects of mutant over-expression thus Sx4 knockout cell lines was considered as an alternative experimental system. Hannah Black, a fellow PhD student, had generated these lines using CRISPR/cas-9, and hence we chose to characterise these cells for our purposes. Immunoblot analysis for Sx4 confirmed the complete knockout of Sx4 (Figure 5-3) and this was accompanied by morphological differences compared to native 3T3-L1 (Figure 5-4) together with slower growth and delayed adipocyte differentiation. These phenotypical features were accompanied by reduced expression levels of protein markers for each stage. One of the important factors in differentiation of 3T3-L1 to adipocytes is PPAR-γ and its level of expression is almost abolished by Sx4 knockout (Figure 5-5) which likely explains the delayed differentiation of knockout cells. Despite this, fat droplets still formed consistent with our observation that fatty acid synthase (FAS) is expressed to a similar level to native adipocytes. We therefore reasoned that despite their reduced growth and differentiation, these cells exhibit adipocyte-like features sufficient for them to be a suitable model for our purposes.

Moving into the main reason for using knockout cells, they were infected with the validated lentivirus for Sx4 over-expression and infection was confirmed by blots (Figure 5-6) and microscopy using the RFP integrated in the lentivirus constructs (Figure 5-8).
Investigation of glucose uptake in infected cells showed the predicted trend where insulin stimulation resulted in increased uptake using wild type Sx4 compared to knockout cells; this was enhanced when the double

phosphomimetic, 2P, was used (Figure 5-6). Double phosphomimetic (2P) was expressed on average in our experiments by about 30% more than wild type and the insulin-stimulated glucose uptake differences are similar (Figure 5-6). Therefore, it is presently difficult to confirm whether increases in glucose transport are evident when Sx4-2P is expressed compared to Sx4 alone. This is also hampered by the fact that lentivirus preps vary in concentrations and transduction efficiency and importantly it should be emphasised that the Sx4 antibody recognition epitope could bind differently depending on protein conformation (Fiona Brandie, PhD thesis, University of Glasgow) thus signal levels may vary between Sx4 and Sx4-2P.

Glucose uptake increased significantly in response to insulin stimulation; for both Sx4 and Sx4-2P a statistically enhanced level of uptake compared to un-infected cells was observed. Importantly, representing an important and novel observation, we show that the fold increase in insulin stimulated glucose transport is markedly impaired upon Sx4 knockout compared to native cells (Figure 5-7 **B**). This could be due to the level of differentiation, maturation into adipocytes and efficiency of the glucose uptake machinery i.e. GLUT4 trafficking/translocation. Therefore, we examined the levels of expression of the GLUT4 translocation machinery. Our preliminary findings (Figure 5-7) are interesting and worthy of deeper exploration, with more variables to consider such as time of exposure to insulin, insulin concentrations and incubation periods, as well as number of cells and usage point from differentiation i.e. longer could result in more adipocytes expressing transduced protein and different results.

An expectation with Sx4 knockout was over-expression of other Sxs in compensation. Surprisingly, expression of the suggested candidates, Sx2 and Sx3, were reduced in the knockout cells (Figure 5-10). Sx3 was of particular interest, as this Qa SNARE has been reported to bind different VAMPs including 2, 3, and 8 (Xu et al., 2015). Presently, we do not have an explanation for these data, but they do suggest that compensatory mechanisms involving other key Qa SNAREs are not invoked by Sx4 knockout.

Knockout cells showed an increase in glucose uptake of 1.3-fold in response to insulin stimulation (Figure 5-6) despite the dramatic reduction of GLUT4 and Munc18c in expression and furthermore reduced levels of compensating SNAREs, Sx2 or Sx3. Therefore, we would predict glucose uptake under basal conditions was mediated by GLUT1 and upon insulin stimulation GLUT4 was functional, though with fewer molecules. Re-expression of Sx4 also rescued Munc18c expression (Figure 5-12) and hence infected cell uptake levels were enhanced pointing to the idea that GLUT4 machinery was fully functional with introduced Sx4 molecules. Interestingly, in vivo, knockout of Sx4 reduced levels of Munc18c in animal models (Yang et al., 2001) as well as cultured cells, as shown in this study. On the other hand, in whole animal studies, Munc18c-knockout does not change levels of Sx4 expression (Oh et al., 2005). However, both Sx4 and Munc18c were heterozygote-knockouts because homozygote is lethal, hence there is the possibility that residual expression of Sx4 in these heterozygous knockout animals is sufficient to maintain elements of functionality. That said, Sx4-KO resulted in 50% reduction in glucose uptake in skeletal muscles but no effect on fat (or liver) tissues, while Munc18c-KO showed >50% reduction GLUT4 translocation in skeletal muscle (Oh et al., 2005).

All in all, our findings hint at a major rule for Sx4 phosphorylation in GLUT4 trafficking and fusion in the case of insulin stimulation in the 3T3-L1 adipocytes. The open conformation of Sx4, produced by Y115 and Y251 phosphorylation (see Chapter XX), might help in the formation of SNARE complexes and hence enhance GLUT4 containing vesicles to fuse with the plasma membrane.

CHAPTER SIX

6 Munc18c phosphorylation effects on SNARE complex

6.1 Introduction

Munc18c is the main regulatory protein controlling Sx4 conformation (opened or closed) thus regulating its participation in SNARE complex formation (Latham et al., 2006). Consistent with this, Munc18c has been shown to play an important role in the regulation of GLUT4 vesicle fusion *in vitro* and insulin-stimulated glucose uptake *in vivo* (Thurmond et al., 2000). Contradictory findings regarding Munc18 binding to Sx showed roles of inhibition or enhancement of SNARE complex formation (Howes et al., 2010; Kioumourtzoglou et al., 2014; Latham et al., 2006). We and others (Yang et al., 2001) have shown that Sx4 knockout reduced dramatically if not abolished Munc18c expression in 3T3-L1 adipocytes or heterozygous knockout mice. On the other hand, Munc18c heterozygous knockout did not affect Sx4 levels (Oh et al., 2005). Munc18c is a soluble protein but is localized to the plasma membrane by association with Sx4, so that overexpression of Sx4 increased Munc18c (Thurmond et al., 1998). This chapter sought to evaluate the role of Munc18c phosphorylation on its interaction with Sx4 using *in vitro* assays. A study used quantitative mass spectrometry to identify insulin-stimulated tyrosine phosphorylation sites in 3T3-L1 adipocytes, and found residue 521 phosphorylated by more than 10 fold upon insulin treatment (Schmelzle et al., 2006). Another study reported tyrosine 219 phosphorylation, insulin-induced, using MIN6 beta cells and 3T3-L1 adipocytes (Oh and Thurmond, 2006) and Sx4-Munc18c binding decreased in pervanadate-treated cells suggesting dissociation of Munc18c from Sx4 due to phosphorylation. Our group showed that Munc18c is a direct tyrosine phosphorylation target by CIRK, *in vitro*, at tyrosine residue 521 and neither CIRK-induced nor phosphomimetic Y521E were able to bind Sx4 (Aran et al., 2011). Also, we showed that pre-incubation Sx4-Munc18c inhibited SNARE complex formation, *in vitro*, while pre-incubation with Munc18c(Y521E) enhanced ternary complex formation (Kioumourtzoglou et al., 2014). Therefore, the Sx4-Munc18c interaction is critical to study especially using codon-optimised gene expression of Munc18c (Rehman et al., 2013).

6.2 Results

6.2.1 Expression of enhanced gene and compare to mouse original sequence

Protein purification of Munc18c was challenging, with low yield and poor expression of Munc18c in bacteria being a common problem (Rehman et al., 2013) and Dr Veronica Aran-Ponte (University of Glasgow, PhD thesis, 2009). A previous study has reported enhanced expression using a different gene sequence, optimised for bacterial expression, resulting in increased yields of Munc18c. Consistent with other reports, we used the His-tagged wild-type protein sequence coding for native mouse Munc18c; however, we found that this was poorly expressed in *E.coli* BL21 (DE3) with a very low yield (Figure 6-1). Similarly, phosphomimetic Munc18c Y251E was poorly expressed (data not shown) in the same system. Trials to optimize protein expression including induction temperature, times, etc. were attempted with no significant improvement in yield.

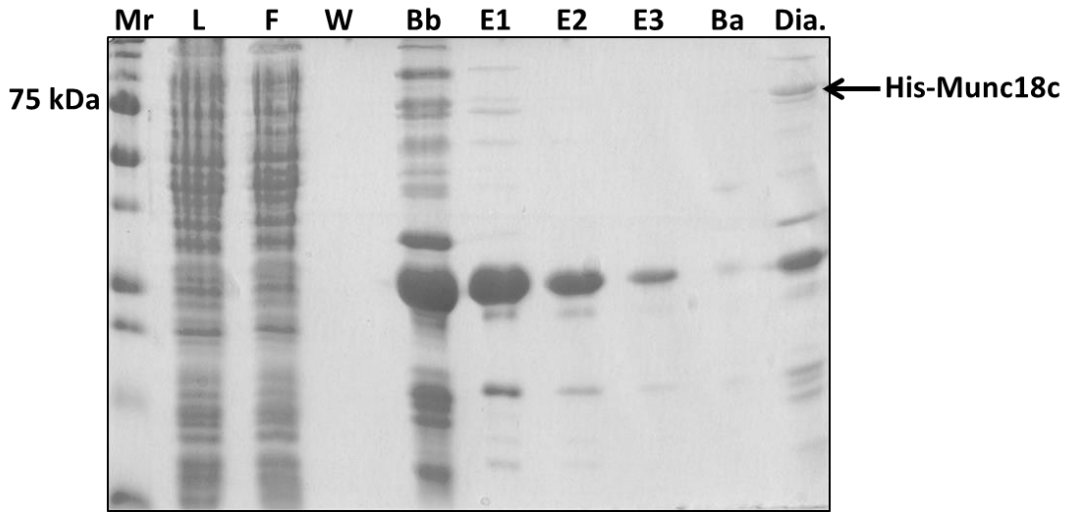

Figure 6-1 Munc18c expression using native mouse sequence.

Samples taken from different protein purification steps were subjected to 12% SDS-PAGE and gel was stained using Coomassie blue. Labels: Mr/ protein ladder, L/ lysate, F/ flow collected after beads incubation with lysate, W/ wash off beads, Bb/ beads before elution, E/ elution, Ba/ beads after elution, Dia./ dialysis sample. Predicted protein size of Munc18c is around 75kDa, indicated by the arrow at the right of the figure.

6.2.2 Cloning enhanced gene into pQE30

A research group have reported the use of an enhanced, codon-optimised, Munc18c gene with good expression level success (Rehman et al., 2013). Hence, we synthesised this gene and sub-cloned it into a bacterial expression vector pQE30. Life technologies assembled the synthetic gene constructs for wild type Munc18c and phosphomimetic Munc18c(Y521E) cloned into plasmid pMA-RQ. Codon optimized Munc18c constructs were sub-cloned into pQE30 digested with restriction enzymes EcoRI and SalI so as to position the Mucn18c species in frame and after six Histidine codons to result later in expression of N-terminus hexa-histidine tagged protein. Positive colonies were tested for the right insert size through mini-prep plasmid DNA extraction followed by restriction enzymes digestion (Figure 6-2). Gene sizes of pQE30 and Munc18c insert are 3461bp and 1971bp, respectively. Positive sub-clones were sequenced for further verification.

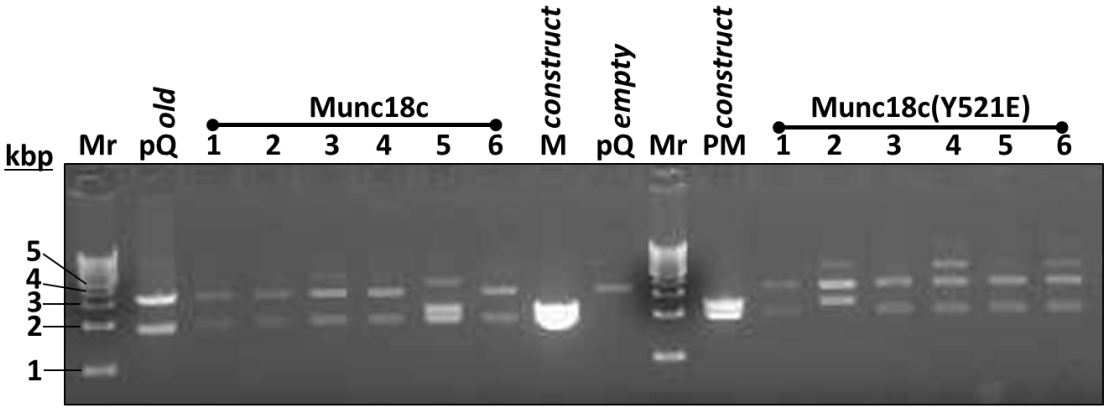

Figure 6-2 Sub-cloning codon-optimised Munc18c into pQE30.

Codon-optimised wild type and phosphomimetic Munc18c(Y521E) constructs were synthesised by Life technologies in pMA-RQ. The Munc18c fragment was released by digestion using EcoRI and SalI restriction enzymes. Following gel purification, Munc18c was ligated into pQE30 and positive colonies were grown followed by DNA extraction and digestion. Digestion patterns analysed by 1% agarose gel electrophoresis stained with Ethidium bromide; shown above are representative clones (labelled 1 to 6) for either wild-type Munc18c or the Y521E mutant. Labels: Mr/ 1kbp DNA-ladder, pQ old/ pQE30 with native mouse M18c sequence, pQ empty/ empty pQE30 plasmid, M/ wild type Munc18c, PM/ phosphomimetic Munc18c(Y521E).

6.2.3 Munc18c codon-optimised expression

The pQE30 expression plasmids containing the enhanced Munc18c sequences were transformed into competent cells *E.coli* BL21 (DE3) and grown in Terrific Broth (TB) media with IPTG induction overnight at 22ºC. Munc18c purified at the expected size of 75kDa (Figure 6-3). Both wild type (M) and phosphomimetic Y521E (PM) expressed significantly better than the wild-type sequence, and were purified to a good level (Figure 6-3) and further cleaned by dialysis (not shown). Expression levels were enhanced dramatically compared to native mouse gene (Figure 6-1).

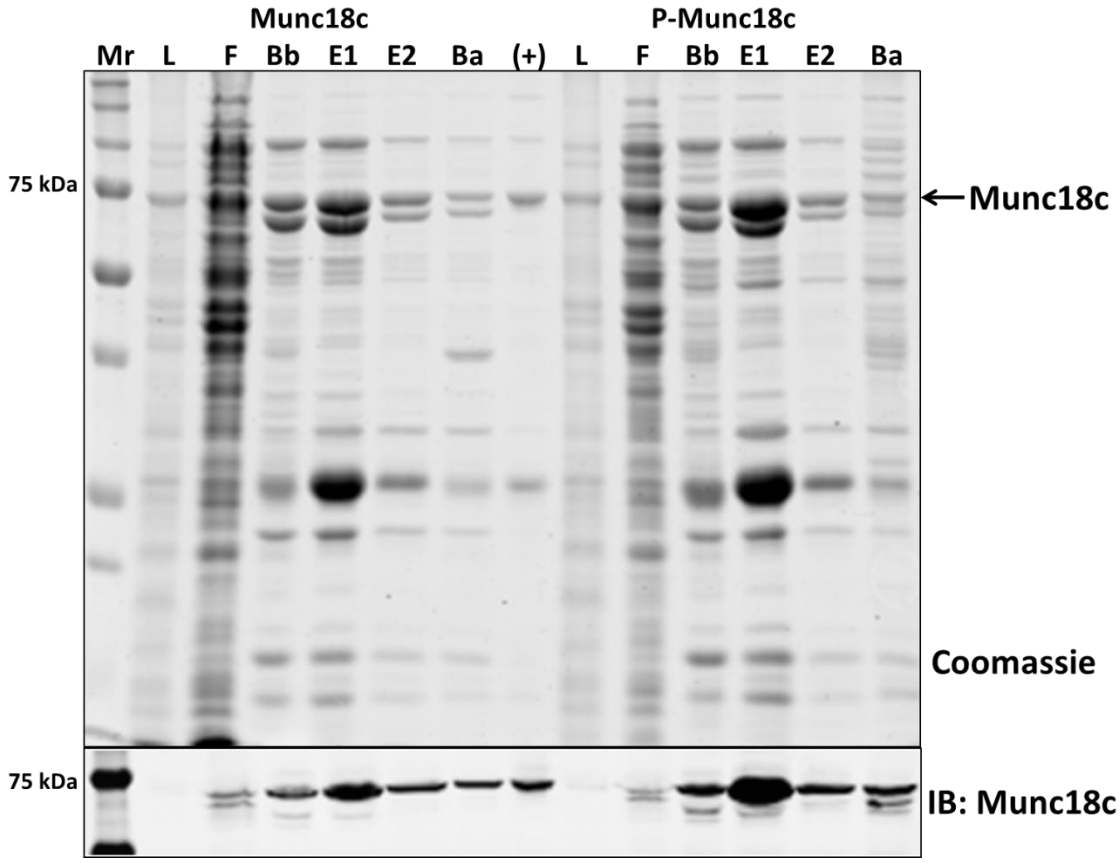

Figure 6-3 Munc18c purifications using codon-optimised gene sequence.

Munc18c expressed using the codon-optimised gene sequence cloned in pQE30 plasmid using *E. coli* BL21 (DE3) competent cells and TB media. Throughout the purification process, samples were taken at different stages and subjected to 12% SDS-PAGE and the gel was stained using coomassie blue, upper panel. Another gel was used to develop an immunoblot for Munc18c, lower panel. Labels: Mr/ protein ladder, L/ lysate, F/ flow collected after beads incubation with lysate, Bb/ beads before elution, E/ elution, Ba/ beads after elution. Predicted protein size of Munc18c is around 75kDa. Lysate sample was over-boiled thus not detected in the blot. It is thought that the additional band co-migrating with Munc18c might be GroEL as this was shown to co-purify with wild-type Munc18c (Veronica Aran, personal communication).

6.2.4 Enhanced Munc18c usage in SNARE complex

Contradictory findings of Munc18c as a Sx4 regulatory protein directed our attention to explore the effect on Sx4 phosphomimetic mutants and resultant SNARE complex to form in the presence and absence of wild-type or phosphomimetic Munc18c. Therefore, Munc18c mutants were used for SNARE complex formation in tandem with Sx4 phosphomimetic mutants comparing presence or absence of Munc18c on the overall complex formation (Figure 6-4). Sx4 mutants were pre-incubated with Munc18c followed by the addition of VAMP2 and SNAP23. Shown in Figure 4 is data from a typical experiment. As expected and previously shown, Sx4-2P formed more SNARE complex than wild-type Sx4. The addition of Munc18c (M) or Munc18c-Y251E (PM) appeared to exert only modest effects in this assay format. Hence, we decided to focus solely on comparing Sx4 and Sx4-2P in subsequent experiments and attempted to quantify many experiments of this type.

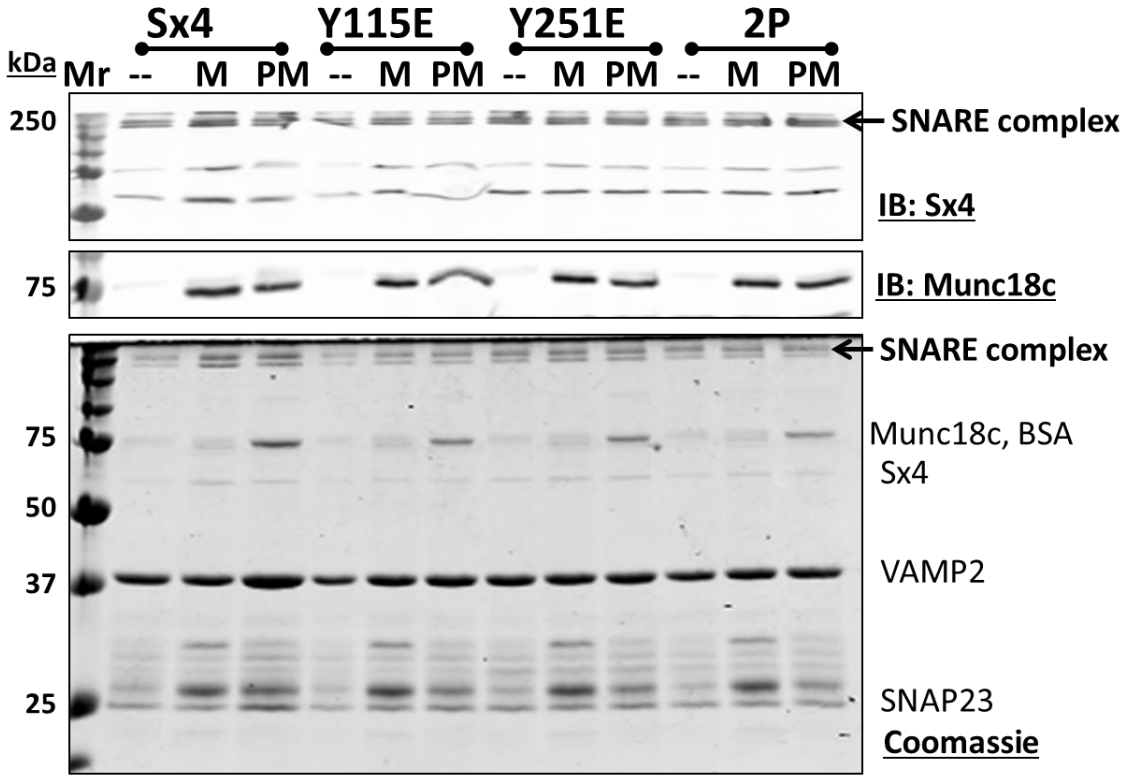

Figure 6-4 Munc18c influence on SNARE complex.

Equimolar (30µg) SNARE complex components, Sx4/SNAP23/VAMP2 were mixed with buffer C (-, i.e. no Munc18c added), wild type M18c (M), or phosphomimetic M18c Y251E (PM) all in buffer C supplemented with BSA. Reaction mixtures were incubated with mixing at 4^{o}C then 2X LSB sample

buffer was added followed by boiling at 95°C for 5 minutes. Samples separated using 12% SDS-PAGE and either stained with Coomassie blue or used for western blot using primary antibody Sx4 or Munc18c. Similar results obtained from repeated trials. Labels: Sx4/ wild type Sx4, Y115E/ Sx4(Y115E), Y251E/ Sx4(Y251E), 2P/ Sx4(Y115/251E), M/ wild type Munc18c, PM/ Munc18c(Y521E), Mr/ protein marker.

Previously, we showed that double phosphomimetic (2P) resulted in more SNARE complex formation over wild type Sx4 (Sx4) thus we thought to focus on these and test for any added effect of Munc18c on complex formed (Figure 6-5). Overall, the double phosphomimetic Sx4 resulted in more complex formed compared to wild type, as previously shown. Normalized data to no Munc18c added showed almost similar trend of differences between M and PM (see graph in Figure 6-5), i.e. wild type displayed less ternary complex amount while the phosphomimetic mutant reinstate levels yet not to the control, no Munc18c.

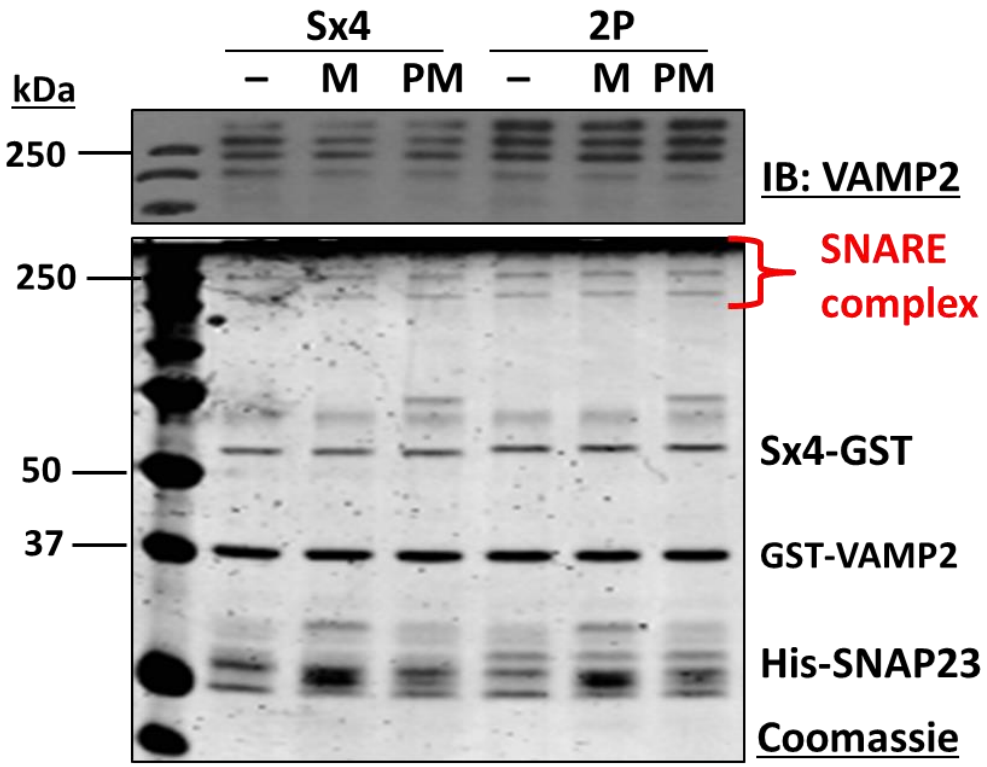

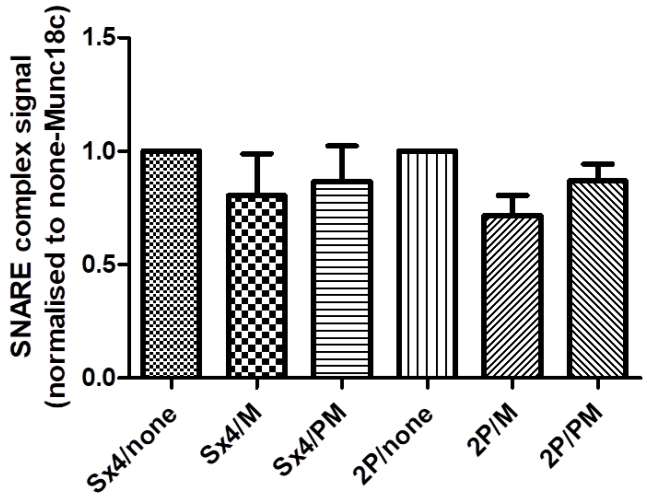

Figure 6-5 SNARE complex formation assay with Munc18c.

SNARE complex components (Sx4/SNAP23/VAMP2), BSA, and Munc18c were mixed, 30µg, in buffer C followed by analysis of complex formation by coomassie-stained gel and immunoblot detection (section-2.3.3 and 2.3.5). Immunoblot for VAMP2 used to quantify SNARE complex band intensity presented in column graph, n=4. Similar results obtained from repeated trials. One-way ANOVA statistical test show no significant differences, p-value 0.1409, GraphPad Prism5.

This data on SNARE complex formation using codon-optimised Munc18c mutants (Figure 6-4 and Figure 6-5) are somewhat different than previous results obtained in our group (Kioumourtzoglou et al., 2014). AS shown in Figure 6-5, Munc18c addition resulted in reduced complex formation, while the phosphomimetic mutant appeared to form more complex. This is broadly similar to a previous study in our group (Kioumourtzoglou et al., 2014) in which wild-type Sx4 pre-incubated with Munc18c was found to exhibit reduced SNARE complex formation, an effect which was over-come by addition of phosphomimetic Munc18c. However, the results with this codon-optimized Munc18c are not as clear-cut as previous studies. Therefore, it was necessary to characterise codon-optimised gene expression and check for any differences compared to the native protein. Protein structural characterization by circular dichroism (CD) spectroscopy was carried out to identify any potential differences. Protein samples were examined for secondary structure using circular dichroism (CD) spectroscopy. It was thought this would allow us to explore any structural changes due to mutations introduced or folding properties arising from enhanced expression (Greenfield, 2007; Kelly et al., 2005).

Newly expressed wild type Munc18c (pQE30-His-M, **A**), phosphomimetic Y521E (pQE30-His-PM, **B**), and native mouse sequence of wild type (pET28b-His-M, **C**) were scanned at far UV region for secondary structure features, individually (Figure 6-6 **A**-**C**). Three spectra were combined in one figure to illustrate differences (Figure 6-6 **D**). Initial measures of these samples were noisy below 195nm and some were contaminated with nucleic acid i.e. DNA/RNA. These were repeated with dilution, giving the presented data. The CD scans of each protein are judged to be not far apart, an indication that their secondary structures are similar, apart from small higher signal detected with pQE30-His-PM sample. It would have been ideal to include a sample of phosphomimetic expressed using the native mouse sequence but unfortunately that was not available.

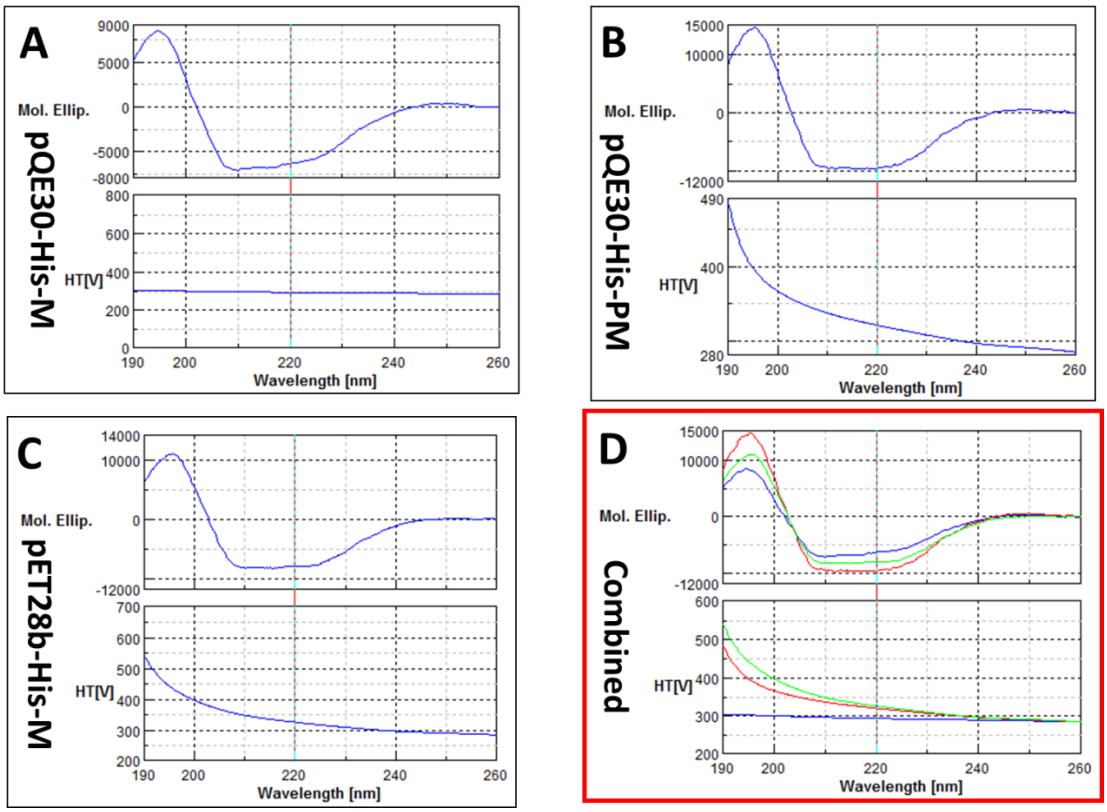

Figure 6-6 Far UV CD spectrum of cytosolic domains of Munc18c expressed by native mouse gene or codon-optimised.

Far UV CD spectra were recorded for the cytosolic domains of recombinant Munc18c mutants using either the codon-optimised gene to express pQE30-His-M (**A**) and pQE30-His-PM (**B**), using native mouse gene expressing pET28b-His-M (**C**). Three spectra combined together for comparison (**D**). CD measurements were collected on a JASCO J-810 spectropolarimeter using a 0.02-cm path length quartz cuvette by Dr Sharon Kelly (University of Glasgow).

Using CD spectroscopy data it is possible to estimate secondary structure elements within each molecule in percentages to a good value of accuracy compared to crystallography (Manavalan and Johnson, 1987). Estimated values (Table 6) were obtained using a reference dataset created for protein secondary structure elucidation by CD (Abdul-Gader et al., 2011). Overall, the three proteins are broadly similar in protein elements content. The exception appears to be α- helix percentage, wild type Munc18c proteins are in close agreement, regardless of gene, while the phosphomimetic is higher in α- helical content. This is in agreement with the obtained spectra (Figure 6-6).

Table 6 Secondary structure content estimates for Munc18c mutants.

Content (%)	α- helices	Strands	Turns	Unordered
pQE30-His-M	20.4	28.7	12.2	38.7
pQE30-His-PM	28.1	24	11.8	36
pET28b-His-M	23.9	26.5	12.2	37.3

DNA contamination influences CD spectra significantly and protein preps should be treated with appropriate nuclease, i.e. DNase prior to analysis (Kelly et al., 2005). Also, protein modifications, such as a point mutation, can lead to structural conformation changes resulting in different binding or interaction affinity. Therefore, it was important to compare spectra of pET28b-His-Munc18c and pQE30-His-PM following normalisation to correct for DNA contamination. The high A_{260} value for pET28b-His-Munc18c suggests contamination with nucleic acid – this would also increase the A_{280} value leading to an over estimation of the protein concentration which would reduce the intensity of the CD signal. Since the A_{260} for pET28b-His-Munc18c was approximately 20% higher than pQE30-His-PM, we have assumed that there is ~20% proportion of DNA contamination. We have subsequently normalised the two spectra by increasing the intensity of the

CD spectrum by 20%. This resulted in a CD spectrum that is almost superimposable on the phosphomimetic Munc18c (Figure 6-7).

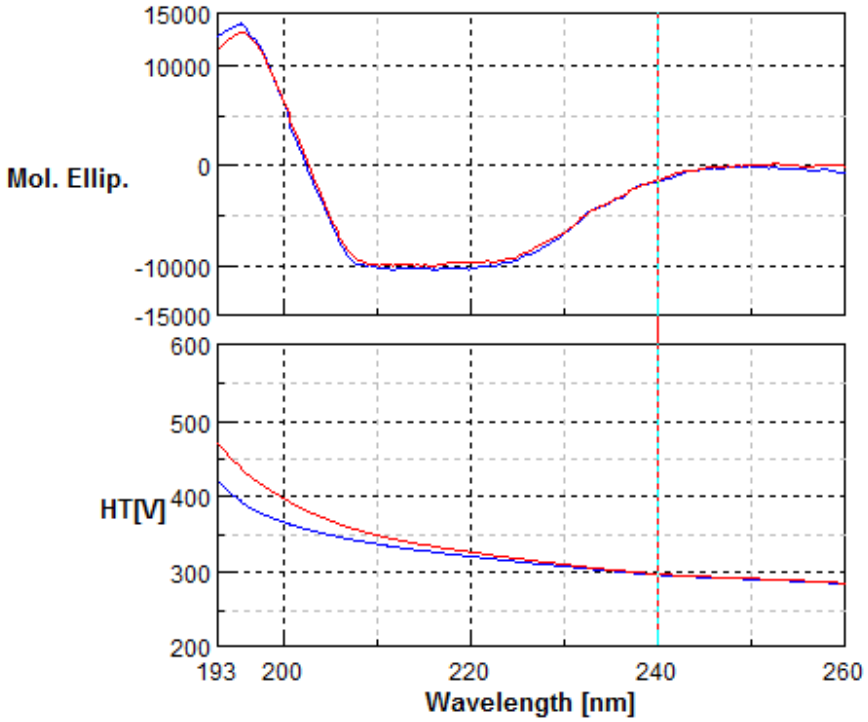

Figure 6-7 Normalised far UV CD spectra of the cytosolic domains of native mouse and codon-optimised Munc18c gene.

Far UV CD spectra were recorded for the cytosolic domains of recombinant pQE30-His-PM (blue) and pET28b-His-M (red). Due to DNA contamination, pET28b-His-M was normalised by 20% in accordance with nucleic acid contamination estimated value. The two spectra are identical and superimpose. CD measurements were collected on a JASCO J-810 spectropolarimeter using a 0.02-cm path length quartz cuvette by Dr Sharon Kelly (University of Glasgow).

When the secondary structure estimates for both pET28b-His-M and pQE30-His-PM are compared, the total alpha helical contents are 31.8% and 32.7% respectively and beta sheet contents are 20.5% and 19.4% respectively. These values suggest that the secondary structures are identical thus the tyrosine-glutamic acid mutation had no effect on secondary structure.

6.2.5 Munc18c pull down assay with cognate SNAREs

Insulin stimulation of 3T3-L1 adipocytes triggers tyrosine phosphorylation of Sx4 at residues 115 and 251 and Munc18c at 521 (Schmelzle et al., 2006). It is not known if these events take place at same time or in sequence, and if so the

order of phosphorylation needs to be determined. We showed (section-3.2.1) that Sx4 and Munc18c co-precipitate in 3T3-L1 adipocyte lysates. Therefore, we decided to examine effects of phosphorylation, of either Sx4 or Munc18c, on binding affinities through a pull down assay using recombinant proteins. Sx4 was immobilised on glutathione sepharose beads and excess of Munc18c was incubated with continuous mixing. Beads were collected and washed thoroughly for non-specific binding followed by addition of equal volume of sample buffer and boiling. Samples were subjected to SDS-PAGE and western blot followed by immunoblot development against Munc18c (Figure 6-8). Although Sx4 mutants, Sx4 and 2P, were concentration normalized their binding affinities appear different. Wild type Sx4 (Sx4) shows a slightly higher binding affinity, overall, to either wild type (M) or phosphomimetic (PM) Munc18c. Interestingly, phosphomimetic Munc18c binds more than wild type to Sx4 regardless of phosphorylation status. Also, it is showing a better tendency to bind to wild type than phosphomimetic, i.e. when both phosphorylated they bind less. Sx4 is GST tagged thus the control was used as GST which showed no binding to Munc18c.

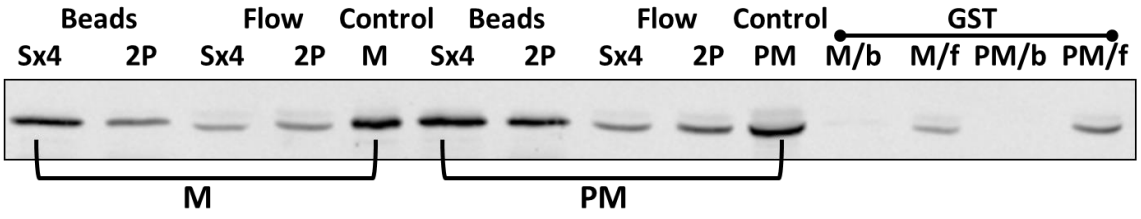

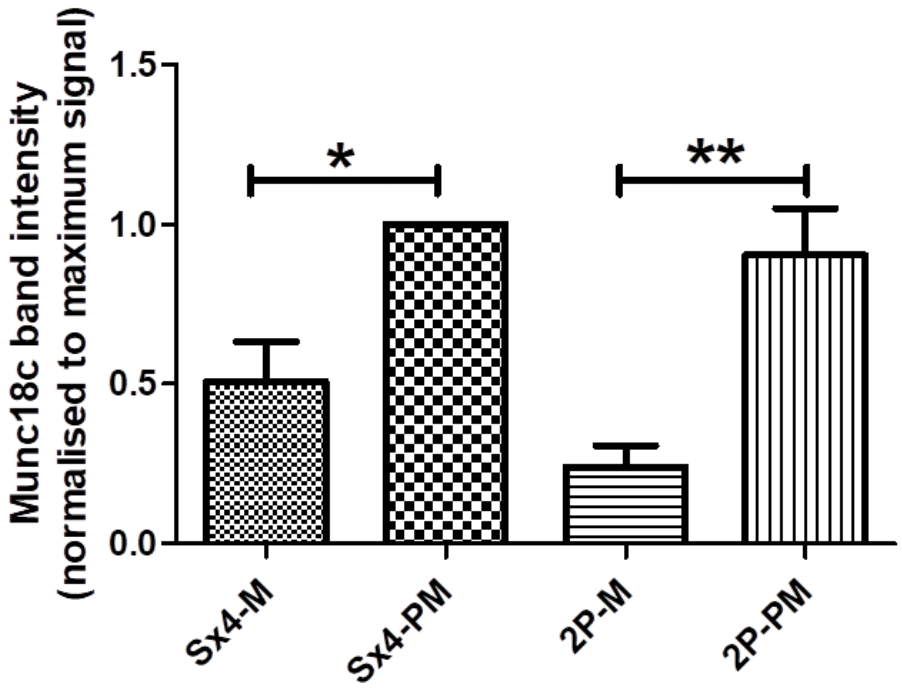

Figure 6-8 Phosphorylation effect on binding affinity of Sx4 and Munc18c.

Syntaxin4, wild type (Sx4) or double phosphomimetic (2P), immobilised in glutathione sepharose beads and Munc18c, wild type (M) or phosphomimetic (PM), was pulled down. Equal protein concentrations of Sx4 and 2P were incubated with excess Munc18c with continuous mixing at 4^{o}C overnight in binding buffer. Beads were washed excessively then mixed with 2X LSB sample buffer and boiled. Proteins resolved through 12% SDS-PAGE and immunoblot were developed using primary antibody of Munc18c. Band intensities were quantified by densitometry using ImageJ software and only beads samples graphed after signal normalization to maximum. Presented data are representative of repeated trials (n=3) with similar results. One-way analysis of variance statistical test showed very significant differences with a P-value of 0.0025. Labels: Sx4/ wild type syntaxin4, 2P/ double phosphomimetic syntaxin4 (Y115/251E), M/ wild type Munc18c, PM/ phosphomimetic Munc18c(Y521E), b/ beads sample, f/ flow sample i.e. unbound, Control/ recombinant protein without beads. Significance asterisks (using GraphPad Prism5) denote *, significant P-value 0.01 to 0.05 and **, very significant P-value 0.001 to 0.01.

6.3 Discussion

The process of GLUT4-vesicle fusion with the plasma membrane is highly regulated; this regulation is achieved, at least in part, through SNARE complex formation such that Sx4 participation is controlled by SM protein Munc18c (D'Andrea-Merrins et al., 2007; Morey and Fasshauer, 2014; Ramalingam et al.,

2014; Thurmond et al., 2000). Insulin stimulation results in tyrosine kinase phosphorylation of Sx4 at 115 and 251 and Munc18c at 521 (Schmelzle et al., 2006). We have shown that Sx4 phosphorylation enhanced the amount of SNARE complex formed in vitro. Here we sought to determine if Munc18c phosphorylation would also influence SNARE complex formation.

Native mouse Munc18c expressed poorly in bacteria with many contaminating bands (Figure 6-1) despite many optimization trials (induction time, temperature, ATP in wash buffers etc.) which were conducted in an effort to improve quality and quantity of Munc18c recovery. Therefore we looked for an alternative which was established by another group using a codon-optimised gene sequence which reportedly gave good expression and purification properties; results which were recapitulated by us (Figure 6-3).

The addition of Munc18c into SNARE complex formation assays using Sx4 phosphomimetic mutants showed indeterminate effects (Figure 6-4). Tyrosine 115 in Sx4 is located in the N-terminus while tyrosine 251 is in the SNARE domain. Munc18c binds Sx4 at the N-terminus when Sx4 is open and also when it is in the closed form such that SNARE and Habc domains are locked by Munc18c (Hu et al., 2007). Hence, further work will be required to ascertain whether these differences in binding to Sx4-Y115E or Y251E represent distinct functional transition states in the SNARE cycle. Similarly, pre-incubation of Sx4 with Munc18c before adding SNAP23 and VAMP2 to form SNARE complex is an area which should be explored. Due to time constraints, these avenues were not pursued.

Previous work in our group, showed that pre-incubation of Sx4 with either M or PM followed by addition of VAMP2 and SNAP23 formed SNARE complexes at different rates (Kioumourtzoglou et al., 2014). The wild type Munc18c (M) reaction formed significantly less complex than was observed when Munc18c was omitted. Interestingly, phosphomimetic Munc18c (PM) resulted in higher complex signal compared to no Munc18c added. The difference in signal between M and PM was statistically significant ($p<0.05$). This was interpreted to imply a role for Munc18c phosphorylation in releasing Sx4 from the closed form or shifting

balance towards open thus facilitating complex formation. It is worth noting here that this was done using Sx4 expressed in bacteria which, as reported here, expresses poorly and at low levels. We sought to determine if the codon-optimised Munc18c would interact similarly to native mouse protein used in previous study; although the amino acid sequences are identical, the different expression levels may result from differences in rates of folding/synthesis, and thus could reflect Munc18c conformation and thus function. The results of this study comparing the same Y521E mutation to wild-type Munc18c are different to those reported by Kioumourtzoglou et al (Figure 6-4). Several potential reasons may underlie this. First, the experimental design is different as we assembled the complex in liquid form compared to immobilised to beads in the previous experiment. This is important, as in Kioumourtzoglou et al, the Munc18c was pre-bound to Sx4 which was immobilized on beads and thus excess, unbound Munc18c was removed in a wash step. This was not the case for our assay.

In a recent study, Rehman *et al.*, 2017, show that C-terminally truncated Sx4 disassembles faster from Munc18c than with a transmembrane domain. Also, SNARE complex formation was inhibited by Munc18c when the truncated Sx4 was used but when an anchored Sx4 was used that did not inhibit the complex formation. Therefore, it is logical, to mimic the physiological condition, to have Sx4 anchored or stabilized when using Munc18c for SNARE complex formation as *in vivo* it is attached to plasma membrane; this was not the case in our assay. Also, as noted above, codon-optimised Munc18c might have a different conformation that might alter protein-protein binding.

Here we sought to ascertain the effect of the Munc18c-Y521E mutation on SNARE complex assembly when Sx4 was also phosphorylated (i.e. Sx4-2P mutation); the latter formed more SNARE complex, but different results were obtained when wild-type or Y521E codon-optimized Munc18c were added (Figure 6-5). Further work will be required to ascertain the validity of these data, and time precluded a rigorous analysis of this type. However, no striking effects were observed. It may be more instructive to recapitulate these analyses using the individual mutations, as the effects of phosphorylation of Sx4 at these two different sites may not be additive.

Examining structural differences in the expressed Munc18c species was deemed to be important. This was conducted using circular dichroism (CD) spectroscopy. The spectra obtained showed slight differences in structures of the proteins derived from the native mouse gene and codon-optimised gene (Figure 6-6). After correction for nucleic acid contamination, the spectrum of the codon-optimised phosphomimetic protein was superimposable with that of the wild type from native mouse gene. Also, secondary structure element estimation showed very similar content (Table 6). Clearly the best way to compare them accurately would be to remove the contaminating nucleic acid (e.g. using a column –anion exchange or increasing the benzonase (DNaseI) concentration during the prep – or both). However, we can say with reasonable confidence that they are similar in their secondary structure.

The direct binary interaction between Munc18c and Sx4 is the most direct and conclusive way to examine their binding affinities to each other. Therefore, a pull down assay was adopted for this purpose (Figure 6-8). It has been shown previously that monomeric Sx4 binding to Munc18c was greatly reduced by phosphorylation of Munc18c (Aran et al., 2011); note however, this used Munc18c expressed in bacteria and not the codon optimized version employed here. Using the same expression plasmid, Sx4 pre-incubation with wild type Munc18c formed less ternary complex, compared to omitted, while phosphomimetic Munc18c resulted in significantly more suggesting alleviation of inhibition by phosphorylation (Kioumourtzoglou et al., 2014). Munc18c is phosphorylated also at tyrosine 219 in MIN6 beta cells (Oh and Thurmond, 2006) which corresponded to a 60% decrease of Munc18c-Sx4 binding and also a switch in binding affinity from Sx4 to a competent protein, double C2 domain Doc2β (Jewell et al., 2008). Platelet-derived growth factor (PDGF)-stimulation resulted in GLUT4 translocation through a mechanism involving phosphorylation of Munc18c at tyrosine 521 simultaneously with Sx4-Munc18c dissociation (Umahara et al., 2008). In our hands, phosphorylated Munc18c (PM) binds more Sx4 regardless of the phosphorylation status of Sx4. However, Sx4 wild-type binds more Munc18c than Sx4-SP, regardless of the phosphorylation status of Munc18c. This might be due to steric hindrance effects of the phosphomimetic negative

charges. This discrepancy between our data and published work, however, requires further clarification. Munc18c is a central yet complicated regulator of SNARE complex formations and its phosphorylation add another layer of complexity to this system.

CHAPTER SEVEN

7 Discussion

7.1 Discussion

Insulin stimulation of GLUT4 translocation in adipocytes and muscle cells is a highly specialised and tightly regulated trafficking event (Bryant et al., 2002). GLUT4 storage vesicles (GSVs) are translocated from intracellular compartments to the plasma membrane (PM) where they fuse through assembly of SNARE proteins into the SNARE complex. The complex consists of syntaxin4 and SNAP23, at PM, and the vesicle's SNARE, VAMP2 (Bryant and Gould, 2011). The complex assembly is regulated by a Sec1/Munc18 protein, Munc18c (Jewell et al., 2010; Latham et al., 2006). Both syntaxin4 and Munc18c are tyrosine phosphorylated upon insulin stimulation; syntaxin4 at 115, 251 and Munc18c at 521 (Schmelzle et al., 2006). At the outset of this work, the biological consequences and effects of these phosphorylation events were not studied or clearly understood in the context of GLUT4 translocation and glucose uptake. Therefore, this study aimed to explore syntaxin4 and Munc18c phosphorylation effects on the overall mechanism of GLUT4 trafficking using techniques analysing binary interactions, *in vitro*, and then moving to cells, including measuring glucose uptake.

Insulin-stimulated Sx4 tyrosine phosphorylation on 115 and 251, was confirmed in fully differentiated 3T3-L1 adipocyte lysates with the help of immunoprecipitation and mass spectroscopy analyses. Syntaxin4 and Munc18c were shown to co-immunoprecipitate at both basal and insulin-stimulation conditions (Figure 3-1). Regardless of extensive efforts to ascertain Munc18c phosphorylation at tyrosine 521, definitive data not obtained for various reasons, discussed in section 3.3. The positions of phosphorylation sites within syntaxin4 have impact on ternary SNARE complex formation as well as on regulatory Munc18c binding at the N-terminus.

Recombinant proteins of syntaxin4 harbouring singular (Y115E or Y251E) or double (Y115,251E) phosphomimetic mutations were expressed by bacteria in a good yield and quality (Figure 3-3). Other SNAREs were expressed including SNAP23 and VAMP2 in addition to the regulatory Sec1/Munc18 protein, Munc18c. In order to mimic physiological conditions, proteins were expressed using different tags at C-terminus or in the cleaved form to avoid any tag dimerization

and to test actual protein-protein interactions. Ternary SNARE complex formation was successfully recapitulated *in vitro* and the complex was found to be SDS and heat resistant (Kioumourtzoglou et al., 2014; Rea et al., 1998; Kawanishi et al., 2000.; St-Denis, Cabaniols, Cushman, & Roche, 1999) (Figure 3-5). Control experiments confirmed that this complex form only between the three SNAREs collectively, Sx4/SNAP23/VAMP2, such that missing any would result in no complex formation (Figure 3-5). Remarkably the syntaxin4 phosphomimetic mutants formed the complex and they showed a higher amount of complex formation compared to wild type syntaxin4. This was encouraging such that we were assured that the introduced mutation has no effect on the protein interaction with other SNAREs and thus we could proceed into using this assay to compare different mutants. The double phosphomimetic Sx4 (2P) formed the highest amount of complex compared to single mutants and the wild type. In an attempt to understand phosphorylation effect on complex formation, binary protein interactions were assessed, Sx4 vs. SNAP23 or VAMP2, and revealed that 2P binds SNAP23 with a higher affinity in comparison to wt.

Target SNAREs are thought to form binary complexes on the plasma membrane and phosphorylation, apparently, enhances this binding and ultimately the ternary complex. Physiologically, these findings correlate nicely such that insulin stimulation leads to Sx4 phosphorylation (Schmelzle et al., 2006) and increases glucose uptake through elevated GSV fusion via effects on SNARE complex assembly (Muretta et al., 2008; Pessin et al., 1999). Our findings support this by showing more SNARE complex formation with phosphomimetic mutants compared to the wild type.

SNARE complex formation assay using fluorometry was used as an alternative and supporting methodology that employee detection of conformational changes using fluorescence changes. In support, 2P showed more complex formation than wild type and in a shorter time too (Figure 3-8). Furthermore, circular dichroism (CD) spectroscopy suggests conformational changes upon ternary complex formation (Figure 3-11). The two complex assembly assays are in agreement and hint at conformational changes taking place during the complex formation;

probably Sx4 phosphomimetic mutants are in a more favourable conformation enhancing the process of complex assembly.

Syntaxin4 exists in two conformations, open and closed (Dulubova et al., 1999). Limited proteolysis assay showed similar digestion degree of open mutant Sx4 (Aran et al., 2009) and the double phosphomimetic (Figure 3-13). Pull down assays, using SNAP23 or VAMP2, also suggested comparable binding affinities of 2P with open mutant (Figure 3-9 and Figure 3-10). A more sophisticated and sensitive technique, isothermal titration calorimetry (ITC), showed a tighter binding of SNAP23 to the double phosphomimetic Sx4 (Figure 3-12). The above mentioned findings suggest the open conformation for Sx4 that enhance complex formation such that open access to the SNARE domain in phosphomimetic Sx4 facilitates the assembly of the ternary complex.

So far the *in vitro* findings are interesting and suggest important effects of posttranslational modification, i.e. phosphorylation, on SNAREs syntaxin4 and Munc18c that affect their interactions in binary or ternary SNARE complex formation. Nevertheless, these are in the *in vitro* context and needed to be tested *in vivo*, which required more sophisticated tools to develop and validate. Phospho-specific antibodies for syntaxin4, Y115 or Y251, and Munc18c, Y521, were generated. These antibodies were not particularly effective in blotting 3T3-L1 adipocyte lysates despite intensive trials. This could be due to antibodies preparation process such that they were not eluted from affinity purification efficiently or as is discussed in section 4.3 other explanation may account for these disappointing results. Recombinant Cytoplasmic Insulin Receptor Kinase (CIRK) can tyrosine phosphorylate syntaxin4 or Munc18c (Aran et al., 2011). Interestingly, the syntaxin4 phospho-specific antibodies recognised phosphorylation sites specifically with high accuracy in CIRK-phosphorylated recombinant syntaxin4 samples (Figure 4-3). A novel finding from CIRK-phosphorylation revealed that both tyrosine sites in syntaxin4 are phosphorylated at the same time. Moreover, syntaxin4 in t-SNARE complex with SNAP23 proved not to be CIRK-phosphorylated in contrast to monomeric syntaxin4 (Figure 4-4).

A non-intrusive method for measuring protein-protein interaction or modification, such as phosphorylation, is the proximity ligation assay, PLA. In contrast to adipocyte lysates, phospho-specific antibodies were recognised in PLA assay such that they were recognised and specific (Figure 4-11) though could not distinguish between insulin-stimulated and basal conditions. Phospho-specific antibodies recognised in PLA assay suggest detection of phosphorylation and specific binding. In addition to the nature of the assay which could be limited to surface interactions and shape of adipocyte cell, fractions of phosphorylated syntaxin4 molecules might vary plus conformation of it could affect epitope binding affinity thus ultimately signal detection. Therefore, future work on optimisation of adipocyte monolayer is essential to have a uniform signal detection that will ensure better insulin-stimulation effect measurement. Preliminary trials gave promising results but time constraints limited further analysis. Also, different timings of insulin stimulation using variable concentrations can work on for better results. Using PLA technique, another study showed that insulin stimulation result in increased SNARE complexes formation that are consisted of syntaxin4, SNAP23, and VAMP2 in 3T3-L1 adipocytes (Kioumourtzoglou et al., 2014).

Genetic modification of fully differentiated 3T3-L1 adipocytes is extremely difficult, yet lentivirus intervention proved to be an efficient approach for genetic material insertion (Carlotti et al., 2004). Through this approach, cellular consequences of phosphorylation could be examined at glucose uptake levels and GLUT4 translocation. Therefore, syntaxin4 phosphomimetic lentivirus molecules were produced and validated for overexpression (Figure 4-14) and functionality (Figure 5-6). Also, a new 3T3-L1 cell line was produced using CRISPR-Cas9 technique that lack syntaxin4, i.e. Sx4 knockout. Re-expression of syntaxin4 in knockout cells rescued functionality (Figure 5-6) and responded to insulin stimulation accordingly such that double phosphomimetic glucose uptake is more than wild type (Figure 5-7). Examination of GLUT4 machinery, protein expression, in knockout cells was not convincing and compensatory Syntaxins, 2 or 3, were not upregulated (Figure 5-10). Characterisation of Sx4 knockout 3T3-L1 adipocytes hint to different protein level expressions compared to native which could explain obtained glucose uptake measurements.

Part of the highly controlled and regulated process of GLUT4 fusion is mediated through interaction of the SM protein, Munc18c, with syntaxin4 and thereafter SNARE complex formation (Hu et al., 2007; Morey and Fasshauer, 2014; Rehman et al., 2017). Moreover, insulin stimulation result in tyrosine kinase phosphorylation of Munc18c at 521 (Schmelzle et al., 2006). In our hands, we showed that Sx4 phosphorylation enhanced amount of SNARE complex formed, *in vitro*, and glucose uptake increased too, *in vivo*. Therefore, we pursued to determine if Munc18c phosphorylation would also influence SNARE complex formation. Munc18c expressed efficiently using codon optimised gene (Figure 6-3) and conformation is comparable to native (Figure 6-6). Addition of Munc18c into the SNARE complex formation assay resulted in indistinguishable outcomes that require further optimisations in future work. Pull-down assay using equal amounts of syntaxin4 mutants resulted in different Munc18c signals detected by immunoblots (Figure 6-8). Phosphomimetic Munc18c presented higher binding affinity to syntaxin4, regardless of phosphorylation state, in comparison to wild type, i.e. significant difference. This suggests an essential effect of phosphorylation on Munc18c such that facilitate syntaxin4 binding.

As a regulatory protein, Munc18c, contradictory findings were reported on the consequences of binding syntaxin4 on the SNARE complex formation. Syntaxin4 binds to Munc18c *via* its N-terminus in an enhancing mode (Hu et al., 2007; Latham et al., 2006) contrary to another study finding as an inhibitor which used liposome fusion assay (Brandie et al., 2008). Phosphorylation adds another layer of complexity such that CIRK-phosphorylated or phosphomimetic Munc18c abrogates binding to syntaxin4 (Aran et al., 2011). In contrast, another study using SNARE complex assay on beads showed more complex formation with phosphomimetic Munc18c and less with wild type, in reference to no Munc18c added in reaction (Kioumourtzoglou et al., 2014). Purification of Munc18c is difficult such that some use chaperones to express (Scott et al., 2004) and also the producing type of cells (Hu et al., 2003) could express differently thus different end results. Therefore, prior to comparisons, structural analysis is important to verify any differences between expressed proteins.

Phosphorylation order could have an effect on SNARE complex formation in sequence such that insulin stimulation might result in phosphorylation of syntaxin4 and/or Munc18c either simultaneously or sequentially, though both were detected by mass spectrometry (Schmelzle et al., 2006). In future complex assay, it is important to quantify proteins used by immunoblots, as Munc18c preps showed coomassie-stained band intensities different than blots, i.e. to achieve similar amounts of reactants in experiments.

Phosphorylation as a regulatory mechanism is reported in many systems such that same protein can be inhibitory or activate a given process depending on its phosphorylation state, detailed in section 1.5.1. It is reviewed in (Laidlaw et al., 2017; Snyder et al., 2006).

7.2 Future work

Glucose homeostasis is a crucial process in physiology as it is the power producer. However, mis-regulation is pathological and failure within this mechanism has major consequence, e.g. Type-2 Diabetes. Therefore, it is important to understand all the signalling pathways involved deeply and in particular how they impact on the GLUT4 trafficking network. Findings in this study support the notion of fundamental importance of phosphorylation by insulin stimulation in GLUT4 translocation and fusion which ultimately regulate blood glucose levels. We found that tyrosine phosphorylation of syntaxin4 at residues 115 and/or 251 are enhancers for SNARE complex formation that is essential in GLUT4 translocation and fusion. Regulatory protein, Munc18c, phosphorylation is involved with more work to clarify its role in the whole process. Results obtained support our theory on importance of phosphorylation on GLUT4 trafficking yet more work to emphasise the detailed mechanism is needed, detailed below.

In order to identify phosphorylated residues in syntaxin4, insulin stimulate adipocytes, using variable time and concentrations, and IP using the phospho-specific antibodies followed by mass spectroscopic analysis for tyrosine

phosphorylated residues. This ensure precipitation of phosphorylated syntaxin4 molecules at the designated residues and hence enrich signal detection.

Further investigation into conformation of syntaxin4 phosphomimetic mutants could include CIRK-phosphorylation of recombinant syntaxin4, wild type, followed by CD spectroscopy comparison with all mutants beside the open syntaxin4 mutant. This will allow for clarification of conformation comparison caused by kinase phosphorylation that we assured happening at tyrosine residues 115 or 251 through the use of phospho-specific antibodies (section 4.2.2). Proteomic mass spectroscopy analysis can ascertain the exact residue number accurately.

Moreover, CIRK-phosphorylated syntaxin4 can be used for ternary SNARE complex formation assay using the liquid method (section 3.2.5) or the fluorometry (section 3.2.7). Thereafter, binary binding affinity to other SNAREs, SNAP23 or VAMP2, would be interesting to measure by pull down assay (section 3.2.8) followed by the sophisticated biophysical methodology, ITC (section 3.2.9).

Another intriguing idea would be to CIRK-phosphorylate for different time points followed by immunoblot using the phospho-specific antibodies. This will reveal if there is any order of phosphorylation between the two residues in syntaxin4. Confirmation by proteomic mass spectroscopic analysis would be the gold-standard technique to use.

The SNARE complex assembly assay is an informative technique yet quantification by immunoblot and densitometry is subjective and exposed to errors from antibodies epitope non-specific bindings or missing binding sites due to changes in conformation at complex. Therefore, alternative detection methods or different assays are important to find. These could include the liposome membrane fusion assay (Brandie et al., 2008; Scott et al., 2003) or surface plasmon resonance, SPR (Rea et al., 1998).

This study explored the consequences of phosphorylation on GLUT4 trafficking by insulin-stimulation or CIRK-phosphorylation or using phosphomimetic proteins. On the other hand, abolishing phosphorylation effects were not tested which can be done by using phosphorylation-resistant mutants. This would show importance of phosphorylation in GLUT4 translocation and ultimately glucose uptake. The phospho-resistant would decrease GLUT4 molecules fused to plasma membrane, probably, thus less glucose uptake. These mutants can be expressed in Hela cells or native 3T3-L1 adipocytes but most appropriate would be the syntaxin4 knockout 3T3-L1 adipocytes.

Revealing the details of the trafficking of GLUT4 is important to understand the machinery behind it which play a crucial role in treatment of Type II diabetes and insulin-resistant patients. These studies could open the horizon for other regulated trafficking pathways discovery that could be an alternative in case of dysfunction or disease.

8 Appendices

8.1 Appendix-I: Primary data obtained from PLA analysis for indicated samples.

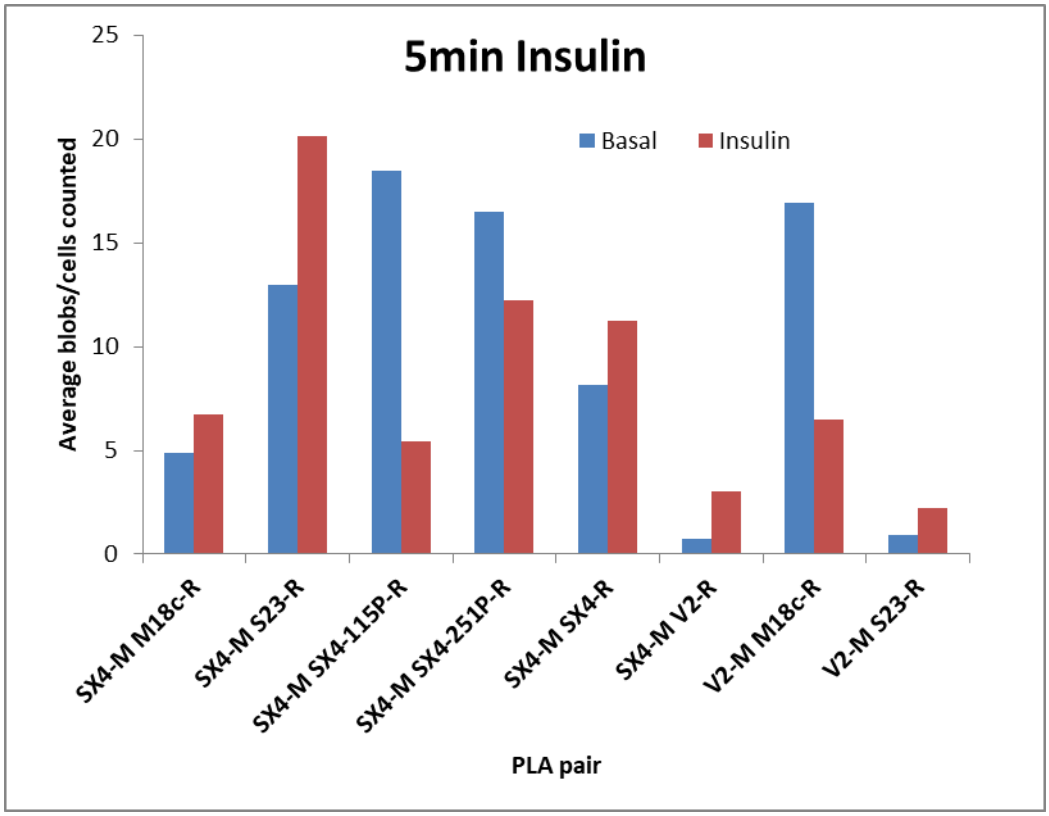

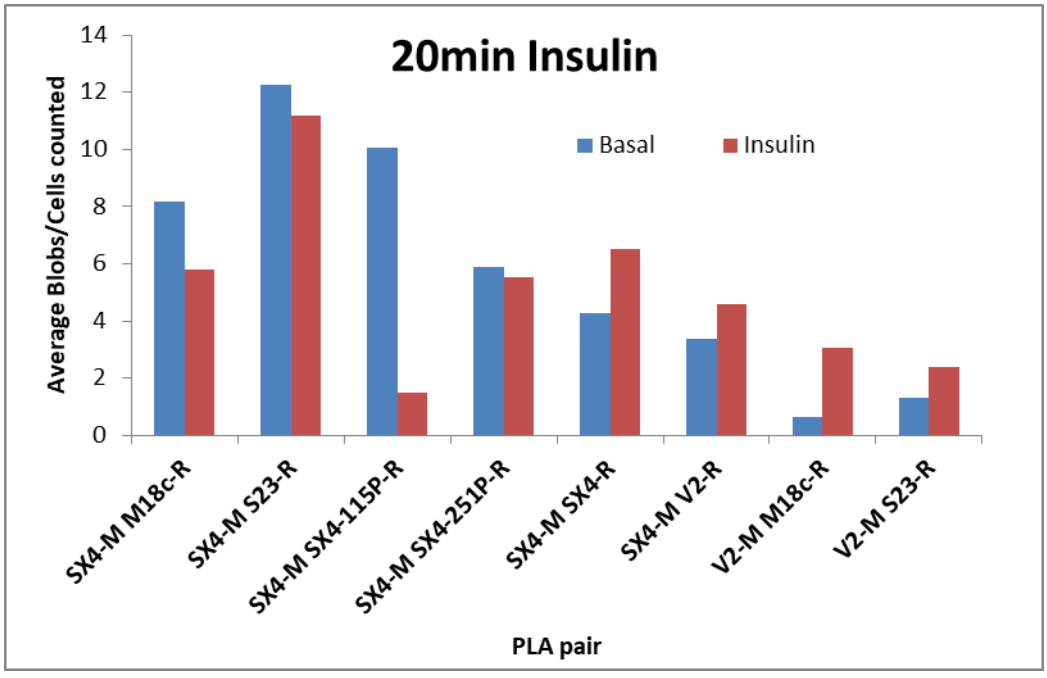

Appendix- 1 Raw average blobs count.

Total blobs, signals, detected in PLA assay from each field counted and divided by number of cells in same field thus average number of blobs plotted. Average counted graphed against pair of antibodies used such that they must be from different species and if there is interaction then signal

would be detected. Upper graph for 3T3-L1 adipocytes insulin-stimulated for 5 minutes and the lower is for 20 minutes.

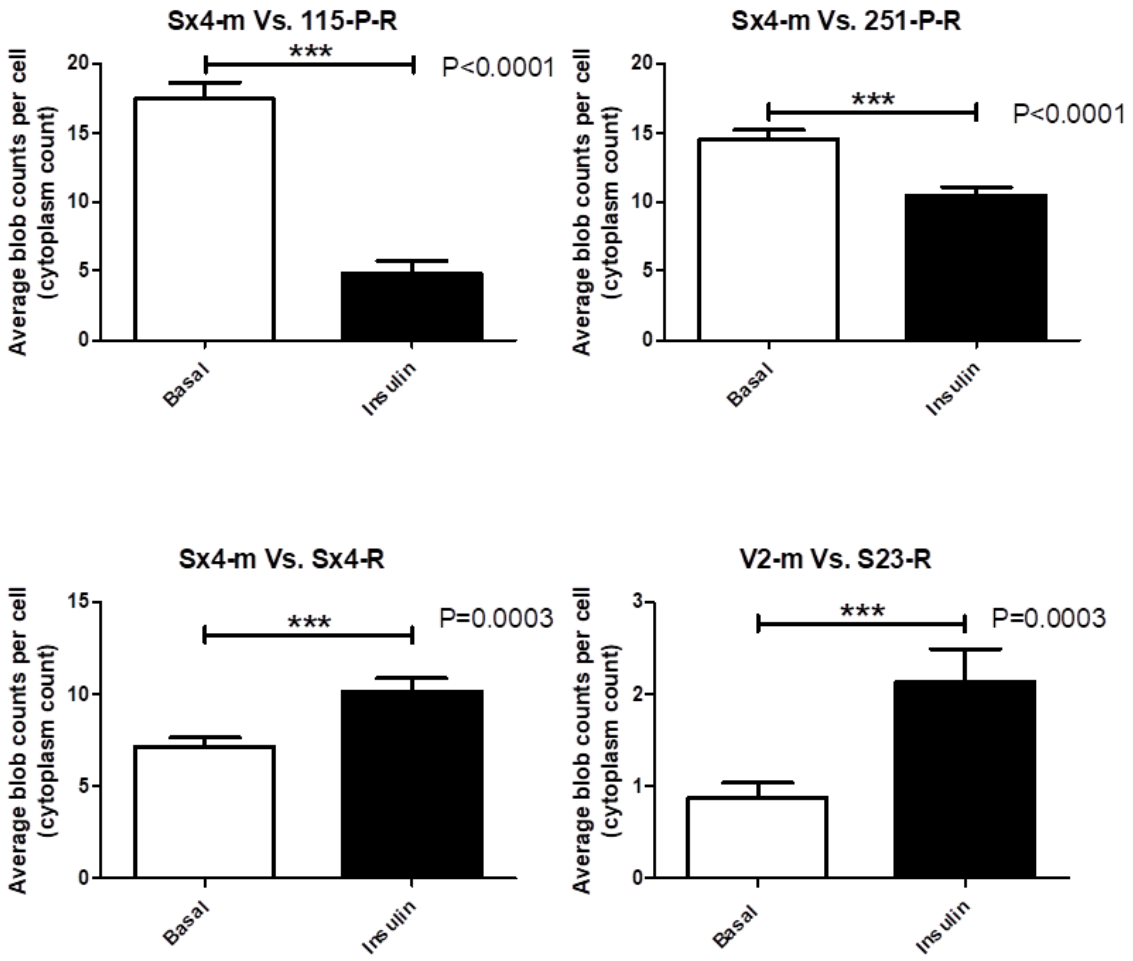

Appendix- 2 Statistical analysis of significant PLA samples.

Phospho-specific antibodies for syntaxin4 blob counts and control pairs analysed statistically using GraphPad software. Unexpectedly, insulin-stimulation resulted in less signal compared to basal. Controls, showed positive significant insulin induction increment as expected. Samples analysed are the 5 minutes stimulation.

8.2 Basal versus 5 minutes insulin stimulation

Following are three examples for each indicated PLA pair taken from the analysis software, BlobFinder, such that red signal for a positive blob and blue for nucleus and green boundary is the cytoplasm.

8.2.1 SX4/M-115P/R BASAL

1

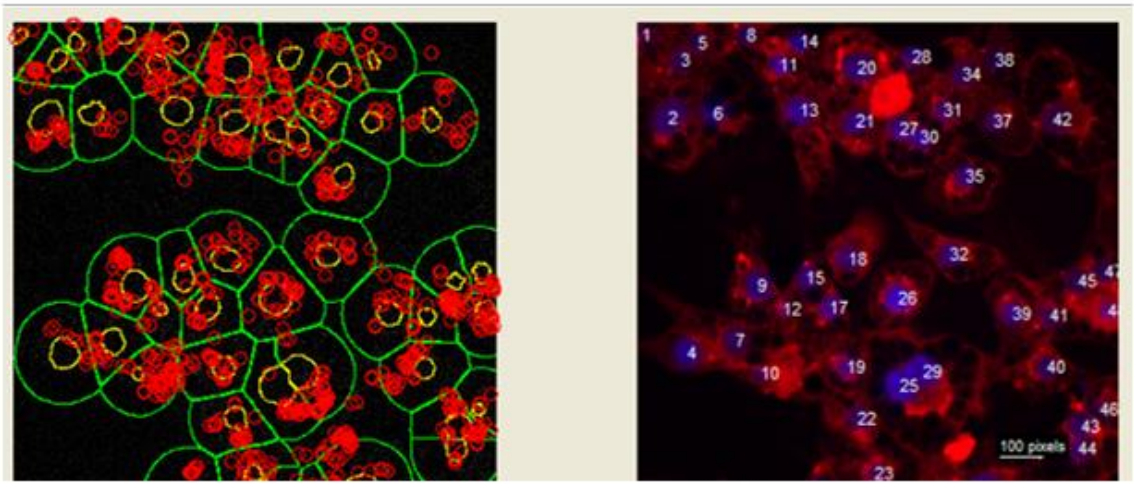

2

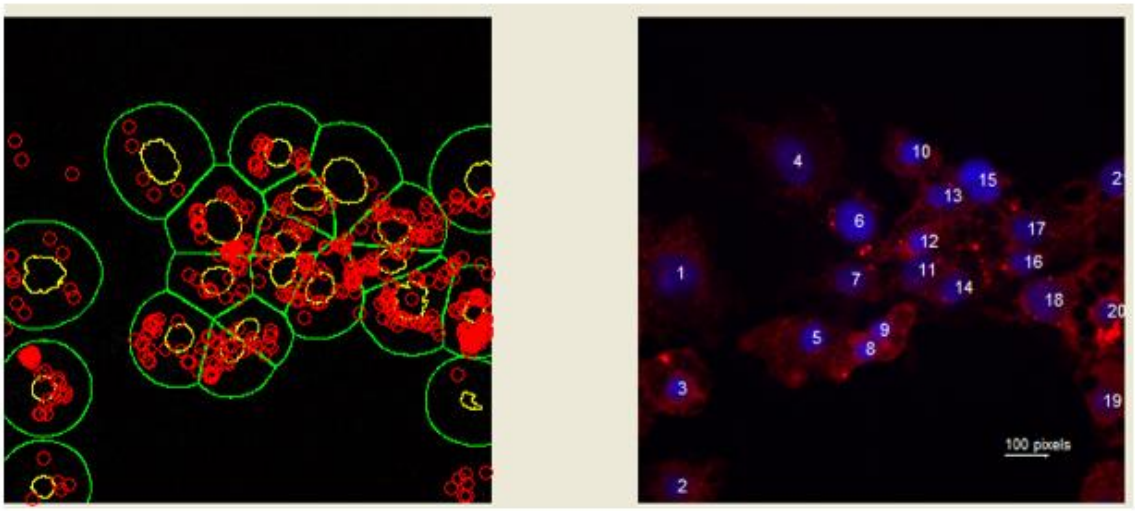

3

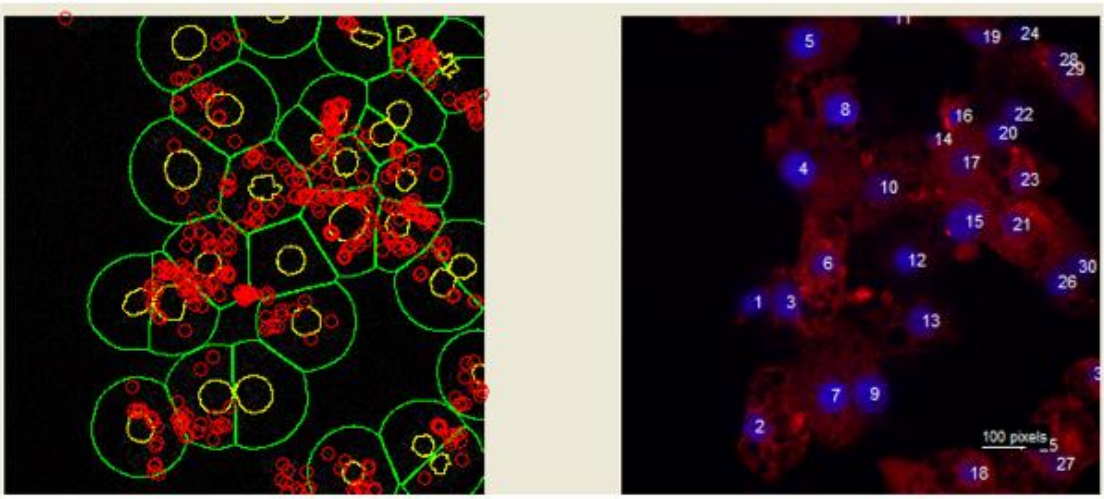

8.2.2 SX4/M-115P/R INSULIN

1

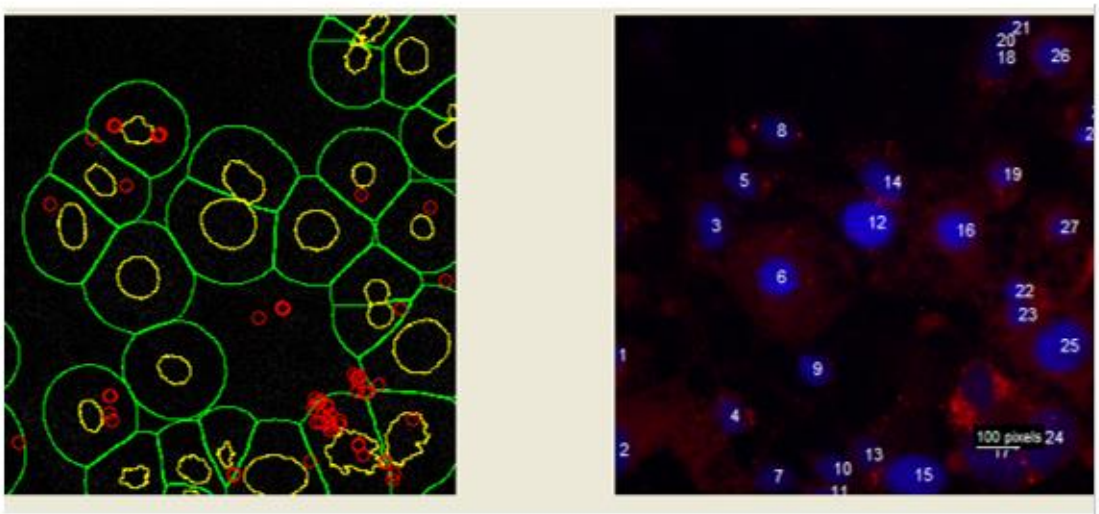

2

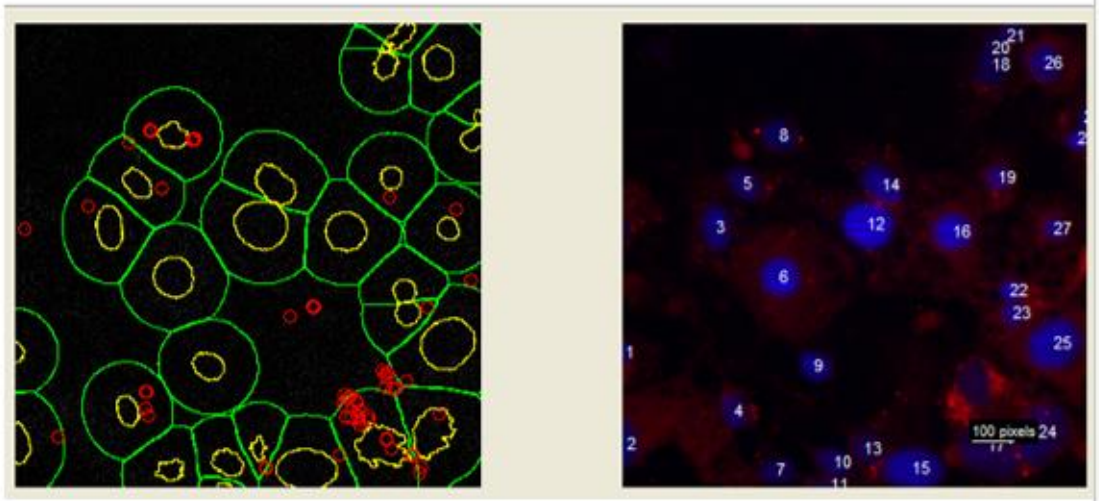

3

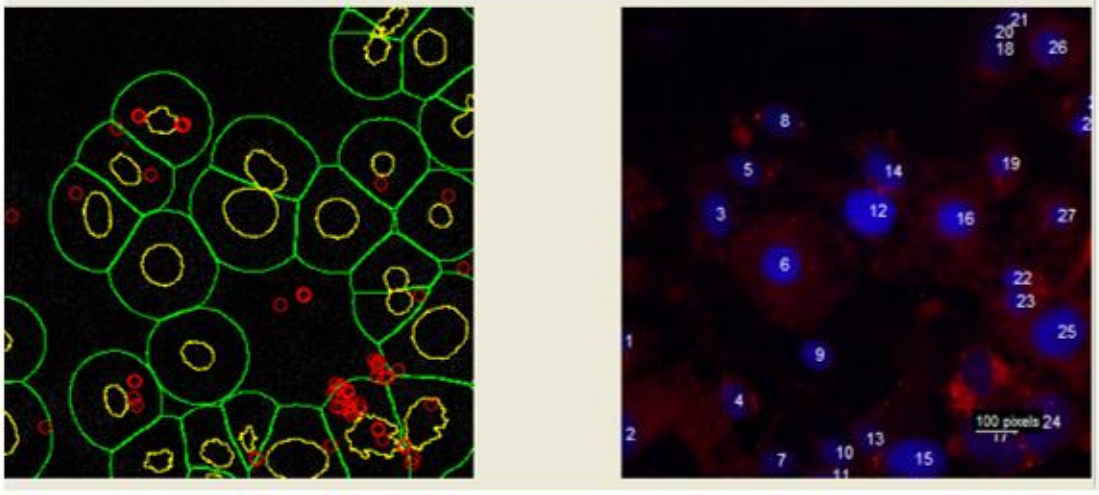

8.2.3 SX4/M-251P/R BASAL

1

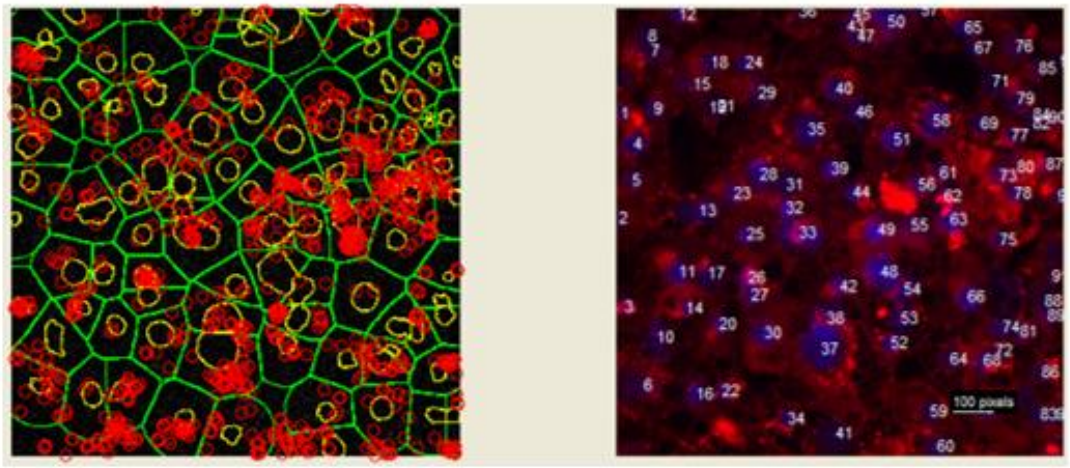

2

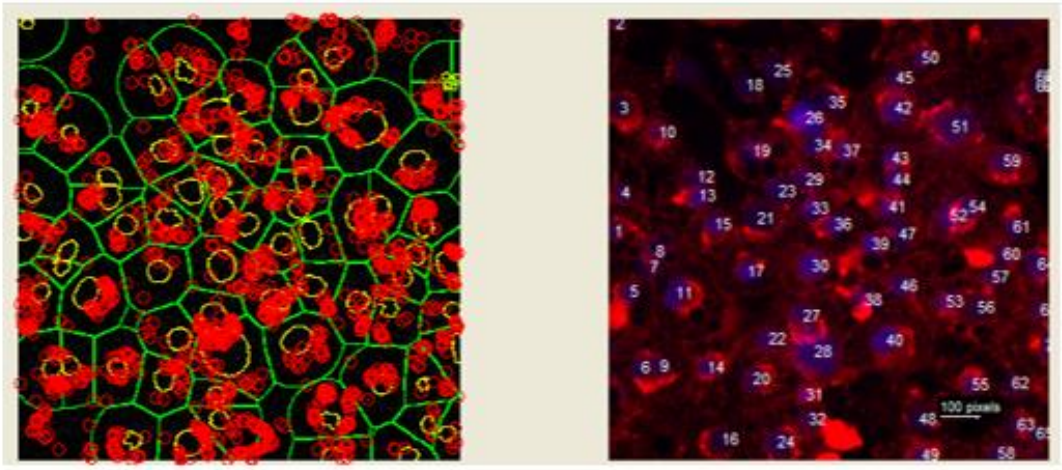

3

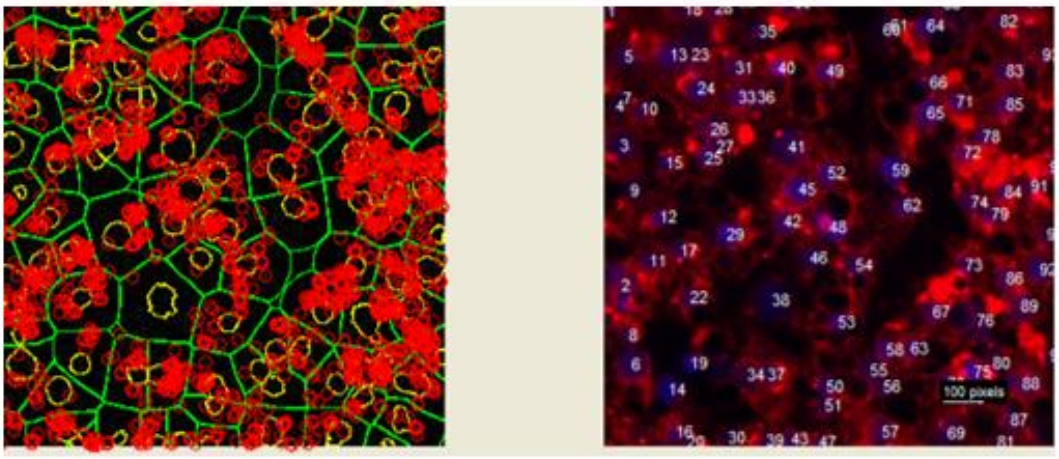

8.2.4 SX4/M-251P/R INSULIN

1

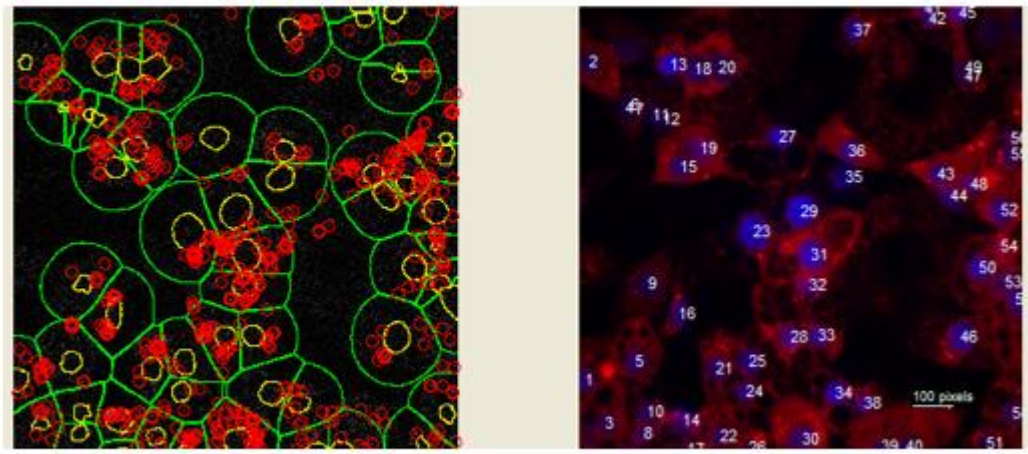

2

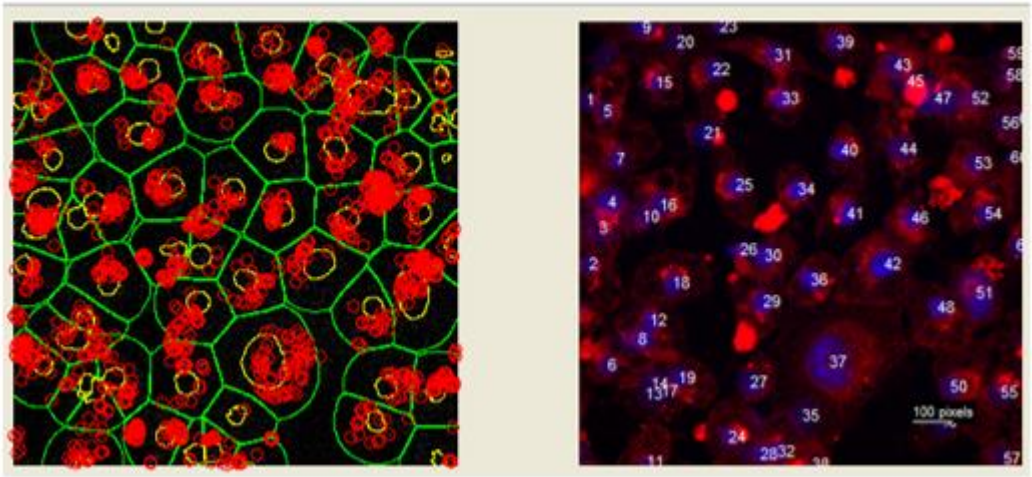

3

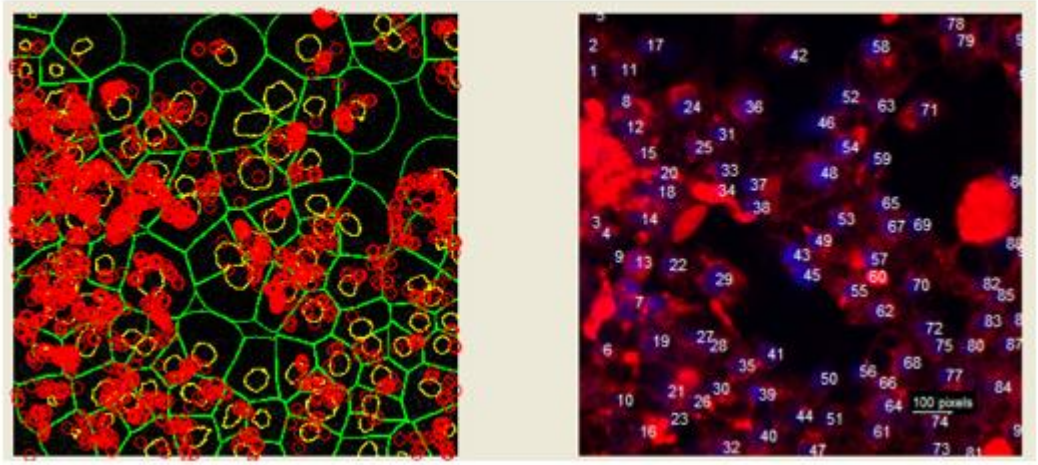

8.2.5 SX4/M-SX4/R BASAL

1

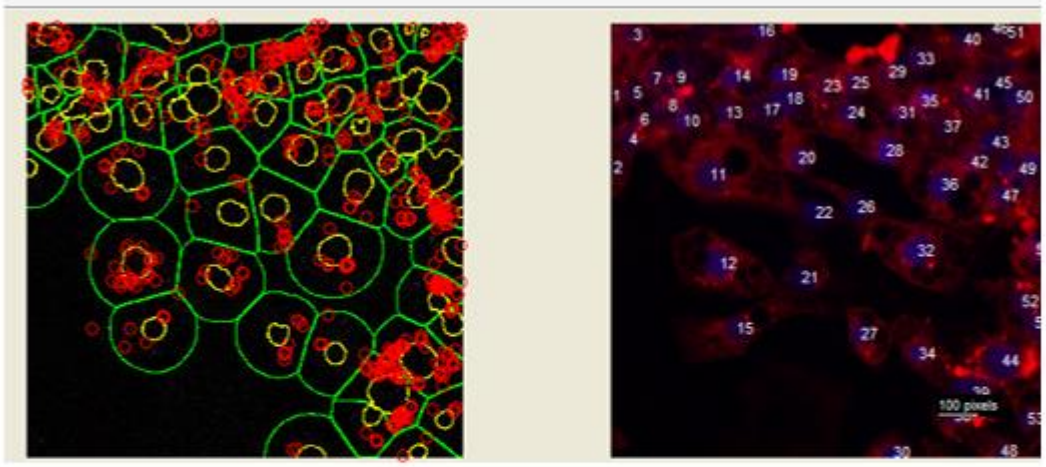

2

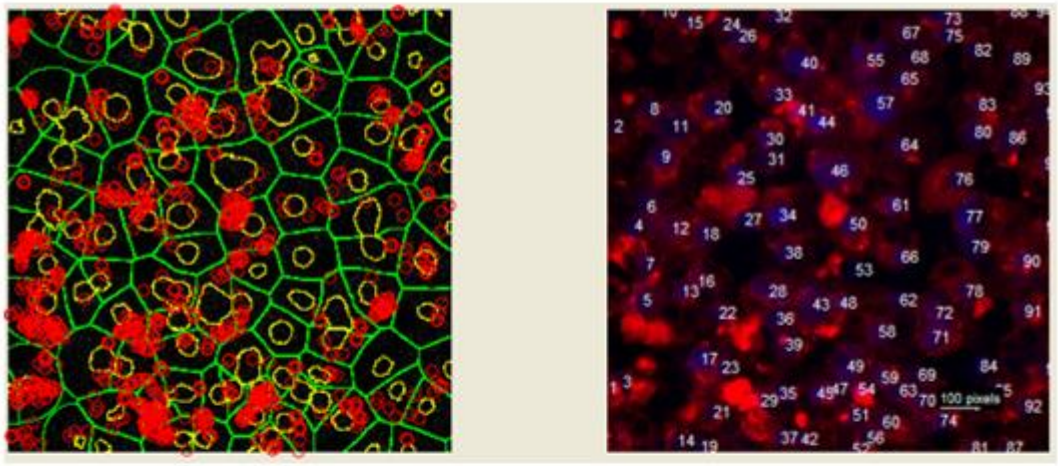

3

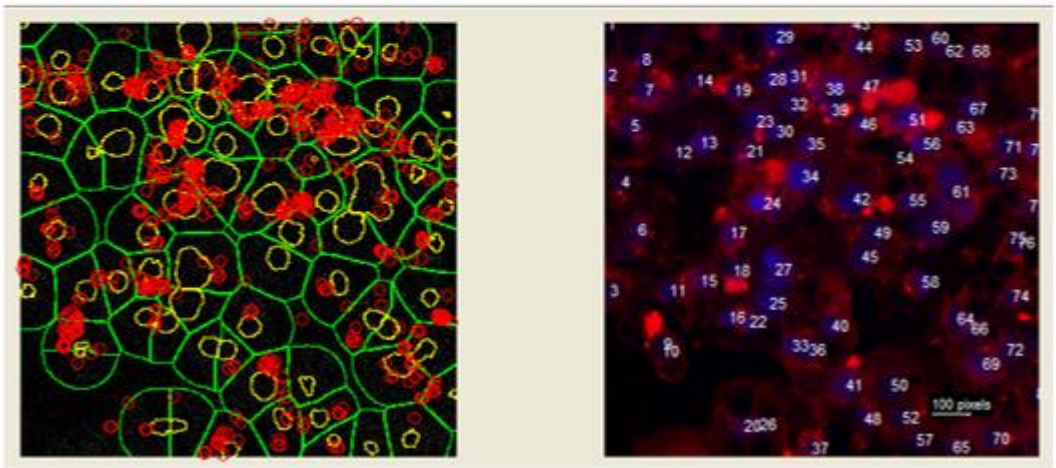

8.2.6 SX4/M-SX4/R INSULIN

1

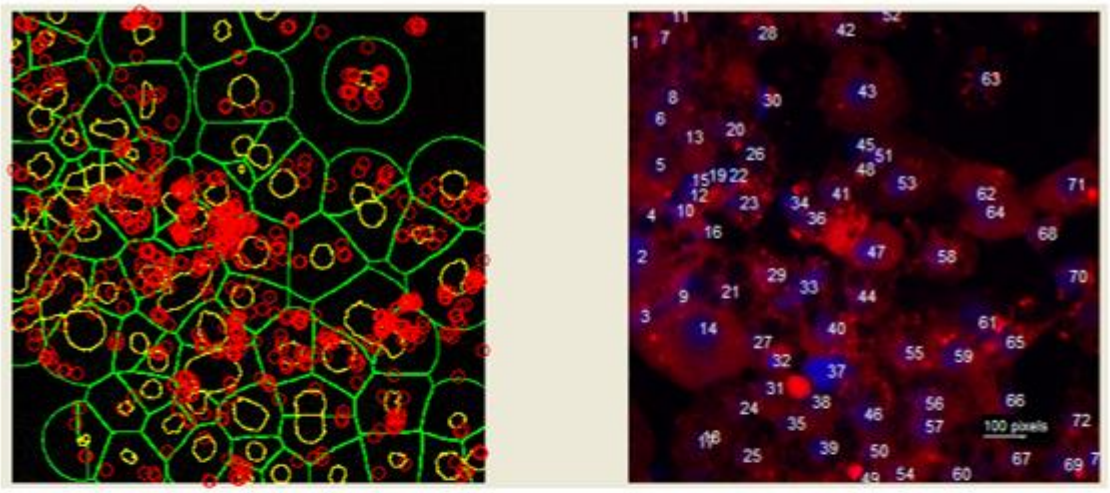

2

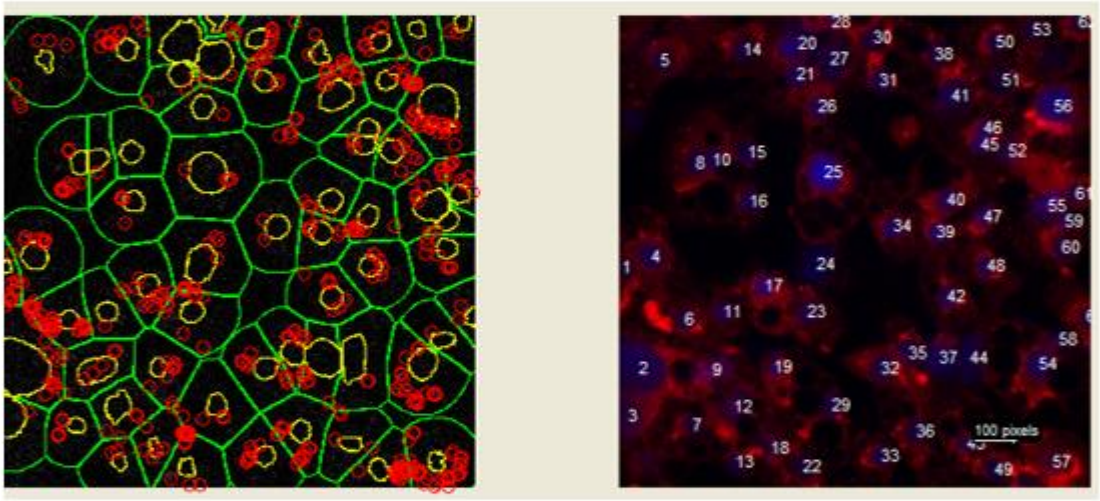

3

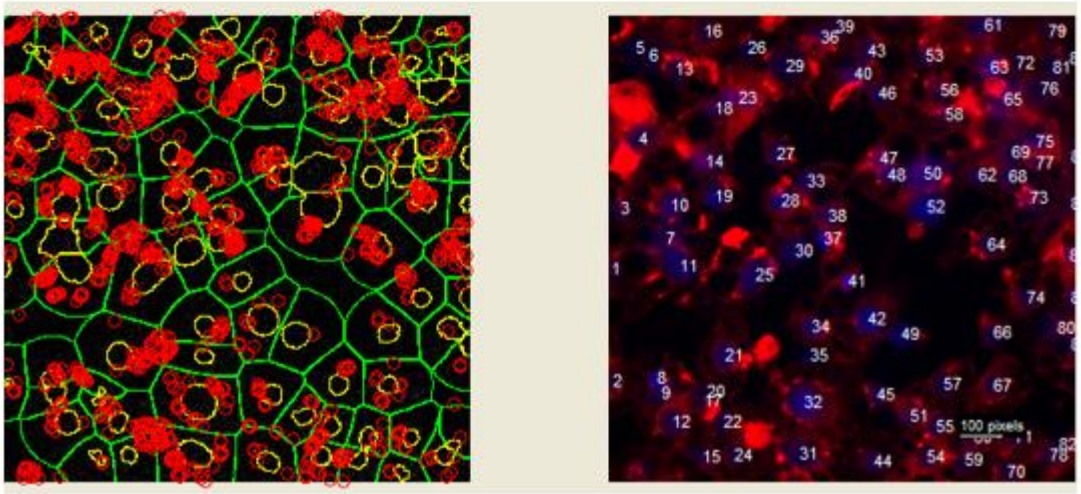

8.2.7 V2/M-S23/R BASAL

1

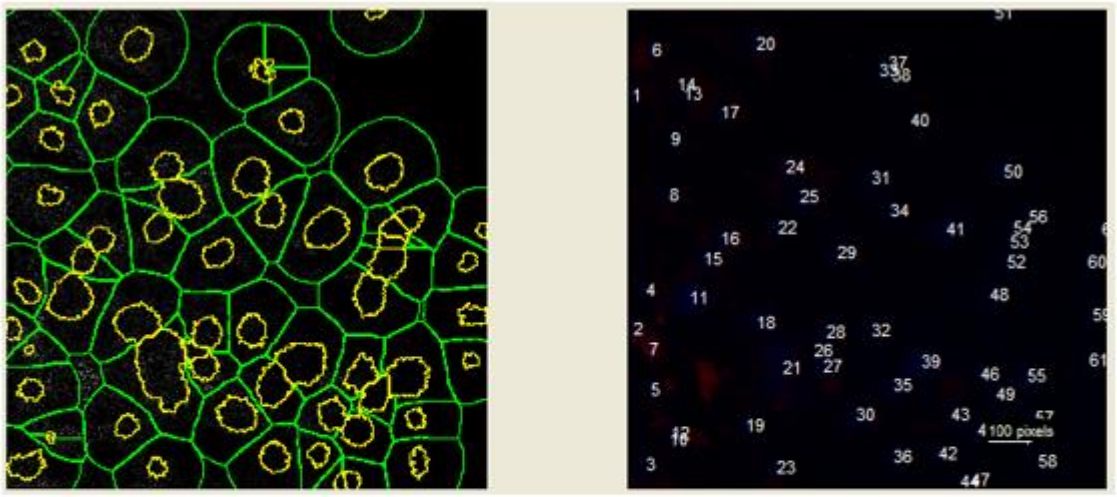

2

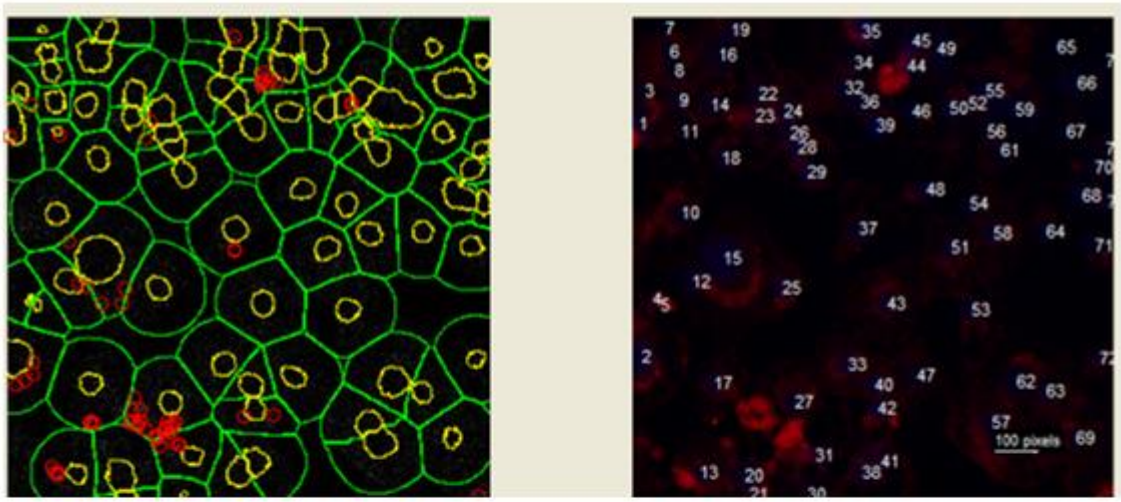

3

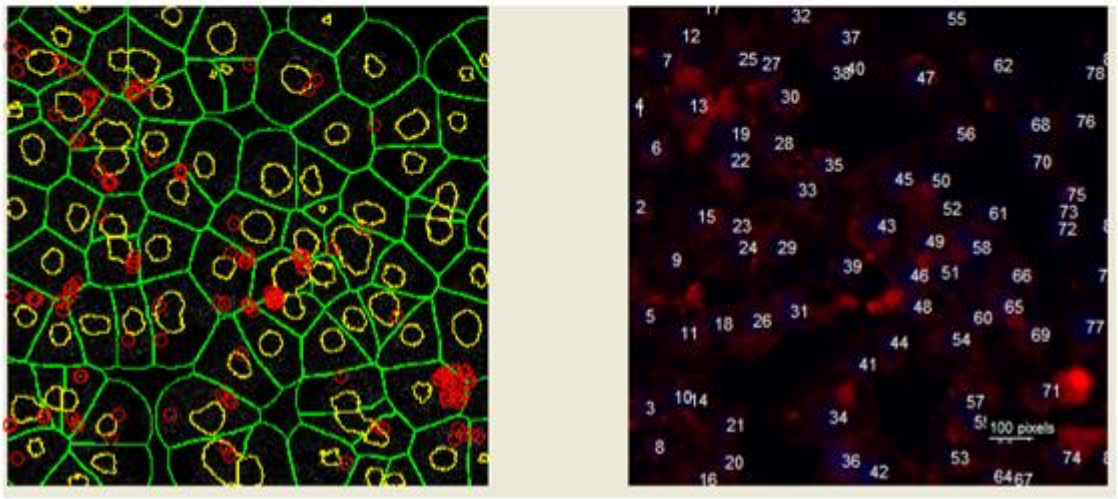

8.2.8 V2/M-S23/R INSULIN

1

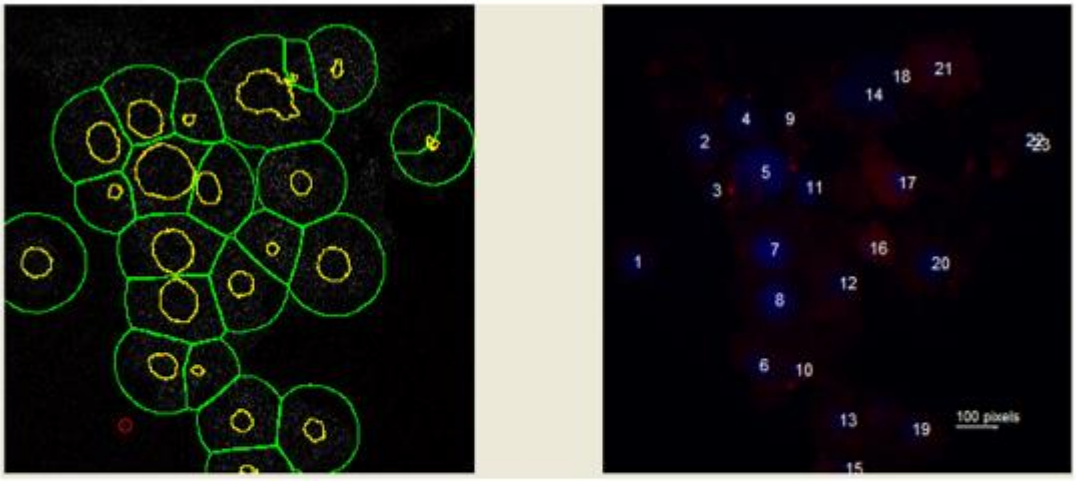

2

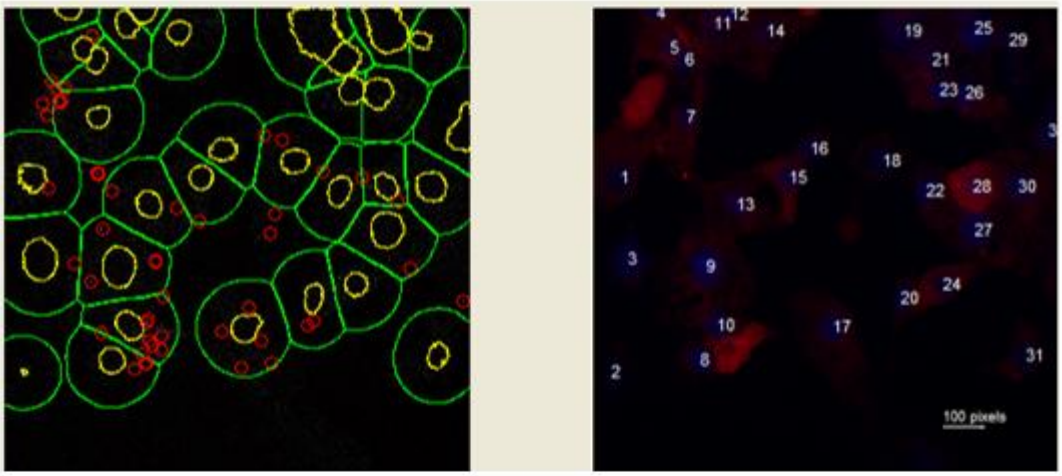

3

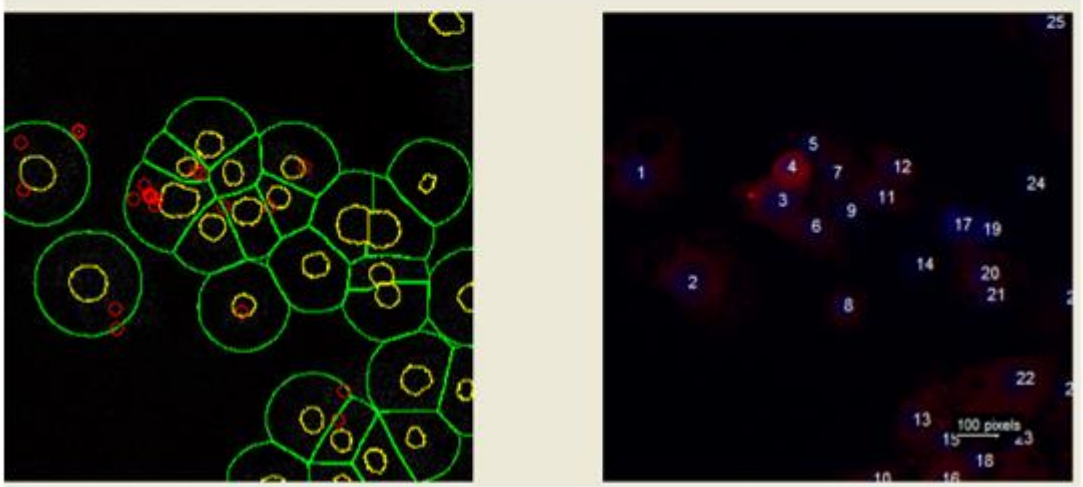

9 List of References

Abdul-Gader, A., Miles, A. J. and Wallace, B. A. (2011). A reference dataset for the analyses of membrane protein secondary structures and transmembrane residuesusing circular dichroism spectroscopy. *Bioinformatics* **27**, 1630–1636.

Abel, E. D., Peroni, O., Kim, J. K., Kim, Y. B., Boss, O., Hadro, E., Minnemann, T., Shulman, G. I. and Kahn, B. B. (2001). Adipose-selective targeting of the GLUT4 gene impairs insulin action in muscle and liver. *Nature* **409**, 729–733.

Adams, M., Reginato, M. J., Shao, D., Lazar, M. A. and Chatterjee, V. K. (1997). Transcriptional activation by peroxisome proliferator-activated receptor γ is inhibited by phosphorylation at a consensus mitogen-activated protein kinase site. *J. Biol. Chem.* **272**, 5128–5132.

Antonin, W., Fasshauer, D., Becker, S., Jahn, R. and Schneider, T. R. (2002). Crystal structure of the endosomal snare complex reveals common structural principles of all snares. *Nat. Struct. Biol.* **9**, 107–111.

Araki, S., Tamori, Y., Kawanishi, M., Shinoda, H., Masugi, J., Mori, H., Niki, T., Okazawa, H., Kubota, T. and Kasuga, M. (1997). Inhibition of the binding of SNAP-23 to syntaxin 4 by Munc18c. *Biochem. Biophys. Res. Commun.* **234**, 257–262.

Aran, V., Brandie, F. M., Boyd, A. R., Kantidakis, T., Rideout, E. J., Kelly, S. M., Gould, G. W. and Bryant, N. J. (2009). Characterization of two distinct binding modes between syntaxin 4 and Munc18c. *Biochem. J.* **419**, 655–660.

Aran, V., Bryant, N. J. and Gould, G. W. (2011). Tyrosine phosphorylation of Munc18c on residue 521 abrogates binding to Syntaxin 4. *BMC Biochem.* **12**, 19.

Aubin, R. A., Weinfeld, M., Mirzayans, R. and Paterson, M. C. (1994). Polybrene/DMSO-assisted gene transfer - Generating stable transfectants with nanogram amounts of DNA. *Mol. Biotechnol.* **1**, 29–48.

Bennett, M. K., Calakos, N. and Scheller, R. H. (1992). Syntaxin: A synaptic protein implicated in docking of synaptic vesicles at presynaptic active zones. *Science (80-.).* **257**, 255–259.

Bermúdez, V., Bermúdez, F., Arraiz, N., Leal, E., Linares, S., Mengual, E.,

Valdelamar, L., Rodríguez, M., Seyfi, H., Amell, A., et al. (2007). Biología molecular de los transportadores de glucosa: Clasificación, estructura y distribución. *Arch. Venez. Farmacol. y Ter.* **26**, 76–86.

Blasic, J. R., Brown, R. L. and Robinson, P. R. (2012). Phosphorylation of Mouse Melanopsin by Protein Kinase A. *PLoS One* **7**,.

Bock, J. B., Lin, R. C. and Scheller, R. H. (1996). A new syntaxin family member implicated in targeting of intracellular transport vesicles. *J. Biol. Chem.* **271**, 17961–17965.

Bock, J. B., Matern, H. T., Peden, A. A. and Scheller, R. H. (2001). A genomic perspective on membrane compartment organization. *Nature* **409**, 839–841.

Bracher, A. and Weissenhorn, W. (2002). Structural basis for the Golgi membrane recruitment of Sly1p by Sed5p. *EMBO J.* **21**, 6114–6124.

Brandie, F. M., Aran, V., Verma, A., McNew, J. A., Bryant, N. J. and Gould, G. W. (2008). Negative regulation of syntaxin4/SNAP-23/VAMP2-mediated membrane fusion by Munc18c In Vitro. *PLoS One* **3**, 1–7.

Brasher, M. I., Martynowicz, D. M., Grafinger, O. R., Hucik, A., Shanks-Skinner, E., Uniacke, J. and Coppolino, M. G. (2017). Interaction of Munc18c and syntaxin4 facilitates invadopodium formation and extracellular matrix invasion of tumor cells. *J. Biol. Chem.* **292**, 16199–16210.

Brenner, S. (2003a). *Nature's gift to science (Nobel lecture)*.

Brenner, S. (2003b). Nature's gift to science (Nobel lecture). *ChemBioChem* **4**, 683–687.

Brun, R. P., Tontonoz, P., Forman, B. M., Ellis, R., Chen, J., Evans, R. M. and Spiegelman, B. M. (1996). Differential activation of adipogenesis by multiple PPAR isoforms. *Genes Dev.* **10**, 974–984.

Bryant, N. J. and Gould, G. W. (2011). SNARE Proteins Underpin Insulin-Regulated GLUT4 Traffic. *Traffic* **12**, 657–664.

Bryant, N. J., Govers, R. and James, D. E. (2002). Regulated transport of the glucose transporter GLUT4. *Nat. Rev. Mol. Cell Biol.* **3**, 267–277.

Cain, C. C., Trimble, W. S. and Lienhard, G. E. (1992). Members of the VAMP family of synaptic vesicle proteins are components of glucose transporter-containing vesicles from rat adipocytes. *J. Biol. Chem.* **267**, 11681–11684.

Carlotti, F., Bazuine, M., Kekarainen, T., Seppen, J., Pognonec, P., Maassen, J. A. and Hoeben, R. C. (2004). Lentiviral vectors efficiently transduce

quiescent mature 3T3-L1 adipocytes. *Mol. Ther.* **9**, 209–217.

Carr, C. M., Grote, E., Munson, M., Hughson, F. M. and Novick, P. J. (1999). Sec1p binds to SNARE complexes and concentrates at sites of secretion. *J. Cell Biol.* **146**, 333–344.

Carroll, K. S., Hanna, J., Simon, I., Krise, J., Barbero, P. and Pfeffer, S. R. (2001). Role of Rab9 GTPase in facilitating receptor recruitment by TIP47. *Science (80-.).* **292**, 1373–1376.

Cheatham, B., Vlahos, C. J., Cheatham, L., Wang, L., Blenis, J. and Kahn, C. R. (1994). Phosphatidylinositol 3-kinase activation is required for insulin stimulation of pp70 S6 kinase, DNA synthesis, and glucose transporter translocation. *Mol. Cell. Biol.* **14**, 4902–11.

Chen, Y. A. and Scheller, R. H. (2001). Snare-mediated membrane fusion. *Nat. Rev. Mol. Cell Biol.* **2**, 98–106.

Chernomordik, L. V. and Kozlov, M. M. (2003). Protein-Lipid Interplay in Fusion and Fission of Biological Membranes. *Annu. Rev. Biochem.* **72**, 175–207.

Cheung, P. P. and Pfeffer, S. R. (2016). Transport Vesicle Tethering at the Trans Golgi Network: Coiled Coil Proteins in Action. *Front. Cell Dev. Biol.* **4**,.

Chiang, S. H., Baumann, C. A., Kanzaki, M., Thurmond, D. C., Watson, R. T., Neudauer, C. L., Macara, I. G., Pessin, J. E. and Saltiel, A. R. (2001). Insulin-stimulated GLUT4 translocation requires the CAP-dependent activation of TC10. *Nature* **410**, 944–948.

Christie, M. P., Whitten, A. E., King, G. J., Hu, S.-H., Jarrott, R. J., Chen, K.-E., Duff, A. P., Callow, P., Collins, B. M., James, D. E., et al. (2012). Low-resolution solution structures of Munc18:Syntaxin protein complexes indicate an open binding mode driven by the Syntaxin N-peptide. *Proc. Natl. Acad. Sci.* **109**, 9816–9821.

Clary, D. O., Griff, I. C. and Rothman, J. E. (1990). SNAPs, a family of NSF attachment proteins involved in intracellular membrane fusion in animals and yeast. *Cell* **61**, 709–721.

Coelen, R. J., Jose, D. G. and May, J. T. (1983). The effect of hexadimethrine bromide (polybrene) on the infection of the primate retroviruses SSV 1/SSAV 1 and BaEV. *Arch. Virol.* **75**, 307–311.

Cushman, S. W. and Wardzala, L. J. (1980). Potential mechanism of insulin

action on glucose transport in the isolated rat adipose cell. Apparent translocation of intracellular transport systems to the plasma membrane. *J. Biol. Chem.* **255**, 4758–4762.

D'Andrea-Merrins, M., Chang, L., Lam, A. D., Ernst, S. A. and Stuenkel, E. L. (2007). Munc18c interaction with syntaxin 4 monomers and SNARE complex intermediates in GLUT4 vesicle trafficking. *J. Biol. Chem.* **282**, 16553–16566.

Dacks, J. B. and Field, M. C. (2007). Evolution of the eukaryotic membrane-trafficking system: origin, tempo and mode. *J. Cell Sci.* **120**, 2977–2985.

Doi, H., Masaki, N., Takahashi, H., Komatsu, H., Fujimori, K. and Satomi, S. (2005). A New Preadipocyte Cell Line, AP-18, Established from Adult Mouse Adipose Tissue. *Tohoku J. Exp. Med.* **207**, 209–216.

Dubuke, M. L. and Munson, M. (2016). The Secret Life of Tethers: The Role of Tethering Factors in SNARE Complex Regulation. *Front. Cell Dev. Biol.* **4**, 42.

Dulubova, I., Sugita, S., Hill, S., Hosaka, M., Fernandez, I., Südhof, T. C. and Rizo, J. (1999). A conformational switch in syntaxin during exocytosis: Role of munc18. *EMBO J.* **18**, 4372–4382.

Dulubova, I., Khvotchev, M., Liu, S., Huryeva, I., Sudhof, T. C. and Rizo, J. (2007). Munc18-1 binds directly to the neuronal SNARE complex. *Proc. Natl. Acad. Sci.* **104**, 2697–2702.

Fernandez, I., Ubach, J., Dulubova, I., Zhang, X., Südhof, T. C. and Rizo, J. (1998). Three-dimensional structure of an evolutionarily conserved N-terminal domain of syntaxin 1A. *Cell* **94**, 841–849.

Flaumenhaft, R., Croce, K., Chen, E., Furie, B. and Furie, B. C. (1998). Proteins of the exocytotic core complex mediate platelet a-granule secretion. *J. Biol. Chem. nicht bekannt* **274**, 2492–2501.

Foster, L. J., Yeung, B., Mohtashami, M., Ross, K., Trimble, W. S. and Klip, A. (1998). Binary interactions of the SNARE proteins syntaxin-4, SNAP23, and VAMP- 2 and their regulation by phosphorylation. *Biochemistry* **37**, 11089–11096.

Gengyo-Ando, K., Kitayama, H., Mukaida, M. and Ikawa, Y. (1996). A murine neural-specific homolog corrects cholinergic defects in Caenorhabditis elegans unc-18 mutants. *J. Neurosci.* **16**, 6695–6702.

Gonzalo, S. and Linder, M. E. (1998). SNAP-25 Palmitoylation and Plasma Membrane Targeting Require a Functional Secretory Pathway. *Mol. Biol. Cell* **9**, 585–597.

Grant, B. D. and Donaldson, J. G. (2009). Pathways and mechanisms of endocytic recycling. *Nat. Rev. Mol. Cell Biol.* **10**, 597–608.

Greenfield, N. J. (2007). Using circular dichroism spectra to estimate protein secondary structure. *Nat. Protoc.* **1**, 2876–2890.

Gross, D. N., Farmer, S. R. and Pilch, P. F. (2004). Glut4 Storage Vesicles without Glut4: Transcriptional Regulation of Insulin-Dependent Vesicular Traffic. *Mol. Cell. Biol.* **24**, 7151–7162.

Gual, P., Le Marchand-Brustel, Y. and Tanti, J. F. (2005). Positive and negative regulation of insulin signaling through IRS-1 phosphorylation. In *Biochimie*, pp. 99–109.

Guerre-Millo, M. (2002). Adipose tissue hormones. *J. Endocrinol. Invest.* **25**, 855–861.

Guo, W., Grant, A. and Novick, P. (1999). Exo84p is an exocyst protein essential for secretion. *J. Biol. Chem.* **274**, 23558–23564.

Hajduch, E., Aledo, J. C., Watts, C. and Hundal, H. S. (1997). Proteolytic cleavage of cellubrevin and vesicle-associated membrane protein (VAMP) by tetanus toxin does not impair insulin-stimulated glucose transport or GLUT4 translocation in rat adipocytes. *Biochem. J.* **321**, 233–238.

Hashiramoto, M. and James, D. E. (2000). Characterization of insulin-responsive GLUT4 storage vesicles isolated from 3T3-L1 adipocytes. *Mol. Cell. Biol.* **20**, 416–27.

Hayashi, T., McMahon, H., Yamasaki, S., Binz, T., Hata, Y., Südhof, T. C. and Niemann, H. (1994). Synaptic vesicle membrane fusion complex: action of clostridial neurotoxins on assembly. *EMBO J.* **13**, 5051–61.

Hernandez, J. M., Stein, A., Behrmann, E., Riedel, D., Cypionka, A., Farsi, Z., Walla, P. J., Raunser, S. and Jahn, R. (2012). Membrane fusion intermediates via directional and full assembly of the SNARE complex. *Science (80-.).* **336**, 1581–1584.

Hirshman, M. F., Goodyear, L. J., Wardzala, L. J., Horton, E. D. and Horton, E. S. (1990). Identification of an intracellular pool of glucose transporters from basal and insulin-stimulated rat skeletal muscle. *J. Biol. Chem.* **265**,

987–991.

Holt, M., Varoqueaux, F., Wiederhold, K., Takamori, S., Urlaub, H., Fasshauer, D. and Jahn, R. (2006). Identification of SNAP-47, a novel Qbc-SNARE with ubiquitous expression. *J. Biol. Chem.* **281**, 17076–17083.

Hong, W. J. (2005a). SNAREs and traffic (vol 1744, pg 120, 2005). *Biochim. Biophys. Acta-Molecular Cell Res.* **1744**, 465–+.

Hong, W. (2005b). SNAREs and traffic. *Biochim. Biophys. Acta - Mol. Cell Res.* **1744**, 120–144.

Hong, W. J. and Lev, S. (2014). Tethering the assembly of SNARE complexes. *Trends Cell Biol.* **24**, 35–43.

Howes, M. T., Mayor, S. and Parton, R. G. (2010). Molecules, mechanisms, and cellular roles of clathrin-independent endocytosis. *Curr. Opin. Cell Biol.* **22**, 519–527.

Hu, S. H., Gee, C. L., Latham, C. F., Rowlinson, S. W., Rova, U., Jones, A., Halliday, J. A., Bryant, N. J., James, D. E. and Martin, J. L. (2003). Recombinant expression of Munc18c in a baculovirus system and interaction with syntaxin. *Protein Expr. Purif.* **31**, 305–310.

Hu, S.-H., Latham, C. F., Gee, C. L., James, D. E. and Martin, J. L. (2007). Structure of the Munc18c/Syntaxin4 N-peptide complex defines universal features of the N-peptide binding mode of Sec1/Munc18 proteins. *Proc. Natl. Acad. Sci.* **104**, 8773–8778.

Hutagalung, A. H. and Novick, P. J. (2011). Role of Rab GTPases in Membrane Traffic and Cell Physiology. *Physiol. Rev.* **91**, 119–149.

Inoue, M., Chang, L., Hwang, J., Chiang, S. H. and Saltiel, A. R. (2003). The exocyst complex is required for targeting of Glut4 to the plasma membrane by insulin. *Nature* **422**, 629–633.

Jahn, R., Lang, T. and Südhof, T. (2003). Membrane fusion. *Cell* **112**, 519–533.

James, D. E., Strube, M. and Muecdler, M. (1989). Molecular cloning and characterization of an insulin-regulatable glucose transporter. *Nature* **338**, 83–87.

Jarvius, M., Paulsson, J., Weibrecht, I., Leuchowius, K.-J., Andersson, A.-C., Wählby, C., Gullberg, M., Botling, J., Sjöblom, T., Markova, B., et al. (2007). *In Situ* Detection of Phosphorylated Platelet-derived Growth Factor Receptor ß Using a Generalized Proximity Ligation Method. *Mol. Cell.*

Proteomics **6**, 1500–1509.

Jedrychowski, M. P., Gartner, C. A., Gygi, S. P., Zhou, L., Herz, J., Kandror, K. V. and Pilch, P. F. (2010). Proteomic analysis of GLUT4 storage vesicles reveals LRP1 to be an important vesicle component and target of insulin signaling. *J. Biol. Chem.* **285**, 104–114.

Jewell, J. L., Oh, E., Bennett, S. M., Meroueh, S. O. and Thurmond, D. C. (2008). The tyrosine phosphorylation of Munc18c induces a switch in binding specificity from syntaxin 4 to Doc2B. *J. Biol. Chem.* **283**, 21734–21746.

Jewell, J. L., Oh, E. and Thurmond, D. C. (2010). Exocytosis mechanisms underlying insulin release and glucose uptake: conserved roles for Munc18c and syntaxin 4. *AJP Regul. Integr. Comp. Physiol.* **298**, R517–R531.

Jewell, J. L., Oh, E., Ramalingam, L., Kalwat, M. A., Tagliabracci, V. S., Tackett, L., Elmendorf, J. S. and Thurmond, D. C. (2011). Munc18c phosphorylation by the insulin receptor links cell signaling directly to SNARE exocytosis. *J. Cell Biol.* **193**, 185–199.

Kahn, S. E., Hull, R. L. and Utzschneider, K. M. (2006). Mechanisms linking obesity to insulin resistance and type 2 diabetes. *Nature*.

Kandror, K. V. and Pilch, P. F. (2011). The Sugar Is sIRVed: Sorting Glut4 and Its Fellow Travelers. *Traffic* **12**, 665–671.

Katz, L. and Brennwald, P. (2000). Testing the 3Q:1R "Rule": Mutational Analysis of the Ionic "Zero" Layer in the Yeast Exocytic SNARE Complex Reveals No Requirement for Arginine. *Mol. Biol. Cell* **11**, 3849–3858.

Kawanishi, M., Tamori, Y., Okazawa, H., Araki, S., Shinoda, H. and Kasuga, M. (2000). Role of SNAP23 in insulin-induced translocation of GLUT4 in 3T3-L1 adipocytes: Mediation of complex formation between syntaxin4 and VAMP2. *J. Biol. Chem.* **275**, 8240–8247.

Kee, Y., Yoo, J.-S., Hazuka, C. D., Peterson, K. E., Hsu, S.-C. and Scheller, R. H. (1997). Subunit structure of the mammalian exocyst complex. *Proc. Natl. Acad. Sci.* **94**, 14438–14443.

Kelly, S. M., Jess, T. J. and Price, N. C. (2005). How to study proteins by circular dichroism. *Biochim. Biophys. Acta - Proteins Proteomics* **1751**, 119–139.

Khvotchev, M., Dulubova, I., Sun, J., Dai, H., Rizo, J. and Sudhof, T. C. (2007). Dual Modes of Munc18-1/SNARE Interactions Are Coupled by

Functionally Critical Binding to Syntaxin-1 N Terminus. *J. Neurosci.* **27**, 12147–12155.

Kioumourtzoglou, D., Gould, G. W. and Bryant, N. J. (2014). Insulin Stimulates Syntaxin4 SNARE Complex Assembly via a Novel Regulatory Mechanism. *Mol. Cell. Biol.* **34**, 1271–1279.

Kioumourtzoglou, D., Pryor, P. R., Gould, G. W. and Bryant, N. J. (2015). Alternative routes to the cell surface underpin insulin-regulated membrane trafficking of GLUT4. *J. Cell Sci.* **128**, 2423–2429.

Kioumourtzoglou, D., Gould, G. W. and Bryant, N. J. (2018). Proximity ligation assay to study the GLUT4 membrane trafficking machinery. In *Methods in Molecular Biology*, pp. 217–227. Humana Press, New York, NY.

Kraegen, E. W., James, D. E., Jenkins, A. B. and Chisholm, D. J. (1985). Dose-response curves for in vivo insulin sensitivity in individual tissues in rats. *Am. J. Physiol. Metab.*

Kuhne, M. R., Zhao, Z., Rowles, J., Lavan, B. E., Shen, S. H., Fischer, E. H. and Lienhard, G. E. (1994). Dephosphorylation of insulin receptor substrate 1 by the tyrosine phosphatase PTP2C. *J. Biol. Chem.* **269**, 15833–15837.

Kupriyanova, T. A. and Kandror, K. V. (2000). Cellugyrin is a marker for a distinct population of intracellular Glut4-containing vesicles. *J. Biol. Chem.* **275**, 36263–36268.

Laidlaw, K. M. E., Livingstone, R., Al-Tobi, M., Bryant, N. J. and Gould, G. W. (2017). SNARE phosphorylation: a control mechanism for insulin-stimulated glucose transport and other regulated exocytic events. *Biochem. Soc. Trans.* **45**, 1271–1277.

Lampson, M. A., Racz, A., Cushman, S. W. and McGraw, T. E. (2000). Demonstration of insulin-responsive trafficking of GLUT4 and vpTR in fibroblasts. *J. Cell Sci.* **113**, 4065–4076.

Lang, T. and Jahn, R. (2008). Core proteins of the secretory machinery. *Handb. Exp. Pharmacol.* **184**, 107–127.

Latham, C. F., Lopez, J. A., Hu, S.-H., Gee, C. L., Westbury, E., Blair, D. H., Armishaw, C. J., Alewood, P. F., Bryant, N. J., James, D. E., et al. (2006). Molecular Dissection of the Munc18c/Syntaxin4 Interaction: Implications for Regulation of Membrane Trafficking. *Traffic* **7**, 1408–1419.

Latham, C. F., Hu, S.-H., Gee, C. L., Armishaw, C. J., Alewood, P. F., James,

D. E. and Martin, J. L. (2007). Crystallization and preliminary X-ray diffraction of the Munc18c–syntaxin4 $_{1-29}$ complex. *Acta Crystallogr. Sect. F Struct. Biol. Cryst. Commun.* **63**, 524–528.

Leavitt, S. and Freire, E. (2001). Direct measurement of protein binding energetics by isothermal titration calorimetry. *Curr. Opin. Struct. Biol.* **11**, 560–566.

Lemberger, T., Saladin, R., Vázquez, M., Assimacopoulos, F., Staels, B., Desvergne, B., Wahli, W. and Auwerx, J. (1996). Expression of the peroxisome proliferator-activated receptor α gene is stimulated by stress and follows a diurnal rhythm. *J. Biol. Chem.* **271**, 1764–1769.

Li, F., Kümmel, D., Coleman, J., Reinisch, K. M., Rothman, J. E. and Pincet, F. (2014). A half-zippered SNARE complex represents a functional intermediate in membrane fusion. *J. Am. Chem. Soc.* **136**, 2456–2464.

Lillie, R. and Ashburn, L. (1943). Supersaturated solutions of fat stains in dilute isopropanol for demonstration of acute fatty degeneration not shown by Herxheimer's technique. *Arch. Pathol.* **36**, 432.

Lisman, J. E., Raghavachari, S. and Tsien, R. W. (2007). The sequence of events that underlie quantal transmission at central glutamatergic synapses. *Nat. Rev. Neurosci.* **8**, 597–609.

Livingstone, C., James, D. E., Rice, J. E., Hanpeter, D. and Gould, G. W. (1996). Compartment ablation analysis of the insulin-responsive glucose transporter (GLUT4) in 3T3-L1 adipocytes. *Biochem. J.* **315**, 487–495.

Lowell, B. B. and Flier, J. S. (1990). Differentiation dependent biphasic regulation of adipsin gene expression by insulin and insulin-like growth factor-1 in 3t3-f442a adipocytes. *Endocrinology* **127**, 2898–2906.

Malhotra, V., Orci, L., Glick, B. S., Block, M. R. and Rothman, J. E. (1988). Role of an N-ethylmaleimide-sensitive transport component in promoting fusion of transport vesicles with cisternae of the Golgi stack. *Cell* **54**, 221–227.

Malmersjö, S., Di Palma, S., Diao, J., Lai, Y., Pfuetzner, R. A., Wang, A. L., McMahon, M. A., Hayer, A., Porteus, M., Bodenmiller, B., et al. (2016). Phosphorylation of residues inside the SNARE complex suppresses secretory vesicle fusion. *EMBO J.* **35**, 1810–1821.

Malsam, J., Kreye, S. and Söllner, T. H. (2008). Membrane traffic in the

secretory pathway: Membrane fusion: SNAREs and regulation. *Cell. Mol. Life Sci.* **65**, 2814–2832.

Manavalan, P. and Johnson, W. C. (1987). Variable selection method improves the prediction of protein secondary structure from circular dichroism spectra. *Anal. Biochem.* **167**, 76–85.

Marash, M. and Gerst, J. E. (2001). t-SNARE dephosphorylation promotes SNARE assembly and exocytosis in yeast. *EMBO J.* **20**, 411–421.

Margittai, M., Fasshauer, D., Pabst, S., Jahn, R. and Langen, R. (2001). Homo- and Heterooligomeric SNARE Complexes Studied by Site-directed Spin Labeling. *J. Biol. Chem.* **276**, 13169–13177.

Martin, O. J., Lee, A. and McGraw, T. E. (2006). GLUT4 distribution between the plasma membrane and the intracellular compartments is maintained by an insulin-modulated bipartite dynamic mechanism. *J. Biol. Chem.* **281**, 484–490.

Masaki, R., Yamamoto, A., Akagawa, K. and Tashiro, Y. (1998). Important roles of the C-terminal portion of HPC-1/syntaxin 1A in membrane anchoring and intracellular localization. *J. Biochem.* **124**, 311–318.

Misura, K. M. S., Scheller, R. H. and Weis, W. I. (2000). Three-dimensional structure of the neuronal-Sec1-syntaxin 1a complex. *Nature* **404**, 355–362.

Mitra, P., Zheng, X. and Czech, M. P. (2004). RNAi-based analysis of CAP, Cbl, and CrkII function in the regulation of GLUT4 by insulin. *J. Biol. Chem.* **279**, 37431–37435.

Molero, J. C., Jensen, T. E., Withers, P. C., Couzens, M., Herzog, H., Thien, C. B. F., Langdon, W. Y., Walder, K., Murphy, M. A., Bowtell, D. D. L., et al. (2004). c-Cbl-deficient mice have reduced adiposity, higher energy expenditure, and improved peripheral insulin action. *J. Clin. Invest.* **114**, 1326–1333.

Morey, C. and Fasshauer, D. (2014). Interaction of Munc18C with Syntaxin4 and the Role of Munc18C in Exocytosis. *Biophys. J.* **106**, 311a.

Muretta, J. M., Romenskaia, I. and Mastick, C. C. (2008). Insulin releases Glut4 from static storage compartments into cycling endosomes and increases the rate constant for Glut4 exocytosis. *J. Biol. Chem.* **283**, 311–323.

Nielander, H. B., Onofri, F., Valtorta, F., Schiavo, G., Montecucco, C., Greengard, P. and Benfenati, F. (1995). Phosphorylation of

VAMP/Synaptobrevin in Synaptic Vesicles by Endogenous Protein Kinases. *J. Neurochem.* **65**, 1712–1720.

Novick, P. and Schekman, R. (1979). *Secretion and cell-surface growth are blocked in a temperature-sensitive mutant of Saccharomyces cerevisiae.*

Novick, P., Field, C. and Schekman, R. (1980). Identification of 23 complementation groups required for post-translational events in the yeast secretory pathway. *Cell* **21**, 205–215.

Oh, E. and Thurmond, D. C. (2006). The stimulus-induced tyrosine phosphorylation of Munc18c facilitates vesicle exocytosis. *J. Biol. Chem.* **281**, 17624–17634.

Oh, E., Spurlin, B. A., Pessin, J. E. and Thurmond, D. C. (2005). Munc18c heterozygous knockout mice display increased susceptibility for severe glucose intolerance. *Diabetes* **54**, 638–647.

Ohya, T., Miaczynska, M., Coskun, Ü., Lommer, B., Runge, A., Drechsel, D., Kalaidzidis, Y. and Zerial, M. (2009). Reconstitution of Rab- And SNARE-dependent membrane fusion by synthetic endosomes. *Nature* **459**, 1091–1097.

Okada, T., Kawano, Y., Sakakibara, T., Hazeki, O. and Ui, M. (1994). Essential role of phosphatidylinositol 3-kinase in insulin-induced glucose transport and antilipolysis in rat adipocytes. Studies with a selective inhibitor wortmannin. *J. Biol. Chem.* **269**, 3568–3573.

Olson, A. L. and Pessin, J. E. (1996). Structure, Function, and Regulation of the Mammalian Facilitative Glucose Transporter Gene Family. *Annu. Rev. Nutr.* **16**, 235–256.

Oyler, G. A., Higgins, G. A., Hart, R. A., Battenberg, E., Billingsley, M., Bloom, F. E. and Wilson, M. C. (1989). The identification of a novel synaptosomal-associated protein, SNAP-25, differentially expressed by neuronal subpopulations. *J. Cell Biol.* **109**, 3039–3052.

Palade, G. (1975). Intracellular Aspects of the Process of Protein Synthesis. *Science (80-.).* **189**, 867–867.

Parkar, N. S., Akpa, B. S., Nitsche, L. C., Wedgewood, L. E., Place, A. T., Sverdlov, M. S., Chaga, O. and Minshall, R. D. (2009). Vesicle Formation and Endocytosis: Function, Machinery, Mechanisms, and Modeling. *Antioxid. Redox Signal.* **11**, 1301–1312.

Perera, H. K. I. (2003). Syntaxin 6 Regulates Glut4 Trafficking in 3T3-L1 Adipocytes. *Mol. Biol. Cell* **14**, 2946–2958.

Pessin, J. E., Thurmond, D. C., Elmendorf, J. S., Coker, K. J. and Okada, S. (1999). Molecular basis of insulin-stimulated GLUT4 vesicle trafficking. Location! Location! Location! *J. Biol. Chem.* **274**, 2593–2596.

Pevsner, J., Hsu, S. C., Braun, J. E. A., Calakos, N., Ting, A. E., Bennett, M. K. and Scheller, R. H. (1994). Specificity and regulation of a synaptic vesicle docking complex. *Neuron* **13**, 353–361.

Pfeffer, S. R. (1999). Transport-vesicle targeting: Tethers before SNAREs. *Nat. Cell Biol.* **1**, E17–E22.

Pierce, M. M., Raman, C. S. and Nall, B. T. (1999). Isothermal titration calorimetry of protein-protein interactions. *Methods A Companion to Methods Enzymol.* **19**, 213–221.

Pobbati, A. V., Stein, A. and Fasshauer, D. (2006). N- to C-terminal SNARE complex assembly promotes rapid membrane fusion. *Science (80-.).* **313**, 673–676.

Proctor, K. M., Miller, S. C. M., Bryant, N. J. and Gould, G. W. (2006). Syntaxin 16 controls the intracellular sequestration of GLUT4 in 3T3-L1 adipocytes. *Biochem. Biophys. Res. Commun.* **347**, 433–438.

Ramalingam, L., Yoder, S. M., Oh, E. and Thurmond, D. C. (2014). Munc18c: A controversial regulator of peripheral insulin action. *Trends Endocrinol. Metab.* **25**, 601–608.

Ran, V. R., Chawla, A. and Roche, P. A. (1996). Identification of a novel syntaxin- and synaptobrevin/ VAMP-binding protein, SNAP-23, expressed in non-neuronal tissues. *J. Biol. Chem.* **271**, 13300–13303.

Randhawa, V. K., Bilan, P. J., Khayat, Z. A., Daneman, N., Liu, Z., Ramlal, T., Volchuk, A., Peng, X.-R., Coppola, T., Regazzi, R., et al. (2000). VAMP2, but Not VAMP3/Cellubrevin, Mediates Insulin-dependent Incorporation of GLUT4 into the Plasma Membrane of L6 Myoblasts. *Mol. Biol. Cell* **11**, 2403–2417.

Rea, S., Martin, L. B., McIntosh, S., Macaulay, S. L., Ramsdale, T., Baldini, G. and James, D. E. (1998). Syndet, an adipocyte target SNARE involved in the insulin-induced translocation of GLUT4 to the cell surface. *J. Biol. Chem.* **273**, 18784–18792.

Rehman, A., Jarrott, R. J., Whitten, A. E., King, G. J., Hu, S. H., Christie, M. P., Collins, B. M. and Martin, J. L. (2013). Milligram quantities of homogeneous recombinant full-length mouse Munc18c from escherichia coli cultures. *PLoS One* **8**,.

Rehman, A., Hu, S. H., Tnimov, Z., Whitten, A. E., King, G. J., Jarrott, R. J., Norwood, S. J., Alexandrov, K., Collins, B. M., Christie, M. P., et al. (2017). The nature of the Syntaxin4 C-terminus affects Munc18c-supported SNARE assembly. *PLoS One* **12**,.

Rickman, C., HU, K., Carroll, J. and Davletov, B. (2005). Self-assembly of SNARE fusion proteins into star-shaped oligomers. *Biochem. J.* **388**, 75–79.

Risinger, C. and Bennett, M. K. (1999). Differential phosphorylation of syntaxin and synaptosome-associated protein of 25 kDa (SNAP-25) isoforms. *J. Neurochem.* **72**, 614–624.

Robinson, L. J., Pang, S., Harris, D. S., Heuser, J. and James, D. E. (1992). Translocation of the glucose transporter (GLUT4) to the cell surface in permeabilized 3T3-L1 adipocytes: Effects of ATP, insulin, and GTPγS and localization of GLUT4 to clathrin lattices. *J. Cell Biol.* **117**, 1181–1196.

Roccisana, J., Sadler, J. B. A., Bryant, N. J. and Gould, G. W. (2013). Sorting of GLUT4 into its insulin-sensitive store requires the Sec1/Munc18 protein mVps45. *Mol. Biol. Cell* **24**, 2389–2397.

Ross, S. A., Song, X., Burney, M. W., Kasai, Y. and Orlicky, D. J. (2003). Efficient adenovirus transduction of 3T3-L1 adipocytes stably expressing coxsackie-adenovirus receptor. *Biochem. Biophys. Res. Commun.* **302**, 354–358.

Rothman, J. E. (1994). Mechanisms of intracellular protein transport. *Nature* **372**, 55–63.

Rowland, A. F., Fazakerley, D. J. and James, D. E. (2011). Mapping Insulin/GLUT4 Circuitry. *Traffic* **12**, 672–681.

Sadler, J. B. A., Lamb, C. A., Gould, G. W. and Bryant, N. J. (2016). Preparation of a total membrane fraction from 3T3-L1 adipocytes. *Cold Spring Harb. Protoc.* **2016**, 276–278.

Sano, H., Roach, W. G., Peck, G. R., Fukuda, M. and Lienhard, G. E. (2008). Rab10 in insulin-stimulated GLUT4 translocation. *Biochem. J.* **411**, 89–95.

Sapperstein, S. K., Lupashin, V. V., Schmitt, H. D. and Waters, M. G. (1996).

Assembly of the ER to Golgi SNARE complex requires Uso1p. *J. Cell Biol.* **132**, 755–767.

Schmelzle, K., Kane, S., Gridley, S., Lienhard, G. E. and White, F. M. (2006). Temporal dynamics of tyrosine phosphorylation in insulin signaling. *Diabetes* **55**, 2171–2179.

Schuck, S. (2004). Polarized sorting in epithelial cells: raft clustering and the biogenesis of the apical membrane. *J. Cell Sci.* **117**, 5955–5964.

Scott, B. L., Van Komen, J. S., Liu, S., Weber, T., Mella, T. J. and McNew, J. A. (2003). Liposome Fusion Assay to Monitor Intracellular Membrane Fusion Machines. *Methods Enzymol.* **372**, 274–300.

Scott, B. L., Van Komen, J. S., Irshad, H., Liu, S., Wilson, K. A. and McNew, J. A. (2004). Sec1 p directly stimulates SNARE-mediated membrane fusion in vitro. *J. Cell Biol.* **167**, 75–85.

Seabra, M. C. and Coudrier, E. (2004). Rab GTPases and myosin motors in organelle motility. *Traffic* **5**, 393–399.

Semerdjieva, S., Shortt, B., Maxwell, E., Singh, S., Fonarev, P., Hansen, J., Schiavo, G., Grant, B. D. and Smythe, E. (2008). Coordinated regulation of AP2 uncoating from clathrin-coated vesicles by rab5 and hRME-6. *J. Cell Biol.* **183**, 499–511.

Shanks, S. G., Carpp, L. N., Struthers, M. S., McCann, R. K. and Bryant, N. J. (2012). The Sec1/Munc18 Protein Vps45 Regulates Cellular Levels of Its SNARE Binding Partners Tlg2 and Snc2 in Saccharomyces cerevisiae. *PLoS One* **7**,.

Shen, J., Tareste, D. C., Paumet, F., Rothman, J. E. and Melia, T. J. (2007). Selective Activation of Cognate SNAREpins by Sec1/Munc18 Proteins. *Cell* **128**, 183–195.

Shewan, A. M. (2003). GLUT4 Recycles via a trans-Golgi Network (TGN) Subdomain Enriched in Syntaxins 6 and 16 But Not TGN38: Involvement of an Acidic Targeting Motif. *Mol. Biol. Cell* **14**, 973–986.

Shimazaki, Y., Nishiki, T. I., Omori, A., Sekiguchi, M., Kamata, Y., Kozaki, S. and Takahashi, M. (1996). Phosphorylation of 25-kDa synaptosome-associated protein: Possible involvement in protein kinase C-mediated regulation of neurotransmitter release. *J. Biol. Chem.* **271**, 14548–14553.

Smith, R. M., Charron, M. J., Shah, N., Lodish, H. F. and Jarett, L. (1991).

Immunoelectron microscopic demonstration of insulin-stimulated translocation of glucose transporters to the plasma membrane of isolated rat adipocytes and masking of the carboxyl-terminal epitope of intracellular GLUT4. *Proc. Natl. Acad. Sci.* **88**, 6893–6897.

Smyth, A. M., Duncan, R. R. and Rickman, C. (2010). Munc18-1 and syntaxin1: Unraveling the interactions between the dynamic duo. In *Cellular and Molecular Neurobiology*, pp. 1309–1313.

Snyder, D. A., Kelly, M. L. and Woodbury, D. J. (2006). SNARE Complex Regulation by Phosphorylation. *Cell Biochem. Biophys.* **45**, 111–124.

Söllner, T., Whiteheart, S. W., Brunner, M., Erdjument-Bromage, H., Geromanos, S., Tempst, P. and Rothman, J. E. (1993a). SNAP receptors implicated in vesicle targeting and fusion. *Nature* **362**, 318–324.

Söllner, T., Bennett, M. K., Whiteheart, S. W., Scheller, R. H. and Rothman, J. E. (1993b). A protein assembly-disassembly pathway in vitro that may correspond to sequential steps of synaptic vesicle docking, activation, and fusion. *Cell* **75**, 409–418.

Spurlin, B. A., Park, S. Y., Nevins, A. K., Kim, J. K. and Thurmond, D. C. (2004). Syntaxin 4 transgenic mice exhibit enhanced insulin-mediated glucose uptake in skeletal muscle. *Diabetes* **53**, 2223–2231.

St-Denis, J. F., Cabaniols, J. P., Cushman, S. W. and Roche, P. A. (1999). SNAP-23 participates in SNARE complex assembly in rat adipose cells. *Biochem. J.* **338 (Pt 3**, 709–15.

Steegmaier, M., Yang, B., Yoo, J. S., Huang, B., Shen, M., Yu, S., Luo, Y. and Scheller, R. H. (1998). Three novel proteins of the syntaxin/SNAP-25 family. *J. Biol. Chem.* **273**, 34171–34179.

Stein, A., Weber, G., Wahl, M. C. and Jahn, R. (2009). Helical extension of the neuronal SNARE complex into the membrane. *Nature* **460**, 525–528.

Südhof, T. C. and Rothman, J. E. (2009). Membrane fusion: Grappling with SNARE and SM proteins. *Science (80-.).* **323**, 474–477.

Sutton, R. B., Fasshauer, D., Jahn, R. and Brunger, A. T. (1998). Crystal structure of a SNARE complex involved in synaptic exocytosis at 2.4 Å resolution. *Nature* **395**, 347–353.

Suzuki, K. and Kono, T. (1980). Evidence that insulin causes translocation of glucose transport activity to the plasma membrane from an intracellular

storage site. *Proc. Natl. Acad. Sci.* **77**, 2542–2545.

Sztul, E. (2005). Role of tethering factors in secretory membrane traffic. *AJP Cell Physiol.* **290**, C11–C26.

Sztul, E. and Lupashin, V. (2009). Role of vesicle tethering factors in the ER-Golgi membrane traffic. *FEBS Lett.* **583**, 3770–3783.

Tamori, Y., Kawanishi, M., Niki, T., Shinoda, H., Araki, S., Okazawa, H. and Kasuga, M. (1998). Inhibition of insulin-induced GLUT4 translocation by Munc18c through interaction with syntaxin4 in 3T3-L1 adipocytes. *J. Biol. Chem.* **273**, 19740–19746.

Teng, F. Y., Wang, Y. and Tang, B. L. (2001). The syntaxins. *Genome Biol.* **2**, REVIEWS3012.

TerBush, D. R., Maurice, T., Roth, D. and Novick, P. (1996). The Exocyst is a multiprotein complex required for exocytosis in Saccharomyces cerevisiae. *EMBO J.* **15**, 6483–6494.

Thien, C. B. F. and Langdon, W. Y. (2005). c-Cbl and Cbl-b ubiquitin ligases: substrate diversity and the negative regulation of signalling responses. *Biochem. J.* **391**, 153–166.

Thorens, B. (1996). Glucose transporters in the regulation of intestinal, renal, and liver glucose fluxes. *Am. J. Physiol.* **270**, G541–G553.

Thurmond, D. C., Ceresa, B. P., Okada, S., Elmendorf, J. S., Coker, K. and Pessin, J. E. (1998). Regulation of insulin-stimulated GLUT4 translocation by Munc18c in 3T3L1 adipocytes. *J. Biol. Chem.* **273**, 33876–33883.

Thurmond, D. C., Kanzaki, M., Khan, A. H. and Pessin, J. E. (2000). Munc18c Function Is Required for Insulin-Stimulated Plasma Membrane Fusion of GLUT4 and Insulin-Responsive Amino Peptidase Storage Vesicles. *Mol. Cell. Biol.* **20**, 379–388.

Toonen, R. F. G. and Verhage, M. (2003). Vesicle trafficking: Pleasure and pain from SM genes. *Trends Cell Biol.* **13**, 177–186.

Umahara, M., Okada, S., Yamada, E., Saito, T., Ohshima, K., Hashimoto, K., Yamada, M., Shimizu, H., Pessin, J. E. and Mori, M. (2008). Tyrosine phosphorylation of Munc18c regulates platelet-derived growth factor-stimulated glucose transporter 4 translocation in 3T3L1 adipocytes. *Endocrinology* **149**, 40–49.

Van Vliet, C., Thomas, E. C., Merino-Trigo, A., Teasdale, R. D. and Gleeson,

P. A. (2003). Intracellular sorting and transport of proteins. *Prog. Biophys. Mol. Biol.* **83**, 1–45.

Vellai, T. and Vida, G. (1999). The origin of eukaryotes: The difference between prokaryotic and eukaryotic cells. *Proc. R. Soc. B Biol. Sci.* **266**, 1571–1577.

Verhage, M., Maia, A. S., Plomp, J. J., Brussaard, A. B., Heeroma, J. H., Vermeer, H., Toonen, R. F., Hammer, R. E., Van Den Berg, T. K., Missler, M., et al. (2000). Synaptic assembly of the brain in the absence of neurotransmitter secretion. *Science (80-.).* **287**, 864–869.

Vishwanath, D., Srinivasan, H., Patil, M. S., Seetarama, S., Agrawal, S. K., Dixit, M. N. and Dhar, K. (2013). Novel method to differentiate 3T3 L1 cells in vitro to produce highly sensitive adipocytes for a GLUT4 mediated glucose uptake using fluorescent glucose analog. *J. Cell Commun. Signal.* **7**, 129–140.

Volchuk, A., Sargeant, R., Sumitani, S., Liu, Z., He, L. and Klip, A. (1995). Cellubrevin is a resident protein of insulin-sensitive GLUT4 glucose transporter vesicles in 3T3-L1 adipocytes. *J. Biol. Chem.* **270**, 8233–8240.

Watanabe, T., Smith, M. M., Robinson, F. W. and Kono, T. (1984). Insulin action on glucose transport in cardiac muscle. *J. Biol. Chem.* **259**, 13117–22.

Watson, R. T., Shigematsu, S., Chiang, S. H., Mora, S., Kanzaki, M., Macara, I. G., Saltiel, A. R. and Pessin, J. E. (2001). Lipid raft microdomain compartmentalization of TC10 is required for insulin signaling and GLUT4 translocation. *J. Cell Biol.* **154**, 829–840.

Watson, R. T., Saltiel, A. R., Pessin, J. E. and Kanzaki, M. (2007). Subcellular compartmentalization of insulin signaling processes and GLUT4 trafficking events. In *Mechanisms of Insulin Action: Medical Intelligence Unit*, pp. 33–51.

Weber, T., Zemelman, B. V., McNew, J. A., Westermann, B., Gmachl, M., Parlati, F., Söllner, T. H. and Rothman, J. E. (1998). SNAREpins: Minimal machinery for membrane fusion. *Cell* **92**, 759–772.

Weibrecht, I., Leuchowius, K. J., Clausson, C. M., Conze, T., Jarvius, M., Howell, W. M., Kamali-Moghaddam, M. and Söderberg, O. (2010). Proximity ligation assays: A recent addition to the proteomics toolbox. *Expert Rev. Proteomics* **7**, 401–409.

Wilkison, W. O., Min, H. Y., Claffey, K. P., Satterberg, B. L. and Spiegelman,

B. M. (1990). Control of the adipsin gene in adipocyte differentiation. Identification of distinct nuclear factors binding to single- and double-stranded DNA. *J. Biol. Chem.* **265**, 477–482.

Williams, D. and Pessin, J. E. (2008). Mapping of R-SNARE function at distinct intracellular GLUT4 trafficking steps in adipocytes. *J. Cell Biol.* **180**, 375–387.

Wong, S. H., Xu, Y., Zhang, T. and Hong, W. (1998). Syntaxin 7, a novel syntaxin member associated with the early endosomal compartment. *J. Biol. Chem.* **273**, 375–380.

Xu, Y., Su, L. and Rizot, J. (2010). Binding of munc 18-1 to synaptobrevin and to the SNARE four-helix bundle. *Biochemistry* **49**, 1568–1576.

Xu, H., Arnold, M. G. and Kumar, S. V. (2015). Differential effects of munc18s on multiple degranulation-relevant trans-SNARE complexes. *PLoS One* **10**,.

Yamaguchi, T., Dulubova, I., Min, S. W., Chen, X., Rizo, J. and Südhof, T. C. (2002). Sly1 binds to Golgi and ER syntaxins via a conserved N-terminal peptide motif. *Dev. Cell* **2**, 295–305.

Yamakawa, H., Seog, D. H., Yoda, K., Yamasaki, M. and Wakabayashi, T. (1996). Uso1 protein is a dimer with two globular heads and a long coiled-coil tail. *J. Struct. Biol.* **116**, 356–365.

Yang, B., Gonzalez, L., Prekeris, R., Steegmaier, M., Advani, R. J. and Scheller, R. H. (1999). SNARE interactions are not selective. Implications for membrane fusion specificity. *J. Biol. Chem.* **274**, 5649–5653.

Yang, C., Coker, K. J., Kim, J. K., Mora, S., Thurmond, D. C., Davis, A. C., Yang, B., Williamson, R. A., Shulman, G. I. and Pessin, J. E. (2001). Syntaxin 4 heterozygous knockout mice develop muscle insulin resistance. *J. Clin. Invest.* **107**, 1311–1318.

Yu, I.-M. and Hughson, F. M. (2010). Tethering Factors as Organizers of Intracellular Vesicular Traffic. *Annu. Rev. Cell Dev. Biol.* **26**, 137–156.

Zerial, M. and McBride, H. (2001). Rab proteins as membrane organizers. *Nat. Rev. Mol. Cell Biol.* **2**, 107–117.

Zhao, P., Yang, L., Lopez, J. A., Fan, J., Burchfield, J. G., Bai, L., Hong, W., Xu, T. and James, D. E. (2009). Variations in the requirement for v-SNAREs in GLUT4 trafficking in adipocytes. *J. Cell Sci.* **122**, 3472–3480.

Zimmet, P., Alberti, K. G. M. M. and Shaw, J. (2001). Global and societal

implications of the diabetes epidemic. *Nature* **414**, 782–787.